Characterization of the Chromatin Remodeling Enzyme Lymphoid-Specific Helicase

Dissertation zur Erlangung des Doktorgrades
der Naturwissenschaften (Dr. rer. nat.)
der Fakultät für Biologie und Vorklinische Medizin
der Universität Regensburg

vorgelegt von
Thomas Gross

aus Hermannstadt (Rumänien)

im Jahr
2016

Das Promotionsgesuch wurde eingereicht am:
19.02.2016

Die Arbeit wurde angeleitet von:
Prof. Dr. Gernot Längst

(Thomas Gross)

Table of contents

List of figures ..... **IV**

List of tables ..... **VI**

List of abbreviations ..... **VII**

1 Summary **1**

2 Introduction **3**

2.1 Chromatin structure **3**

2.2 Histone modifications **5**

2.3. DNA methylation **7**

2.3.1 Mammalian DNA methyltransferases 7

2.3.2 Reaction mechanism of DNA methyltransferases 11

2.3.3 Biological role of DNA methylation 11

2.4 DNA demethylation **14**

2.4.1 Tet mediated DNA demethylation 14

2.5. Chromatin remodeling **17**

2.5.1 Remodeler families 18

2.5.2 Mechanism of nucleosome remodeling 22

2.5.3 Association of non-coding RNAs with chromatin remodelers 24

2.6 DNA methylation in the context of chromatin **25**

2.6.1 *In vitro* studies on DNA methylation in chromatin 25

2.6.2 Interplay between chromatin remodeling enzymes and DNA methylation 26

2.7 The Snf2 family member Lymphoid-specific helicase **27**

3 Results **32**

3.1 Protein sequence motifs favoring the proposed function of Lsh as a chromatin remodeling enzyme **32**

3.2 Expression and purification of human Lsh **37**

3.3 Lsh preferentially binds to longer DNA molecules *in vitro* **40**

3.4 Lsh binding to nucleosomes is facilitated by the availability of linker DNA **42**

3.5 Lsh shows no remodeling activity *in vitro* **45**

3.6 Basic studies on the ATPase activity of Lsh **47**

3.6.1 Establishing reaction conditions for ATPase assays 47

3.6.2 The *in vitro* ATPase activity of Lsh is not stimulated by DNA and nucleosomes 48

3.7 Expression and purification of Lsh KR mutant **50**

3.8 Study of the interplay between Lsh and 5-hmC **51**

3.8.1 Lsh binds to hydroxy-methylated and methylated DNA with higher affinity than to unmodified DNA 52
3.8.2 Dinucleosomes stimulate Lsh ATPase activity only under specific assay conditions but not in general 53
3.9 The stimulation of the ATPase activity of Lsh is induced by RNA and enhanced by nucleosomes 60
3.9.1 Lsh binds to single-stranded RNA with higher affinity than to DNA 60
3.9.2 The ATPase activity of Lsh is stimulated by total RNA 61
3.9.3 Lsh ATPase activity is enhanced by nucleosomes in the presence of total RNA 63
3.9.4 Competitive binding of RNA, naked DNA and nucleosomal DNA to Lsh 68
3.9.5 The capability of Lsh to hydrolyze ATP improves the binding affinity of Lsh towards RNA 73
3.9.6 Lsh ATPase activity is preferentially induced by structured RNAs 75
3.10 DNA methyltransferases do not activate the ATPase function of Lsh *in vitro* 78
4 Discussion 80
4.1 Basic studies on the chromatin remodeling capabilities of Lsh 80
4.1.1 Lsh preferentially binds longer DNA, prefers nucleosomes with linkers to the nucleosomal core and binds cooperatively 81
4.1.2 Lsh does not remodel nucleosomes *in vitro*, and the *in vitro* ATPase activity of Lsh is not stimulated by DNA and nucleosomes 83
4.2 The role of Lsh in the recognition of the epigenetic landmark 5-hmC 84
4.3 The ATPase activity of Lsh is induced by RNA and enhanced by nucleosomes. 87
4.3.1 Lsh binds to RNA with greater affinity than to DNA 87
4.3.2 Nucleosomes contribute to RNA induced ATPase activity of Lsh 88
4.3.3 Displacement of RNA by DNA and nucleosomes indicates a dynamic interaction between RNA and Lsh 89
4.3.4 ATP hydrolysis changes binding dynamics of Lsh 91
4.3.5 The ATPase activity of Lsh is preferentially induced by structured RNAs 93
4.3.6 Lsh – an RNA helicase? 94
4.4 DNA methyltransferases do not activate Lsh ATPase *in vitro* 96
4.5 Working model of the mechanism of action 97
4.6 Perspectives 99
5 Materials and Methods 103

5.1 Materials 103
5.1.1 Technical devices 103
5.1.2 Software tools 104
5.1.3 Chemicals and consumables 105
5.1.4 Standard solutions 108
5.1.5 Enzymes 112
5.1.6 Kits 112
5.1.7 Standard DNA and protein marker 113
5.1.8 Protease inhibitors, RNase inhibitors and antibiotics 113
5.1.9 Bacterial cell lines and media 113
5.1.10 Eukaryotic cell lines and media 115
5.1.11 Antibodies 115
5.1.12 Oligonucleotides 115
5.1.13 Plasmids 118
5.1.14 Baculoviruses 120
5.1.15 Histones 120
5.2 Methods 121
5.2.1 Working with DNA 121
5.2.2 Working with RNA 126
5.2.3 Protein biochemical methods 128
5.2.4 *E. coli* culture and methods 129
5.2.5 GATEWAY cloning system 130
5.2.5.5 Recombination into baculovirus bacmid DNA 132
5.2.6 Sf21 insect cell culture and baculovirus protein expression 134
5.2.7 Purification of recombinant proteins form Sf21 insect cells 136
5.2.8 *In vitro* reconstitution of chromatin 137
5.2.9 Functional assays 143
6 Appendix 150
7 Acknowledgements 154
8 Bibliography 155

List of figures

Fig 2.1: Structure of the nucleosome core particle. 3
Fig 2.2: Model of hierarchical levels of DNA compaction. 4
Fig 2.3. Histone modifications involved in chromatin reorganization. 6
Fig 2.4: Domain structures of mammalian DNA methyltransferases. 7
Fig 2.5: Overview of Dnmt1 interacting proteins. 9
Fig 2.6: Schematic representation of the DNA methylation reaction. 11
Fig 2.7: DNA methylation and demethylation dynamics in pre-implantation embryos. 13
Fig 2.8: Schematic diagrams of Tet proteins. 14
Fig 2.9: Oxidized cytosines and potential active demethylation pathways. 16
Fig 2.10: Passive DNA demethylation after oxidation by Tet proteins. 17
Fig 2.11: Different activities of chromatin remodeling enzymes. 17
Fig 2.12: Snf2 family of ATPases. 18
Fig 2.13. Organization of remodeler families defined by their ATPase. 19
Fig 2.14: DNA movement around the histone octamer during the remodeling reaction. 23
Fig 2.15: Protein interaction network of Lsh. 29
Fig 2.16: Schematic representation and assigned domains of Lsh. 30
Fig 2.17: Hypothetical model of how Lsh facilitates DNA methylation. 30
Fig 3.1: Multiple sequence alignments of regions encompassing DExx- and HELICc domains of all human representatives of the Snf2-like group. 35
Fig 3.2: Expresssion and purification of 6x His-tagged human full-length Lsh. 38
Fig 3.3: Binding affinities of Lsh towardsDNA fragments of different sizes. 40
Fig 3.4: Binding affinity of Lsh to nucleosomes. 43
Fig 3.5: Analysis of the capability of Lsh to mobilize nucleosomes *in vitro*. 45
Fig 3.6: ATPase activity of Chd3. 48
Fig 3.7: Analysis of the influence of DNA and nucleosomes on the *in vitro* ATPase activity of Lsh. 49
Fig 3.8: Generation of an ATPase inactive version of Lsh. 50
Fig 3.9: Binding affinities of Lsh towards 5-hmC and 5-mC modified and unmodified DNA fragments. 53
Fig 3.10: Analysis of the influence of unmodified dinucleosomes on the ATPase activity of Lsh. 55
Fig 3.11: Analysis of the influence of hydroxy-methylated dinucleosomes on the ATPase activity of Lsh. 57

Fig 3.12: Analysis of the influence of methylated dinucleosomes on the ATPase activity of Lsh. 59
Fig 3.13: Binding affinities of Lsh to RNA and DNA. 60
Fig 3.14: Effect of total RNA on the ATPase activity of Lsh. 62
Fig 3.15: Nucleosome assemblies used in ATPase assays. 64
Fig 3.16: Effect of total RNA in combination with nucleosomes on the ATPase activity of Lsh. 67
Fig 3.17: Competitive binding of RNA and DNA to Lsh. 69
Fig 3.18: Competitive binding of RNA and nucleosomes to Lsh. 71
Fig 3.19: Binding affinity of Lsh towards nucleosomes in the presence of ATP. 73
Fig 3.20: Binding affinity of Lsh towards RNA in the presence of ATP. 74
Fig 3.21: Competitive binding of RNA and nucleosomes to Lsh in the presence of ATP. 75
Figure 3.22: Predicted secondary structures and minimum free energy values of the individual RNAs. 76
Fig 3.23: Effects of structured RNAs on the ATPase activity of Lsh. 77
Fig 3.24: Purifications of His-tagged DNA methyltransferases. 78
Fig 3.25: Effects of Dnmts on the ATPase activity of Lsh. 79
Fig 4.1: Cartoon illustrating the suggested binding mode of Lsh to nucleosomes. 82
Fig 4.2: Competitive interactions with different rates of binding. 91
Fig 4.3: Working model of the mechanistic mode of action of Lsh. 98
Fig 4.4: Multiple sequence alignments of Lsh (Hells) and HSA/post-HSA domains and chromodomains of chromatin remodelers. 100
Fig 4.5: Multiple sequence alignments of Lsh (Hells) and AutoN and NegC domains of ISWI homologs. 102
Fig 5.1: Histone octamers purified from chicken erythrocytes. 120
Fig 5.2: Analysis of incorporation of 5-hmC and 5-mC into the BN601 DNA fragment. 125
Fig 5.3: BP reaction–GATEWAY technology 130
Fig 5.4: LR reaction–GATEWAY technology 131
Fig 5.5: Analysis of incorporation of 5-hmC and 5-mC into the 601-10N-601 DNA fragment. 140
Fig 5.6: Analysis of a typical *in vitro* chromatin assembly. 141
Fig 5.7: Partial MNase digestion of *in vitro* assembled circular chromatin. 142
Fig 5.8: The concept of microscale thermophoresis. 146

List of tables

Table 3.1: Pairwise protein sequence alignments of human Lsh and human members of the Snf2-like group of the Snf2 superfamily. 32
Table 3.2: Overview on nucleosomal substrates used in combination with total RNA in ATPase assays. 63

List of abbreviations

°C	Degree Celsius
aa	Amino acid
ACF	ATP-utilizing chromatin assembly and remodeling factor
ADP	Adenosine-5'-diphosphate
Air	Antisense Igf2r RNA
Amp	Ampicillin
APS	Ammonium persulfate
ARPs	Actin-Related Proteins
ATP	Adenosine-5'-triphosphate
ATRX	Alpha Thalassemia/Mental Retardation Syndrome X-Linked
BAF	Brahma-Associated Factor
bp	base pair
BPTF	Bromodomain PHD Finger Transcription Factor
Brg1	Brahma-Related Gene 1
BRM	Brahma
BSA	Bovine Serum Albumine
C-terminal	Carboxy-terminal
CAF1	Chromatin Assembly Factor 1
CDK4	Cyclin-dependent kinase 4
ChIP	Chromatin immunoprecipitation
CHD	Chromo-ATPase/Helicase-DNA-binding protein
CHRAC	Chromatin Accessibility Complex
Ci	Curie
CpG	Cytosine-phosphatidyl-guanosine
Dbp2	DEAD box protein 2
DDM1	Decrease in DNA methylation protein 1
DDX21	DEAD Box Helicase 21
DEAD	(asp-glu-ala-asp)
DLX1	Distal-less homeobox 1
DMSO	Dimethylsulfoxide
DNA	Deoxyribonucleic acid
Dnmt	DNA-Cytosine-5-Methyltransferase
dNTP	2'-Deoxynucleotide-triphosphate
DTT	Dithiothreitol
E. coli	Escherichia coli
EC_{50}	Equilibrium constant
EDTA	Ethyleneiaminotetraacetate
EGTA	Ethylene Glycol Tetraacetic Acid
EMSA	Electrophoretic mobility shift assay
ESCs	Embryonic Stem Cells
EtBr	Ethidium bromide
FCS	Fetal Calf Serum
Fig	Figure
for	forward

FRAP	Fluorescence Recovery After Photobleaching
g	Gram
g	Relative centrifugal force
GFP	Green fluorescent protein
GOI	Gene of interest
h	Hour, human
H1	Histone 1
H2A	Histone 2A
H2B	Histone 2B
H3	Histone 3
H4	Histone 4
H3Kxme3	Tri-methylation at lysine x of histone H3
H4Kxac	Acetylation at lysine x of histone H4
HAT	Histone Acetyltransferase
HDAC	Histone Deacetylase
HELICc	Helicase superfamily C-terminal domain
His-tag	histidine tag
HMT	Histone Methyltransferase
HOTAIR	HOX antisense intergenic RNA
HP1	Heterochromatin binding Protein 1
INK4	Inhibitors of CDK4
INO80	Inositol requiring
IPTG	Isopropylthiogalactoside
Isw1/Isw2	Imitating Switch (Sacharomyces cerevisiae)
ISWI	Imitating Switch (Drosophila melanogaster)
kb	Kilobases
kDa	kilo-Dalton
KO	knock-out
l	Litre
LB	Luria-Bertani
LINE	Long interspersed nuclear element
lncRNA	Long non-coding RNA
Lsh	Lymphoid-specific helicase
M	Molar
µM	Micromolar
MBD	Methyl-CpG-binding-Domain protein
MeCP	5-Methyl-Cytosine Binding Protein
MENT	Methylated In Normal Thymocytes
MEP-1	Metalloproteinase 1
Mhrt	Myosin heavy-chain-associated RNA transcript
min	Minute
MNase	Micrococcal nuclease
MOI	Multiplicity of Infection
MW	Molecular Weight
n	Hill coefficient
NCP	Nucleosome core particle
ncRNA	non-coding RNA
Ni-NTA	Nickel-nitroacetic acid

NLS	nuclear localization sequence
nM	Nanomolar
N-terminal	Amino-terminal
NoRC	Nucleolar Remodeling Complex
NPS	Nucleosome Positioning Sequence
nt	nucleotide
NuRD	Nucleosome Remodeling and Deacetylase
NURF	Nucleosome Remodeling Factor
OD	optical density
PAA	Polyacrylamide
PAGE	Polyacrylamide Gel Electrophoresis
PBS	Phosphate Buffered Saline
PCR	Polymerase Chain Reaction
PHD	Plant Homeodomain
PRC	Polycomb-group repressive complex
PTMs	Post-translational Modifications
rDNA	ribosomal DNA
rev	reverse
RIG1	Retionic acid inducible gene 1 protein
RNA	Ribonucleic Acid
rpm	rounds per minute
RSF	Remodeling and Spacing Factor
RSC	Remodels the structure of chromatin
RT	room temperature
s, sec	Second
SAH	S-adenosyl-L-homocysteine
SAM	S-adenosyl-L-methionine
SANT	SWI3, ADA2, N-CoR and TFIIIB
SDS	Sodium Dodecyl Sulfate
SDS-PAGE	Sodium Dodecyl Sulfate Polyacrylamide Gel Electrophoresis
SF2	Super family 2
Sf21	Spodoptera frugiperda 21 cells
SINE	Short interspersed nuclear element
SLIDE	SANT-Like Domain
Snf	Sucrose non-fermenting
Snf2H	Snf2 homolog protein
Snf2L	Snf2 like protein
SU(VAR)3-9	suppressor of variegation 3-9
Sth1	Snf2 homologous 1
SWI/SNF	Switching defective/Sucrose Non-Fermenting
Swr1	SWI/SNF-related 1
TAM	Tip5/ARBP/MBD
Taq	Thermus aquaticus
TBE	Tris Borate EDTA
TE	Tris EDTA
Tet	Ten-eleven translocation
TEMED	N,N,N’,N’-tetramethylethylenediamine
TIP5	TTF-I interacting protein 5

TLC	Thin-layer chromatography
Tris	Tris(hydroxymethyl)aminomethane
tRNA	transfer RNA
TTF1	Transcription Termination Factor 1
U	Unit
UHRF1	Ubiquitin-Like PHD And RING Finger Domain-Containing Protein 1
V	Volt
WDR5	WD repeat-containing protein 5
WICH	WSTF-ISWI chromatin remodeling complex
WSTF	Williams syndrome transcription factor
WT	wild-type
w/v	Weight per volume
XIST	X(inactive)-specific transcript
YFP	Yellow fluorescent protein

1 Summary

Lsh is an essential epigenetic regulator protein and is required for both *de novo* and *maintenance* DNA methylation (Zhu et al., 2006) (Myant and Stancheva, 2007) (Dunican et al., 2015). Lsh deficiency results in perturbed heterochromatin structure, abnormal mitosis and de-repression of transcription (Huang, 2004) (Yan et al., 2003b), which is mainly due to a severe decrease in DNA methylation levels. Loss of Lsh preferentially reduces DNA methylation at repetitive elements (Dennis, 2001) (Geiman et al., 2001), but also at stem cell genes (Xi et al., 2009) and imprinted regions (Fan et al., 2005). Lsh is thus considered as an important player in the establishment of transcriptionally inactive chromatin.

As DNA methylation is repressed by nucleosomes, allowing DNA methylation only in the linker regions, DNA in a nucleosomal complex requires active changes in nucleosome structure to render DNA accessible for Dnmts (Robertson et al., 2004) (Takeshima et al., 2006) (Felle et al., 2011a) (Schrader et al., 2015). Due to its conserved ATPase domain and its chromatin-specific functions, the Snf2-like family member Lsh (Flaus et al., 2006) is supposed to mobilize nucleosomes in an ATP-dependent manner, regulating DNA accessibilty and thus DNA methylation. However, its capability to move nucleosomes has not been addressed so far.

Therefore, a detailed characterization of the chromatin remodeling functions of Lsh was performed *in vitro*.

Gel retardation assays and MST measurements demonstrate a preferred binding to longer DNA molecules, a preference in the binding to nucleosomes containing symmetric linkers, and reveal cooperative binding. Collectively, the binding assays suggest multimerization upon binding to DNA at the entry/exit sites of nucleosomes. This implies the spreading of Lsh in a nucleosomal array, probably marking genomic regions by this way *in vivo*. Despite its relationship to chromatin remodeling enzymes, Lsh did not mobilize nucleosomes *in vitro*. In addition, nucleosomes by their own, or in combination with Dnmts, did not stimulate its ATPase activity. However, RNA was found to associate with Lsh and to exhibit stimulatory effects on Lsh ATPase activity. The RNA-stimulated activity is further enhanced by nucleosomes, realizing that RNA-dependent ATPase activity of Lsh works best with arrays. Competitive EMSAs show that nucleosomes and RNA occupy the same binding site on Lsh. RNA is displaced from Lsh at increased nucleosome concentrations, suggesting dynamic binding of substrates that may be required for its ATPase activity. RNA appears to be the limiting factor in terms of the activity of Lsh, and the enzyme is probably inactive when it is tightly bound to nucleosomes.

Moreover, Lsh exhibits increased ATPase activity with complex structured RNAs, indicating that the ATPase activity could be stimulated by specific RNAs.
Besides, the presented work offers data to unveil whether the proposed remodeling capability of Lsh could play a role in the interpretation of 5-hmC as an epigenetic mark (Shen and Zhang, 2013) (Spruijt et al., 2013). The binding affinity of Lsh to 5-hmC modified DNA is higher than to unmodified DNA, and the ATPase activity of Lsh is stimulated, yet weakly, by hydroxy-methylated dinucleosomes.

2 Introduction

2.1 Chromatin structure

The length and complexity of eukaryotic genomes confronts cells with several constraints, as genomic DNA has to be compacted to fit into the nucleus, yet genetic information has to be readily accessible. Furthermore, multi-cellular organisms contain a number of widely different and specialized cell types, requiring differential gene expression. Cells meet these requirements by the assembly of the genome into a structure termed chromatin, which is of high plasticity.

Chromatin consists of DNA, histones and non-histone proteins (Olins and Olins, 2003) and presents the substrate for all kinds of DNA-dependent processes, such as the control of gene expression, DNA replication, recombination and DNA repair (Felsenfeld et al., 2004) (Khorasanizadeh, 2004). Notably, there is evidence that besides DNA and proteins, RNA forms an integral component of chromatin regarding chromatin structure and stability (Rodríguez-Campos and Azorín, 2007). DNA compaction in chromatin is achieved by the folding into several layers of structural hierarchy. The nucleosome core particle (NCP) is the universal repeat unit in chromatin with a molecular weight of 210 kilo Dalton (kDa) (Kornberg, 1974). High-resolution crystal structures revealed that 147 bp of DNA are wrapped around an octameric histone core in 1.65 helical turns of a flat left-handed superhelix (Luger et al., 1997) (Fig 2.1).

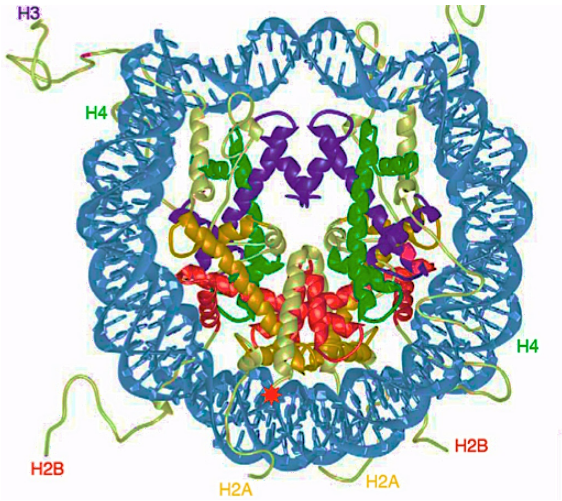

Fig 2.1: Structure of the nucleosome core particle.
147 bp of DNA (colored in light blue) are wrapped around the histone octamer in 1.65 turns. The histone octamer is composed of two copies of each histone H2A (yellow), H2B (red), H3 (violet) and H4 (green). Histone tails protrude from the nucleosome core particle. The red star indicates the site of ubiquitination in yeast (adapted from Luger, Current Opinion in Genetics & Development, 2003).

Distortion of the DNA is caused by the tight interaction between the rigid framework of the histone proteins with the DNA at 14 specific DNA-binding sites (Luger and Richmond, 1998). The histone octamer itself is composed of two copies of each of the four canonical histone proteins H2A, H2B, H3 and H4 (Luger et al., 1997). The canonical histones are small basic proteins (11–16 kDa) that are highly conserved throughout evolution and are made of a carboxy-terminal three-helix 'histone fold' domain and less structured amino-terminal domains, the 'histone tails' (Richmond and Davey, 2003) (Luger, 2006). These histone tails exhibit numerous lysine, arginine and serine residues, and are targets for post-translational modifications. Furthermore, canonical histones in the nucleosome can be exchanged by histone variants that either differ in their amino acid sequence or contain a additional protein domains or both in comparison to their canonical counterparts. Histone variants are assumed to be involved in transcriptional regulation, development and tissue-specific gene expression, thus adding an additional layer of plasticity to the epigenetic regulation of chromatin (Weber and Henikoff, 2014).

Eukaryotic DNA is many orders of magnitude longer than the diameter of the nucleus. Therefore, DNA has to be compacted in order to fit into the nucleus, which as achieved by the folding of chromatin into higher-order structures (Woodcock and Dimitrov, 2001) (Woodcock, 2006) (Horn and Peterson, 2002) (Fig 2.2).

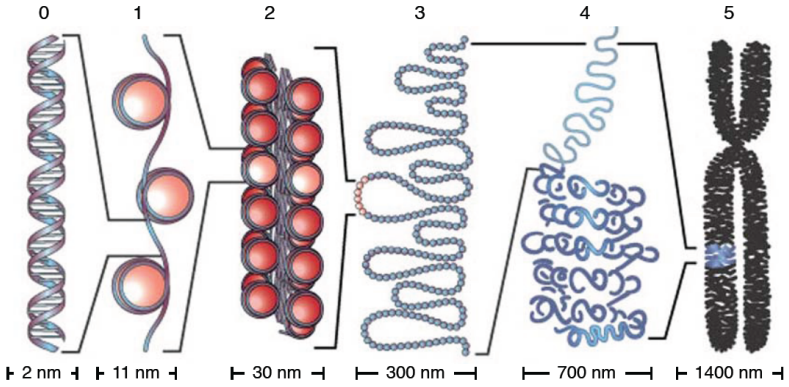

Fig 2.2: Model of hierarchical levels of DNA compaction.
A linear DNA molecule (1) is compacted into a nucleosomal array (2). This so-called 10 nm fiber is believed to be wound into the 30 nm fiber (3) that is depicted according to the solenoid model. Higher-order chromatin structures (4 and 5) contribute to the formation of the highly organized structure of mitotic chromsomes (modified and adapted from Felsenfeld and Groudine, Nature, 2003).

The first level of compaction is the 10 nm fiber, a succession of nucleosomes linked by short stretches of DNA (15–60 bp) into a flexible chain, also referred to as 'beads on a string'. The second level of organization is the so-called 30 nm fiber that still remains elusive in its structure despite of intense work on this topic. Two architectural concepts on how nucleosomes are arranged within the 30 nm fiber are under discussion. In the 'solenoid model', nucleosomes are spiraled into a one-start helix (Robinson and Rhodes, 2006) (Routh

et al., 2008), wherein the nucleosomes are gradually coiled around a central axis (6–8 nucleosomes per turn). The other model proposed a 'zig-zag' packaging that features a two-start helix in which the 10 nm fiber criss-crosses between two helical turns (Dorigo et al., 2004) (Khorasanizadeh, 2004) (Schalch et al., 2005).
Very little is known about the compaction of chromatin above the 30 nm fiber. However, chromatin is suggested to be further organized into higher-order fiber-like structures that are based on fiber-fiber interactions (Li and Reinberg, 2011).
The highest level of DNA compaction is found during M-phase in the mitotic metaphase chromosomes. The metaphase chromosome, condensing chromatin 10.000–20.000 times, represents the most consistent higher-order structure of chromatin (Hancock, 2012).
Conventionally, chromatin can be categorized into two main classes, euchromatin and heterochromatin. Heterochromatin is highly condensed, gene-poor, and transcriptionally silent, whereas euchromatin is less condensed, gene-rich, and more easily transcribed (Huisinga et al., 2006). Heterochromatin can be further classified as constitutive and facultative heterochromatin. Constitutive heterochromatin is found at pericentromeric, telomeric, and ribosomal regions, and mainly comprises repetitive elements. Constitutive heterochromatin is enriched in H3K9me3, primarily set by the histone methyltransferase SU(VAR)3-9 and recognized by the H3K9me3-specific binder Heterochromatin Protein 1 (HP1), recruiting additional chromatin modifiers. By contrast, facultative heterochromatin can form anywhere in the nucleus, and its formation is required for mating-type gene silencing in budding yeast, and X-chromosome inactivation and developmental progression in mammalian cells (Grewal and Jia, 2007) (Craig, 2005) (Saksouk et al., 2015).

2.2 Histone modifications

The architecture of chromatin and the activity state of genomic regoins are dynamically regulated by mechanisms such as post-translational modifications (PTMs) of histones (Vaquero et al., 2003) (Fischle, 2008), the exchange of canonical histones by histone variants (Weber and Henikoff, 2014), and ATP-dependent chromatin remodeling (Varga-Weisz and Becker, 2006).
The usually unstructured histone tails are the primary target sites for PTMs that are highly dynamic and well regulated by specific enzymes (Kouzarides, 2007). The vast variety of PTMs and the combinatorial complexity, which generates histone patterns, led to the proposal of a so-called 'histone code' hypothesis. According to this, a specific combinatorial set of histone modifications, either in '*cis*' (on same tail) or in '*trans*' (on proximal tails), can trigger the recruitment of specific reader or effector proteins (Fischle et al., 2003a) (Strahl and Allis, 2000).

The defined histone patterns therefore specifically regulate the activity of chromatin regions. PTMs of canonical histone proteins include methylation of lysine and arginine residues, phosphorylation of serine and threonin residues as well as lysine acetylation and ubiquitylation, and also lysine sumoylation (Bönisch et al., 2008) (Cosgrove et al., 2004) (Fischle et al., 2003b) (Fig 2.3).

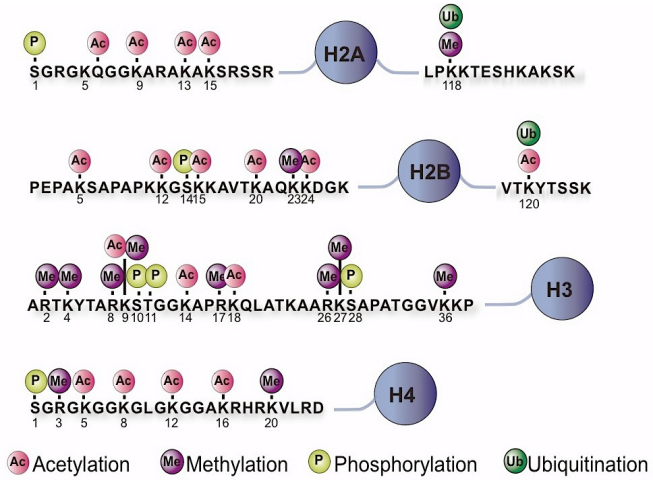

Fig 2.3. Histone modifications involved in chromatin reorganization.
Histone N-terminal tails are post-translationally modified, and certain combinations of histone modifications appear to generate a "histone code" that defines the chromatin state (adapted from Kato et al., IBMS BoneKEy, 2010).

Methylation of H3K4 is involved in the activation of gene transcription (Santos-Rosa et al., 2003) (Bannister and Kouzarides, 2005) (Bernstein et al., 2006), whereas methylation of H3K9 is associated with heterochromatin formation and transcriptional repression. H3K9m3 is mainly found in pericentromeric regions, together with mono-methylated H3K27 (Peters et al., 2003) (Martens et al., 2005). Yet, H3K9me3 was also detected at certain active genes (Margueron and Reinberg, 2010) (Campos and Reinberg, 2009).
Histone methylation is catalyzed by histone methyltransferases (HMTs), such as SU(VAR)3-9 or G9a that catalyze the methylation of histone H3 at lysine 9 (Zhang and Reinberg, 2001). Demethylation is carried out by histone lysine demethylases (Hoffmann et al., 2012).
Another well-studied PTM is acetylation of histones, carried out by histone acetyltranferases (HAT). This modification is observed at the amino-terminal (N-terminal) domains of all four core histones (Vaquero et al., 2003). In general, histone H3 and H4 acetylation is related to active gene transcription. Acetyl groups can be removed by histone deacetylases (HDACs) (Dovey et al., 2010) (Jacobson et al., 2000), which correlates with transcriptional repression (Vaquero et al., 2003).
Further histone modifications are phosphorylation and ubiquitination. All four nucleosomal histone tails contain acceptor sites that can be phosphorylated by a number of protein kinases and dephosphorylated by phosphatases. Histone phosphorylation can occur at serine, threonine and tyrosine residues (Rossetto et al., 2012).

One prominent example of histone phosphorylation is the phosphorylation of the histone variant H2A.X, in its phosphorylated form commonly referred to as γH2A.X. Phosphorylation of H2A.X plays a major role in DNA damage response and takes place on serine 139 (Celeste et al., 2003). H2A and H2B are two of the most abundant ubiquitinated proteins in the nucleus. Histone ubiquitination plays a role in many processes, including transcription, maintenance of chromatin structure, and DNA repair (Cao and Yan, 2012).

2.3. DNA methylation

2.3.1 Mammalian DNA methyltransferases

The mammalian group of DNA methyltransferases (Dnmts) comprises Dnmt1, Dnmt2, Dnmt3a, Dnmt3b and Dnmt3L. The Dnmt3 family establishes the initial CpG methylation pattern, therefore its members are termed *de novo* methyltransferases, while Dnmt1 maintains the methylation pattern during replication (Chen and Li, 2006) and repair (Mortusewicz et al., 2005). The Dnmt3 family includes two active *de novo* Dnmts (Dnmt3a, Dnmt3b) and one regulatory factor, the Dnmt3-Like factor (Dnmt3L). DNA methyltransferases generally comprise two domains: a conserved catalytic domain in the carboxy-terminal (C-terminal) part of the protein and a more variable regulatory domain in the N-terminal region (Fig 2.4) (for review, see (Denis et al., 2011)).

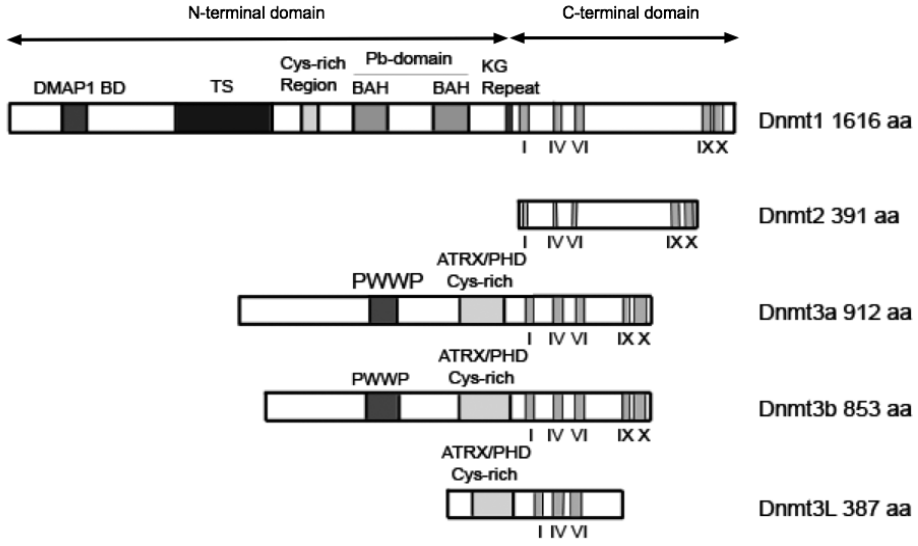

Fig 2.4: Domain structures of mammalian DNA methyltransferases.
The mammalian DNA methyltransferases are divided into an N-terminal regulatory domain and a C-terminal catalytic domain, with the latter showing strong amino acid sequence homology to prokaryotic DNA methyltransferases (conserved catalytic motifs I, IV, VI, IX and X are indicated). Dnmt1: DMAP1 (Dnmt1 associated protein 1)-binding domain, TS (targeting sequence) domain, Cys-rich region (ATRX type zinc finger, mediates DNA-binding), Pb-domain (polybromo-1 protein homologous region containing two BAH domains), KG (lysine-glycine) repeats. Dnmt3 family: PWWP domain, ATRX/PHD (cysteine-rich zinc finger domain of the ATRX/ plant homeodomain type) (modified and adapted from Ryazanova et al., InTech article, chapter 2: Diverse Domains of (Cytosine-5)-DNA Methyltransferases: Structural and Functional Characterization, 2013).

2.3.1.1 The *maintenance* methyltransferase Dnmt1

Dnmt1 was the first mammalian DNA methyltransferase to be characterized (Bestor et al., 1988). Enzymatic studies revealed high methylation processivity of hemi-methylated (hm) DNA as well as a high preference of Dnmt1 activity towards hm DNA. The activity of Dnmt1 towards hm DNA is approximately 20–25-fold higher in comparison to its activity towards non-methylated DNA (Hermann et al., 2004b) (Bacolla et al., 1999) (Pradhan et al., 1999). Taken together, this reflects the role of *maintenance* methylation in the course of DNA replication *in vivo* (Bestor, 2000).

Dnmt1 comprises a large N-terminal regulatory domain, linked via a lysine-glycine-rich (KG) stretch to the conserved C-terminal catalytic domain (Fig 2.4). The N-terminal domain contains a PCNA (Proliferating cell nuclear antigen)-binding domain (Pb-domain), including two bromo adjacent homology domains (BAH1 and BAH2) (Goll and Bestor, 2005) (Rottach et al., 2009). The Pb-domain is responsible for the interaction with PCNA, which serves as a loading platform and processivity factor for proteins contributing to DNA replication and repair (Maga and Hubscher, 2003) (Sporbert et al., 2005) (Mortusewicz et al., 2005). The two BAH domains are likely involved in protein-protein interactions (Oliver et al., 2005).

The TS domain of Dnmt1 was identified as the key determinant for dimerization of Dnmt1 in a head-to-head orientation (Fellinger et al., 2009). In addition, the TS domain mediates the recruitment of Dnmt1 to replication foci through its interaction with the SRA domain of UHRF1 (Leonhardt et al., 1992) (Achour et al., 2008). UHRF1 binds preferentially to hm DNA (Bostick et al., 2007). In addition, UHRF1 not only increases the accessibility for DNA inside the catalytic center of DNMT1 but also determines the specificity of Dnmt1 for hm CpG sites (Bashtrykov et al., 2014) (Berkyurek et al., 2014).

Apart from its association with UHRF1, Dnmt1 is regulated in a tightly cross-linked network of interactions, coordinating Dnmt1 methylation activity together with other chromatin modifications (Fig 2.5) (for review on Dnmt1 interactions, see (Qin et al., 2014)).

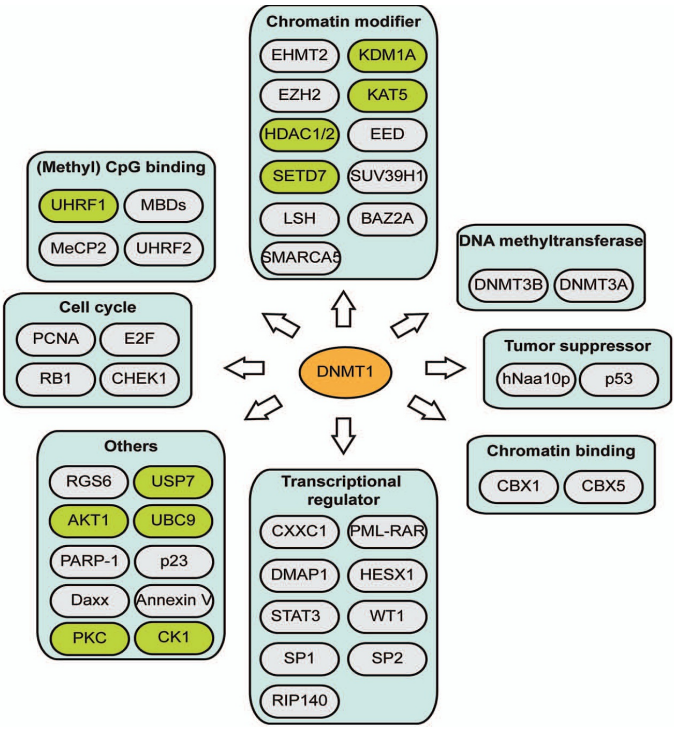

Fig 2.5: Overview of Dnmt1 interacting proteins.
Interacting proteins range from DNA methyltransferases, DNA-binding proteins, chromatin modifiers and chromatin-binding proteins to tumor suppressors, cell cycle regulators and transcriptional regulators. Proteins involved in the post-translational modification of Dnmt1 are highlighted in green (adapted from Qin et al., Nucleus, 2011).

Amongst others, Dnmt1 interacts with proteins such as histone methyltransferases, histone deacetylases and chromatin remodelers. For instance, Dnmt1 forms a complex with the Nucleolar Remodeling Complex (NoRC), Dnmt3b and HDAC1 in order to mediate silencing of ribosomal DNA (rDNA) (Zhou and Grummt, 2005). Interestingly, the ATPase subunit of NoRC, hSnf2H, increases the binding affinity of DNMT1 to mononucleosomes (Robertson et al., 2004), indicating that the interaction with chromatin remodeling factors may help Dnmt1 to access substrate sites in heterochromatic regions. In addition, Dnmt1 interacts with Lsh, a protein required for maintaining DNA methylation in mammals. Lsh is related to the Snf2 family of chromatin-remodeling ATPases and is suggested to cooperate with Dnmt1, Dnmt3b and HDACs in order to establish transcriptional repression (Dennis, 2001) (Myant and Stancheva, 2007). Recently, the regulation of Dnmt1 by long non-coding RNAs has been demonstrated as well (Di Ruscio et al., 2014).

2.3.1.2 The Dnmt3 family

Both Dnmt3a and Dnmt3b do not exhibit any preference for hemi-methylated DNA *in vitro* and thus have been termed *de novo* methyltransferases (Okano et al., 1998) (Gowher and Jeltsch, 2001) (Suetake et al., 2003). *De novo* methyltransferase activity exerted by Dnmt3a and Dnmt3b was substantiated by *in vivo* findings. Disruption of the genes for Dnmt3a and Dnmt3b blocked *de novo* methylation in ES cells and early embryos, yet had no effect on the maintenance of imprinted methylation patterns (Okano et al., 1999). Furthermore, their localization to heterochromatin is not dependent on pre-existing methylation marks (Bachman et al., 2001). Dnmt3a and Dnmt3b are highly related proteins, and contain protein domains for interactions with chromatin-associated factors. Dnmt3a and Dnmt3b share a homologous C-terminal catalytic domain as well as a homologous cysteine-rich region (also referred to as ATRX/PHD domain) (Xie et al., 1999) and a PWWP domain (Qiu et al., 2002). The PWWP domain exhibits DNA-binding properties (Qiu et al., 2002) (Chen et al., 2004). Notably, disruption of the PWWP domain in Dnmt3a and Dnmt3b abolished their association with pericentromeric heterochromatin (Chen et al., 2004). The ATRX/PHD domain of these two proteins is characterized by a conserved Cys_4-$HisCys_3$ zinc-binding motif and is mainly found in proteins involved in eukaryotic transcriptional regulation (Hermann et al., 2004a). Dnmt3a is known to associate with proteins such as the histone methyltransferases SU(VAR)3-9 and SETDB1, the HP1 protein, transcription factors like SALL3, the arginine methyltransferase PRMT5, or the chromatin remodelers Brg1 and Lsh (Li et al., 2006) (Fuks et al., 2003a) (Shikauchi et al., 2009) (Zhao et al., 2009) (Datta et al., 2005) (Myant and Stancheva, 2007).

Like Dnmt3a, Dnmt3b has been shown to interact with factors involved in gene silencing such as SU(VAR)3-9, HDAC1 and 2, HP1 and the chromatin remodeling enzymes hSnf2H and Lsh (Lehnertz et al., 2003) (Geiman et al., 2004) (Myant and Stancheva, 2007).

The third member of the Dnmt3 family, Dnmt3L, lacks some essential catalytic motifs and has no methyltransferase activity. However, Dnmt3L serves as a cofactor for Dnmt3a and Dnmt3b and stimulates their activity via direct interaction (Hata et al., 2002) (Chedin et al., 2002) (Suetake et al., 2004) (Jia et al., 2007).

Several findings indicate complementary functions of Dnmt1 and *de novo* Dnmts. Whereas Dnmt3a and Dnmt3b are involved in maintaining DNA methylation patterns (Chen et al., 2003) (Rhee et al., 2002), *in vitro* and *in vivo* studies provide evidence that Dnmt1 has *de novo* methylation activity (Arand et al., 2012) (Felle et al., 2011b). Furthermore, Dnmt3a appears to functionally cooperate with Dnmt1, stimulating methyltransferase activity (Fatemi et al., 2002).

2.3.2 Reaction mechanism of DNA methyltransferases

The reaction catalyzed by Dnmts is the conversion of one molecule of S-adenosyl-methionine (SAM) and an unmethylated cytosine residue within double-stranded DNA to one molecule of S-adenosyl-homocysteine (SAH) and a cytosine residue methylated on carbon C5 (Fig 2.6). For detailed description of the reaction mechanism, see (Pradhan and Estève, 2003). In contrast to other eukaryotic Dnmts, the catalytic domain of Dnmt1 is not catalytically active by itself but requires allosteric activation by its N-terminal domain (Fatemi et al., 2001).

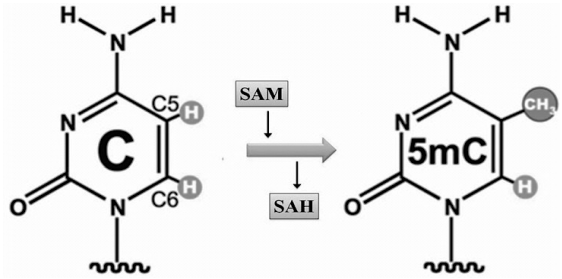

Fig 2.6: Schematic representation of the DNA methylation reaction.
DNA methyltransferases transfer a methyl-group onto carbon C5 of the cytosine residue of the double-stranded DNA, by using *S*-adenosyl-methionine (SAM) as methyl donor. *S*-adenosyl-homocysteine (SAH) is the cofactor product (adapted from Cheng and Blumenthal, Cell, 2008).

As shown for prokaryotic Dnmts, DNA methylation requires the accessibility of the target cytosine by a base flipping mechanism, which is also suggested for mammalian Dnmts (Huang et al., 2003) (Jia et al., 2007). Indeed, crystal structures of Dnmt1 in a complex with DNA revealed a structure with the flipped-out target cytosine anchored within the catalytic pocket of Dnmt1 (Song et al., 2012). Initially, base flipping was described for the uracil-DNA glycosylase in DNA repair (Jeltsch, 2002), while the SRA domain of UHRF1 was identified as the first example of a DNA-binding module that uses this mechanism for sequence-specific DNA recognition (Arita et al., 2008) (Hashimoto et al., 2008).

2.3.3 Biological role of DNA methylation

DNA methylation has a variety of important functions in mammals such as gene repression, control of cellular differentiation and development, preservation of chromosomal integrity, parental imprinting and X-chromosome inactivation (Bird, 2002) (Hermann et al., 2004a). CpG methylation induces interaction changes between DNA and DNA-binding proteins. For instance, binding of transcription factors such as E2F or NFκB can be abolished, whereas recruitment of 5-methyl-cytosine-binding proteins (MECPs) that ‘read’ DNA methylation patterns, is enhanced. MECPs and Dnmts are associated with HDACs and other

factors like chromatin remodelers and histone methyltransferases, in order to induce chromatin compaction and stable transcriptional repression (Robertson, 2002) (Fuks et al., 2003b) (Rountree et al., 2001) (Yang et al., 2015) (Qin et al., 2014).

The human genome contains approximately 50% of repetitive elements. Of these, about 60% are sequences like LINEs, SINEs and IAPs that originate from transposable elements (de Koning et al., 2011). Since integration of transposable elements into the genome is a source for mutations, their spreading in the genome is inhibited by silencing such regions through extensive DNA methylation. In addition, pericentromeric satellite repeats and telomeres are highly methylated and densely packaged into heterochromatin, impairing homologous recombination events and thus providing chromosomal stability (Smith and Meissner, 2013) (Slotkin and Martienssen, 2007).

Aberrations in DNA methylation play a causal role in a variety of diseases, including defects in genome-wide hypo- and hypermethylation of specific CpG islands, as well as loss of genomic imprinting. Global DNA hypomethylation, which promotes stimulation of oncogenes as well as reactivation of retrotransposons and genomic instability, occurs concomitantly with local hypermethylation of tumor suppressor genes and is often found in a significant subset of melanomas and colon cancers (Feinberg, 2004).

Furthermore, DNA methylation has been shown to be involved in ICF (Immunodeficiency, Centromeric instability, Facial abnormalities) and the Rett syndrome. ICF is an autosomal recessive disease, characterized by hypomethylation of pericentromeric satellite repeats. Hypomethylation in ICF is caused by mutations in the *DNMT3B* gene, negatively affecting the activity of the Dnmt3b protein (Moarefi and Chedin, 2011). The Rett syndrome is an X-chromosomal dominant disease that results from a mutation in the MeCP2 protein (Kriaucionis and Bird, 2003).

Genomic imprinting is a mammalian-specific phenomenon that refers to parental-origin-dependent mono-allelic expression in spite of identical nucleotide sequences (Li, 2002). The existence of genomic imprinting in mammals was proven by the identification of the gene *Igf2r* (Insulin-like growth factor type 2 receptor) and the *H19* locus, which both are maternally expressed imprinted genes, and by the identification of the *Igf2* gene as a paternally expressed imprinted gene (Bartolomei et al., 1991) (DeChiara et al., 1991) (Regha et al., 2006). To date, there are about 150 imprinted genes known in humans and mice. Most imprinted genes are found in clusters that include multiple protein-coding mRNAs and at least one non-coding RNA. The imprinting mechanism is acting *in cis*, and imprinted expression is controlled by an imprint control element (ICE) that is epigenetically marked by DNA methylation, inherited from one parental gamete (Barlow and Bartolomei, 2014) (Barbaux et al., 2012). Imprinting defects due to aberrant DNA methylation are found in solid tumors in childhood that arise from embryonic tissues. These so-called embryonic tumors,

comprising neuroblastoma (NB), Wilms tumor, medulloblastoma (MB), rhabdomyosarcoma (RMS) and hepatoblastoma (HB), have been extensively studied in regard to epigenetic defects at the *Igf2/H19* locus. Interestingly, defective imprinting of *Igf2* and thus inappropriate activation of the maternal allele of the *Igf2* gene are found in about 50% of all Wilms tumors (Ogawa et al., 1993) and RMS cases (Zhan et al., 1994) as well as in about 25% of HB (Rainier et al., 1995).

In mammals, genome-wide reprogramming of DNA methylation patterns occurs during germ-cell development and after fertilization. Typically, a substantial part of the genome is demethylated and after some time remethylated, which occurs in a cell- or tissue-specific pattern (Morgan et al., 2005). During gametogenesis, primordial germ cells undergo demethylation-independent of replication, erasing parental imprinting marks (Abdalla et al., 2009). In the course of oogenesis and spermatogenesis, maternal and paternal-specific genomic imprints are re-established through *de novo* methylation activities of Dnmt3a and Dnmt3b and the associated Dnmt3L protein (Hata et al., 2002) (Kato et al., 2007).

After zygote formation, the paternal DNA is demethylated. Loss of paternal DNA methylation was observed to correlate with a rapid increase in 5-hydroxy-methylcytosine (5-hmC), 5-formylcytosine (5-fC) and 5-carboxyl-cytosine (5-caC), suggesting active, i. e. Tet-driven DNA demethylation (Iqbal et al., 2011) (Inoue et al., 2011) (Inoue and Zhang, 2011)). The maternal DNA is demethylated over several cell divisions by the lack of *maintenance* DNA methylation (Frauer et al., 2011) (Hashimoto et al., 2012).

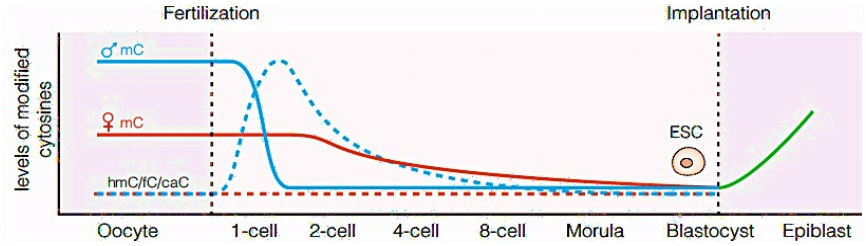

Fig 2.7: DNA methylation and demethylation dynamics in pre-implantation embryos.
Immediately after fertilization, paternal 5-mC is rapidly oxidized by Tets, most probably by Tet3. Oxidized 5-mC levels in the paternal genome and 5-mC in the maternal genome are diluted through passive demethylation. After implantation, DNA methylation is re-established (modified and adapted from Wu and Zhang, Cell, 2014).

After the paternal and the maternal pronuclei fuse, 5-hmC, 5-fC and 5-caC in sperm-derived chromosomes and 5-mC in oocyte-derived chromosomes are lost by passive DNA demethylation (Inoue et al., 2011) (Inoue and Zhang, 2011). Yet, several maternally derived methylated CpG-rich regions remain fully or partially methylated, including maternal imprinting control regions (ICRs) (Smallwood et al., 2011) (Smith et al., 2012).

Following implantation, embryonic methylation patterns are re-introduced by a wave of *de novo* DNA methylation. Genetic studies on zygote formation revealed that both *maintenance*

and *de novo* methylation activities are indispensible for the formation of methylation patterns, and thus essential for embryonic development (Okano et al., 1999) (Li et al., 1992).

2.4 DNA demethylation

2.4.1 Tet mediated DNA demethylation

2.4.1.1 Tet proteins

The Ten-eleven-translocation (Tet) family of Fe(II)-2-oxoglutarate-dependent dioxygenases were identified as the enzymes that convert 5-mC to 5-hmC (Tahiliani et al., 2009). Subsequent studies showed that Tet proteins can further oxidize 5-hmC to 5-fC and 5-caC (Ito et al., 2011) (Pfaffeneder et al., 2014). These discoveries contributed to the understanding of the molecular mechanisms leading to active DNA demethylation in mammals.

First experiments on Tet proteins revealed that overexpression of Tet1 results in a decrease of genomic 5-mC levels, and that recombinant Tet1 protein can oxidize 5-mC to 5-hmC *in vitro* (Tahiliani et al., 2009). A similar enzymatic activity was also demonstrated for Tet2 and Tet3, the two other members of the Tet protein family (Ito et al., 2010).

Structurally, all Tet family members contain a C-terminal catalytic domain, including a cysteine-rich (Cys-rich) domain and the double-stranded beta helix (DSBH) domain. In addition, the binding sites for the cofactors Fe(II) and 2-oxoglutarate (2-OG) are located in the C-terminal catalytic domain (Zhao and Chen, 2013) (Fig 2.8).

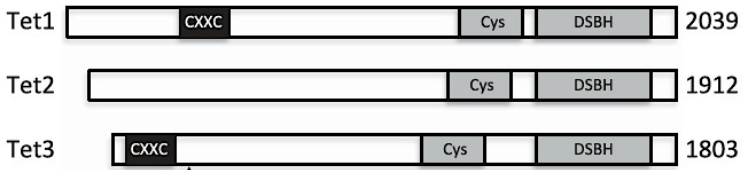

Fig 2.8: Schematic diagrams of Tet proteins.
All of the three Tet proteins Tet1, Tet2 and Tet3 have a C-terminal catalytic domain, consisting of a cysteine-rich region and the double-stranded beta-helix (DSBH) fold that is characteristic of the 2-oxoglutarate- and Fe(II)-dependent dioxygenase family. Tet1 and Tet3, but not Tet2, contain an N-terminal CXXC zinc finger domain, which is a DNA-binding domain (adapted from Zhao and Chen, Journal of Human Genetics, 2013).

An unstructured region of great variation across Tet family members separates the DSBH domain from the Cys-rich domain. In addition, *TET1* and a long splicing variant of *TET3* encode a CXXC zinc finger domain at their N-termini (Liu et al., 2013) (Iyer et al., 2009). The CXXC domain is present in many chromatin-associated proteins and has a strong preference for unmethylated CpGs (Long et al., 2013). Biochemical and structural analyses indicate that at least the Tet3 CXXC domain can target unmethylated cytosines within both CpG and non-

CpG contexts (Xu et al., 2012). Therefore, unlike other CXXC domains that only bind to unmethylated CpG sites, CXXC domains of Tet proteins are supposed to be more flexible in sequence selectivity and might target the enzyme to its specific genomic site (Zhang et al., 2010) (Xu et al., 2011) (Xu et al., 2012).
A recent crystal structure of the Tet2 catalytic domain in complex with DNA revealed insights into the mechanism of Tet-driven oxidation of 5-mC. Tet2 specifically recognizes CpG dinucleotides, with 5-mC inserted into the catalytic cavity by a base flipping mechanism. Since the methyl group is not involved in the Tet2-DNA interaction, the composition of the catalytic cavity allows Tet2 to accommodate 5-mC derivatives for further oxidation (Hu et al., 2013).

2.4.1.2 Tet mediated active DNA demethylation

Several mechanisms have been proposed that couple oxidation of 5-mC with base excision repair (Fig 2.9). According to the mechanism that is best verified, Tet proteins further oxidize 5-hmC to generate 5-fC or 5-caC. 5-fC and 5-caC are supposed to be excised by the thymine DNA glycosylase (TDG) and replaced by cytosine via base excision repair (BER) (He et al., 2011) (Maiti and Drohat, 2011). Another mechanism, yet less well-proven, proposes the deamination of 5-hmC to 5-hydroxy-uracil (5-hmU) by the cytidine deaminases AID (activation-induced cytidine deaminase) and APOBEC (apolipoprotein B mRNA editing enzyme-catalytic polypeptide). Subsequently, 5-hmU could be removed by SMUG1 (single-strand-selective monofunctional uracil DNA glycosylase 1) or TDG and ultimately replaced by cytosine (Guo et al., 2011) (Fig 2.9). In support of such a mechanism, TDG can excise 5-hmU:G mismatches *in vitro*. However, arguing against a deamination based mechanism, the AID enzyme primarily acts on single-stranded DNA, and APOBEC enzymes display no detectable activity on 5-hmC (Nabel et al., 2012). Other mechanisms of demethylation that also are less well-established, include decarboxylation of 5-caC (Schiesser et al., 2012) and Dnmt mediated removal of the hydroxy-methyl group of 5-hmC (Fig 2.9). Monitoring the conversion of 5-hmC to C in a hydrolysis-TLC assay, recombinant Dnmt3a and Dnmt3b but not Dnmt1 functioned as 5-hmC-dehydroxy-methylases. However, whether Dnmts demethylate in living cells is unknown, and demethylation activity is contradictory to their function as methyltransferases.

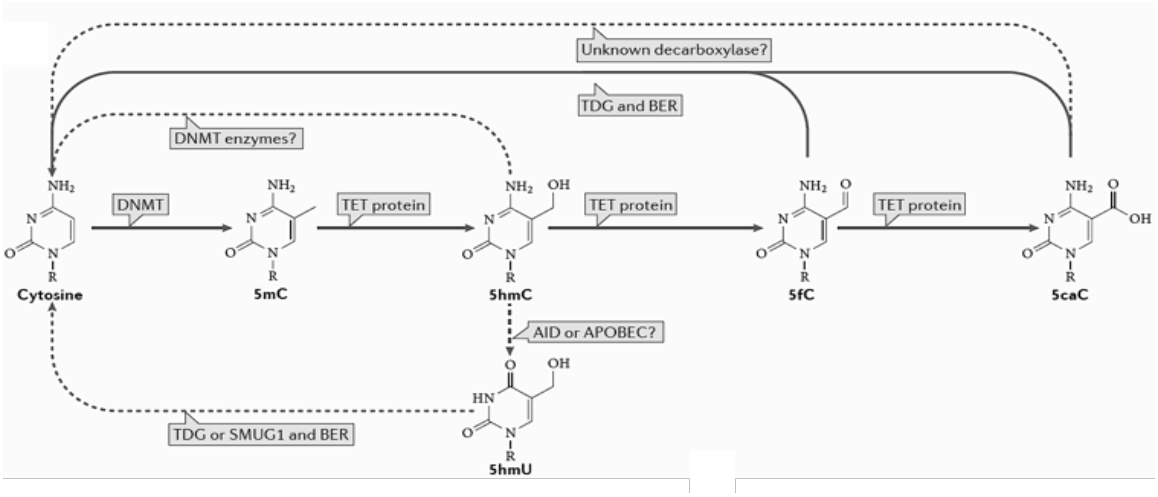

Fig 2.9: Oxidized cytosines and potential active demethylation pathways.
The cytosine modification pathway starts with Dnmts that catalyze methylation at the C5-position of cytosine. Tet proteins subsequently oxidize 5-mC to 5-hmC, 5-fC and 5-caC. 5-fC and 5-caC can be removed by TDG and replaced by cytosine via BER. Deamination of 5-hmC leads to the formation of 5-hmU. 5-hmU:G mismatches are proposed to be excised by SMUG1 or TDG followed by BER. Other direct mechanisms are less well-established, including dehydroxy-methylation by Dnmts or decarboxylation (adapted from Pastor et al., Nature Reviews Mol. Cell. Biol., 2013).

2.4.1.3 Tet mediated passive DNA demethylation

The presence of oxidized 5-mC bases at CpG sites may contribute to passive replication-dependent loss of 5-mC (Fig 2.10). While there are conflicting results whether UHRF1 can specifically recognize hemi-hydroxymethylated CpG sites, Dnmt1 has been shown to methylate hemi-hydroxymethylated CpGs less efficiently than hemi-methylated sites *in vitro* (Frauer et al., 2011) (Hashimoto et al., 2012). Thus, Tet proteins may initiate a two-step demethylation process in dividing cells: The initial oxidation of 5-mC could be subsequently followed by a replication-dependent passive dilution of 5-hmC or potentially 5-fC and 5-caC. This mode of DNA demethylation is distinct from simple passive dilution of 5mC, as such a oxidation-based loss may be effective even in the presence of functional *maintenance* methylation machinery.

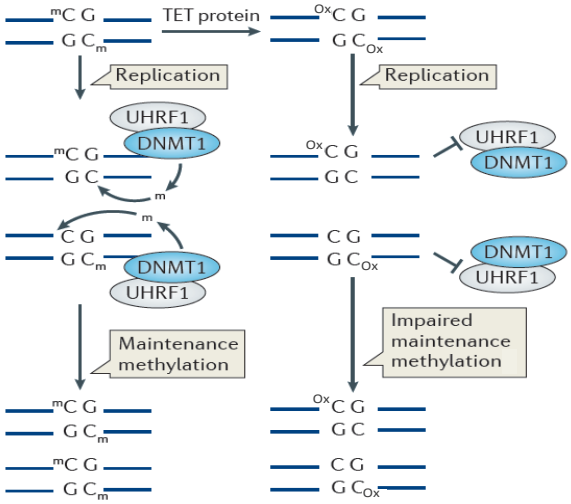

Fig 2.10: Passive DNA demethylation after oxidation by Tet proteins.
A symmetrically methylated CpG sequence is converted during DNA replication into two asymmetrically methylated DNA strands. Hemi-methylated CpG sites are recognized by UHRFI, the obligate partner of the *maintenance* DNA methyltransferase Dnmt1, which restores symmetrical methylation. Tet proteins oxidize methylated CpG sites (^{m}CG) to generate symmetrically oxidized CpGs (^{Ox}CG). During DNA replication, the oxidized cytosines may interfere with *maintenance* methylation by inhibiting UHRF1 binding or Dnmt1 activity. Thus, the CpG sites progressively lose methylation through successive DNA replication cycles (modified and adapted from Pastor et al., Nature Reviews Mol. Cell. Biol., 2013).

2.5. Chromatin remodeling

A fluid state of chromatin is necessary to enable DNA-dependent processes. This dynamic balance between genome packaging and genome access is enabled by the tight interplay between histone and DNA modifying enzymes and ATP-dependent nucleosome remodeling enzymes. Remodeling enzymes utilize the energy of ATP hydrolysis to mobilize nucleosome (Becker and Hörz, 2002) (Fig 2.11), thereby inhibiting or facilitating the access to DNA for regulatory factors.

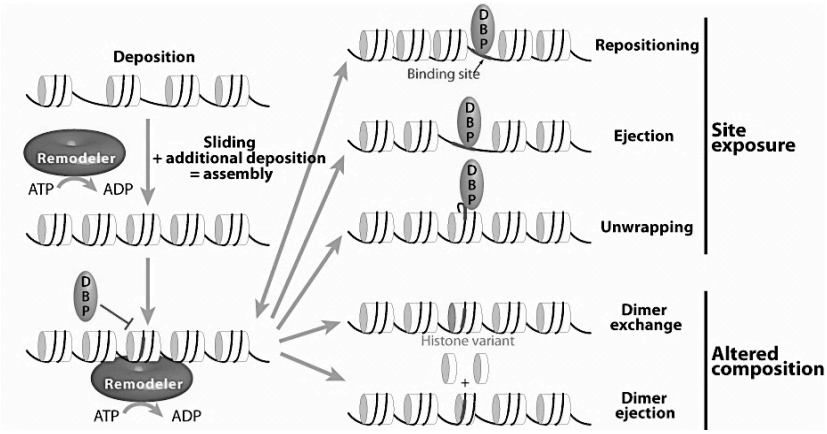

Fig 2.11: Different activities of chromatin remodeling enzymes.
Remodelers can assist in chromatin assembly and regularly space assembled nucleosomes, generating room for additional deposition of histone octamers. Nucleosome sliding (Repositioning) or nucleosome eviction (Ejection) of a nucleosome generates access to DNA for a DNA-binding protein (DBP). The same accounts for local unwrapping of nucleosomal DNA. Remodeling enzymes also catalyze changes in the chromatin composition by exchange of histone dimers (e. g. H2A/H2B dimers) with an alternative dimer containing a histone variant, or by ejection of dimers (modified and adapted from Clapier and Cairns, Annu. Rev. Biochem., 2009).

2.5.1 Remodeler families

Almost all chromatin remodelers are large multi-protein complexes consisting of an ATPase subunit and unique regulatory subunits. The human genome encodes for 32 genes of non-redundant remodeling enyzmes. The combinatorial assembly of several hundred different chromatin remodeling complexes further expands their biological specificity (Rippe et al., 2007) (Ho and Crabtree, 2010).

All ATP-dependent DNA translocases show two recA-like helicase domains in their active center, which as a feature of the helicase-like superfamily 2 (SF2). Based on sequence similarity to the Snf2 protein from *S. cerevisiae*, a number of SF2 members have been grouped into the Snf2 family, and 24 distinct subfamilies of the Snf2 family have been identified (Flaus et al., 2006) (Fig 2.12).

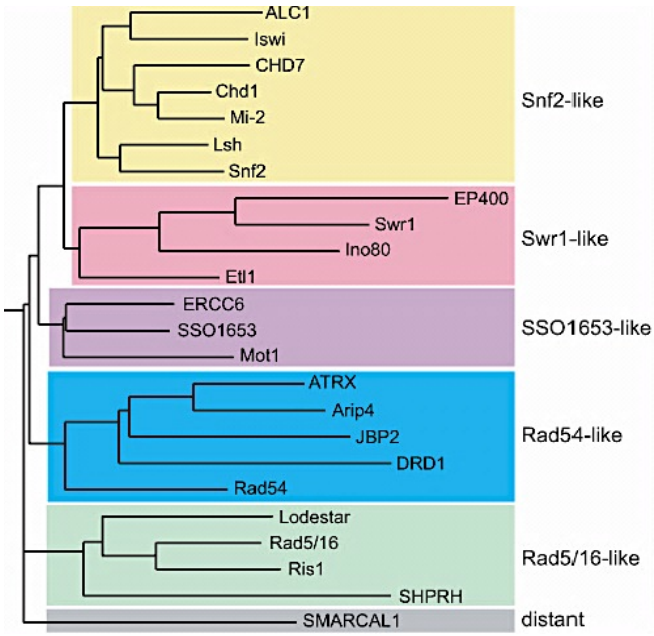

Fig 2.12: Snf2 family of ATPases.
Illustration of the relationship between Snf2 subfamilies based on a HMM (Hidden Markov model) profile for full-length alignments of the helicase regions of the respective enzymes. Grouping into subfamilies is indicated by coloring (modified and adapted from Flaus *et al.*, Nucleic Acid Research, 2006).

Although the Snf2 family is a large group of ATP-dependent enzymes, not all members of this family are DNA tranlocases. For example, Rad54 and Rad51 promote strand pairing, while Mot1 displaces the TATA-binding protein from DNA (Flaus et al., 2006). Nevertheless, a large pool of Snf2 family members displays chromatin remodeling activity and participates in a number of DNA-mediated processes like transcriptional regulation, DNA repair, homologous recombination and chromatin assembly (Lusser and Kadonaga, 2003) (Clapier and Cairns, 2009).

Apart from the classification based on multiple sequence alignments, the remodeling enzymes are also grouped according to domains flanking the catalytic helicase domains. Four major classes of chromatin remodeling enzymes can be distinguished: SWI/SNF, CHD, INO80 and ISWI (Clapier and Cairns, 2009) (Fig 2.13). According to the subfamily classification introduced by Flaus and colleagues (Fig 2.12), the INO80 class is formed by subfamily members of the Swr1-like group, whereas SWI/SNF, CHD and ISWI classes belong to the Snf2-like group (Flaus et al., 2006).

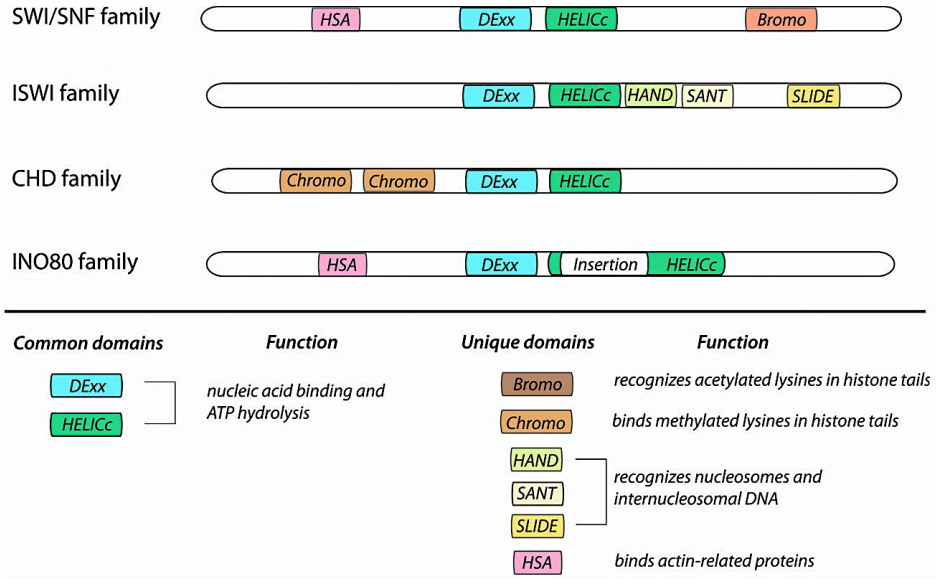

Fig 2.13. Organization of remodeler families defined by their ATPase.
All remodeling enzymes contain a ATPase subunit characterized by shared catalyic helicase domains (Dexx and HELICc) and by unique flanking domains. Remodelers of the SWI/SNF, ISWI, and CHD families each have a distinctive short insertion within the ATPase domain, whereas remodelers of INO80 family contain a long insertion. Each family is further defined by distinct combinations of flanking domains: Bromodomain and HSA (helicase-SANT) domain for the SWI/SNF family, HAND-SANT-SLIDE module for the ISWI family, tandem chromodomains for the CHD family, and HSA domain for the INO80 family (modified and adapted from Manelyte and Längst, Chromatin Remodelers and Their Way of Action, Chromatin Remodelling, ISBN 978-953-51-1087- 3, InTech).

2.5.1.1 SWI/SNF family

The SWI/SNF (SWItching defective/Sucrose Non-Fermenting) family members are defined by the presence of an N-terminally located HSA (helicase-SANT) domain, which is known to recruit actin and actin-related proteins (ARPs), and a C-terminally located bromo domain, that is suggested to bind to the acetylated lysines of histones. In yeast, SWI/SNF complexes are built around the catalytic subunits Swi2/Snf2 or Sth1. Mammalian genomes encode two homologous ATPases of SWI/SNF, BRM (Brahma) and Brg1 (Brahma-Related Gene 1), which are present in large multi-subunit complexes of at least eight proteins, called BAF complexes (Brahma-Associated Factor) (Clapier and Cairns, 2009) (Manelyte and Längst, 2013). Human BAF and PBAF complexes are distinguished by the presence of unique

subunits: BAF180, BAF200 and BRD7 for PBAF and BAF250a for BAF (Wilson and Roberts, 2011). These BAF complexes play an important roles during development (Ho and Crabtree, 2010) and are essential for maintaining pluripotency and self-renewal in mouse ESCs (Yan et al., 2008) (Ho et al., 2009).

2.5.1.2 ISWI family

The ISWI (Imitation SWItch) family of ATPases can be regarded as the subfamily that is most closely related to the SWI/SNF ATPases (Gangaraju and Bartholomew, 2007). ISWI members contain three characteristic binding domains at the C-terminal end, the HAND domain, the SANT (SWI3, ADA2, N-CoR and TFIIIB) domain, and the positively charged SLIDE domain (SANT-Like Domain). Together, they form a nucleosome recognition module (HSS module) that binds to DNA and unmodified tails of histone H4 (Clapier and Cairns, 2009). Indeed, the H4 tail was shown to be required for efficient ATPase and remodeling activity of ISWI (Clapier et al., 2001) (Georgel et al., 1997). However, subsequent studies revealed that the islolated ATPase domain of *D. melanogaster* ISWI is sufficient for nucleosome remodeling, suggesting that the HSS module serves to increase the affinity to nucleosomes, enhances remodeling efficiency and directs repositioning (Mueller-Planitz et al., 2012). Furthermore, Clapier and Cairns identified two regulatory domains, named NegC and AutoN, exerting inhibitory effects on ISWI ATPase activity (Clapier and Cairns, 2012). ISWI ATPase subunits show nucleosome spacing activity *in vitro*, facilitating the assembly and regular distribution of nucleosomes in arrays. Furthermore, the nucleosome mobilizing activity of ISWI assists DNA-binding factors to gain access to target sequences within chromatin (Langst et al., 1999) (Whitehouse et al., 2003).
D. melanogaster ISWI is known to be present in several chromatin remodeling complexes such as NURF, CHRAC and ACF (Clapier and Cairns, 2009), and homologs to *D. melanogaster* ISWI have been identified in numerous other organisms: Isw1 and Isw2 in yeast (Mellor and Morillon, 2004), xISWI in *Xenopus* (Guschin et al., 2000), and Snf2H and Snf2L in mammals. Snf2H and Snf2L can act on their own or in combination with one or more additional subunits such as Tip5, Rsf1 or WSTF to form the complexes NoRC, RSF and WICH, respectively (Strohner et al., 2001) (Poot et al., 2000) (LeRoy et al., 2000). Dependent on the auxilary subunits of the respective complex, these complexes are involved in a variety of functions, including activation and repression of transcription initation and elongation as well as replication and chromatin assembly (Clapier and Cairns, 2009).

2.5.1.3 CHD family

The CHD (Chromodomain, Helicase, DNA-binding) family comprising Chd1, Chd3, Chd4 and Chd7 (Flaus et al., 2006) is characterized by the presence of two chromodomains that mediate binding to methylated lysine residues of histone tails, but are also able to interact with DNA and RNA (Brehm et al., 2004). Additionally to the chromodomains, distinct CHD remodelers can harbour specific regulatory domains. For instance, Chd1 contains a SANT-SLIDE-like fold, which was shown to be required for the remodeling activity of Chd1 (Ryan et al., 2011), whereas Chd3 and Chd4 differ from other CHD members by the possession of PHD (plant homeodomain) domains that regulate ATPase and remodeling activity (Watson et al., 2012). Chd1 ATPase from *D. melanogaster* is active as monomeric protein, yet has the ability to associate with additional regulatory subunits (Lusser et al., 2005). Like ISWI remodelers, Chd1 shows chromatin spacing and assembly activity *in vitro*, but does not incorporate the linker histone H1 into nucleosomal arrays. Furthermore, it generates a shorter nucleosome repeat length compared to other remodeling factors (Lusser et al., 2005). In mouse ESCs, Chd1 is essential to keep chromatin in an hyperdynamic euchromatic state, therefore maintaining pluripotency (Gaspar-Maia et al., 2009). In contrast, complexes that incorporate Chd3 and Chd4, such as NuRD, act as repressors. The Methyl-CpG-Binding Domain (MBD) within the NuRD complex links DNA methylation to histone deacetylase activity to mediate gene silencing (Flaus et al., 2006).

2.5.1.4 INO80 family

The yeast INO80 enzyme is the archetype ATPase of the INO80 family (Ebbert et al., 1999). Remodeling ATPases of this group are characterized by the relatively large insertion in the ATPase domain. This unique module retains ATPase activity and acts as a scaffold for the association with the RuvB-like proteins Rvb1 and Rvb2. RuvB is a bacterial ATP-dependent helicase that forms a double hexamer around Holliday junctions to promote their migration during homologous recombination (West, 1997). Since the purified INO80 complex is active as an ATP-dependent helicase, INO80 and possibly also SWR1 may represent eukaryotic homologous of RuvB. The helicase activity in combination with the nucleosome remodeling capacity suggests that the INO80 complex participates in multiple DNA repair pathways by regulating the accessibility of DNA repair proteins to double-strand breaks (Shen et al., 2000) (Bao and Shen, 2007). The SWR1 complex consists of 13 further subunits, including actin, ARP4, Rvb1 and Rvb2, that are also present in the yeast INO80 complex. In humans, SRCAP (Snf2-Related CREB-binding Protein Activator Protein) is the homolog to yeast SWR1. An active complex with SRCAP as motor protein catalyzes the exchange of H2A/H2B dimers with variant H2A.Z/H2B, thereby integrating this alternative form into chromatin (Flaus et al., 2006) (Bao and Shen, 2007).

2.5.2 Mechanism of nucleosome remodeling

To understand how the distinct remodeling complexes move nucleosomes, the detailed steps of the translocation reaction had been considered, essentially proposing two models. The ‘twist diffusion’ model suggests the rotation of DNA in 1 bp intervals over the surface of the histone octamer, implying that the distortion of a single base pair is continuously propagated through the nucleosome. The ‘twist diffusion’ model is supported by nucleosomal crystal structures exhibiting this single base pair ‘twist defect’ (Davey et al., 2002) (Luger et al., 1997). However, several studies didn’t confirm such a translocation model (Aoyagi et al., 2003) (Längst and Becker, 2004). The second proposed model, the ‘loop recapture’ model, is based on the conformational change induced by the catalytic translocase domain, wich results in a relative change of the distance of both nucleosome-binding domains. This coordinated movement of the DNA-binding domain and the translocase domain disrupts local histone-DNA contacts and forms a small DNA loop. The DNA loop propagates over the surface of the histone octamer by releasing and rebinding adjacent sequences on the protein surface. This stepwise disruption and reformation of histone-DNA contacts is driven by the mechanical stress introduced by the initial conformational changes and does not cost further energy. When the loop meets the distal nucleosomal boundary, it resolves when detaching from the histone octamer surface. As a consequence, DNA has moved around the histone octamer surface. From this point on, a new round of loop initiation and propagation can start (Strohner et al., 2005) (Clapier and Cairns, 2009) (Fig 2.14).

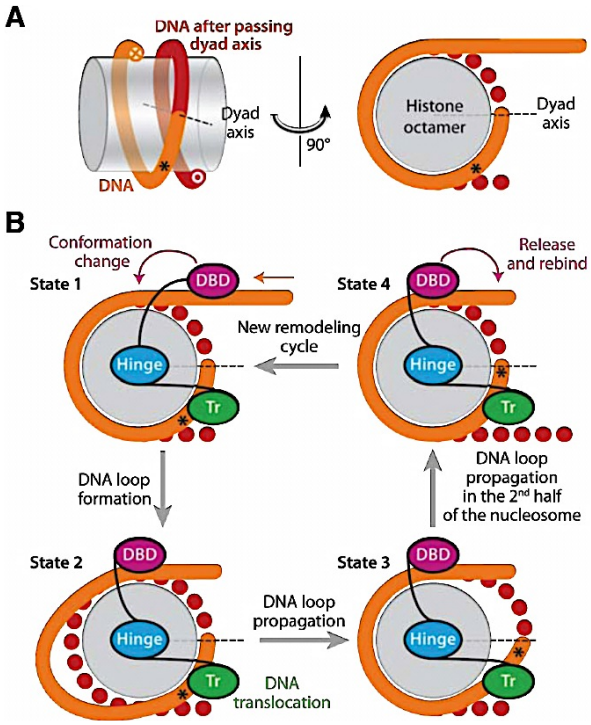

Fig 2.14: DNA movement around the histone octamer during the remodeling reaction.
(A) DNA (red/orange) is wrapped in two helical turns around the disc-shaped histone core (grey). The asterisks (*) marks a reference point to illustrate movement of the DNA. **(B)** According to the „loop recapture“ model, the translocation reaction is initiated (State 1) by binding of the DNA-Binding Domain (DBD: pink) and the catalytical translocase domain (Tr: green) to the nucleosomal DNA. (State 2) A conformational change induced by the translocase domain leads to local disruption of DNA-histone contacts and formation of a DNA loop. (State 3) The remodeling enzyme stays fixed to the substrate, therefore the loop propagates into the nucleosome. (State 4) After the loop has resolved and the conformation of the remodeler is reset, the system can initiate a new remodeling cycle (adapted from Clapier and Cairns, Annu. Rev. Biochem., 2009).

The currently favored ‘loop recapture’ model, explaining the mechanism of translocation activity of remodeling ATPases, is strengthened by biochemical and single-molecule studies (Strohner et al., 2005) (Liu et al., 2011) (Zhang et al., 2006).

After a successful remodeling reaction, different endpoints are possible. For ACF and Chd1, it was shown that these machines dissociate from the nucleosome after remodeling due to a reduced affinity to the end-products of the translocation reaction, proposing the so-called ‘release’ model. The enzymes are released and can again adopt an active conformation to start a new remodeling reaction. Theoretically, an inverse mechanism is also possible, called ‘arrest’ model, where the remodeling reaction is driven to end-product formation by an increased affinity to the remodeled nucleosome. In this case, the remodeling complex stays bound to the nucleosome, resembling sort of a structural component of chromatin (Rippe et al., 2007).

2.5.3 Association of non-coding RNAs with chromatin remodelers

98% of the cellular transcription results in non-coding RNAs (ncRNAs). Initially being considered as non-functional junk, there is increasing evidence that ncRNAs regulate gene activity by their association with chromatin modifiers and remodeling enzymes, and thereby affect chromatin organization. In general, non-coding RNAs can be classified according to their length. Small non-coding RNAs such as microRNAs, small-interfering RNAs (siRNAs) and Piwi-interacting RNAs (piRNAs) are definded by sizes less than 200 nucleotides. Long non-coding RNAs (lncRNAs) are non-protein coding transcripts with sizes longer than 200 nucleotides (Pang et al., 2006).

One of the best known examples of lncRNA mediated chromatin regulation occurs during X-chromosome dosage compensation in mammals. The lncRNA Xist is expressed from one of the two X-chromosomes in female cells and results in altering chromatin structure of the X-chromosome where most genes are transcriptionally silenced (Wutz, 2011). Xist physically associates with the histone methyltransferase Polycomb repressive complex 2 (PRC2), localizing H3K27me3 to the inactive X-chromosome (Zhao et al., 2008).

Notably, the chromatin remodeling factor ATRX was found to direct the binding of PRC2 to Xist (Sarma et al., 2014).

Recently it was shown that the lncRNA Evf2 co-localizes with the chromatin remodeler Brg1 in a complex with the transcriptional activator DLX1 in murine embryonic forebrains and inhibits Brg1 ATPase- and chromatin remodeling activity *in vitro* (Cajigas et al., 2015).

Others reported that the cardiac-specific lncRNA Mhrt prevents Brg1 from recognizing its genomic DNA targets, thus inhibiting chromatin targeting and gene regulation by Brg1 (Han et al., 2014). A ncRNA termed pRNA (promoter-associated RNA) appears to functionally interact with NoRC, regulating the enzyme by switching off its ATPase activity (Manelyte et al., 2014). In contrast, studies on *D. melanogaster* ISWI revealed ATPase activating effects by a ncRNA (Onorati et al., 2011). Interestingly, both studies indicate rather competing than synergistic effects of nucleosomes and RNA on the ATPase activity of the respective remodeler (Manelyte et al., 2014) (Onorati et al., 2011).

In addition, it is of note that RIP analyses showed the interaction of Lsh with the lncRNA HOTAIR in human adenocarcinoma cell lines (Wang et al., 2015).

2.6 DNA methylation in the context of chromatin

2.6.1 *In vitro* studies on DNA methylation in chromatin

DNA methyltransferases have been extensively studied with regard to their enzymatic properties (Hermann et al., 2004b) (Bacolla et al., 1999) (Pradhan et al., 1999) (Okano et al., 1998) (Gowher and Jeltsch, 2001) (Suetake et al., 2003). All these results were obtained by *in vitro* studies using naked DNA as substrate. However, the DNA of eukaryotic cells is packaged into a compact nucleoprotein complex with nucleosomes as its elementary structure (Woodcock and Horowitz, 1995), and several studies on DNA methylation in the context of chromatin reported that DNA methylation is at least restricted within the chromatin environment. Okuwaki and Verreault found that Dnmt1 was intrinsically capable to methylate DNA within the nucleosome core. Yet, this activity was slightly inhibited in comparison to Dnmt1 activity towards naked DNA, and was highly dependent on the DNA sequence (Okuwaki and Verreault, 2004). On the contrary, Gowher and colleagues found comparable methylation efficiencies towards naked and nucleosomal templates (147bp in size) for Dnmt1 and Dnmt3a, irrespective of the sequence (Gowher et al., 2005). Another study used a 208 bp sequence that is a well-characterized nucleosome positioning sequence (5S rDNA from sea urchin) (Robertson et al., 2004). The catalytic efficiency of Dnmt1 and Dnmt3a to the mononucleosomal substrate decreased 8-fold and 17-fold, respectively, in comparison to their activities on the naked DNA. Interestingly, the ability of both enzymes to bind the substrate was not significantly altered by the chromatin structure (Robertson et al., 2004). Recently, it was reported that Dnmt1 binds to the entry/exit sites of the nucleosome and efficiently methylates DNA in the linker regions, whereas DNA protected by the nucleosome is almost free of DNA methylation (Schrader et al., 2015). Similar results were obtained by the analysis of nucleosomal DNA methylation by the *de novo* methyltransferases Dnmt3a and Dnmt3b, showing that compared to linker DNA, nucleosomal DNA is largely devoid of CpG methylation (Felle et al., 2011a).

Others described distinct roles for Dnmt3a and Dnmt3b with respect to the methylation of DNA and nucleosomes. Whereas the methylation activity of Dnmt3b showed low but significant methylation within the nucleosome core region (Takeshima et al., 2006), Dnmt3a preferentially methylated linker DNA, which was impaired by the binding of histone H1 (Takeshima et al., 2008).

2.6.2 Interplay between chromatin remodeling enzymes and DNA methylation

In this context, it is important to note that in addition to the intrinsic properties of the DNA methyltransferases also components of ATP-dependent chromatin remodeling factors seem to have an effect on the methylation in chromatin, providing evidence for a tight interplay between chromatin remodeling and DNA methylation.
For instance, Dnmt3a directly interacts with components of the Brg1 complex in mouse lymphosarcoma cells. In these cells, the cooperation of the two proteins is involved in the repression of the metallothionein promoter. In this regard, the catalytic function of Dnmt3a was dispensable for repression, whereas Brg1 activity was crucial for promoter silencing (Datta et al., 2005). The nucleolar remodeling factor NoRC plays a role in promoting the methylation and silencing at the rDNA gene locus. NoRC interacts with Dnmt1 and Dnmt3a *in vivo* and targets the DNA methyltransferases to the rDNA to repress rDNA transcription (Santoro et al., 2002). Robertson and colleagues demonstrated direct association between Dnmt1 and Snf2H by co-immunoprecipitation, and immunofluorescence microscopy revealed that a significant fraction of both enzymes co-localized in heterochromatic regions of HeLa cells. Furthermore, the addition of recombinant Snf2H enhanced the binding affinity of Dnmt1 to nucleosomes by 3-fold in an ATP-independent manner *in vitro*, but had no effect on the enzymatic activity of Dnmt1 on mononucleosomal substrates (Robertson et al., 2004). Others could show co-localization of Dnmt3a as well as Dnmt3b with human Snf2H at heterochromatic regions of HeLa cells (Geiman et al., 2004). In addition, it was demonstrated that human Snf2H stimulates *de novo* DNA methylation by the remodeling of nucleosomes in an ATP-dependent manner (Felle et al., 2011a). A recent study on Dnmt1 activity and its binding characteristics showed that Dnmt1 interacts with specific chromatin remodeling enzymes to enable methylation of hm DNA in chromatin (Schrader et al., 2015), supporting the idea that ATP-dependent chromatin remodeling is required to render nucleosomal DNA that otherwise would be refractory to DNA modifications.
Mutations of genes encoding chromatin remodeling factors further indicate co-actions of chromatin remodeling and DNA methylation. Mutations in the *ATRX* gene, that belongs to the Rad54 subfamily (Flaus et al., 2006), cause a human genetic disease called X-linked α-thalassemia mental retardation (ATRX) syndrome. Methylation defects in ATRX patients are restricted to selected regions of the genome such as rDNA repeats, and are characterized by both hypo- and hypermethylation (Gibbons et al., 2000). Mutations in *DDM1* lead to a 70 % decrease of whole genomic 5-methylcytosine (Martienssen and Henikoff, 1999). Similar results were obtained with the mammalian homolog of *DDM1, LSH* (Jeddeloh et al., 1999).

2.7 The Snf2 family member Lymphoid-specific helicase

The *LSH* gene (Lymphoid-specific helicase, Hells, PASG, SMARCA6) encodes a DEAD/H helicase that belongs to the Snf2 family of helicase-like proteins (Flaus et al., 2006). Lsh showed highest expression in T-lymphocytes in fetal mouse thymus (Jarvis et al., 1996). However, Lsh is generally expressed in proliferating cells (Geiman et al., 2001).
Later, it was found that the transcriptin factor FOXM1 acts as a central regulator of Lsh expression (Waseem et al., 2010).
With respect to its biological functions, there is evidence that, depending on cell type, Lsh may both promote and prevent carcinogenesis (Mjelle et al., 2015). Overexpression of Lsh is suggested to contribute to tumor progression in prostate cancer, which may in part be explained by its function as a co-activator for the transcription factor E2F3, whose amplified expression is linked with tumorigenesis (Eyss et al., 2011). Lsh silences expression of the CDK4-inhibitor $p16^{INK4}$ by recruiting HDACs to the *p16INK4* gene promoter, thereby increasing cell proliferation and delaying senescence (Zhou et al., 2009) (Sun, 2004). A recent report suggests that Lsh is a critical component of the p63 pathway to bypass senescence in skin cancer cells (Keyes et al., 2011). In contrast, deficiency of Lsh causes erythroleukemia in mice (Fan et al., 2008), and deletions are associated with acute myeloblastic and acute myelogenic leukemia in humans (Lee et al., 2000).
Lsh contributes to DNA methylation and also has a role in histone deacetylation and methylation of histone H3K4, which is why Lsh is considered to be an important player in the establishment of heterochromatin (Zhu et al., 2006) (Zhou et al., 2009) (Yan et al., 2003b) (Dennis, 2001), especially during gametogenesis and embryonic development. Lsh deficiency results in perturbed heterochromatin structure, abnormal mitosis and de-repression of transcription (Huang, 2004) (Yan et al., 2003b). Most strikingly, Lsh deficient mice died soon after birth with reduced lymphoid numbers, renal lesions with signs of necrosis, and a 20% weight reduction at birth. Analyses of genomic DNA methylation patterns from fibroblasts, brain, liver, intestine, heart and lung, as well as thymus obtained from Lsh deficient mice exhibited 50–60 % reductions in DNA methylation levels, mainly affecting repetitive elements such as major satellite sequences, IAPs, SINEs and LINEs, or telomeric sequences (Dennis, 2001) (Geiman et al., 2001). However, Lsh globally regulates DNA methylation, and reduced DNA methylation levels have also been observed at unique sequences like stem cell genes (*OCT4, NANOG, SOX2*) (Xi et al., 2009), single genomic imprinting control regions (*CDKN1c*) (Fan et al., 2005), or *HOX* genes (Xi et al., 2007). Recently published data, generated by applying more advanced technologies like whole-genome bisulfite sequencing, confirmed global loss of CpG methylation in the absence of Lsh and the critical role of Lsh for the repression of repeat elements. For such studies,

murine embryonic fibroblasts (MEFs) derived from Lsh wild-type (WT) and Lsh knock-out (KO) mice had been used to basically compare differences in CpG methylation levels between WT and KO MEFs (Tao et al., 2011) (Yu et al., 2014). In addition, these results indicate that Lsh is important for the establishment of CpG methylation at a nuclear compartment that is in part defined by so-called Lamin B1 attachment domains (LADs). More than 60% of repeat elements showing DNA methylation reduction in Lsh deficient MEFs were located in LADs (Yu et al., 2014).

Other studies using Lsh knock-out mice strains revealed reduced proliferation of spermatogonia and arrest of germ cell differentiation, suggesting an essential role for Lsh during male meiosis (Zeng et al., 2011). The knock-out of Lsh during oogenesis induced a similar phenotype, including arrest of oocyte differentation and abnormally low levels of 5-mC on major and minor satellite sequences (La Fuente et al., 2006). As satellite sequences are the main components of pericentromeric DNA, these results support the idea that Lsh plays a role in the formation of pericentromeric heterochromatin, which is substantiated by fluorescence microscopy studies and western blot analyses, showing localization of Lsh to pericentromeric heterochromatin (Yan et al., 2003b) (Lungu et al., 2015). Furthermore, several ChIP data provide evidence that Lsh is directly recruited to repetitive sites in the genome (Huang, 2004), indicating that Lsh guards preferentially genomic regions embedded in repressive chromatin.

Lsh has been suggested to be dispensable for *maintenance* DNA methylation but primarily participate in *de novo* DNA methylation (Yan et al., 2003a) (Zhu et al., 2006). In this regard, it was shown that acquisition of DNA methylation of non-methylated episomes required Lsh, and that Lsh interacts specifically with the *de novo* DNA methyltransferases Dnmt3a and Dnmt3b (Zhu et al., 2006). In particular, Lsh was demonstrated to recruit Dnmt3b to *HOX* genes and to regulate Dnmt3b-dependent DNA methylation as well as polycomb repressive complex (PRC) mediated histone modifications to control silencing of *HOX* genes during embryonic development (Xi et al., 2007) (Tao et al., 2010). However, others reported direct interactions between Lsh and Dnmt1 and suggest Lsh-dependent recruitment of Dnmt1 to chromatin (Dunican et al., 2015). Thus, Lsh may be required for both *de novo* and *maintenance* DNA methylation. Indeed, according to Myant and Stancheva, Lsh cooperates with Dnmt1 and Dnmt3b. In addition, they showed by *in vitro* pull downs association of Lsh with HDAC1 and HDAC2 (Fig 2.15).

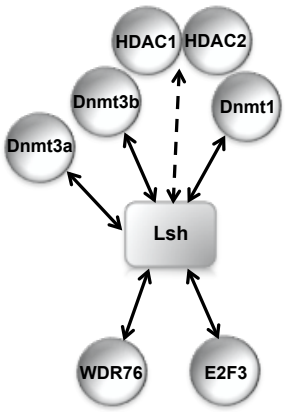

Fig 2.15: Protein interaction network of Lsh.
Interaction partners of Lsh identified by literature search. Co-IPs and pull down assays revealed direct association of Lsh with Dnmt3b (Myant and Stancheva, 2007) (Zhu et al., 2006), Dnmt3a (Zhu et al., 2006) and Dnmt1 (Myant and Stancheva, 2007) (Dunican et al., 2015). Lsh may also cooperate, yet rather indirectly, with HDAC1 and 2 (Zhou et al., 2009) (Myant and Stancheva, 2007), probably mediated by Dnmts. Furthermore, association of Lsh with the transcription factor E2F3 is reported (Eyss et al., 2011). Recently, WDR76 was found to interact with Lsh. WDR76 is a 5-hmC specific reader (Spruijt et al., 2013) and has been proposed to keep genome stability (Gallina et al., 2015).

Yet, transcriptional repression by Lsh and its interactions with HDACs were lost in Dnmt1- and Dnmt3b-knock-out cells (Myant and Stancheva, 2007). Therefore, Lsh may rather indirectly interact with HDACs, probably via Dnmts, which is supported by interaction studies of Zhou and colleagues (Zhou et al., 2009). Interestingly, native Lsh was not detected in a large protein complex. Hence, it was proposed that Lsh transiently interacts with chromatin-associated proteins (Myant and Stancheva, 2007) and could serve as a recruiting factor for Dnmts and HDACs to establish transcriptionally repressive chromatin.
Apart from its crucial role in the regulation of DNA methylation during development, Lsh may have additional functions. Lsh was found to contribute to DNA double-strand break repair by promoting phosphorylation of H2AX to γH2AX (Burrage et al., 2013). Furthermore, Lsh was identified as a specific reader for 5-hmC in neural progenitor cells (Spruijt et al., 2013), emphasizing the function of 5-hmC as a landmark in the epigenetic landscape that might recruit specific readers to direct dynamic remodeling and organization of chromatin.
The biological importance of Lsh mediating gene silencing is well documented.
However, the molecular processes of how Lsh is mechanistically involved in the formation of transcriptionally repressive chromatin have not been addressed.
Lsh is classified into the Snf2-like group comprising enzymes like *D.melanogaster* ISWI, mouse Chd1 and human Brg1, which are the catalytic core subunits of well-known ATP-dependent chromatin remodeling complexes. The respective classification is based on alignments of the helicase regions comprising the Dexx and the HELICc domains. Dexx and HELICc represent essential domains of Snf2-like ATPases in terms of ATP hydrolysis and the coupling of the energy derived from ATP hydrolysis to the mobilization of nucleosomes (Flaus et al., 2006) (Clapier and Cairns, 2009). Apart from its nuclear localization sequence

(NLS) and in part the coiled-coil domain that could mediate protein-protein interactions (Hu, 2000), these two domains are the only domains of Lsh of assigned functions (Fig 2.16).

Fig 2.16: Schematic representation and assigned domains of Lsh.
Lsh comprises 838 aa with a coiled-coil domain at the N-terminus. The nuclear localization domain (NLS) is positioned adjacent to the coiled-coil domain. The Snf2 family specific helicase domains (Dexx and HELICc) are seperated by about 200 amino acids. Relative positions and domain length are indicated by numbers in brackets indicating first and last amino acid of the respective domain.

Consequently, due to its conserved ATPase domain and its chromatin-specific functions, it is generally believed that Lsh moves nucleosomes by using ATP as energy source, thereby facilitating DNA methyltransferases access to DNA and allow DNA methylation within nucleosomes (Fig 2.17).

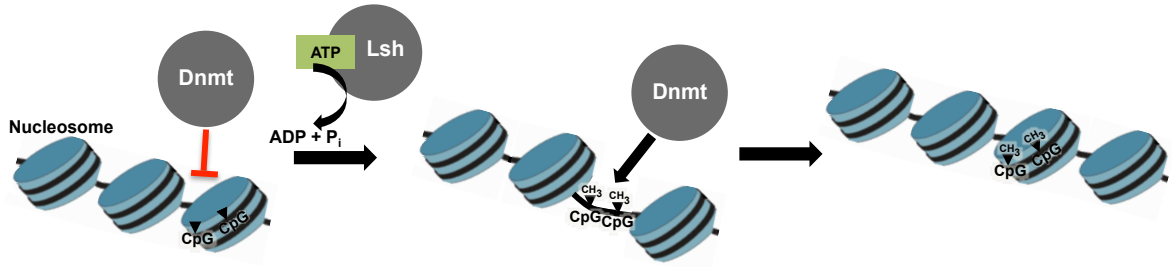

Fig 2.17: Hypothetical model of how Lsh facilitates DNA methylation.
Dnmts are unable to recognize and modify DNA in the nucleosomal context. Lsh moves nucleosomes in an ATP-dependent fashion, which enables a Dnmt to access and methylate its target sites on the DNA (as presented by the methylation of CpG sites). Eventually, the concerted action of Lsh and Dnmts contributes to the establishment of heterochromatin. Triangles illustrate CpG sites.

Eventually, the concerted action of Lsh and Dnmts might result in gene silencing, and is most probably accompanied by histone deacetylation and the setting of repressive histone marks such as H3K9 and H3K27 di- and trimethlyation, in order to complete the establishment of heterochromatin. At least, it is reported that Lsh mediates gene silencing not only by cooperating with Dnmts and HDACs but also by promoting the recruitment of histone methyltransferase complexes such as G9a/GLP to specific loci during lineage commitment and cell differentiation (Myant et al., 2011).
Since nucleosomes represent a repressive structure for DNA-dependent processes, altering chromatin structure by the mobilization of nucleosomes in order to regulate DNA accessibility appears to be an important process for the successive methylation of DNA (Geiman et al., 2004) (Felle et al., 2011a) (Schrader et al., 2015) (see also chapter 2.6). Indeed, recently published data provide evidence for the connection between DNA methylation and the

proposed chromatin remodeling activity of Lsh. Ren and colleagues re-expressed an ATPase deficient version of Lsh in ESCs derived from Lsh knock-out mice and observed reduced CpG methylation levels at repeat elements if compared to wild-type (Ren et al., 2015), indicating the requirement of a functional Lsh ATPase for efficient CpG methylation.

As there is still neither proof that Lsh opens up chromatin and allows access to Dnmts, nor have the molecular mechanisms of this process been addressed so far, the aim of the presented work is the molecular analysis and description of the chromatin remodeling and ATPase function of Lsh and its interaction with nucleosomes *in vitro*

3 Results

3.1 Protein sequence motifs favoring the proposed function of Lsh as a chromatin remodeling enzyme

In order to gain first insights into the suggested mechanistic properties of Lsh, pairwise protein sequence alignments with human Lsh as query and one prominent human member of each subfamily of the Snf2-like group (Flaus et al., 2006) as target were performed with EMBOSS Needle using EMBOSS Needle's default parameters (Rice et al., 2000). Apart from its coiled-coil domain, the DExx domain and the HELICc domain of Lsh are the only assigned ones (http://www.ncbi.nlm.nih.gov/Structure/cdd/wrpsb.cgi). Together, DExx and HELICc domains share about 35% to 40% sequence identity with DExx and HELICc domains of human members of the Snf2-like group. In contrast, the overall protein sequence identity of full-length Lsh with the targets' full-length sequences ranges from 10% to 23%, depending on the protein Lsh was compared to (Table 3.1).

Pairwise protein sequence alignments of human Lsh and human members of the Snf2-like group of the Snf2 superfamily		
	Lsh (human) – hSnf2H (ISWI subfamily)	
	full-length	DExx/HELICc domain
Sequence identity (%)	23,08	40,19
	Lsh (human) - Chd1 (CHD1 subfamily)	
	full-length	DExx/HELICc domain
Sequence identity (%)	16,21	35,58
	Lsh (human) – Chd8 (CHD7 subfamily)	
	full-length	DExx/HELICc domain
Sequence identity (%)	10,01	35,55
	Lsh (human) – Brg1 (SWI/SNF subfamily)	
	full-length	DExx/HELICc domain
Sequence identity (%)	15,74	36,62
	Lsh – Chd4 (Mi-2 subfamily)	
	full-length	DExx/HELICc domain
Sequence identity (%)	12,5	35,57
	Lsh (human) – Chd1L (ALC1 subfamily)	
	full-length	DExx/HELICc domain
Sequence identity (%)	19,69	36,89

Table 3.1: Pairwise protein sequence alignments of human Lsh and human members of the Snf2-like group of the Snf2 superfamily.
Pairwise protein sequence alignments were performed with EMBOSS Needle. Lsh was used as query, and one prominent human member of each subfamily of the Snf2-like group as target. The table shows the percentage of sequence identity of full-length Lsh with the target's full-length protein sequence and the percentage of sequence identity of combined DExx and HELICc domains of Lsh with the target's combined DExx and HELICc domains. For analysis, the program's default parameters were used.

This indicates that the relationship of Lsh with its members of the Snf2-like group is mainly referred to the DExx domain and the HELICc domain but not to other regions of Lsh. In fact, it is not known whether Lsh contains so called interaction or reader domains that are typical for catalytic ATPase subunits of chromatin remodeling complexes.
Within or close to the DExx and HELICc domains, the Snf2 family shares eight SF2 superfamily characteristic motifs known as helicase motifs I, Ia, II, III, IV, V and VI, and Q motif. In addition, Snf2 family proteins share conserved blocks distinguishing them from other members of the SF2 superfamily (Flaus et al., 2006). Focusing on human Lsh, a bioinformatic analysis of the sequences of DExx and HELICc domains was done by perfoming multiple protein sequence alignments (MSA) with MSAProbs using the program's default parameters (Liu et al., 2010). The amino acid sequence of full-length human Lsh was used as query and was compared to the full-length protein sequences of all human representatives of the Snf2-like group. The helicase motifs I, Ia, II and III are present in the DExx domain, while motifs IV, V and VI are present in the HELICc domain. According to Flaus and colleagues, the Snf2-specific blocks are termed A to N. To be mentioned, the conserved blocks B and C overlap with previously described Snf2-specific sequence motifs (Thomä et al., 2005). Lsh shares all annotated motifs with all human members of the other subfamilies of the Snf2-like group (Fig 3.1).

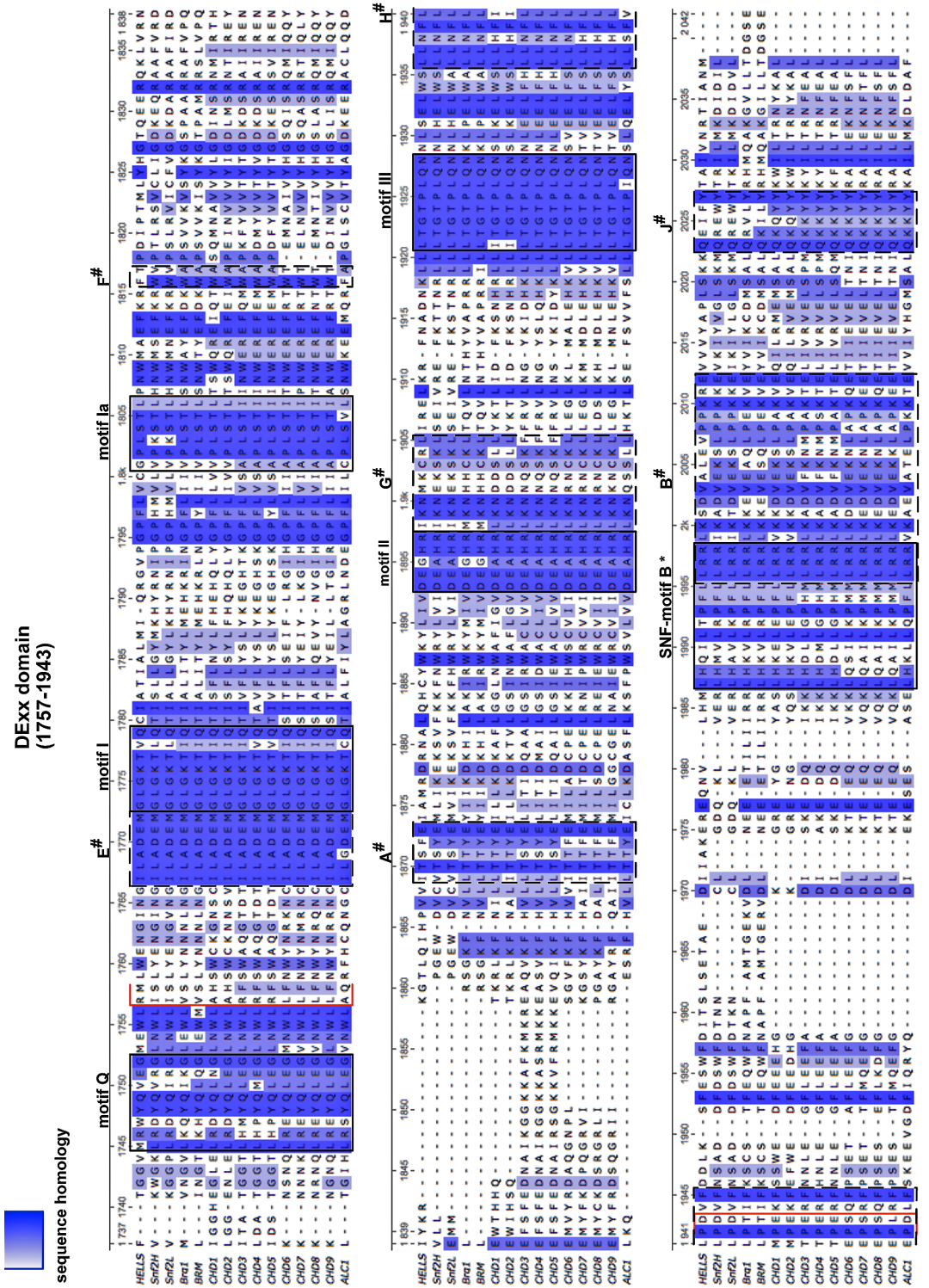
DExx domain
(1757-1943)
sequence homology
motif Q
motif I
motif Ia
motif II
motif III
SNF-motif B *
HELLS
Snf2H
Snf2L
Brg1
BRM
CHD1
CHD2
CHD3
CHD4
CHD5
CHD6
CHD7
CHD8
CHD9
ALC1

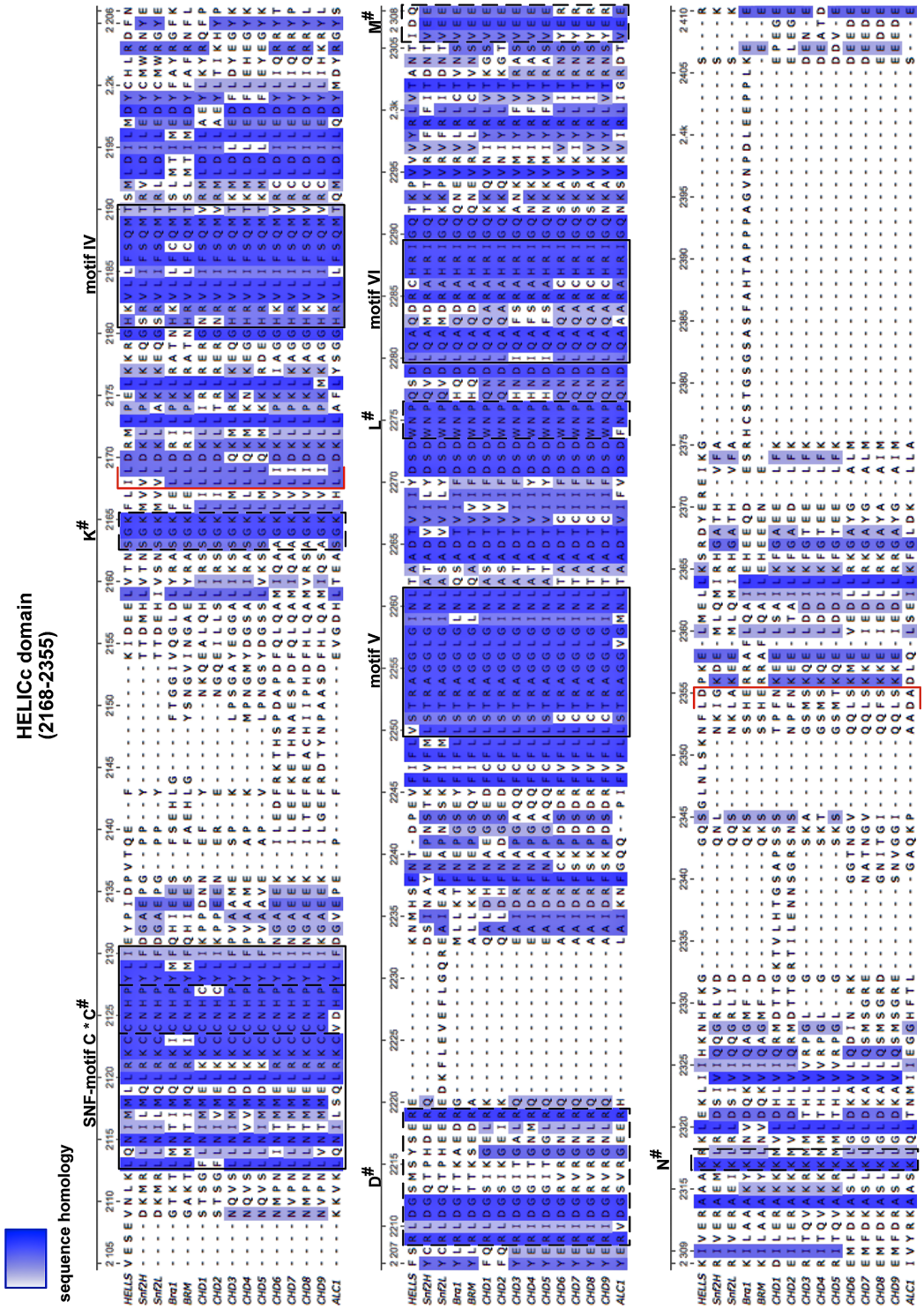

Fig 3.1: Multiple sequence alignments of regions encompassing DExx- and HELICc domains of all human representatives of the Snf2-like group.
The protein sequences of all human members of the Snf2-like group have been aligned to each other with MSAProbs and were visualized with the UGENE software tool. Lsh (referred to as Hells) is shown in the top line of the alignment. The degree of sequence similarity is color coded (background in white: no similarity, background in brilliant blue: completely identical). The DExx domain and the HELICc domains are surrounded by red brackets. Helicase motifs (motif I, Ia, II, III, IV, V and VI, and motif Q) are shown in rectangles (solid lines). Structural motifs conserved in Snf2 subfamilies according to Flaus and colleagues (Flaus et al., 2006) ($E^{\#}$, $F^{\#}$, $A^{\#}$, $G^{\#}$, $H^{\#}$, $B^{\#}$, $J^{\#}$, $C^{\#}$, $K^{\#}$, $D^{\#}$, $L^{\#}$, $M^{\#}$, and $N^{\#}$) are shown in rectangles (dashed lines). SNF-motif B and SNF-motif C have been described as Snf2 specific sequence motifs by Thomä and colleagues (Thomä et al., 2005).

The alignments demonstrate the high degree of conservation of the motifs implying that the helicase domains are conserved amongst chromatin remodelers. All of the seven helicase motifs have been described to play roles either in ATP hydrolysis or ATP binding, or DNA interactions. Motif I (also known as Walker A motif) is the nucleotide binding region but is also important for hydrolyzing nucleotides since the conserved lysine in the GKT box of motif I is required for ATP hydrolysis (Nongkhlaw et al., 2012). Functional characterization of motif I revealed that mutation of this conserved lysine to alanine or arginine abolishes the ATPase activity of chromatin remodeling enzymes, as it was shown for Snf2, Sth1, and Brg1 (Du et al., 1998) (Khavari et al., 1993). The conserved glutamine one amino acid downstream of the GKT box and the conserved glutamine in motif Q regulate the catalytic efficiency of the ATPase reaction as it was shown for Active DNA-dependent ATPase A Domian (ADAAD), a proteolytic fragment of the Snf2 family protein SMARCAL1 (Nongkhlaw et al., 2012). Motif II including the DEXX box, and motifs III, IV and VI are involved in ATPase activity either by regulating the ATP hydrolysis rate or by binding ATP, as indicated by mutagenesis experiments (Brosh and Matson, 1995) (Richmond and Peterson, 1996) (Dürr et al., 2005). Motifs Ia and V, as well as motifs IV and VI may play a role in DNA interactions (Thomä et al., 2005). Interestingly, Motif V is suggested to couple ATP hydrolysis to nucleosome mobilization activity since a mutant of the *S. cerevisiae* SWI/SNF ATPase subunit lacking several amino acids of motif V is still able to hydrolyze ATP but is, in contrast to wild type, defective for mobilization of nucleosomes (Smith and Peterson, 2005). The conservation of the motifs and their functions in ATPase activity implies that Snf2 family members share mechanistic features, which is supported by analyses of crystal structures of the SWI2/SNF2 ATPase core from *S. solfataricus* and zebrafish (Dürr et al., 2005) (Thomä et al., 2005). The crystal structures of the catalytic core that includes the helicase domains indicate that the core has a bi-lobal structure made out of two RecA-like domains fused to Snf2 specific structural elements (Flaus et al., 2006). The RecA-like domains are structurally closely related to the architecture found in SF2 helicases (Duerr et al., 2006). This suggests that Snf2 family enzymes and SF2 helicases have a basic ATP hydrolysis mechanism in common.

Although all chromatin remodeling complexes have a conserved and Snf2 family specific catalytic core, they differ in their biochemical activities exhibiting diverse biological and physiological functions. Most probably, this is due to the additional proteins of the large remodeler complexes as well as to characteristic domains of the ATPase subunit of the complex. For instance, SWI/SNF members contain a bromodomain recognizing acetylated histone tails. ISWI members contain a HAND-SANT-SLIDE domain binding to unmodified histone tails and nucleic acids. CHD members contain chromodomains interacting with methylated histones (Duerr et al., 2006) (Erdel et al., 2011). The importance of these

domains on chromatin remodeling has been demonstrated. For example, removing the chromodomains of Mi-2 or the SLIDE domain of Isw2 compromises nucleosome mobilization *in vitro* (Bouazoune et al., 2002) (Boyer et al., 2004). Taken together, chromatin remodelers have diverse domain organization reflecting different substrate specificities and functional roles. However, the conserved helicase domains suggest common features in terms of the basic remodeling mechanism.
In contrast to most other Snf2 family enzymes with intrinsic ATPase activity, Lsh does not seem to be part of a large protein complex (Myant and Stancheva, 2007). In addition, it appears as if Lsh does not contain other remodeler typical domains beside the DExx and HELICc domains. Nevertheless, its Snf2-like group membership, primarily based on protein sequence similarities, and the already mentioned analyses of crystal structures revealing conserved properties of chromatin remodelers, give rise to the assumption that Lsh acts as a chromatin remodeling enzyme. In addition, since ATPase subunits of chromatin remodeling complexes by their own are capable of remodeling nucleosomes (Brehm et al., 2000) (Corona et al., 1999) (Phelan et al., 1999), Lsh may not need to be associated with other proteins in a stable complex in order to mobilize nucleosomes. In conclusion, the alignments suggest that Lsh is a chromatin remodeler and support the hypothesis that Lsh facilitates DNA methylation by moving nucleosomes.

3.2 Expression and purification of human Lsh

To study the functional interactions between Lsh and chromatin *in vitro*, attempts to express and purify recombinant full-length human Lsh (isoform 1) were first done using *E. coli* as expression system. Different bacterial strains, expression vector systems and temperature conditions during protein expression were tested. However, Lsh was either in the pellet, and therefore not soluble, or hardly detectable on sodium dodecyl sulfate polyacrylamide gels (SDS-gels) (data not shown). Still, purification was performed if Lsh was expressed and soluble. Purification attempts with different systems (column purification, batch-purification, different buffer systems, two different tags namely His-tag and FLAG-tag, different purification protocols with varying sonication settings) failed, as SDS-gels revealed that Lsh was either not in the supernatant after sonication or the elution fractions were clearly impure, if Lsh was soluble and not lost before (data not shown). For this reason, the expression system was changed to insect cells. Using the Gateway system (Invitrogen), the *LSH* cDNA was cloned into a vector suited for protein expression in insect cells. After bacmid isolation and virus generation, 6x C-terminal His-tagged human full-length Lsh was expressed in insect cells, as shown by SDS-polyacrylamide gelelectrophoresis (SDS-PAGE) and western blot (see 5.2.5 and 5.2.6) (Figs 3.2 A and B).

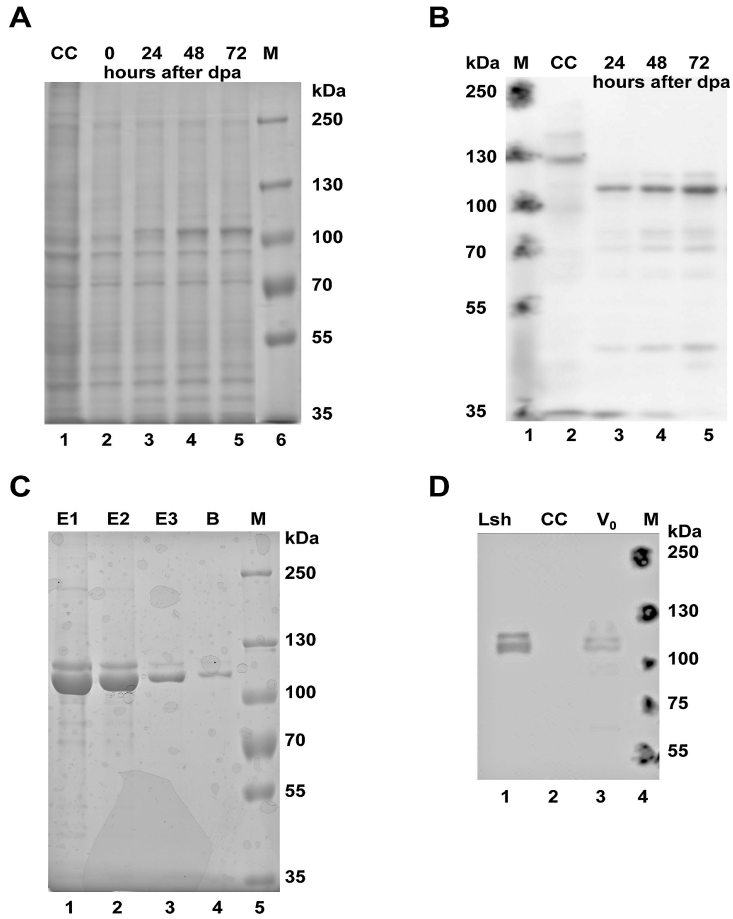

Fig 3.2: Expresssion and purification of 6x His-tagged human full-length Lsh.
(A) Lsh was expressed in Sf21 insect cells after infection of cells with 200 µl of virus per 200 ml cell culture. At indicated time points, samples of $1x10^6$ cells were taken, and cell extracts were prepared as described (see 5.2.6.3). Protein expression was analyzed by loading cell extracts on a 7.5% SDS gel. The gel was stained with Coomassie blue and destained with water. Non-infected cells (CC; lane 1) served as negative control. **(B)** Additionally, protein expression was analyzed by western blotting using an anti-His antibody (HisProbe-HRP; ThermoFisher) for detection of the C-terminal His-tag (see 5.2.3.3). Non-infected cells (CC; lane 2) served as negative control. **(C)** Lsh was batch-purified (see 5.2.7) from 200 ml Sf21 insect cells expressing 6x His tagged human full-length Lsh. For analysis, samples taken during protein purification were loaded on a 7.5% SDS gel. The gel was stained with Coomassie blue and destained with water. The SDS gel illustrates samples taken during protein elution (lanes 1–3) showing successful purification of Lsh. E1–E3: elution fractions. B: Ni-NTA beads after elution. **(D)** Purified Lsh (lane 1) was further analyzed by western blotting using a Lsh specific antibody (sc-46665; Santa Cruz). Non-infected cells (CC) (lane 2) and cells expressing Lsh (V_0) (lane 3) served as controls.

Lsh has a molecular weight of about 100 kilo Daltons (kDa). The SDS-gel reveals the increased expression of the Lsh protein over time while the intensities of all other bands remain the same (Fig 3.2 A, lanes 2–5). During western blotting, the membrane was incubated with an anti-His antibody to detect His-tagged Lsh (Fig 3.2 B). On the western blot's negative control (CC, non-infected cells; lane 2), there is no signal appearing that would match Lsh. Corresponding to the result of the SDS-PAGE, signal intensities of the expressed Lsh protein increase with time (Fig 3.2 B, lanes 3–5). The results of SDS-PAGE and western blot strongly suggest a successful expression of recombinant human full-length Lsh in insect cells, which is why the protein was subjected to purification.

The protein was purified by batch-purification, using Nickel-NTA (Ni-NTA) beads for the capture and imidazole for the elution of the protein (see 5.2.7) (Fig 3.3).
In general, the purification resulted in highly pure protein fractions with no obvious contaminations, as illustrated by an SDS-gel of one of the purifications. The few existing contaminants are only faintly visible while Lsh appears as a prominent double band in the elution fractions (Fig 3.2 C, lanes 1–3). A western blot was performed in order to prove if one of the two bands of the double band is derived from a contaminating protein. Both bands were detected with a Lsh specific antibody (sc-46665; Santa Cruz) in purified Lsh (Lsh) and in insect cells expressing Lsh (V_0). In contrast, the negative control (CC) did not yield any signal (Fig 3.2 D, lanes 1–3). Altogether, the result of the western blot confirms the specificity of the antibody and shows that the double band matches Lsh. The upper band probably emerges from posttranslational modifications. Indeed, a query at PhosphoSitePlus (http://www.phosphosite.org/homeAction.do) revealed a number of Lsh amino acid residues prone to posttranslational modifications such as phosphorylation, ubiqitination and acetylation.
The theoretical molecular weight of 6x His tagged Lsh was calculated with ProtParam (http://web.expasy.org/protparam/) and is 98.93 kDa. However, Lsh eluted at a size greater than 100 kDa (approximately 115 kDa). In a study by Myant and Stancheva, recombinant Lsh appears in the elution fractions of a size exclusion chromatography experiment with a peak corresponding to a molecular mass of about 150 kDa. Applying the Stokes radius and the sedimentation coefficient of Lsh they determined a molecular mass of 91.5 kDa. Therefore, the running behavior of Lsh seems to vary, depending on the applied method of choice, and may not correspond to the actual molecular weight of the protein. For subsequent experiments, molarities were calculated with the theoretical molecular weight of 98.93 kDa.

3.3 Lsh preferentially binds to longer DNA molecules *in vitro*

Little is known about the binding behavior of Lsh towards nucleosomes. Therefore, a basic characterization on the DNA binding properties was done first. In an initial binding assay, increasing amounts of protein were incubated with an ultra-low-range DNA marker (Fermentas) (Fig 3.3 A).

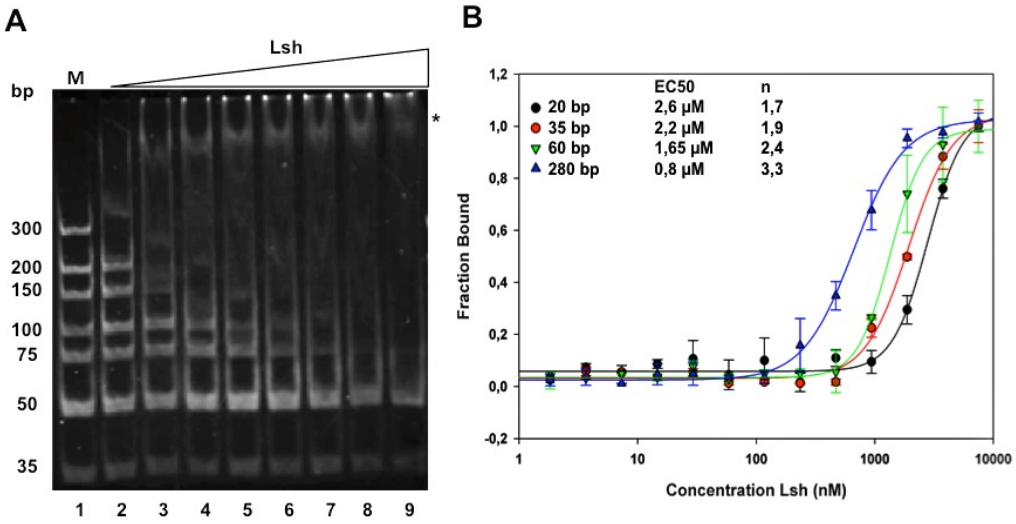

Fig 3.3: Binding affinities of Lsh towardsDNA fragments of different sizes.
The binding affinity of Lsh to differently sized DNA fragments was studied by electrophoretic mobility shift assay (EMSA) and microscale thermophoresis (MST). **(A)** For analysis by EMSA, increasing concentrations of Lsh (125 nM–1 µM; lanes 2–9) were titrated to the DNA (125 ng ultra-low-range DNA marker per lane; lanes 1–9) in a final volume of 20 µl. Reactions were incubated for 30 min at 26 °C, and DNA-protein complexes (indicated by an asterisk) were separated from unbound DNA on a 12% native PAA gel. For visualization, the gel was stained with ethidium bromide and destained with water. **(B)** For analysis by MST, increasing concentrations of Lsh (4 nM–8000 nM) were incubated with 40 nM of the respective Cy5 labeled dsDNA fragment [(AIR 20, 20 bp in size) (AIR 35, 35 bp in size) (AIR 60, 60 bp in size) (-190/+90, 280 bp in size)] at 30 °C for 10 min before starting the measurement. For data evaluation, the thermophoresis signals were normalized to fraction bound (X) by X = (Y(c)-Min)/(Max-Min). EC_{50} values and Hill coefficients were obtained according to the Hill equation f = min+(max-min)/(1+(EC_{50}/abs(x))^n) and are indicated in line with the respective DNA fragment (the size of the respective DNA fragment Lsh was incubated with is indicated). Each MST measurement was done in triplicates, each time using a different fraction of purified Lsh and freshly prepared fluorescently labeled DNA, and mean values and standard deviations were calculated.

Reactions were loaded on a 12% native PAA gel that was stained with ethidium bromide (see 5.2.9.1). Lsh first binds to the longest DNA fragments, visible as DNA-protein complexes shifted to the well of the gel, whereas smaller DNA fragments are only bound at higher protein concentrations (Fig 3.3 A). As the DNA amount (weight) remains constant (exception: 50bp; 2.5x as much), the preferred binding to longer free DNA fragments suggests a cooperative binding mechanism. In order to prove cooperative binding behavior and preferential binding to longer DNA molecules, a method differing from EMSA was applied. Microscale thermophoresis (MST) is a technique that is based on the movement of molecules in temperature gradients and that allows real-time quantification of binding affinities in solution (Baaske et al., 2010) (Zillner et al., 2011) (see 5.2.9.4.1). The

thermophoretic mobility of fluorescently labeled double-stranded (ds) DNA molecules differing in size was recorded at Lsh concentrations ranging from 4 nM to 8 µM (Fig 3.3 B). Data were then used to calculate binding affinities by applying the Hill equation:

$f = min+(max-min)/(1+(EC_{50}/abs(x))^n)$

The Hill equation is commonly used to study the kinetics of reactions that exhibit a sigmoidal behavior. The EC_{50} value is the median concentration that causes 50% of the maximal response, meaning it is the enzyme concentration at which the binding is halfway between the baseline and the maximum. Hence, lower EC_{50} values imply that less protein is needed to reach saturation. The Hill coefficient (n) is used to provide a quantitative measure of cooperativity of substrate binding with values of $n > 1$ indicating positive cooperativity. Positive cooperativity occurs when the binding of one ligand or substrate molecule promotes the binding of a second or more substrate molecules, as the other binding partner is either a monomer and has two or more binding sites, or multimerizes upon binding (Hernan G Garcia, 2011). Lsh exhibits a binding affinity (EC_{50}) of 0.8 µM towards the 280 bp long dsDNA while binding affinities to the shorter fragments are much lower, displaying EC_{50} values that increase (1.65 µM, 2.2 µM and 2.6 µM) with decreasing size of the DNA molecule (60 bp, 35 bp and 20 bp) (Fig 3.3 B). Thus, the MST data confirm the preferential binding to longer dsDNA fragments as previously indicated by the results of the electromobility shift assay. Moreover, the binding reactions indicate cooperative binding.

In summary, two different techniques to study the DNA binding properties of Lsh have been applied and show independently from each other that Lsh prefers to bind to longer dsDNA molecules *in vitro*. Interestingly, MST reveals that DNA is bound cooperatively, and binding to longer DNA molecules enhances cooperativity ($n > 3$).

3.4 Lsh binding to nucleosomes is facilitated by the availability of linker DNA

Lsh is known to associate with chromatin, and especially localizes to pericentromeric heterochromatin (Yan et al., 2003a). However, on the molecular level it has not been addressed how Lsh does bind to nuclesomes. To characterize the binding behavior of Lsh to nucleosomes, the affinity of Lsh to different nucleosomal substrates was studied *in vitro* by performing EMSA as well as MST experiments (see 5.2.9.2.1 and 5.2.9.4). Subsequent to the generation of the DNA fragments, either by restriction enzyme digestion (NPS-AvaI and NPS NotI) or by PCR (-190/90, 77-NPS-77, 0-NPS-0), the templates were used for chromatin assembly. By salt gradient dialysis (Rhodes and Laskey, 1989) nucleosomes were either reconstituted on the 601 nucleosome positioning sequence (NPS) (Lowary and Widom, 1998) or on the rDNA promoter fragment comprising 190 bp upstream and 90 bp downstream to the transcription start site (-190/+90) (see 5.2.8). Nucleosomes reconstituted on the rDNA promoter region occupied multiple positions on the DNA whereas the 601 sequence containing DNA fragments provide one single position for nucleosome assemby, as demonstrated by native PAGE (see 5.2.8.3). Additional bands in mononucleosome preparations can be explained by the occupancy of DNA with histones at positions differing from the 601 nucleosome positioning sequence, which usually make a minor fraction and therefore have no influence on the quality of the nucleosomes. Nucleosomes were incubated with increasing amounts of Lsh, and reactions were analyzed on native PAA gels visualized either by ethidium bromide staining (NPS-AvaI and NPS-NotI) or by fluorescence scanning (-190/90, 77-NPS-77, 0-NPS-0; DNA templates are fluorescently labeled).

In general, the gel retardation assays demonstrate that Lsh interacts with chromatin *in vitro,* since the mobility shifts are due to the specific binding of Lsh to the nucleosomes (Figs 3.4 A–E).

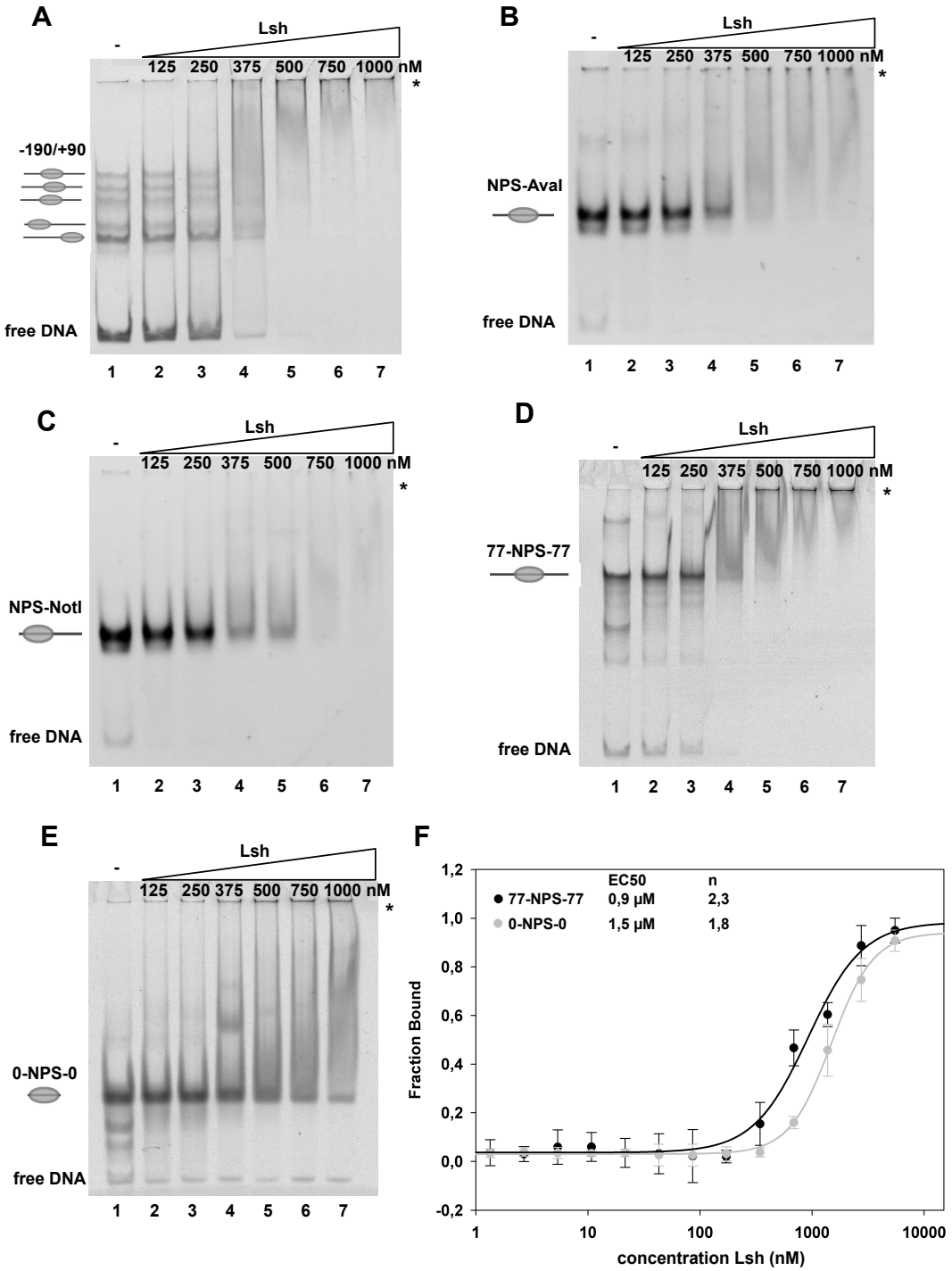

Fig 3.4: Binding affinity of Lsh to nucleosomes.
The binding affinity of Lsh to different nucleosomal substrates was studied by EMSA and MST. **(A–E)** Analysis of the binding affinities of Lsh towards nucleosomes by EMSA. Increasing concentrations of Lsh (125 nM–1 µM) were incubated with constant amounts (20 nM) of **(A)** nucleosomes positioned on the Cy5 labeled murine rDNA promoter region (-190/+90), **(B)** a centrally-positioned mononucleosome with 27 bp linker DNA (NPS-AvaI), **(C)** a mononucleosome positioned at the border of the DNA template (NPS-NotI), **(D)** a centrally-positioned Cy5 labeled mononucleosome with 77 bp linker DNA (77-NPS-77), and **(E)** the Cy3 labeled nucleosomal core (0-NPS-0). Reactions were incubated for 30 min at 30 °C and were analyzed on 5% native PAA gels. Gels were visualized on a fluorescence image reader, or by staining with ethidium bromide. Protein-nucleosome complexes are indicated by asterisks. **(F)** Analysis of binding affinities of Lsh towards Cy5 labeled 77-NPS-77 and Cy3 labeled 0-NPS-0 by MST. Increasing concentrations of Lsh (2 nM–7500 nM) were incubated with 50 nM of the respective nucleosomal substrate at 30 °C for 10 min before starting the measurement. For data evaluation the thermophoresis signals were normalized to fraction bound (X) by X = (Y(c)-Min)/(Max-Min). EC_{50} values and Hill coefficients were obtained according to the Hill equation f = min+(max-min)/(1+(EC_{50}/abs(x))^n) and are indicated in line with the respective nucleosome (77-NPS-77 and 0-NPS-0, respectively). Each measurement was done in triplicates, and mean values and standard deviations were calculated.

Nucleosomes differently positioned on the rDNA promoter region are bound by Lsh as indicated by the disappearance of the nucleosomal bands, but also the free DNA is bound. The nucleosomal DNA-protein complex is shifted to the well as indicated by an asterisk (Fig 3.4 A). The EMSA indicates preferential binding of Lsh to centrally-positioned nucleosomes than to nucleosomes positioned at the border. To prove this, mononucleosomes positioned either at the center or at the border of the template and flanked with DNA differing in size (Figs 3.4 B–E) were used. NPS-AvaI and NPS-NotI were both prepared from the same plasmid but with different restriction enzymes. Digestion with AvaI leads to a centrally-positioned nucleosome, with about 27 bp linker DNA on both sites. Digestion of the plasmid with NotI generates a mononucleosome positioned at the border and flanked with about 55 bp linker DNA on one site of the nucleosome. In both cases, EMSAs suggest that Lsh binds to the free DNA before it binds to the nucleosome. The centrally-positioned NPS-AvaI is bound at a protein concentration of 500 nM (Fig 3.4 B, lane 5) while binding of NPS-NotI affords higher protein concentrations (Fig 3.4 C, lane 6). The results confirm the preferred binding to centrally-positioned nucleosomes, suggesting symmetric binding of Lsh. As for the binding of Lsh to 77-NPS-77 (77 bp symmetric linker DNA), Lsh starts to bind the free DNA at stages where the nucleosome is still not fully bound (Fig 3.4 D). Since Lsh prefers to bind to longer free DNA *in vitro* (see 3.3) one may conclude that longer linkers facilitate the binding to nucleosomes. 77-NPS-77 comprises linker DNA that is about 50 bp longer in comparison to NPS-AvaI that contains 27 bp symmetric linker DNA. By visual inspection of the native PAA gels of the EMSAs with NPS-AvaI and 77-NPS-77, one could draw the conclusion that longer linkers improve the binding affinity of Lsh as it appears that Lsh shows slightly enhanced binding to 77-NPS-77 compared to the binding to NPS-AvaI (Figs 3.4 B and D). Yet, this is derived from indirect comparisons, as the substrates were not combined in a reaction to compete with each other. EMSAs with the nucleosomal core (0-NPS-0) demonstrate that lack of linker DNA impedes the binding to the nucleosome. The nucleosomal core is weakly bound, even at higher protein concentrations. The free DNA that is still present and makes only a few base pairs (about 3 to 5 bp on both sites of the core), is not bound since there is less free DNA in size to be bound by Lsh (Fig 3.4 E). Therefore, a certain minimal linker length may be necessary to facilitate the binding of nucleosomes.

The ability of Lsh to interact with chromatin was further confirmed by MST experiments. Reconstituted mononucleosomes with (77-NPS-77) and without (0-NPS-0) DNA linkers were incubated with increasing amounts of Lsh. Lsh exhibits a binding affinity of 0.9 µM towards 77-NPS-77. In contrast to the gel retardation assay, Lsh binds to the nucleosomal core when applying MST and displays an EC_{50} value of 1.5 µM (Fig 3.4 F). Nevertheless, and as suggested by the results of the EMSAs, the MST data demonstrate increased

affinity of Lsh towards the nucleosome in the presence of linker DNA. The data reveal Hill coefficients with values of n > 1 and a relatively higher Hill coefficient if the substrate has linker DNA (Fig 3.4 F). This suggests cooperative binding of Lsh to nucleosomes with an increase in cooperativity in the presence of extranucleosomal DNA.

3.5 Lsh shows no remodeling activity *in vitro*

Since it is not known if Lsh is able to move nucleosomes, *in vitro* nucleosome mobilization assays using substrates with nucleosomes occupying terminal (NPS-NotI), central (NPS-AvaI and 77-NPS-77) and multiple (-190/+90) positions on the DNA were done. In the presence of constant amounts of ATP nucleosomes were incubated with increasing concentrations of Lsh. NoRC (nucleolar remodeling complex) was used as positive control, which is an ISWI type remodeling enzyme that consists of two subunits, Tip5 and the Snf2H ATPase (Manelyte et al., 2014). Reactions were stopped by the addition of competitor DNA and were analyzed on native PAA gels (Fig 3.5) (for detailed description of the nucleosome mobilization assay, see 5.2.9.5).

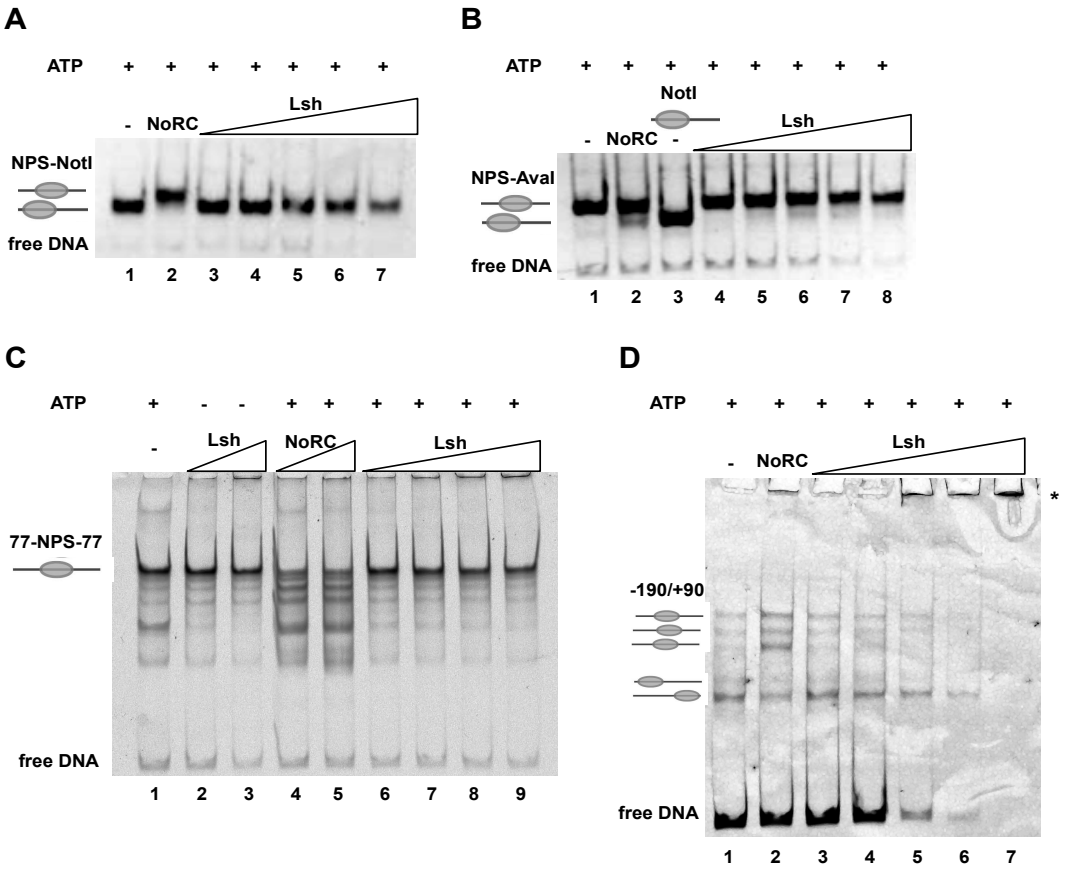

Fig 3.5: Analysis of the capability of Lsh to mobilize nucleosomes *in vitro*.
The capability of Lsh to remodel nucleosomes was studied in *in vitro* nucleosome mobilization assays using different nucleosomal substrates. Reactions were carried out in the presence or absence of ATP (1 mM) as indicated. Constant amounts of nucleosomes were incubated with increasing concentrations of Lsh for 60 min at 30 °C. Reactions were stopped by the addition of competitor DNA and analyzed on 5% native PAA gels. **(A)** Increasing concentrations of Lsh (50 nM–800 nM) were incubated with constant amounts (100 nM) of an end-

positioned mononucleosome (NPS-NotI). The chromatin remodeling complex NoRC served as positive control and moved the nucleosome to a central position on the DNA fragment (remodeled and non-remodeled nucleosome are illustrated as sketch). **(B)** Increasing concentrations of Lsh (50 nM–800 nM) were incubated with constant amounts (100 nM) of a centrally-positioned mononucleosome (NPS-AvaI). NoRC moved the nucleosome to an end-position on the DNA fragment (remodeled and non-remodeled nucleosome are illustrated as sketch). For better visualization of the directional nucleosome movement, non-remodeled NPS-NotI was included (lane 3). **(C)** 50 nM (lane 2) and 400 nM (lane 3) as well as 50–400 nM (lanes 6–9) of Lsh were incubated with 30 nM of the centrally-positioned Cy5 labeled mononucleosome 77-NPS-77.
The positive control NoRC moved the nucleosome to end-positions. **(D)** Increasing concentrations of Lsh (50 nM–800 nM) were incubated with 30 nM of nucleosomes positioned on the Cy5 labeled murine rDNA promoter region (-190/+90). Nucleosomes were bound by Lsh at higher protein concentrations, and protein-nucleosome complexes shifted to the well of the gel, as indicated by an asterisk. NoRC served as positive control and moved nucleosomes to central positions on the DNA fragment.

NoRC translocates the NPS-NotI mononucleosome from an end-position to a central position (Fig 3.5 A, lane 2), showing that the assay conditions are suitable to study chromatin remodeling. The movement of the nucleosome to a central position results in slower migration of the nucleosome through the matrix of a native PAA gel, allowing the discrimination between end-positioned and more centrally located nucleosomes (Linxweiler and Hörz, 1984) (Pennings et al., 1991). Whilst the positive control moves the nucleosome as expected, Lsh shows no remodeling activity on NPS-NotI (Fig 3.5 A, lanes 3–7). However, end-positioned nucleosomes are probably not the optimal substrate, as suggested by the binding assays. Lsh binding affinity towards the nucleosome seems to be slightly impeded if there is no linker DNA protruding only from one site of the nucleosomal core (see chapter 3.4, Figs 3.4 B–D). For this reason, centrally-positioned mono-nucleosomes (NPS-AvaI and 77-NPS-77) were assayed in the presence of Lsh and ATP. NPS-AvaI is not repositioned by Lsh (Fig 3.5 B, lanes 4–8) whereas NoRC moves the nucleosome to an end-position that is equivalent to the position of the NPS-NotI mononucleosome (Fig 3.5 B, lanes 2 and 3). The shadow-like band beneath the nucleosomal band in lane 6 is not derived from remodeling. It rather must be a gel artefact and disappears at higher Lsh concentrations. In addition, the ATPase activity of Lsh is not stimulated by the NPS-AvaI mononucleosome (see chapter 3.6.2, Fig 3.7 B). Testing the centrally-positioned 77-NPS-77 that contains longer linkers in comparison to NPS-AvaI, Lsh again did not exhibit chromatin remodeling activity (Fig 3.5 C). The position of the mononucleosome does not change throughout the titration series of Lsh in the presence of constant amounts of ATP (Fig 3.5 C, lanes 6–9). In contrast, the positive control NoRC moves the 77-NPS-77 mononucleosome from its central position to end-positions (Fig 3.5 C, lanes 4 and 5). Faster migrating bands representing nucleosomes on undefined positions lose intensity in lanes 6 to 9 where Lsh and ATP are present. However, this is not an ATP-dependent effect, as illustrated by lanes 2 and 3, which represent reactions including Lsh without ATP. Therefore, those nucleosomes are simply bound by Lsh and are not relocated on the basis of ATP hydrolysis. By the reconstitution of mononucleosomes on the rDNA promoter fragment (position −190 to +90, relative to the transcription start site), a

more complex and natural substrate with nucleosomes placed on different positions on the fragment was prepared (Fig 3.5 D, lane 1). A substrate with multiple nucleosomes potentially allows Lsh more flexibilty in terms of nucleosome mobilization. NoRC served as positive control. As previously reported, NoRC-dependent remodeling results in a pattern of nucleosome positions that are preferably located close to the center of the DNA (Manelyte et al., 2014) (Fig 3.5 D, lane 2). Lsh did not move the nucleosomes in a chromatin remodeling like fashion (Fig 3.5 D, lanes 3–5). However, the nucleosomal DNA and the free DNA were bound by Lsh and formed a complex that was not able to enter the gel, which is probably due to underestimated competitor DNA concentrations (Fig 3.5 D, lanes 5–7). Taken together, despite its ability to bind DNA and nucleosomes and its close relationship to ATPase subunits of chromatin remodeling complexes, Lsh did not exhibit chromatin remodeling activity *in vitro*.

3.6 Basic studies on the ATPase activity of Lsh

Nucleosome mobilization is an ATP-driven process. The energy released from ATP hydrolysis is coupled to the remodeling of nucleosomes, which means that the ATPase subunit of a chromatin remodeling enzyme is the core for the catalysis of the remodeling reaction. Nucleosomes are a natural substrate for chromatin remodelers and usually activate the ATPase function of those enzymes. In order to figure out whether the ability of Lsh to hydrolyze ATP is stimulated by nucleosomes, a series of ATPase assays was performed.

3.6.1 Establishing reaction conditions for ATPase assays

To determine assay conditions, the ATPase activity of Chd3 was tested using dsDNA, mononucleosomes and a nucleosomal array as substrates. Chd3 is a component of the NuRD (nucleosome remodeling and histone deacetylase) complex and, as in the case of Lsh, contains the Snf2 typical ATPase domain motifs. Recombinant Chd3 was shown to be a nucleosome stimulated ATPase that remodels nucleosomal substrates in an ATP-dependent manner (Murawska et al., 2008).
For our purposes, the following conditions were used: 150 nM of Chd3 were incubated with DNA (80 nM) or nucleosomes (80 nM mononucleosomes, 43 ng/µl nucleosomal array) in the presence of 200 µM ATP (non-radioactive) and [γ-32P]-ATP (0.2 µCi/µl) in the reaction buffer (2 mM Tris, 120 mM KCl, 0.15 mM $MgCl_2$, 50 µM EGTA, 1mM DTT, 25 mM imidazole final concentrations) for 45 minutes at 30 °C in a final reaction volume of 10 µl. [γ-32P]-ATP was added to the reaction mix to monitor ATP hydrolysis. The hydrolyzed phosphate was

separated from unreacted ATP by thin layer chromatography. Non-hydrolyzed ATP and hydrolyzed phosphate spots were quantified, and amounts of hydrolyzed ATP were calculated (see 5.2.9.6).

Chd3 had weak basal ATPase activity but was stimulated by DNA (2–3-fold) and to a significantly greater extent by nucleosomes (4–6-fold), with polynucleosomes (nucleosomal array) having the strongest stimulatory effect (Fig 3.6). The results of the ATPase assays with Chd3 show that the reaction conditions can be used to examine ATPase activity.

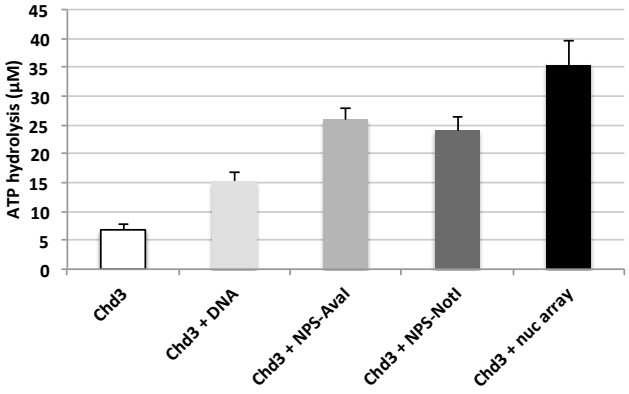

Fig 3.6: ATPase activity of Chd3.
The ATPase activity of recombinant Chd3 (150 nM per reaction) was tested using plasmid DNA (puC18 12x 601, 80 nM), mononucleosomes (NPS-AvaI and NPS-NotI, 80 nM each), and a nucleosomal array (12x 601, 43 ng/µl) as substrates. Basal activity of Chd3 was derived by incubating Chd3 only with reaction buffer (white bar). Reactions were carried out in 10 µl volumes in the presence of 200 µM ATP (non-radioactive) and minor amounts of radioactive ATP (0.2 µCi/µl). Reactions were incubated for 45 min at 30 °C, then pipetted onto a TLC plate to separate the hydrolyzed phosphate from unreacted ATP. The percentage of hydrolyzed ATP was calculated according to the equation: $\%_{(\text{hydrolyzed ATP})} = P_i*100/(P_i + ATP_{\text{non-hydr}})$, and was corrected for background activity arising from non-radioactive ATP. Corrected values were then used to calculate the amount of hydrolyzed ATP in µM. Experiments were carried out in biological triplicates, and mean values of hydrolyzed ATP in µM and standard deviations were calculated.

3.6.2 The *in vitro* ATPase activity of Lsh is not stimulated by DNA and nucleosomes

To elucidate a stimulatory effect of DNA and nucleosomes on the ATPase activity of Lsh, ATPase assays were carried out as described for Chd3 (see 3.6.1), with the exception that Lsh was added to increasing amounts of substrate. Chd3 was included as positive control. Both Lsh and Chd3 showed weak basal ATPase activity (Figs 3.7 A–D, black and white bars).

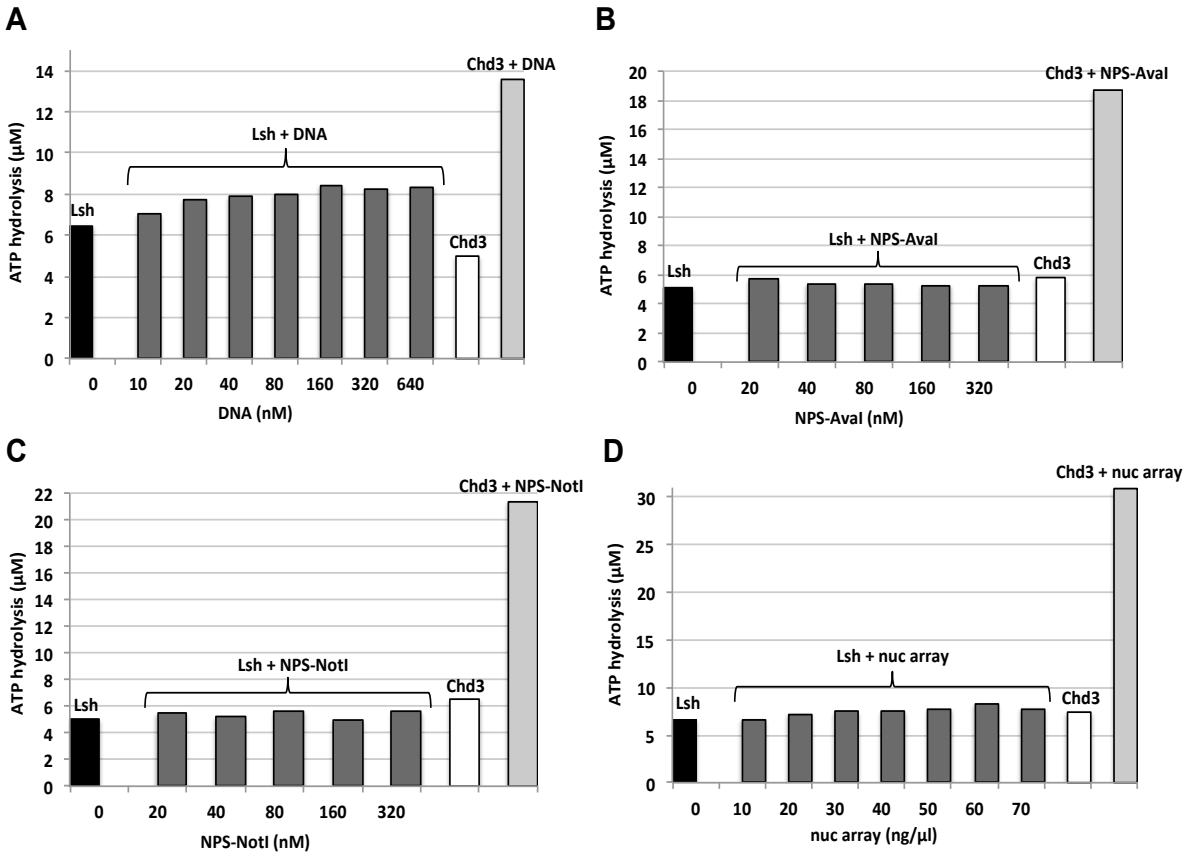

Fig 3.7: Analysis of the influence of DNA and nucleosomes on the *in vitro* ATPase activity of Lsh.
The ATPase activity of recombinant human Lsh (200 nM per reaction) was tested using **(A)** plasmid DNA (puC18 12x 601, 10–160 nM), **(B, C)** mononucleosomes (NPS-AvaI and NPS-NotI, 20–320 nM each), and **(D)** a nucleosomal array (12x 601, 10–70 ng/µl) as substrates. Basal activity of Lsh was derived by incubating Lsh only with reaction buffer (black bars). Chd3 (150 nM) served as positive control and was incubated with buffer only (white bars), and with buffer supplied with DNA (puC18 12x 601, 80 nM), mononucleosomes (NPS-AvaI and NPS-NotI, each 80 nM) or a nucleosomal array (12x 601, 43 ng/µl) (light grey bars). Reactions were carried out in 10 µl volumes in the presence of 200 µM ATP (non-radioactive) and minor amounts of radioactive ATP (0.2 µCi/µl). Reactions were incubated for 45 min at 30 °C, then pipetted onto a TLC plate to separate the hydrolyzed phosphate from unreacted ATP. The percentage of hydrolyzed ATP was calculated according to the equation: $\%_{(\text{hydrolyzed ATP})} = P_i*100/(P_i + ATP_{\text{non-hydr}})$, and was corrected for background activity arising from non-radioactive ATP. Corrected values were then used to calculate the amount of hydrolyzed ATP in µM.

However, in contrast to the positive control Chd3, Lsh ATPase was neither activated by DNA (Fig 3.7 A) nor by nucleosomes, no matter if mononucleosomes (Figs 3.7 B and C) or a nucleosomal array (Fig 3.7 D) were used. Varying concentrations of Lsh (40 nM–1 µM) and ATP (10 µM–2 mM) in different molar ratios to each other or changing incubation time (30 min–60 min) or salt concentrations (80 mM–150 mM) did not improve the results of the ATPase assays (data not shown). Under all the conditions tested, DNA and nucleosomes did not stimulate Lsh ATPase activity.

Contradictory to its proposed function as a chromatin remodeler, the basic *in vitro* studies to characterize a chromatin remodeling enzyme suggest that Lsh is not a nucleosome stimulated ATPase and does not mobilize nucleosomes. The lack of an essential interaction partner to trigger ATPase activity cannot be ruled out though. Furthermore, Lsh possibly possesses a so far not described domain inhibiting ATP binding or hydrolysis, or it needs to

recognize certain histone or DNA modifications in order to perform its function. In the following, alternative ATPase activating substrates were screened, and it was tried to generate deletion mutants of Lsh in order to characterize its ATPase function.

3.7 Expression and purification of Lsh KR mutant

At this point, a His-tagged KR mutant of Lsh was included as an internal negative control in the ATPase assays. The KR mutant was generated by introducing a point mutation by site-directed mutagenesis resulting in the exchange of lysine residue K254 to arginine (see 5.2.1.10). This lysine residue resides in the Walker A motif that is important for ATP binding and hydrolysis (Fig 3.8 A).

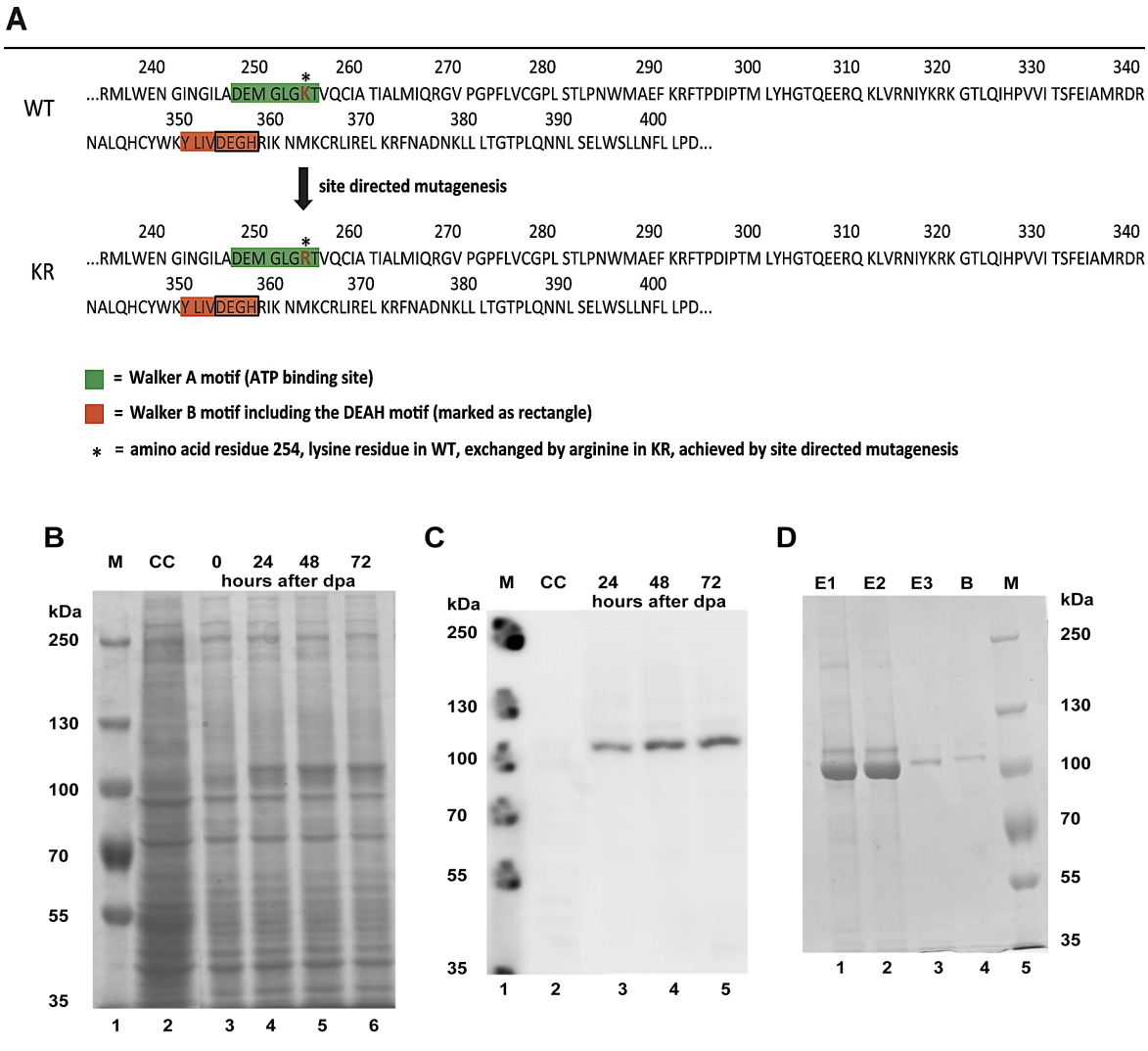

Fig 3.8: Generation of an ATPase inactive version of Lsh.
A version of Lsh deficient of ATPase activity was generated. **(A)** Illustration of the DExx domain of Lsh. Walker A (green) and Walker B motifs (red) are highlighted. Exchanging the lysine residue (K254) by arginine (marked by asterisks) in the Walker A motif by site-directed mutagenesis resulted in an ATPase inactive version of Lsh, and is called KR mutant. **(B, C)** Expresssion of 6x His-tagged KR mutant in SF21 insect cells. KR mutant was expressed in Sf21 insect cells after infection of cells with 400 µl of virus per 200 ml cell culture. At indicated time points, samples of $1x10^6$ cells were taken, and cell extracts were prepared as described (5.2.6.3). **(B)** Protein expression was analyzed by loading cell extracts on a 7.5% SDS gel.
The gel was stained with Coomassie blue and destained with water. Non-infected cells (CC; lane 2) served as

negative control. **(C)** Additionally, protein expression was analyzed by western blotting using an anti-His antibody (HisProbe-HRP; ThermoFisher) for detection of the C-terminal His-tag (see 5.2.3.3). Non-infected cells (CC; lane 2) served as negative control. **(D)** Purification of 6x His-tagged KR mutant. KR mutant was batch-purified from 200 ml Sf21 insect cells expressing 6x His tagged KR mutant. For analysis, samples taken during protein purification were loaded on a 7.5% SDS gel. The gel was stained with Coomassie blue and destained with water. The SDS gel illustrates samples taken during protein elution (lanes 1–3) showing successful purification of Lsh. E1–E3: elution fractions. B: Ni-NTA beads after elution.

Mutation of the equivalent lysine residue in other Snf2 family proteins has been shown to abolish ATPase activity, and consequently nucleosome remodeling activities (Côté et al., 1994) (Bouazoune and Kingston, 2012). In the presence of ATPase stimulating substrates, the ATPase activity of Lsh KR mutant usually was similar to the basal ATPase activity of Lsh wild-type enzyme, showing that the KR mutant was fairly inactive and hence is a proper internal negative control (see 3.9.2 and 3.9.3). 6x C-terminal His-tagged KR mutant was expressed in insect cells as described (see 5.2.6). Expression was analyzed by SDS-PAGE and western blotting. The SDS-gel reveals increased protein expression over time, while the intensities of all other bands remain the same (Fig 3.8 B). During western blotting the membrane was incubated with an anti-His antibody to detect His-tagged Lsh KR mutant. On the western blot's negative control (CC) there is no signal appearing, and corresponding to the results of the SDS-PAGE, signal intensities of the expressed KR mutant increase with time (Fig 3.8 C). Recombinant KR mutant was purified by batch-purification as described (see 5.2.7). Lsh KR mutant was eluted with few contaminants that are only faintly visible. As for Lsh wild type, the KR mutant appears as a double band in the elution fractions (Fig 3.8 D).

3.8 Study of the interplay between Lsh and 5-hmC

5-hydroxy-methylcytosine (5-hmC) is an intermediate in the course of the Ten-eleven translocation (Tet) protein-driven DNA demethylation process. The Tet proteins remove methyl groups from the DNA by the successive oxidation of 5-mC to 5-hmC, to 5-formyl-cytosine (5-fC) and to 5-carboxyl-cytosine (5-caC) (Tahiliani et al., 2009) (Ito et al., 2011). During Tet mediated DNA demethylation, the oxidized derivatives of 5-mC can be converted to cytosine by base excision repair mechanisms (He et al., 2011) (Maiti and Drohat, 2011).

There is evidence suggesting that 5-hmC not only serves as an intermediate of DNA demethylation, but also functions as an epigenetic mark with unique regulatory functions (Yildirim et al., 2011) (Hashimoto et al., 2012) (Choi et al., 2014).

Still, several important questions remain regarding the functions of 5-hmC and the other oxidized versions of 5-mC. Lsh was identified as a specific reader for 5-hmC in mouse neural progenitor cells (NPCs) in a screen for readers for methylcytosine and its oxidized

derivates (Spruijt et al., 2013). Lsh promotes phosphorylation of H2AX to γH2AX, and thereby contributes to efficient repair of DNA double strand breaks (Burrage et al., 2013). Therefore, it has been assumed that Lsh could be involved in a Tet mediated DNA demethylation pathway that converts 5-hmC to cytosine via DNA repair mechanisms (Spruijt et al., 2013). However, since Lsh is important to maintain and establish DNA methylation, it is questionable wether Lsh participates in active DNA demethylation. Lsh more likely recognizes 5-hmC and conducts signals mediated by 5-hmC in terms of its function as an epigenetic landmark. For example, recruitment of Lsh to 5-hmC could result in the stimulation of Lsh ATPase and remodeling activity.

3.8.1 Lsh binds to hydroxy-methylated and methylated DNA with higher affinity than to unmodified DNA

The binding of Lsh to 5-mC and 5-hmC modified DNA fragments and unmodified DNA fragments was studied by MST in order to confirm specific interaction between Lsh and 5-hmC, and to quantify binding affinities. For this purpose, the differently modified DNA substrates were prepared by PCR. By using a dNTP mix including methyl-dCTP, hydroxy-methyl-dCTP or dCTP in combination with a fluorescently labeled primer and an unlabeled primer, 310 bp long DNA fragments were generated. The DNA fragments contain two HpaII restriction sites. Incorporation of methyl groups and hydroxy-methyl groups was analyzed by restriction endonuclease digestion with HpaII and its isoschizomer MspI (see 5.2.1.9). Subsequently, binding affinities of Lsh to 5-mC and 5-hmC modified DNA as well as unmodified DNA were examined by MST. The fluorescently labeled DNA substrates were incubated with increasing concentrations of Lsh. Afterwards, the thermophoretic mobility was recorded, and the data were used to calculate binding affinities by applying the Hill equation (see 5.2.9.4). Lsh exhibits identical binding affinities towards the 5-hmC and 5-mC modified DNA fragments (EC_{50} = 0.3 µM each). In comparison, Lsh has a 3-fold lower binding affinity towards unmodified DNA (EC_{50} = 1µM) (Fig 3.9).

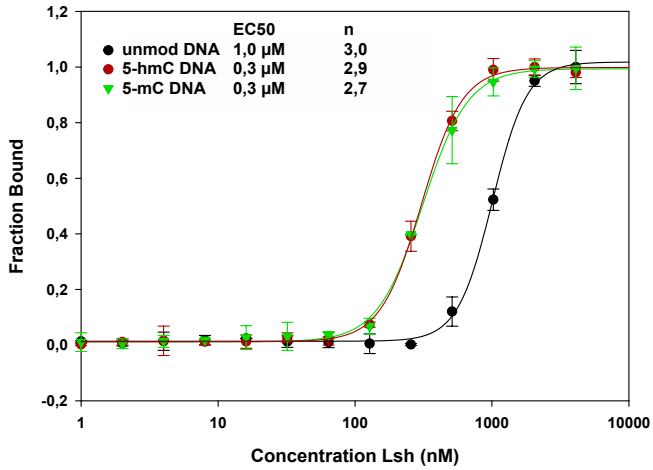

Fig 3.9: Binding affinities of Lsh towards 5-hmC and 5-mC modified and unmodified DNA fragments. The binding affinity of Lsh to 5-hmC and 5-mC modified and to unmodified DNA fragments was studied by MST. Increasing concentrations of Lsh (2 nM–6200 nM) were incubated with 30 nM of the respective Cy5 labeled DNA fragment at 30 °C for 15 min before starting the measurement. For data evaluation the thermophoresis signals were normalized to fraction bound (X) by X = (Y(c)-Min)/(Max-Min). EC_{50} values and Hill coefficients were obtained according to the Hill equation f = min+(max-min)/(1+(EC_{50}/abs(x))^n) and are indicated in line with the respective DNA fragment. Each MST measurement was done in triplicates, each time using a different fraction of purified Lsh and freshly prepared fluorescently labeled DNA, and mean values and standard deviations were calculated.

Hill coefficients (n = 2.7 or higher) confirm the high cooperative binding to long dsDNA that was already noticed in the MST measurements to differently sized DNA fragments (Fig 3.3 B). However, DNA modifications do not appear to affect cooperativity indicating that the protein's binding site somehow adopts a structure that fits better to modified DNA substrates than to unmodified DNA. Contradictory to the findings by Spruijt and colleagues, similar binding of Lsh to both 5-hmC and 5-mC was observed. However, the performed *in vitro* analysis is based on a completely different method. Still, the results of the MST measurements are in line with the hypothesis that Lsh interacts with 5-hmC to direct the organization of chromatin structures.

3.8.2 Dinucleosomes stimulate Lsh ATPase activity only under specific assay conditions but not in general

In order to examine, if the intrinsic capability of Lsh to hydrolyze ATP is stimulated through its preferential recognition of 5-mC or 5-hmC in the context of chromatin, dinucleosomes containing either methylcytosine, 5-hydroxy-methylcytosine or unmodified cytosine were generated and used as substrates in ATPase assays. For this purpose, a DNA sequence harbouring two 601 nucleosome positioning sequences seperated by 10 bp (601-10N-601) served as template. The differently modified DNA templates were generated by PCR. Analysis of incorporation of methylcytosine and 5-hydroxy-methylcytosine was performed as described (see 5.2.8.2.3). In combination with chicken histones, 5-hmC and 5-mC

modified and unmodified DNA templates were subjected to chromatin assembly. Reconstituted dinucleosomes were analyzed on 5% native PAA gels. In contrast to mononucleosomes, dinucleosomes may allow Lsh greater flexibility in terms of substrate recognition.

Subsequently, the stimulatory effect of 5-hmC and 5-mC modified and unmodified dinucleosomes on Lsh ATPase activity was studied (Figs 3.10–3.12). Buffer compositions and incubation time and temperature were kept as described (see 3.6.1). Lsh wild-type (WT) and KR mutant (KR) were added in concentrations ranging from 100 nM to 1 µM to increasing concentrations of nucleosomal substrates, and different ATP concentrations were tested (10 µM ATP, 100 µM ATP, 1 mM ATP). Rates of ATP hydrolysis were normalized to the ATP hydrolysis levels exhibited by WT and KR lacking nucleosomal substrates (referred to as “Lsh only”). Bars displaying values < 1 mirror signal intensities that are weaker than signal intensities of “Lsh only” and thus are not relevant. Therefore, values > 1 for WT are supposed to be compared to “Lsh only”, if values for the corresponding KR are < 1. In all other cases, WT and corresponding KR are compared to each other. A ratio of ATP hydrolysis levels of WT to ATP hydrolysis levels of KR above 2-fold is interpreted as a stimulatory effect on ATPase activity. Ratios below 2-fold are interpreted as “no stimulation of ATPase activity”.

3.8.2.1 Unmodified dinucleosomes do not strongly stimulate Lsh ATPase activity

In the presence of 1mM ATP, unmodified dinucleosomes do not stimulate Lsh ATPase (Fig 3.10 A). Lowering the ATP concentration to 100 µM led to ATP hydrolysis levels of WT that were about 1.5-fold higher in comparison to KR or “Lsh only”, independent of nucleosome concentrations (Fig 3.10 B). 10 µM ATP and 200 nM protein resulted in a 2-fold higher ATPase activity of WT in comparison to KR. Lowering protein concentrations to 100 nM and increasing protein concentrations to 500 nM reduced the ATPase activating effect of dinucleosomes on WT to 1.5-fold relative to KR, and a further increase in protein concentration equalled the hydrolytic activity of WT and KR (Fig 3.10 C).

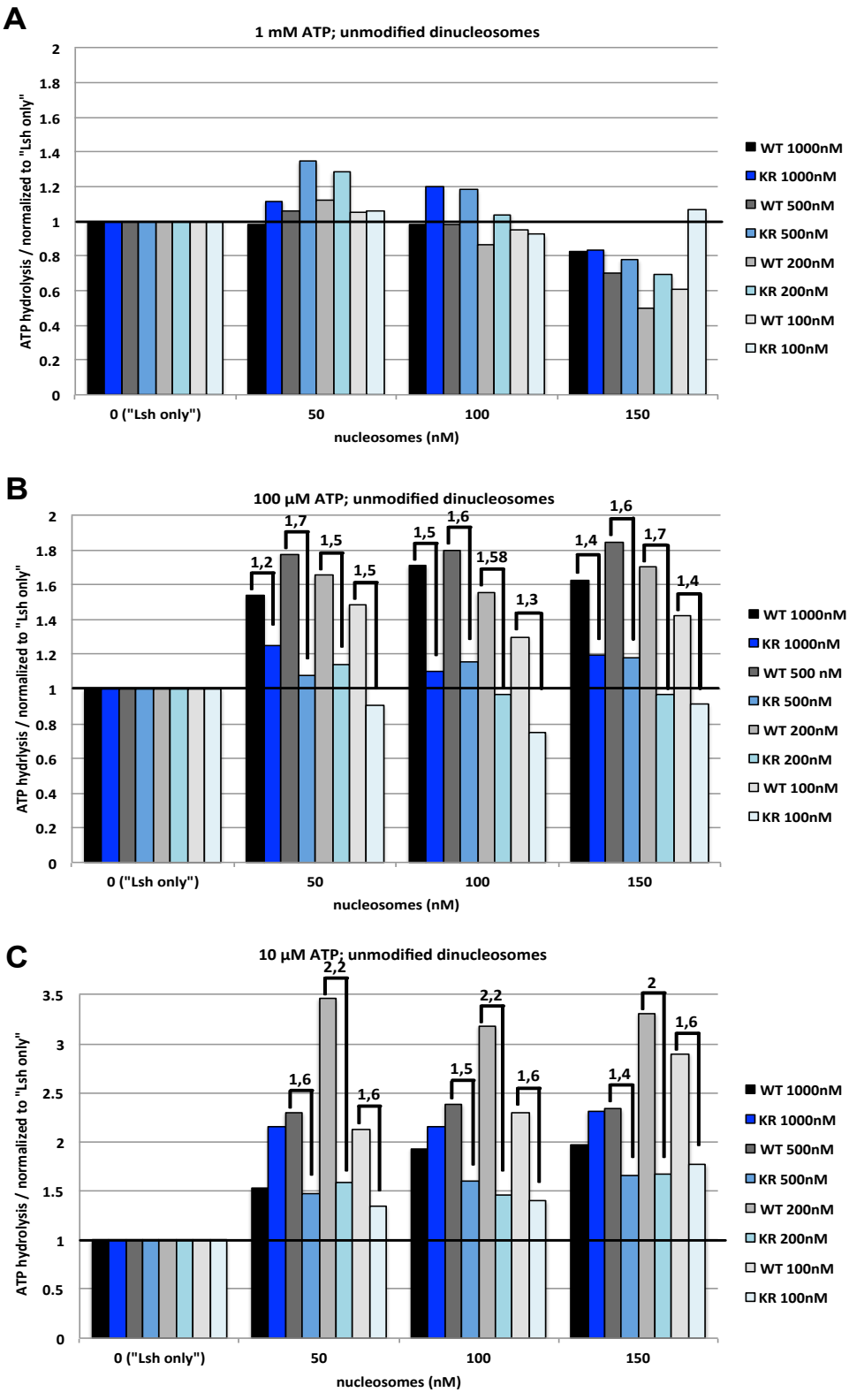

Fig 3.10: Analysis of the influence of unmodified dinucleosomes on the ATPase activity of Lsh.
The effect of unmodified dinucleosomes on the ATPase activity of Lsh was studied at **(A)** 1mM ATP, **(B)** 100 µM ATP and **(C)** 10 µM ATP. Nucleosome concentrations varied from 50 to 150 nM, and concentrations of Lsh WT and KR varied from 100 nM to 1000 nM, as indicated. WT is illustrated in black and grey scale bars, KR in blue scale and white bars. Reactions were carried out in 10 µl volumes in the presence of the indicated amount of ATP (non-radioactive) and minor amounts of radioactive ATP (0.2 µCi/µl). Reactions were incubated for 45 min at 30 °C, then pipetted onto a TLC plate to separate the hydrolyzed phosphate from unreacted ATP. The percentage of hydrolyzed ATP was calculated according to the equation: $\%_{(\text{hydrolyzed ATP})} = P_i*100/(P_i + ATP_{\text{non-hydr}})$, and was corrected for background activity arising from non-radioactive ATP. Corrected values were then used to calculate the amount of hydrolyzed ATP in µM. Afterwards, values were normalized to “Lsh only” (WT and KR lacking

nucleosomes). WT and corresponding KR were compared to each other, and calculated ratios are displayed, if values for WT are > 1 and exceed values for the corresponding KR. Values > 1 for WT were compared to “Lsh only” (corresponds to a value = 1, indicated by a black line), if values for the corresponding KR are < 1. Values < 1 can be ignored as signal intensities are weaker than for “Lsh only”.

Repetition of these assays (see Appendix) confirmed the results shown here, demonstrating that WT ATPase activity in general is only about 1.5-fold higher in comparison to the ATPase activity of KR at ATP concentrations below 1 mM. Therefore, unmodified dinucleosomes in general do not significantly stimulate Lsh ATPase activity. Nevertheless, under specific reaction conditions, a mild stimulatory effect on the protein’s ATPase activity in the range of 2-fold was observed.

3.8.2.2 5-hmC modified dinucleosomes considerably stimulate Lsh ATPase but only under specific assay conditions

As in the case of unmodified dinucleosomes, hydroxy-methylated dinucleosomes have no stimulating impact on Lsh ATPase in the presence of 1 mM ATP (Fig 3.11 A). Reduction to 100 µM ATP results in an overall 1.5-fold higher WT ATPase activity in relation to the corresponding KR mutant or “Lsh only” (Fig 3.11 B). With 10 µM ATP, lowering protein concentrations from 1 µM to 100 nM causes a stepwise increase in the hydrolytic activity of WT ranging from about 1.4-fold (500 nM Lsh) to about 2.3-fold (200 nM Lsh) to about 2.5–3-fold (100 nM Lsh) relative to the hydrolytic activity of KR (Fig 3.11 C).

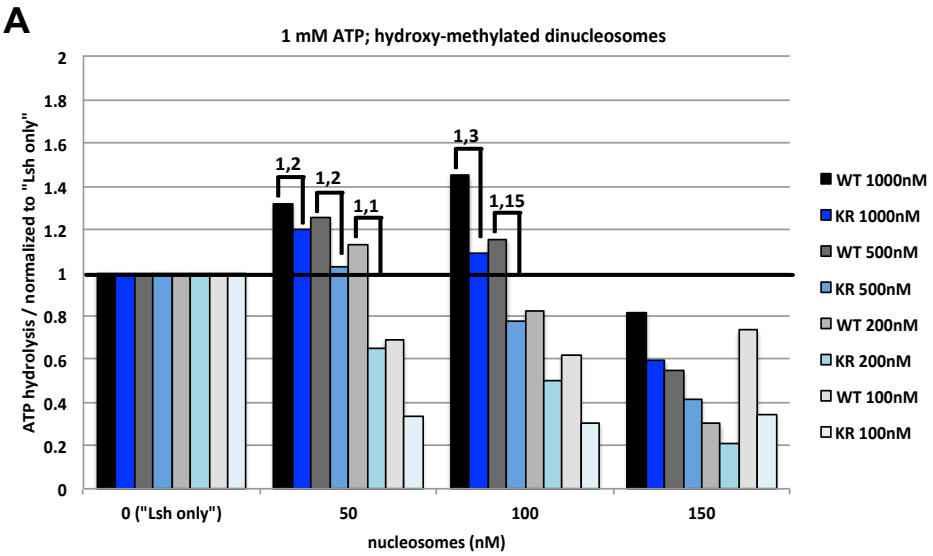

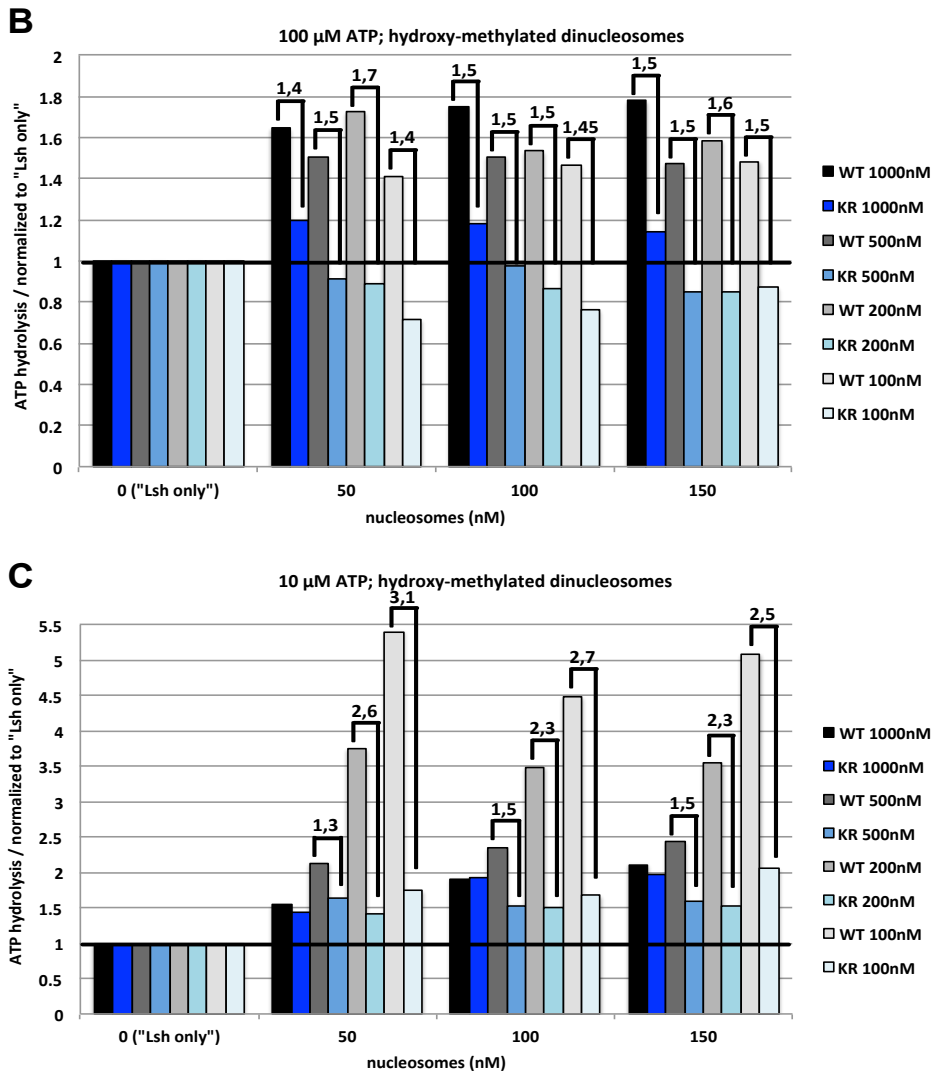

Fig 3.11: Analysis of the influence of hydroxy-methylated dinucleosomes on the ATPase activity of Lsh. The effect of hydroxy-methylated dinucleosomes on the ATPase activity of Lsh was studied at **(A)** 1mM ATP, **(B)** 100 µM ATP and **(C)** 10 µM ATP. Nucleosome concentrations varied from 50 to 150 nM, and concentrations of Lsh WT and KR varied from 100 nM to 1000 nM, as indicated. WT is illustrated in black and grey scale bars, KR in blue scale and white bars. Reactions were carried out in 10 µl volumes in the presence of the indicated amount of ATP (non-radioactive) and minor amounts of radioactive ATP (0.2 µCi/µl). Reactions were incubated for 45 min at 30 °C, then pipetted onto a TLC plate to separate the hydrolyzed phosphate from unreacted ATP. The percentage of hydrolyzed ATP was calculated according to the equation: $\%_{(\text{hydrolyzed ATP})} = P_i*100/(P_i + ATP_{\text{non-hydr}})$, and was corrected for background activity arising from non-radioactive ATP. Corrected values were then used to calculate the amount of hydrolyzed ATP in µM. Afterwards, values were normalized to “Lsh only” (WT and KR lacking nucleosomes). WT and corresponding KR were compared to each other, and calculated ratios are displayed, if values for WT are > 1 and exceed values for the corresponding KR. Values > 1 for WT were compared to “Lsh only” (corresponds to a value = 1, indicated by a black line), if values for the corresponding KR are < 1. Values < 1 can be ignored as signal intensities are weaker than for “Lsh only”.

Repeating the experiments (see Appendix) substantiated the findings. 5-hmC modified dinucleosomes have no strong stimulatory effect on Lsh ATPase activity in the presence of 1 mM ATP and 100 µM ATP. In contrast, 5-hmC modified dinucleosomes in combination with 10 µM ATP and specific Lsh concentrations enabled stimulation of Lsh WT ATPase activity that was about 2–3-fold higher relative to the activity of KR. This indicates that 5-hmC modified dinucleosomes can considerably stimulate Lsh, but only under very well defined experimental conditions.

3.8.2.3 The Lsh ATPase is not stimulated by methylated dinucleosomes

Using methylated dinucleosomes in various concentrations in combination with different protein concentrations and ATP concentrations of 1 mM ATP, 100 µM ATP and 10 µM ATP, the ratios of ATP hydrolysis levels of WT to ATP hydrolysis levels of KR were far below 2-fold (Figs 3.12 A–C). Therefore, methylated dinucleosomes represent an even weaker substrate and do not stimulate Lsh ATPase activity.

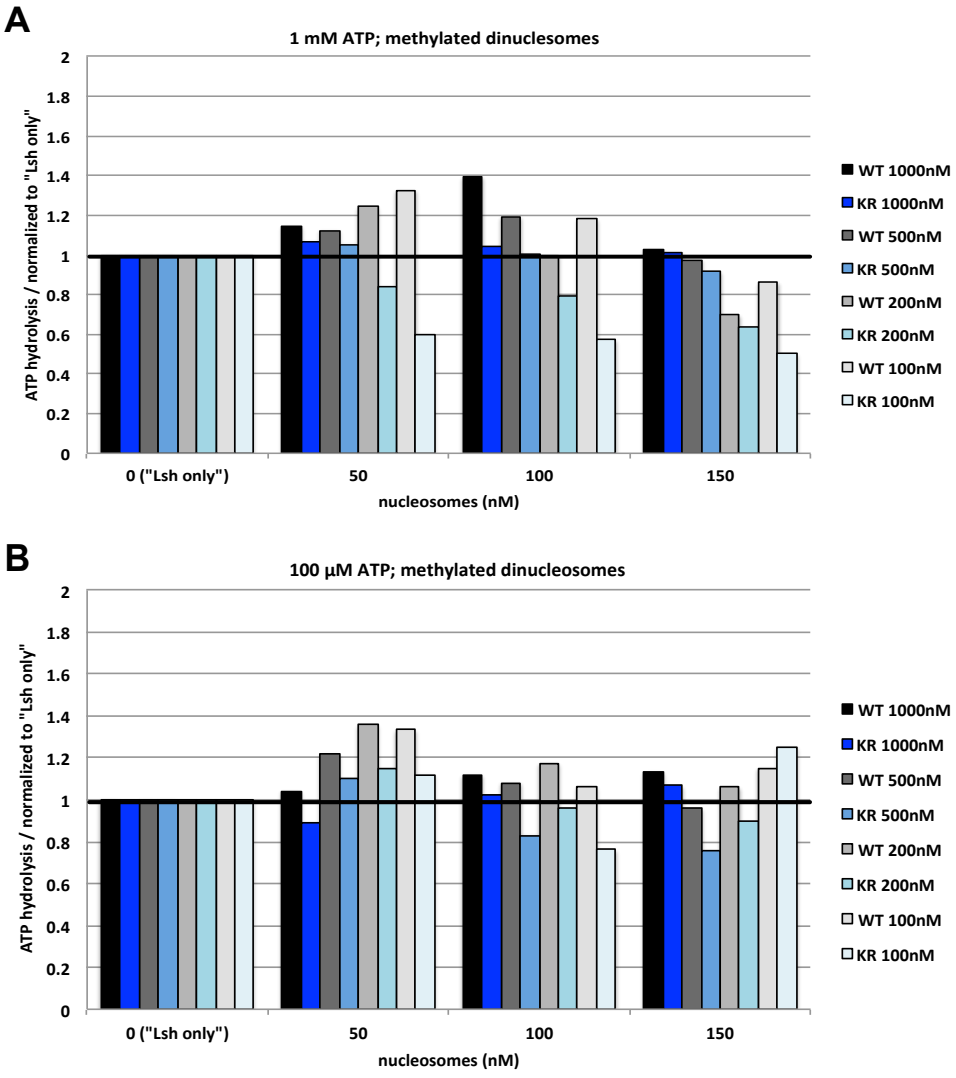

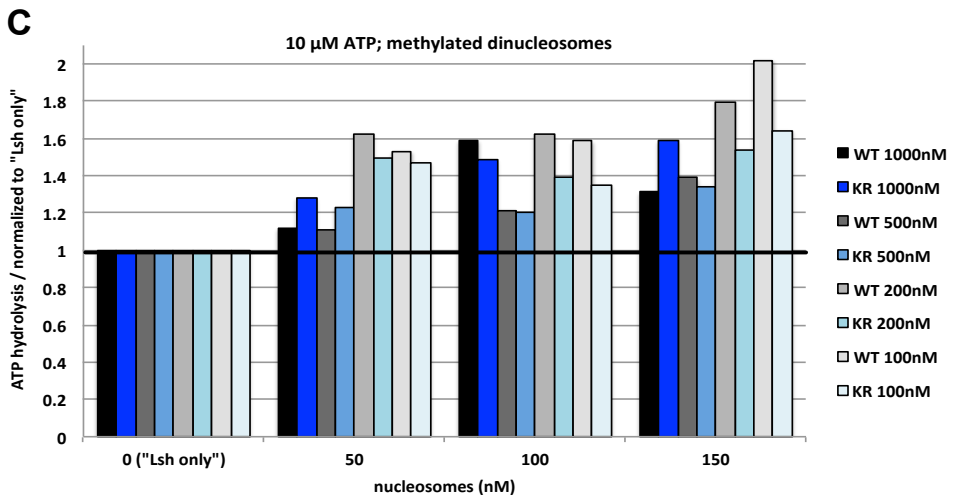

Fig 3.12: Analysis of the influence of methylated dinucleosomes on the ATPase activity of Lsh.
The effect of methylated dinucleosomes on the ATPase activity of Lsh was studied at **(A)** 1mM ATP, **(B)** 100 µM ATP and **(C)** 10 µM ATP. Nucleosome concentrations varied from 50 to 150 nM, and concentrations of Lsh WT and KR varied from 100 nM to 1000 nM, as indicated. WT is illustrated in black and grey scale bars, KR in blue scale and white bars. Reactions were carried out in 10 µl volumes in the presence of the indicated amount of ATP (non-radioactive) and minor amounts of radioactive ATP (0.2 µCi/µl). Reactions were incubated for 45 min at 30 °C, then pipetted onto a TLC plate to separate the hydrolyzed phosphate from unreacted ATP. The percentage of hydrolyzed ATP was calculated according to the equation: $\%_{(\text{hydrolyzed ATP})} = P_i*100/(P_i + ATP_{\text{non-hydr}})$, and was corrected for background activity arising from non-radioactive ATP. Corrected values were then used to calculate the amount of hydrolyzed ATP in µM. Afterwards, values were normalized to “Lsh only” (WT and KR lacking nucleosomes). WT and corresponding KR were compared to each other. Values > 1 for WT were compared to “Lsh only” (corresponds to a value = 1, indicated by a black line), if values for the corresponding KR are < 1. Values < 1 can be ignored as signal intensities are weaker than for “Lsh only”.

Taken together, this work shows biochemical analyses to unveil whether the proposed remodeling capability of Lsh plays a role in the interpretation of 5-hmC as an epigenetic mark that is suggested to recruit specific readers to direct changes in chromatin structure. In doing so, 5-hmC and 5-mC modified and unmodified substrates were used in *in vitro* binding studies and ATPase assays. Lsh shows higher binding affinity to 5-hmC and 5-mC modified DNA than to unmodified DNA, and its ATPase activity is relatively strongly stimulated by 5-hmC modified dinucleosomes. However, it is of note that considerable ATPase stimulation was only detected at an ATP concentration of 10 µM, indicating a low ATP hydrolysis rate.

3.9 The stimulation of the ATPase activity of Lsh is induced by RNA and enhanced by nucleosomes

At this point, it still remains unclear what kind of substrate is required to induce stimulation of Lsh ATPase activity at conditions that are closer to physiological ones, meaning ATP concentrations higher than 10 µM, at best in the millimolar range, implying a relative increase in the ATP hydrolysis rate. In addition, it has to be mentioned that relative and not absolute values of ATP hydrolysis have been inspected in the previous chapter, which was mainly due to the large amount of tested combinations.
Further screenings for ATPase activating substrates examined RNA as a potential target.

3.9.1 Lsh binds to single-stranded RNA with higher affinity than to DNA

To unveil if RNA is a candidate that could activate the ATPase function of Lsh, the binding affinity of Lsh to single-stranded (ss) RNA was initially investigated by EMSA (see 5.2.9.2.2). Increasing concentrations of Lsh were incubated with constant amounts of FAM labeled ssRNA with a size of about 30 bp, and reactions were analyzed on a 5% native PAA gel. As illustrated, Lsh binds the RNA forming a Lsh-RNA complex that is shifted to the well of the gel (Fig 3.13 A).

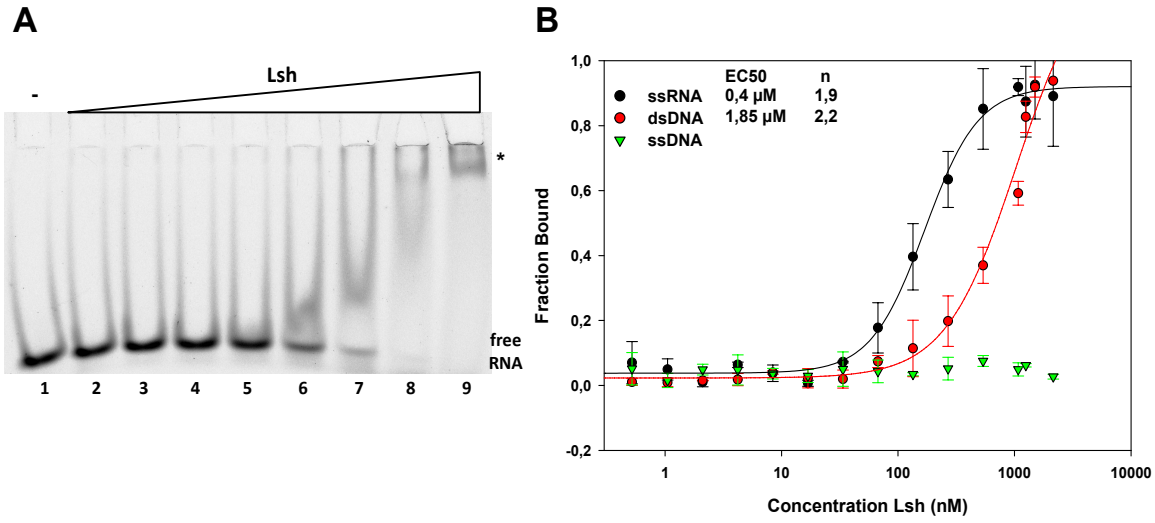

Fig 3.13: Binding affinities of Lsh to RNA and DNA.
(A) The binding affinity of Lsh to RNA was studied by EMSA. Increasing concentrations of Lsh (12.5 nM–1.6 µM) were titrated to 25 nM FAM labeled ssRNA of 30 bp in size (En3D_RNA). After incubation for 30 min at 30 °C protein-RNA complexes were separated from free RNA on a 5% native PAA gel. The gel was visualized on a fluorescence image reader. The protein-RNA complex shifted to the well of the gel is indicated by an asterisk. **(B)** Binding affinities of Lsh towards RNA and DNA were measured by MST. Increasing concentrations of Lsh (0.5 nM–2200 nM) were titrated to 40 nM of either ssRNA (En3D_RNA; FAM labeled), dsDNA (En3D_DNA; Cy5 labeled), or ssDNA (En3D_rev; Cy5 labeled). RNA and DNA substrates are of the same size (30 bp) and sequence. Reactions were incubated at 30 °C for 15 min before starting the measurement. For data evaluation, the thermophoresis signals were normalized to fraction bound (X) by X = (Y(c)-Min)/(Max-Min). EC_{50} values and Hill coefficients were obtained according to the Hill equation f = min+(max-min)/(1+(EC_{50}/abs(x))^n) and are indicated in line with the respective substrate. Each measurement was done in triplicates, each time using a different fraction of purified Lsh. Mean values and standard deviations were calculated.

In a next step, the binding affinity of Lsh towards ssRNA in comparison to the affinity of Lsh to dsDNA and ssDNA was analyzed by microscale thermophoresis (see 5.2.9.4). The ssRNA is FAM labeled, dsDNA and ssDNA are Cy5 labeled, and all the three nucleic acids have the same sequence and a size of 30 bp. Constant amounts of the respective nucleic acid were added to increasing concentrations of Lsh. The thermophoretic mobility was recorded on a Nanotemper device, and binding affinities were calculated by applying the Hill equation. Lsh binds to ssRNA with comparably high affinity exhibiting an EC_{50} value of 0.4 µM, whereas the dsDNA is bound with an affinity that is nearly 5 times lower (EC_{50} = 1.85 µM). Hill coefficients > 1 with negligible differences to each other indicate similar cooperative binding to ssRNA and dsDNA. Interestingly, ssDNA with the same size and same sequence as the ssRNA is not bound by Lsh, confirming the preferential binding of Lsh towards RNA (Fig 3.13 B).

3.9.2 The ATPase activity of Lsh is stimulated by total RNA

Observing binding of Lsh to a ssRNA oligonucleotide, RNA was used as substrate in ATPase assays. As it is not known what sort of RNA stimulates Lsh ATPase, total RNA was extracted with TRIzol® (Thermofisher) from two different types of cells, namely *D. melanogaster* and HeLa cells. The quality of isolated total RNA was analyzed by agarose gel electrophoresis (see 5.2.2). ATPase assays were performed with increasing concentrations of total RNA and constant amounts of Lsh (200 nM). Apart from this, assays were carried out as described (see 3.6.1 and 5.2.9.6). In most of the cases, about two times more ATP was hydrolyzed when RNA was present, if compared to the basal activity of Lsh, which was quite low. This indicates that RNA stimulates Lsh ATPase activity (Fig 3.14 A).

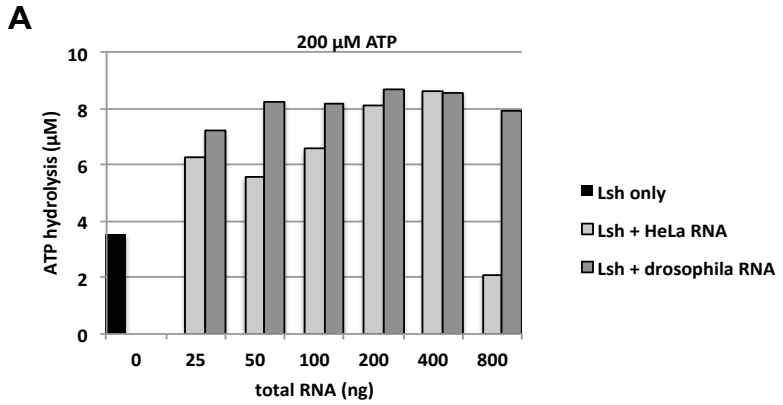

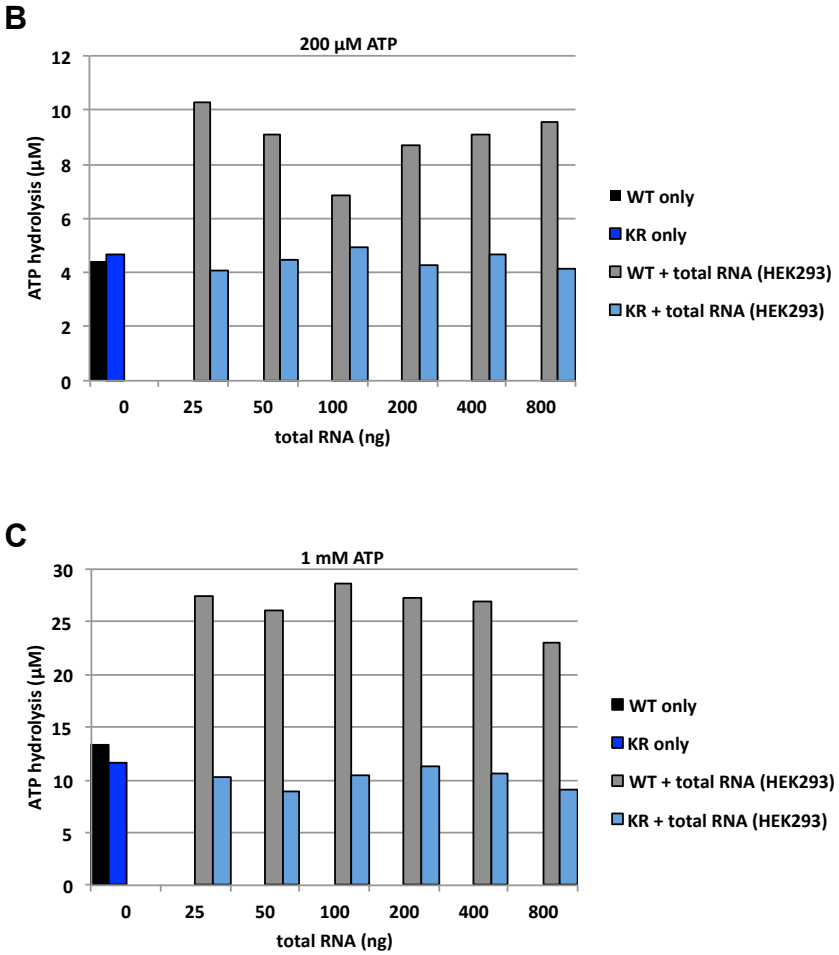

Fig 3.14: Effect of total RNA on the ATPase activity of Lsh.
The ATPase activity of Lsh was studied using total RNA as substrate. **(A)** Increasing amounts of total RNA (25 ng–800 ng) isolated from *D. melanogaster* and HeLa cells were incubated with 200 nM of Lsh WT in the presence of 200 µM non-radioactive ATP. **(B)** Increasing amounts of total RNA (25 ng–800 ng) isolated from HEK293 cells were incubated with 200 nM of Lsh WT (grey bars) and Lsh KR (light blue bars) in the presence of 200 µM non-radioactive ATP. **(C))** Increasing amounts of total RNA (25 ng–800 ng) isolated from HEK293 cells were incubated with 200 nM of Lsh WT (grey bars) and Lsh KR (light blue bars) in the presence of 1 mM non-radioactive ATP. Lsh WT (black bars) and Lsh KR (dark blue bars) lacking total RNA in the mixture served as controls. Reactions were incubated with minor amounts of radioactive ATP (0.2 µCi/µl) for 45 min at 30 °C in a volume of 10 µl, and were pipetted onto a TLC plate to separate hydrolyzed phosphate from unreacted ATP. Percentage of hydrolyzed ATP was calculated according to the equation: $\%_{(\text{hydrolyzed ATP})} = P_i*100/(P_i + ATP_{\text{non-hydr}})$, and was corrected for background activity arising from non-radioactive ATP and total RNA preparations. Corrected values were used to calculate hydrolyzed ATP in µM.

However, the KR mutant as an internal control was not integrated in these assays. Therefore, the assay was repeated but with total RNA isolated from HEK293 cells, and including the KR mutant. KR including total RNA displayed levels of hydrolyzed ATP that were comparable to the levels exhibited by Lsh WT and KR lacking RNA. Lsh WT was mostly about two times more active than KR (Fig 3.14 B), showing that Lsh WT is stimulated by total RNA and confirming that the KR mutant is basically inactive.
Since ATP concentrations in cells are in the millimolar range, an ATPase assay with total RNA isolated from HEK 293 cells was performed, this time with 1 mM ATP. The results of the assay demonstrate the ATPase activating effect of total RNA. In the presence of RNA, ATP hydrolysis levels exhibited by Lsh WT were at least two times higher than ATP

hydrolysis levels exhibited by KR (KR with and without RNA) and WT lacking RNA (Fig 3.14 C). To ensure that it is RNA that causes the ATPase stimulation and not a contamination coming from the preparation of the total RNA, the assay was repeated with preceding isolation of total RNA using the NucleoSpin® RNA isolation kit (Macherey-Nagel) instead of TRIzol. The results confirmed the findings of the previous assays (see Appendix).
Still, the question remains open how Lsh is mechanistically involved in DNA methylation. In view of the hypothesis that Lsh is a chromatin remodeler enabling Dnmts to methylate DNA, RNA could act as a trigger inducing Lsh ATPase activity, and could therefore be essential for the proposed chromatin remodeling function of Lsh. If Lsh was an RNA activated remodeler, Lsh would have to interact with both RNA and nucleosomes.

3.9.3 Lsh ATPase activity is enhanced by nucleosomes in the presence of total RNA

In order to find out, if the combination of RNA and nucleosomes leads to stimulation of Lsh ATPase activity exceeding the impact of RNA by its own, different nucleosomes (Table 3.2) combined with total RNA isolated from HEK293 cells were tested as substrates in ATPase assays.

nucleosome	complexity	modification
NPS-AvaI	mononucleosome	n/a
NPS-NotI	mononucleosome	n/a
77-NPS-77	mononucleosome	n/a
unmod 601-10n-601	dinucleosome	n/a
5-hmC 601-10n-601	dinucleosome	5-hmC
5-mC 601-10n-601	dinucleosome	5-mC
12x601	array	n/a

Table 3.2: Overview on nucleosomal substrates used in combination with total RNA in ATPase assays. The name of the nucleosome, its complexity (mono- or dinucleosome or nucleosomal array) and DNA modifications (none, hydroxy-methylated or methylated cytosine residues) on the substrate are indicated.

Nucleosomes were prepared as described (see 5.2.8) and were analyzed on 5% native PAA gels (Fig 3.15).

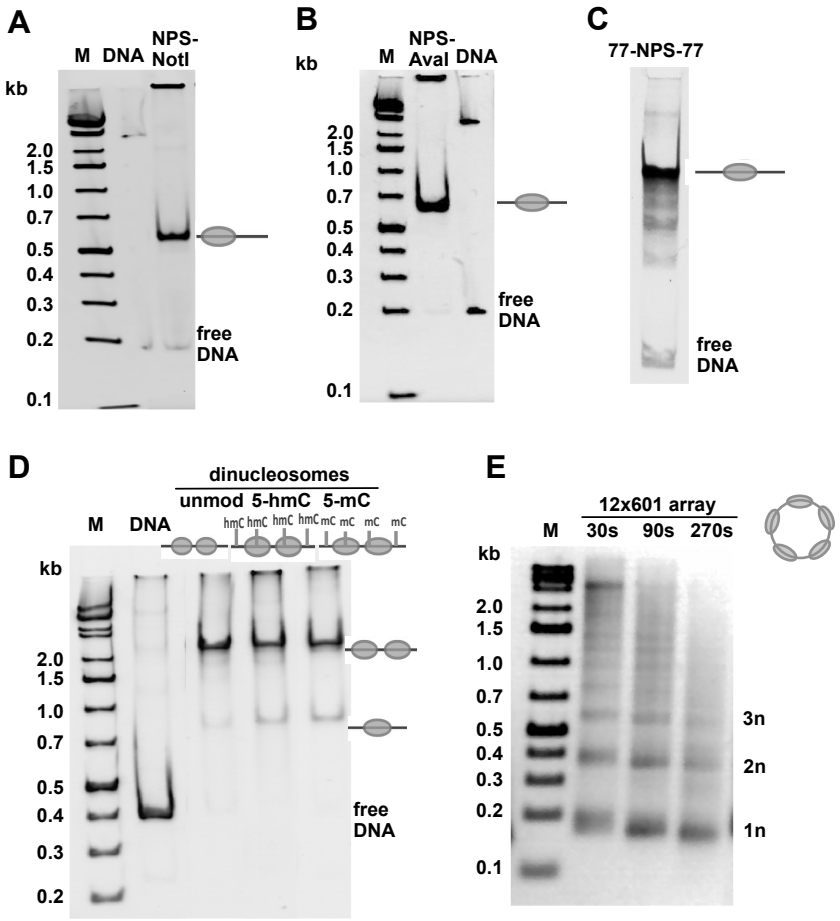

Fig 3.15: Nucleosome assemblies used in ATPase assays.
Nucleosomes were reconstituted on the DNA templates with chicken histones by salt gradient dialysis. **(A)** and **(B)** The DNA templates NPS-NotI and NPS-AvaI were generated by digesting the plasmid pUC18 12x601 either with NotI or AvaI. Nucleosomes were reconstituted, and assemblies were analyzed on 5% native PAA gels. The position of the nucleosome on the DNA fragment is outlined. **(C)** The DNA fragment 77-NPS-77 was generated by PCR, assembled into chromatin and analyzed on 5% native PAA gels. Nucleosome positions on the DNA fragments are illustrated. **(D)** To generate differently DNA modified dinucleosomes, hydroxy-methylated, methylated and unmodified templates were produced by PCR, incorporation of the modification was analyzed by restriction enzyme digestion, and nucleosomes were reconstituted on the DNA templates. Assemblies were analyzed on 5% native PAA gels. Unmod: Unmodified dinucleosome; 5-hmC: hydroxy-methylated dinucleosome; 5-mC: methylated dinucleosome. **(E)** Circular chromatin was assembled on pUC18 12x601 plasmid DNA, and the assembly was analyzed by the digestion of 2 µg of chromatin with MNase. Reaction was stopped after 30, 60 and 270 sec incubation time. After digestion with proteinase K, DNA was precipitated and analyzed on a 1.3% agarose gel stained with ethidium bromide. The nucleosomal ladder generated by MNase digestion is shown, and mono- di- and trinucleosomes are indicated (1n–3n).

In the activity assays, Lsh WT and KR as well as total RNA were kept constant, while nucleosomes were added in increasing concentrations. WT and KR without substrate (WT only and KR only) and only with total RNA as substrate (WT+RNA and KR+RNA) served as controls. Since the ATPase activity of Lsh is not induced by nucleosomes, Lsh WT and KR with nucleosomes as sole substrate were included as reference for comparison. As expected, Lsh WT was about two times more active than KR when only total RNA was present as substrate. Throughout the experiments, Lsh WT and KR in combination solely with nucleosomes showed ATPase activity that was similar to the basal activity of WT and KR lacking substrates (Figs 3.16 A–C).

A

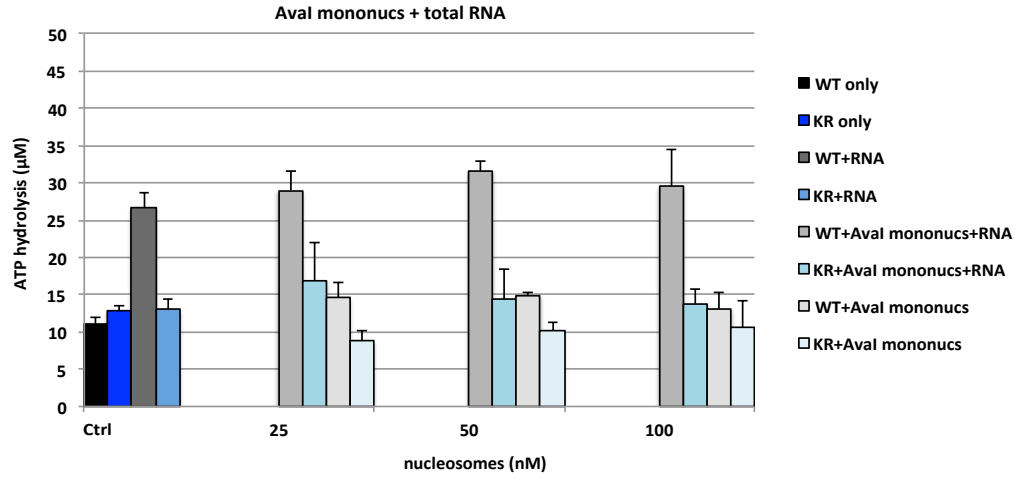
AvaI mononucs + total RNA
ATP hydrolysis (µM)
50
45
40
35
30
25
20
15
10
5
0
Ctrl
25
50
100
nucleosomes (nM)
WT only
KR only
WT+RNA
KR+RNA
WT+AvaI mononucs+RNA
KR+AvaI mononucs+RNA
WT+AvaI mononucs
KR+AvaI mononucs

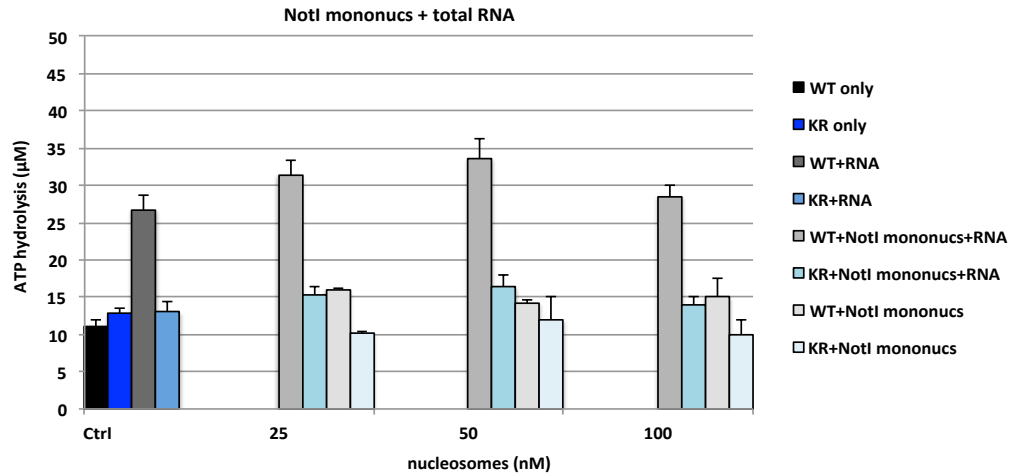
NotI mononucs + total RNA
ATP hydrolysis (µM)
50
45
40
35
30
25
20
15
10
5
0
Ctrl
25
50
100
nucleosomes (nM)
WT only
KR only
WT+RNA
KR+RNA
WT+NotI mononucs+RNA
KR+NotI mononucs+RNA
WT+NotI mononucs
KR+NotI mononucs

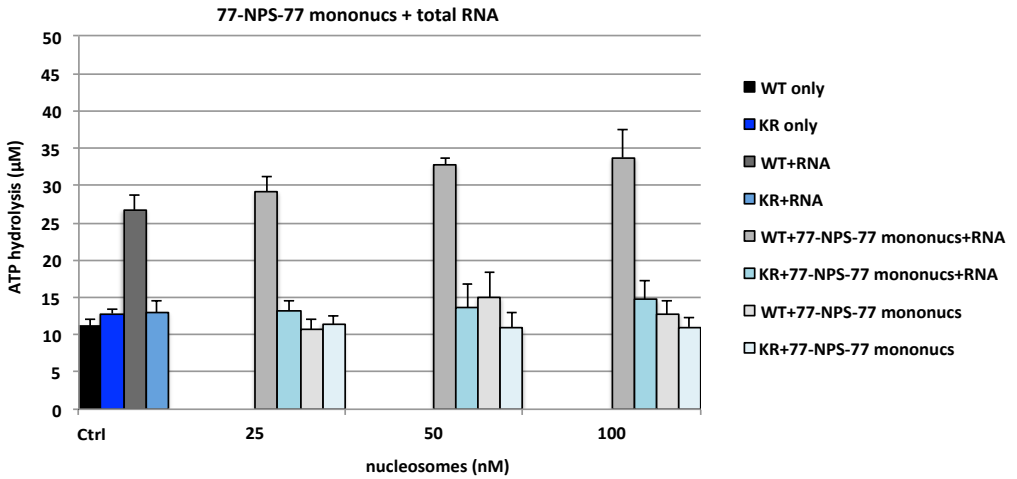
77-NPS-77 mononucs + total RNA
ATP hydrolysis (µM)
50
45
40
35
30
25
20
15
10
5
0
Ctrl
25
50
100
nucleosomes (nM)
WT only
KR only
WT+RNA
KR+RNA
WT+77-NPS-77 mononucs+RNA
KR+77-NPS-77 mononucs+RNA
WT+77-NPS-77 mononucs
KR+77-NPS-77 mononucs

B

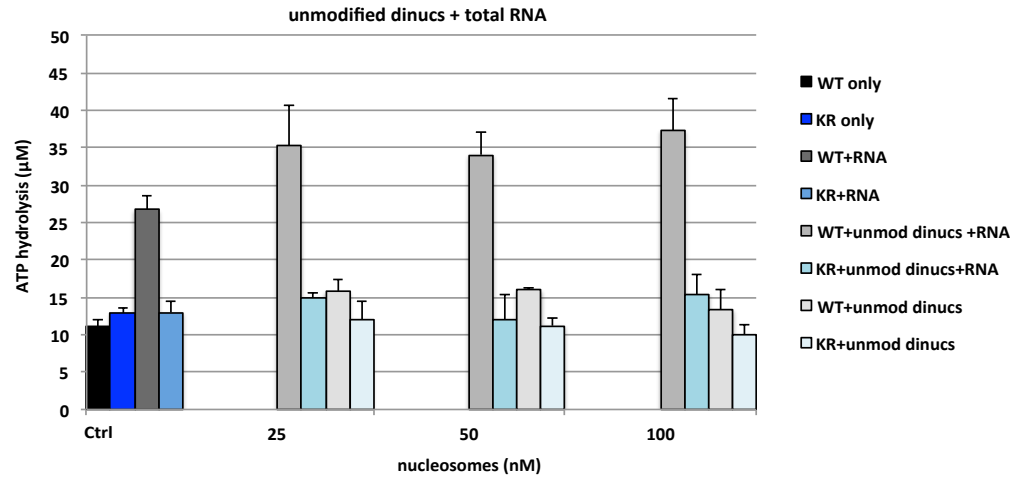
unmodified dinucs + total RNA
ATP hydrolysis (µM)
50
45
40
35
30
25
20
15
10
5
0
Ctrl
25
50
100
nucleosomes (nM)
WT only
KR only
WT+RNA
KR+RNA
WT+unmod dinucs +RNA
KR+unmod dinucs+RNA
WT+unmod dinucs
KR+unmod dinucs

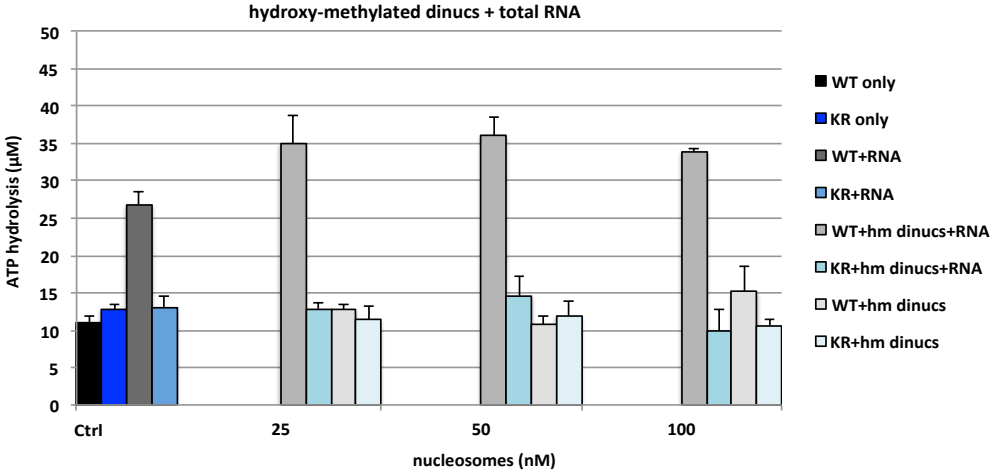
hydroxy-methylated dinucs + total RNA
ATP hydrolysis (µM)
50
45
40
35
30
25
20
15
10
5
0
Ctrl
25
50
100
nucleosomes (nM)
WT only
KR only
WT+RNA
KR+RNA
WT+hm dinucs+RNA
KR+hm dinucs+RNA
WT+hm dinucs
KR+hm dinucs

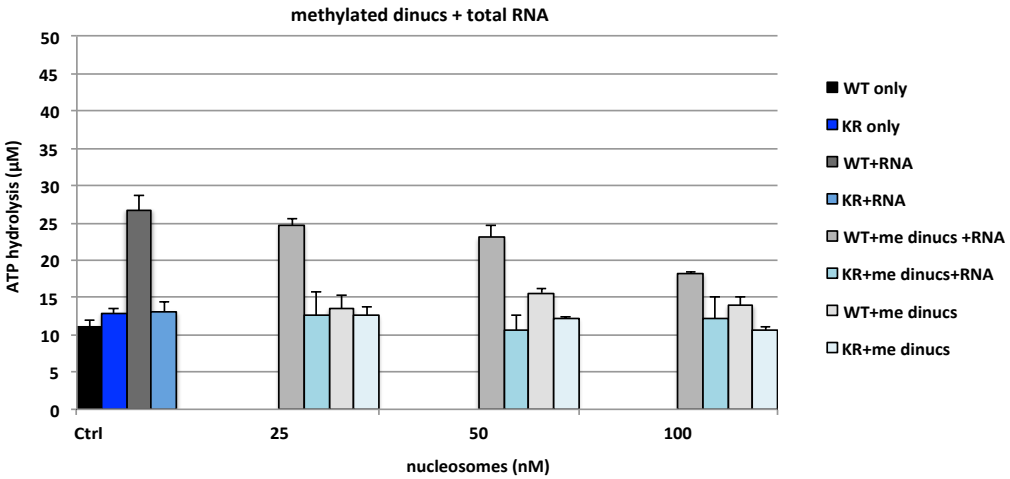
methylated dinucs + total RNA
ATP hydrolysis (µM)
50
45
40
35
30
25
20
15
10
5
0
Ctrl
25
50
100
nucleosomes (nM)
WT only
KR only
WT+RNA
KR+RNA
WT+me dinucs +RNA
KR+me dinucs+RNA
WT+me dinucs
KR+me dinucs

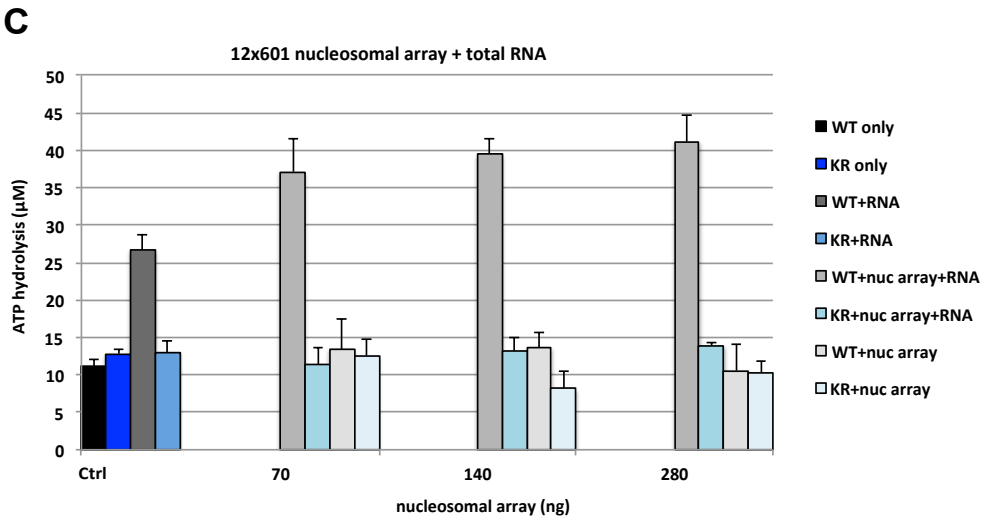

Fig 3.16: Effect of total RNA in combination with nucleosomes on the ATPase activity of Lsh.
The ATPase activity of Lsh was studied using combinations of total RNA and nucleosomes as substrates. Increasing amounts of **(A)** mononucleosomes (25 nM–100 nM of NPS-AvaI; upper panel, NPS-NotI; middle panel, and 77-NPS-77; lower panel), **(B)** dinucleosomes (25 nM–100 nM of unmodified dinucs; upper panel, hydroxy-methylated dinucs; middle panel, and methylated dinucs; lower panel) and **(C)** nucleosomal array (70–140 ng of 12x601 nuc array) were incubated with 200 nM of Lsh WT or Lsh KR in the presence (grey and turquoise bars) or absence (light grey and white bars) of total RNA isolated from HEK293 cells. Lsh WT (black bars) and Lsh KR (dark blue bars) lacking total RNA as well as Lsh WT+RNA (dark grey bars) and Lsh KR+RNA (light blue bars) served as controls. Mixtures contained 1 mM non-radioactive ATP and minor amounts of radioactive ATP (0.2 µCi/µl) and were incubated for 45 min at 30 °C in a total volume of 10 µl. Reactions were pipetted onto a TLC plate to separate the hydrolyzed phosphate from unreacted ATP. The percentage of hydrolyzed ATP was calculated according to the equation: $\%_{(\text{hydrolyzed ATP})} = P_i*100/(P_i + ATP_{\text{non-hydr}})$, and was corrected for background activity arising from non-radioactive ATP and total RNA preparations. Corrected values were then used to calculate the amount of hydrolyzed ATP in µM. Experiments were carried out in biological triplicates, each time using a different fraction of purified Lsh WT and KR, and mean values of hydrolyzed ATP in µM and standard deviations were calculated.

AvaI mononucleosomes did not cause additional ATPase activation when they were combined with RNA (Fig 3.16 A, upper panel). In comparison to levels of WT+RNA, ATP hydrolysis levels were increased to some extent when Lsh WT was incubated with NotI mononucleosomes and RNA. Yet, there were also minor increases in ATP hydrolysis levels exhibited by the KR mutant when the mutant was combined with RNA and NotI mononucleosomes (Fig 3.16 A, middle panel). With increasing concentrations, the 77-NPS-77 nucleosomal substrate appears to slightly increase WT ATPase activity in the presence of RNA (Fig 3.16 A, lower panel). However, in a sum, the addition of mononucleosomes does not seem to result in a stimulation of Lsh WT ATPase activity that clearly exceeds the impact of RNA alone on the ATPase activity of Lsh.
ATPase assays with differently DNA modified dinucleosomes displayed a divergent picture. Unmodified and hydroxy-methylated dinucleosomes combined with total RNA enhanced WT ATPase activity, and this effect was stronger than the effect of the 77-NPS-77 mononucleosome. (Fig 3.16 B, upper panel and middle panel). With a view to the suggested active involvement of Lsh in DNA demethylation (Spruijt et al., 2013) but also considering the interpretation of 5-hmC as an epigenetic mark, it is to note that

differences in the modification status of the DNA template, unmodified or hydroxy-methylated, had no influence on ATPase activity (Fig 3.16 B, upper panel and middle panel). This argues against a participation of Lsh in DNA demethylation and questions whether Lsh responds to the epigenetic signaling function of 5-hmC by mobilizing nucleosomes. Interestingly, methylated dinucleosomes rather seem to repress RNA induced ATPase activity, especially at higher nucleosome concentrations (Fig 3.16 B, lower panel).
Stimulation of Lsh ATPase activity was even more pronounced when total RNA was combined with a nucleosomal array. The ATPase activity of WT was consistently three times stronger relative to the activity of WT and KR lacking substrates, and also relative to the activity of KR that was incubated with total RNA and nucleosomal array (Fig 3.16 C). Taken together, the results indicate a stimulatory effect of nucleosomes on RNA-induced ATPase activity of Lsh. Furthermore, boosting impacts of nucleosomes on the Lsh ATPase appear to depend on the complexity of the nucleosomal substrate.

3.9.4 Competitive binding of RNA, naked DNA and nucleosomal DNA to Lsh

The capability of Lsh to bind nucleosomal DNA and RNA has been demonstrated (Fig 3.4 and Fig 3.13). Nevertheless, the binding experiments were performed independently of each other. To figure out how RNA and nucleosomes have an influence on each other's interaction with Lsh we aimed to study the binding behavior of Lsh to RNA in the presence of nucleosomal DNA *in vitro*. Therefore, the binding of Lsh to RNA was first examined in the presence of naked DNA by performing competitive EMSAs (see 5.2.9.3). Cy5 labeled dsDNA and FAM labeled ssRNA oligonucleotides of the same size and sequence served as substrates. First, a Lsh-RNA complex was built by incubating Lsh with RNA, using a ratio of concentrations that would result in a band shift in the gel indicating the formation of a complex as previously demonstrated (see chapter 3.9.1; Fig 3.13 A). Afterwards the Lsh-RNA complex was added to increasing concentrations of dsDNA. Binding reactions were analyzed on native PAA gels by scanning both of the fluorescent signals. Images were merged, in order to present them as an overlay picture. To view all image details, images are also shown individually (Fig 3.17).

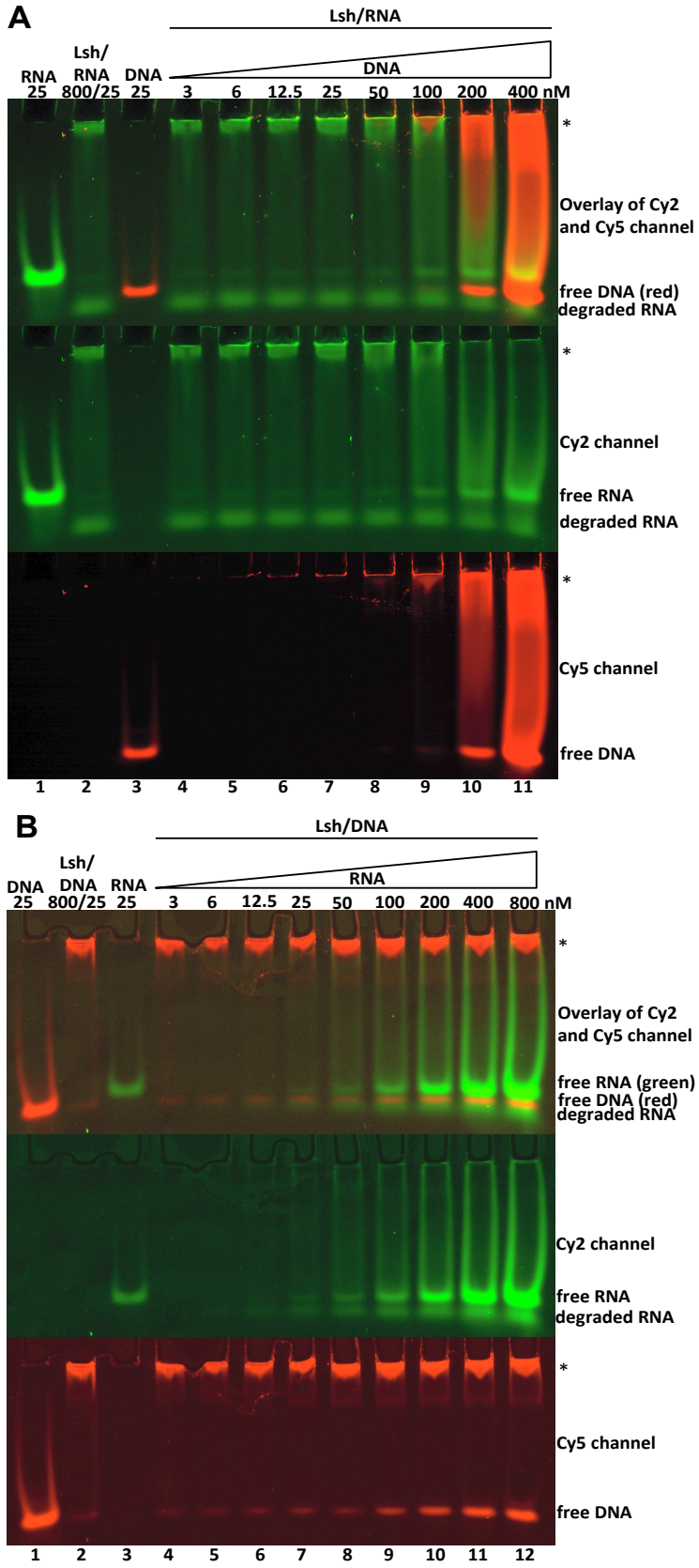

Fig 3.17: Competitive binding of RNA and DNA to Lsh.
The influence of RNA and DNA on their respective interaction with Lsh was studied in competitive EMSAs. **(A)** Increasing conentrations (3–400 nM) of a 30 bp long Cy5 labeled dsDNA oligonucleotide (En3D_DNA) were incubated with a pre-formed complex of Lsh (800 nM) and a 30 bp FAM labeled ssRNA (En3D_RNA; 25 nM). **(B)** Increasing concentrations (3–800 nM) of 30 bp long FAM labeled ssRNA oligonucleotide (En3D_RNA) were incubated with a pre-formed complex of Lsh (800 nM) and 30 bp long Cy5 labeled dsDNA (En3D_DNA; 25 nM).

The RNA and DNA as well as Lsh/RNA and Lsh/DNA complexes served as controls. Reactions were incubated for 15 min at 30 °C, loaded on 5% native PAA gels and analyzed by fluorescence scanning. Gel images are illustrated as channel overlays (upper panels) and single representation of channels (middle panels and lower panels). Free DNA, free RNA and degraded RNA are indicated. Asterisks indicate complex formations.

As expected, Lsh forms a complex with RNA that shifts to the well of the gel (Fig 3.17 A, lane 2). The DNA begins to displace the RNA at a molar ratio of 4:1 of DNA:RNA (100 nM DNA:25 nM RNA) (Fig 3.17 A, lane 9) until all of the RNA is set free and the DNA exists in excess amounts (Fig 3.17 A, lanes 10 and 11). However, even at a molar ratio of 4:1 some of the RNA still seems to be bound by Lsh, as fluorescent signals overlap (Fig 3.17 A, lane 9). Overlapping signals plus the displacement of RNA at increased DNA concentrations suggest that both substrates interact with the same binding site of Lsh.
Next, the vice-versa experiment was done, building a Lsh-DNA complex (Fig 3.17 B, lane 2) and incubating the Lsh-DNA complex with increasing concentrations of RNA. The DNA remains associated with Lsh even at excess amounts of RNA (Fig 3.17 B, lanes 10–12), although some of the DNA is released, starting at a molar ratio of DNA to RNA of 1:4 (25 nM DNA:100 nM RNA) (Fig 3.17 B, lanes 9–12). In conclusion, this competitive EMSA indicates that Lsh and DNA form a stable complex, and RNA as a second binding partner is not able to remove the DNA from its binding site, or at least not completely.
At first glance, the result appears to be contradictory to the findings that Lsh binds to ssRNA with higher affinity than to dsDNA (see chapter 3.9.1, Fig 3.13 B). Usually, high affinity interactions imply fast complex formation (high on-rate) combined with slow complex dissociation (slow off-rate). However, high affinity binding can also be characterized by a high on-rate and a high off-rate. Assuming that a second binding partner reveals slow on- and off-rates, one would obtain the following picture: Since the MST data suggest faster binding of Lsh to RNA than to dsDNA, RNA is bound to Lsh relatively quickly but the half-life of the complex is probably quite short (high on/off-rate). Thus, a competing binding partner is able to displace the RNA. The comparably slower binding of Lsh to dsDNA could be explained with a slow on-rate, which is usually accompanied by a slow off-rate. This would mean, once the Lsh-DNA complex is formed, the complex is relatively stable. Hence, the Lsh-DNA complex may have a relatively long half-life, which is why displacement of the DNA was not observed in the competitive binding assays.
Following the competitive EMSAs with RNA and naked DNA, competitive EMSAs were performed again with RNA, but this time using nucleosomal DNA instead of naked DNA (Fig 3.18).

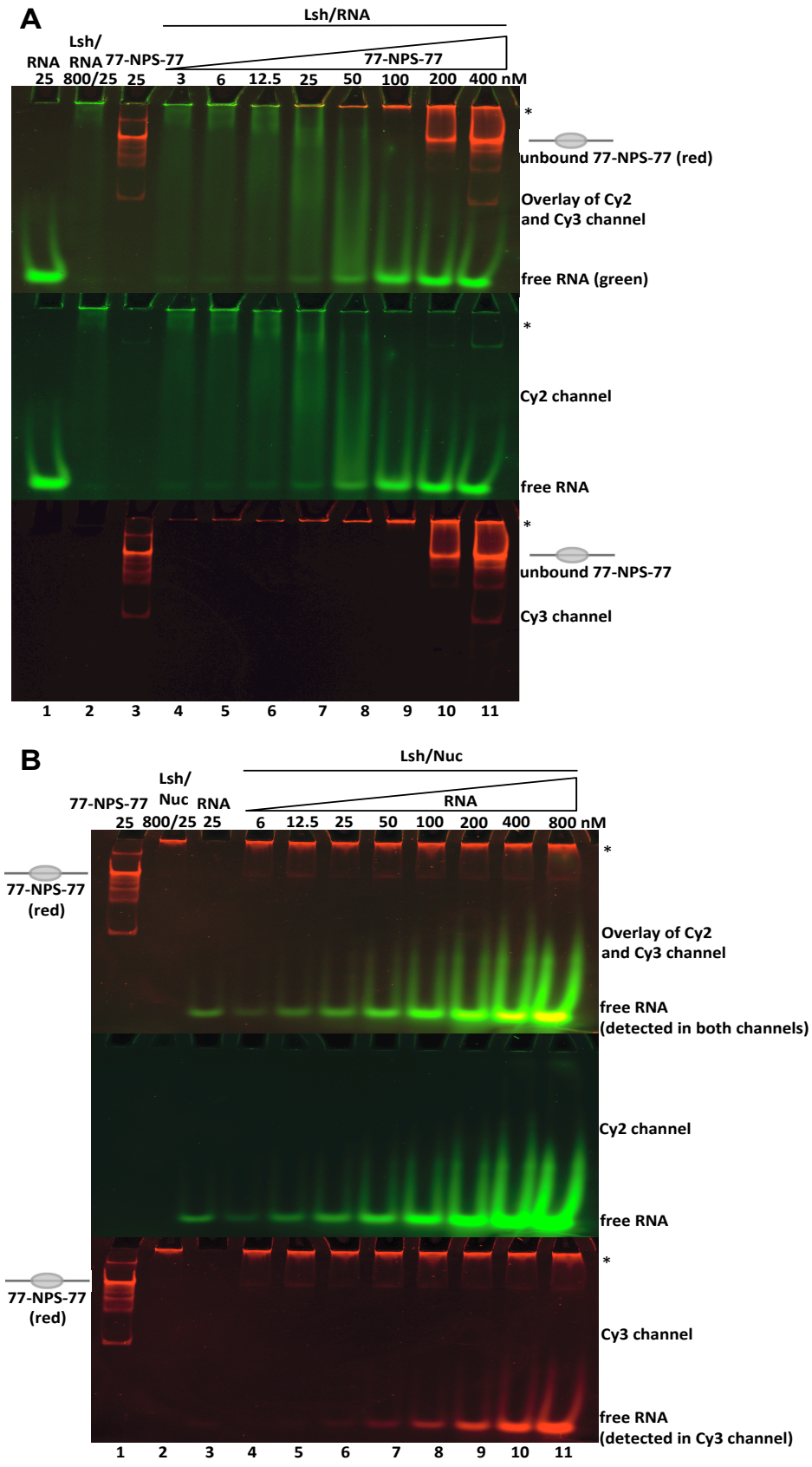

Fig 3.18: Competitive binding of RNA and nucleosomes to Lsh.
The influence of RNA and nucleosomes on their respective interaction with Lsh was studied in competitive EMSAs. **(A)** Increasing concentrations (3–400 nM) of a Cy3 labeled mononucleosome (77-NPS-77) were incubated with a pre-formed complex of Lsh (800 nM) and a 30 bp FAM labeled ssRNA (En3D_RNA; 25 nM).

(B) Increasing concentrations (6–800 nM) of 30 bp FAM labeled ssRNA oligonucleotide (En3D_RNA) were incubated with a pre-formed complex (referred to as Lsh/Nuc) of Lsh (800 nM) and Cy3 labeled 77-NPS-77 (25 nM). RNA and 77-NPS-77 as well as Lsh/RNA and Lsh/Nuc complexes served as controls. Reactions were incubated for 15 min at 30 °C, loaded on 5% native PAA gels and analyzed by fluorescence scanning. Gel images are illustrated as channel overlays (upper panels) and single representation of channels (middle panels and lower panels). Unbound nucleosome and RNA are indicated. Asterisks indicate complex formations.

The FAM labeled RNA was incubated with Lsh in order to form a complex that was added to increasing amounts of Cy3 labeled nucleosomal DNA. For this purpose, the 77-NPS-77 nucleosome was chosen, a nucleosome bound quite well by Lsh (see Figs 3.5 D and F). RNA remains associated with Lsh at lower nucleosome concentrations, up to a molar ratio of nucleosome to RNA of 1:1 (25 nM nucleosomes:25 nM RNA). At a molar ratio of 1:1, fluorescent signals overlap in the well of the gel, pointing to a simultaneous binding of RNA and nucleosome by Lsh at this stage (Fig 3.18 A, lane 7). Then, the nucleosome begins to displace the RNA (Fig 3.18 A, lane 8) until the RNA is completely released and the nucleosome is present in excess amounts (Fig 3.18 A, lanes 9 to 11). The result indicates that RNA and nucleosomal DNA interact with the same binding region of Lsh. In the vice-versa experiment with a Lsh-nucleosome complex and increasing concentrations of ssRNA, the nucleosome remained stably bound and was not displaced by the RNA, not even at excess amounts of RNA (Fig 3.18 B).

Considering the individual MST experiments, Lsh seems to bind to ssRNA with higher affinity than to the 77-NPS-77 nucleosome (see Figs 3.4 F and 3.13 B). However, these experiments were not done in parallel, which may be delicate in terms of an interpration as direct comparisons. However, if one again assumes a high on/off-rate when Lsh binds to RNA and a comparably slow on/off-rate when Lsh binds to nucleosomes, the MST data and the results of the competitive EMSAs fit together, as explained previously.

The competitive binding assays presented in this chapter did not include ATP in the reaction buffer. Since RNA stimulates the ATPase activity of Lsh *in vitro*, competitive binding behavior of Lsh to RNA and naked DNA or nucleosomal DNA might change in the presence of ATP. This is why ATP was included in the binding assays presented in the following.

3.9.5 The capability of Lsh to hydrolyze ATP improves the binding affinity of Lsh towards RNA

To figure out whether the capability to hydrolyze ATP makes an impact on the binding of Lsh to RNA and nucleosomes, EMSAs were performed in the presence of ATP, and binding affinities of Lsh WT and Lsh KR were compared. FAM labeled RNA and a Cy3 labeled nucleosome (77-NPS-77) were used as substrates. First, the binding of WT and KR to the 77-NPS-77 nucleosome was analyzed by adding increasing concentrations of either WT or KR to constant amounts of nucleosome. Reactions were loaded on 5% native PAA gels, and gels were documented on a laser scanner. WT and KR appear to have similar binding affinities towards the 77-NPS-77 nucleosome (Fig 3.19), which was expected as nucleosomes by their own do not stimulate Lsh ATPase.

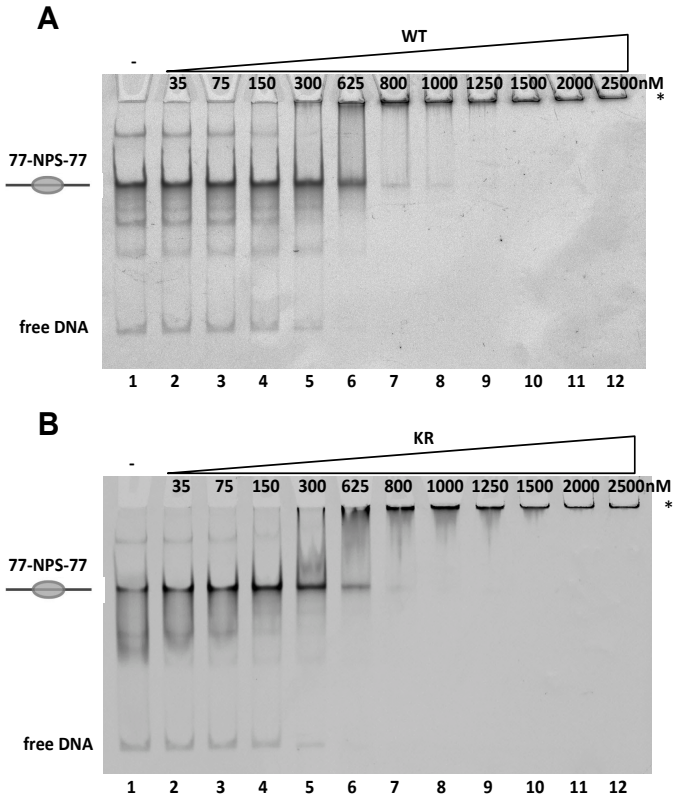

Fig 3.19: Binding affinity of Lsh towards nucleosomes in the presence of ATP.
The binding of Lsh to mononucleosomal DNA in the presence of ATP was studied by EMSA. Increasing concentrations (35 nM–2.5 µM) of **(A)** Lsh WT and **(B)** Lsh KR mutant were incubated with constant amounts of Cy3 labeled mononucleosomal DNA (77-NPS-77; 25 nM) in the presence of 1 mM ATP for 30 min at 30 °C. Reactions were analyzed on 5% native PAA gels and visualized by fluorescence scanning. Asterisks indicate protein-nucleosome complexes.

EMSAs using the RNA as substrate revealed minor but detectable differences in the binding behavior of Lsh WT in comparison to KR. Retarded mobility due to complex formation and the entire shift of the complex to the well of the gel appear to happen at lower concentrations of WT (Fig 3.20 A) relative to concentrations of KR (Fig 3.20 B).
The findings suggest that the capability to hydrolyze ATP is beneficial to the binding affinity of Lsh towards RNA.

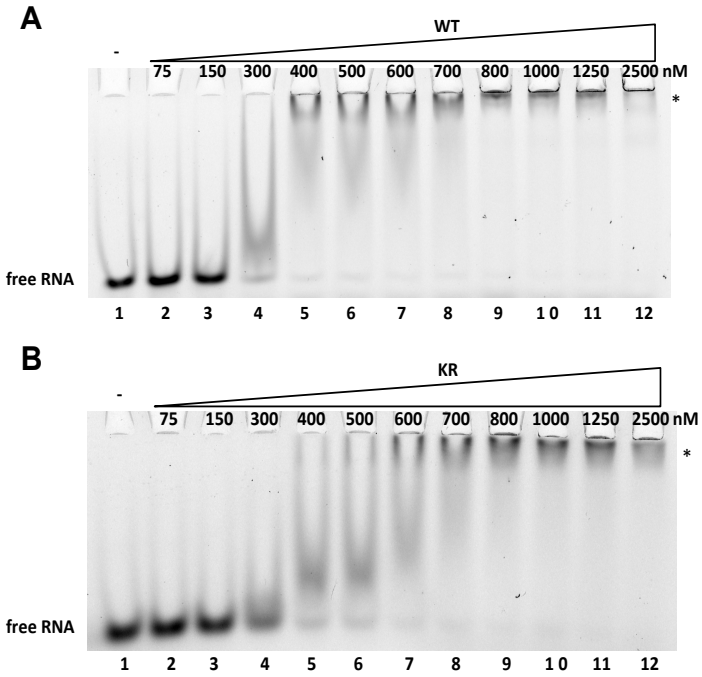

Fig 3.20: Binding affinity of Lsh towards RNA in the presence of ATP.
The binding of Lsh to ssRNA in the presence of ATP was studied by EMSA. Increasing concentrations (75 nM–2.5 µM) of **(A)** Lsh WT and **(B)** Lsh KR mutant were incubated with constant amounts of FAM labeled 30 bp long ssRNA (En3D_RNA; 25 nM) in the presence of 1 mM ATP for 30 min at 30 °C. Reactions were analyzed on 5% native PAA gels and visualized by fluorescence scanning. Asterisks indicate protein-RNA complexes that are shifted to the well of the gel.

In competitive EMSAs with pre-incubated Lsh-RNA complexes (WT/RNA in Fig 3.21 A, and KR/RNA in Fig 3.21 B) and increasing amounts of nucleosome, it seems that in comparison to KR, higher amounts of nucleosome are needed to completely displace the RNA from WT (Fig 3.21). In consequence of the higher binding affinity of RNA to WT than to KR (see Fig 3.20) and more rapidly occuring dissociation of RNA from KR than from WT in the presence of ATP, the results emphasize the importance of RNA for nucleosome-enhanced ATPase activity.

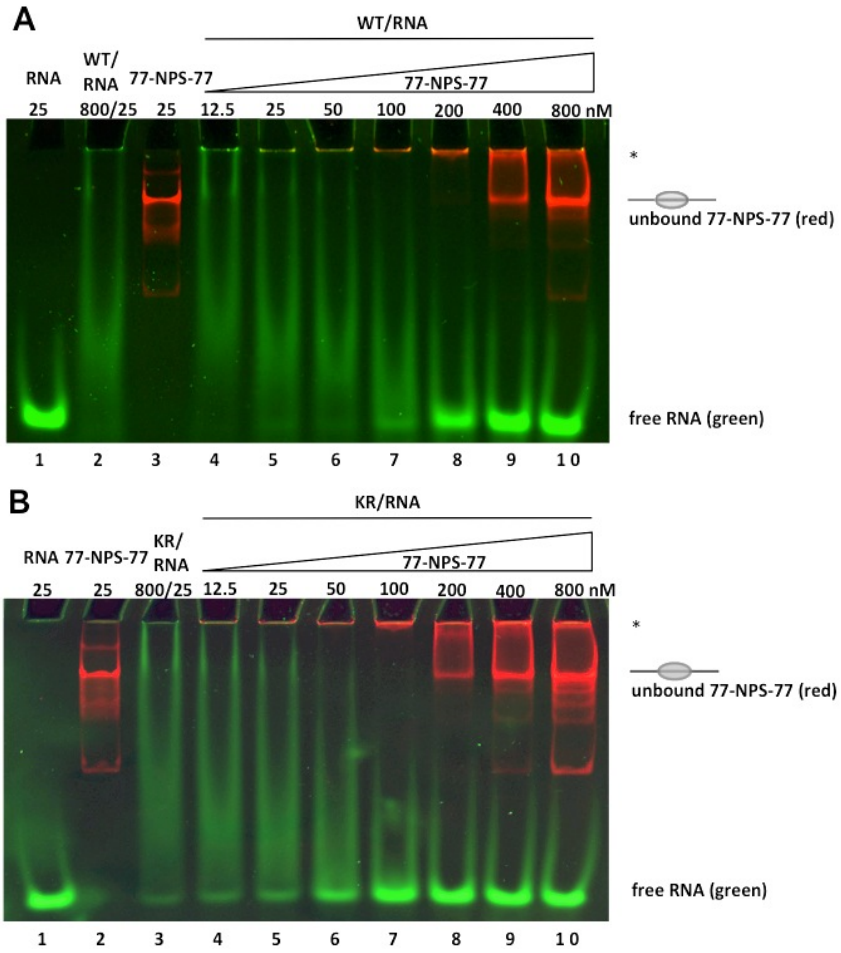

Fig 3.21: Competitive binding of RNA and nucleosomes to Lsh in the presence of ATP.
The influence of RNA and nucleosomes on each other's interaction with Lsh in the presence of ATP was studied in competitive EMSAs. Increasing conentrations (12.5–800 nM) of Cy3 labeled mononucleosomal DNA (77-NPS-77) were incubated with a pre-formed complex of **(A)** Lsh WT (800 nM) and 30 bp long FAM labeled ssRNA (25 nM) and **(B)** Lsh KR mutant (800 nM) and 30 bp long FAM labeled ssRNA (En3D_RNA; 25 nM) for 15 min at 30 °C. RNA, 77-NPS-77 as well as WT/RNA and KR/RNA complexes served as controls. Reactions were loaded on 5% native PAA gels and analyzed by fluorescence scanning. Gel images are illustrated as channel overlays. Unbound nucleosome and RNA are indicated. Asterisks indicate complexes shifted to the wells of the gel.

3.9.6 Lsh ATPase activity is preferentially induced by structured RNAs

To figure out how RNA structure influences the enzyme's ATPase activity, differently structured RNAs of different length were tested in ATPase assays. Two different about 60 nt long RNAs that form stem-loops in solution (L10 and L17; precursor-microRNAs from *D. melanogaster*) and two about 500 nt long, GC rich and highly structured RNAs that depict parts from the long non-coding RNA TINCR (T546 and T3460; (Kretz et al., 2013)), as well as a 30 nt long single stranded RNA that is unable to-fold into stem-loops (En3D) served as substrates. RNA secondary structures were predicted on the RNAfold web server (http://rna.tbi.univie.ac.at/cgi-bin/RNAfold.cgi) (Lorenz and Bernhart, 2011), using the program's default parameters and are illustrated in Fig 3.22. Values for the calculated minimum free energy (MFE) are indicated.

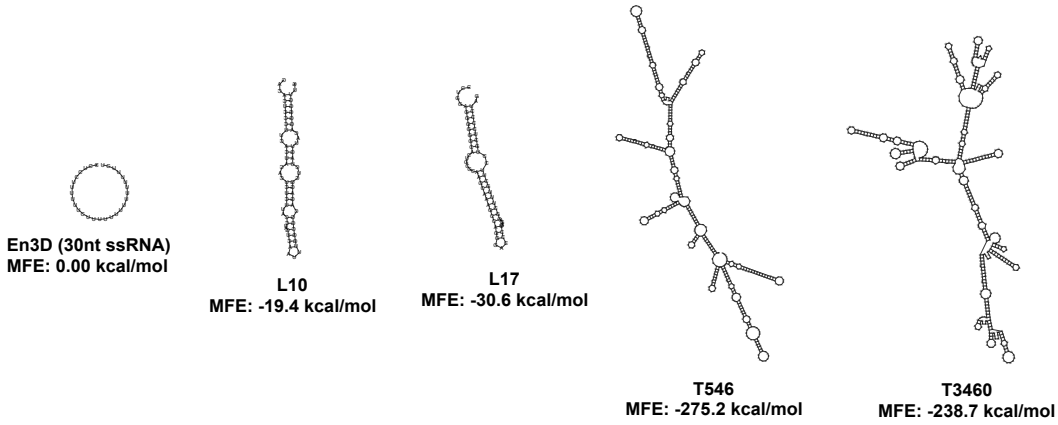

Figure 3.22: Predicted secondary structures and minimum free energy values of the individual RNAs. Secondary structures including the corresponding minimum free energy were predicted with RNAfold.

RNAs L10, L17, T546 and T3460 were a gift from Thomas Treiber from the department Biochemistry I, who prepared the RNAs by *in vitro* transcription followed by gel purification. Overall, KR mutant combined with RNA exhibited only basal ATPase activity. Points in the titration series, where the mutant shows levels of hydrolyzed ATP that are fairly below levels of KR lacking RNA (KR only), are due to a certain background activity coming from the purification of the structured RNAs. Background activity exclusively arising from RNA was substracted from ATP hydrolysis levels exhibited by WT and KR that were incubated with RNA. The results of the ATPase assays with the stem-loop forming RNAs L10 and L17 as substrates overall showed a stimulation of WT ATPase activity that was about twice as high as basal activity (Fig 3.23 A).

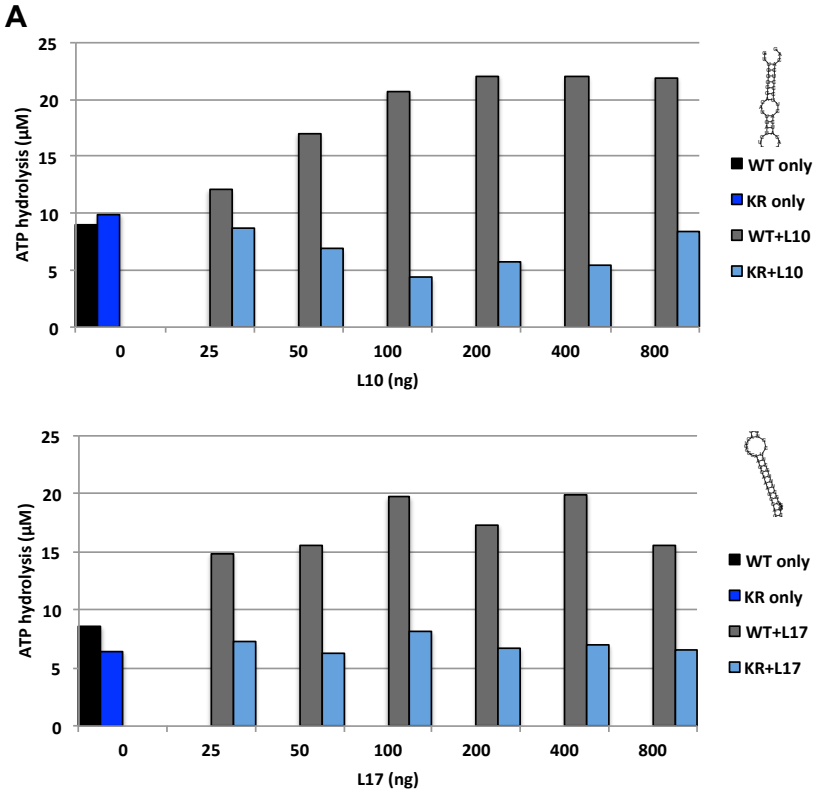

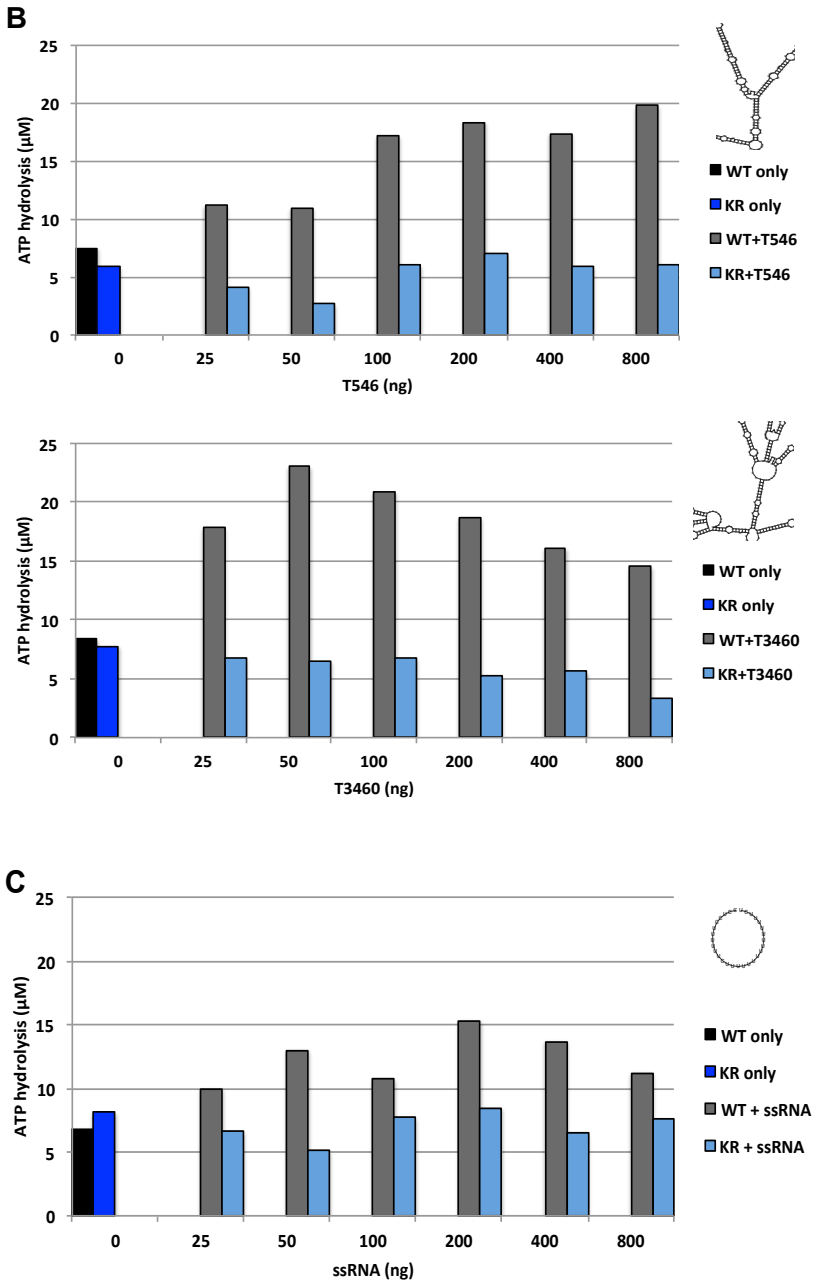

Fig 3.23: Effects of structured RNAs on the ATPase activity of Lsh.
The influence of differently structured RNAs on the ATPase activity of Lsh was studied in ATPase assays. 200 nM of Lsh WT or Lsh KR were incubated with increasing amounts (25 ng–800 ng) of **(A)** ~ 60 nt long stem-loop forming RNAs (L10; upper panel, and L17; lower panel) **(B)** ~ 500 nt long, GC rich and highly structured parts from the long non-coding RNA TINCR (T546; upper panel, and T3460; lower panel) and **(C)** a 30 nt long ssRNA (En3D_RNA) in the presence of 1 mM non-radioactive ATP and minor amounts of radioactive ATP (0.2 µCi/µl) for 45 min at 30 °C in a total volume of 10 µl. Lsh WT (black bars) and Lsh KR (dark blue bars) lacking RNA in the mixture served as controls. Reactions were pipetted onto a TLC plate to separate the hydrolyzed phosphate from unreacted ATP. The percentage of hydrolyzed ATP was calculated according to the equation: $\%_{(\text{hydrolyzed ATP})} = P_i*100/(P_i + ATP_{\text{non-hydr}})$, and was corrected for background activity arising from non-radioactive ATP and RNA preparations. Corrected values were then used to calculate the amount of hydrolyzed ATP in µM. The respective RNA is indicated as a piece of its predicted secondary structure next to the bar graph.

Similar results were obtained with the about 500 nt long RNAs originated from TINCR (T546 and T3460). Generally, WT was at least two times more active than WT and KR lacking substrate or KR incubated with the respective RNA (Fig 3.23 B).

Activating effects of the 30 nt long ssRNA on Lsh ATPase are not clearly detectable. There are few points in the titration series suggesting stimulation, but by tendency the ssRNA, that appears to have no secondary structure, does not induce ATPase activity (Fig 3.23 C). However, the assay was done just once. Therefore, at least mild stimulatory effects on Lsh WT cannot be excluded.
In conclusion, the results indicate that the recognition of certain RNA secondary structure elements such as stem-loops is beneficial for the stimulation of the ATPase function of Lsh. In addition, the data demonstrate that activating effects of total RNA on the enzyme's ATPase activity are specifically based on RNAs and not on contaminations in RNA preparations.

3.10 DNA methyltransferases do not activate the ATPase function of Lsh *in vitro*

Interactions of Lsh with Dnmts and the influence of Lsh on CpG methylation are reported. However, it is not known if Dnmts contribute to the ATPase activity of the Lsh enzyme. In order to study an activating influence of Dnmts on Lsh ATPase, recombinant Dnmt1, Dnmt3a and Dnmt3b2 were included in ATPase assays. All the three Dnmts are His-tagged and were purified by batch-purification using Ni-NTA beads for the capture and imidazole for the elution of the proteins (see 5.2.7). Eluted fractions of Dnmts were analyzed by SDS-PAGE (Fig 3.24).

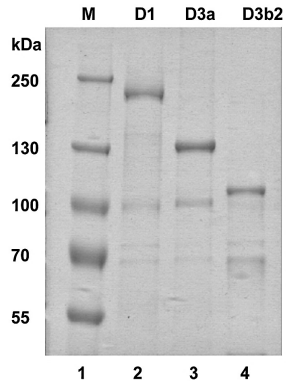

Fig 3.24: Purifications of His-tagged DNA methyltransferases.
DNA methyltransferases Dnmt1 (D1, lane 2), Dnmt3a (D3a, lane 3) and Dnmt3b2 (D3b2, lane 4) were batch-purified from SF21 insect cells expressing the respective His-tagged Dnmt. For analysis, samples taken during protein purification were loaded on 7.5% SDS gels. Gels were stained with Coomassie blue and destained with water. The SDS gel illustrates samples taken during the elution of the proteins.

Activity of purified Dnmts was tested with the Dnmt Activity/Inhibition Assay Kit (Active Motif). In ATPase assays, Dnmts were titrated in the presence of a nucleosomal array in combination with Lsh WT or Lsh KR (Fig 3.25). Lsh WT and KR lacking substrates as well as Lsh WT and KR both incubated solely with a nucleosomal array served as controls.

Recombinant Dnmts by themselves showed ATPase activity. Therefore, Dnmt based ATPase activity, which was probably due to contaminations in the preparations of the Dnmts, was substracted from the ATPase activity of Dnmt containing samples. Because of this, Lsh KR can display relatively low levels of ATP hydrolysis when incubated with the respective Dnmt. According to the ATPase assays, all Dnmts have no stimulatory effect on the ATPase activity of Lsh (Figs 3.25 A–C). As the experiments were performed only once, replicates would be needed to confirm the results.

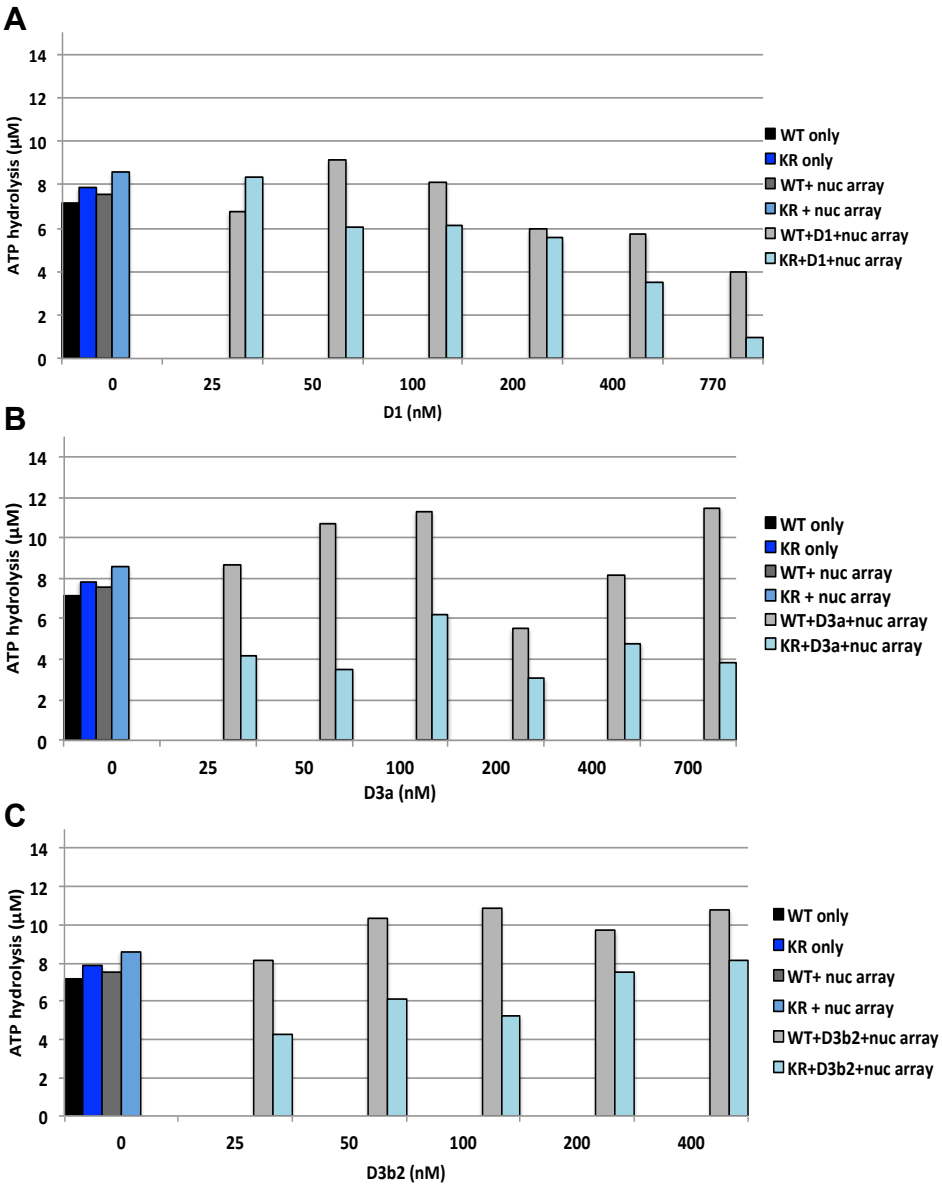

Fig 3.25: Effects of Dnmts on the ATPase activity of Lsh.
The contribution of Dnmts to the ATPase activity of Lsh was studied in ATPase assays. 200 nM of Lsh WT or Lsh KR were incubated with increasing concentrations of **(A)** Dnmt1 (D1; 25–770 nM) **(B)** Dnmt3a (D3a; 25–700 nM) and **(C)** Dnmt3b2 (D3b2; 25–400 nM) in the presence of a 12x601 nucleosomal array (nuc array),1 mM non-radioactive ATP and minor amounts of radioactive ATP (0.2 µCi/µl) for 45 min at 30 °C in a total volume of 10 µl. Lsh WT (black bars) and Lsh KR (dark blue bars) lacking the respective Dnmt and nuc array in the mixture as well as Lsh WT (dark grey bars) and Lsh KR (light blue bars) solely incubated with nuc array served as controls. Reactions were pipetted onto a TLC plate to separate the hydrolyzed phosphate from unreacted ATP. The percentage of hydrolyzed ATP was calculated according to the equation: $\%_{(\text{hydrolyzed ATP})} = P_i*100/(P_i + ATP_{non\text{-}hydr})$, and was corrected for background activity arising from non-radioactive ATP and Dnmt preparations. Corrected values were then used to calculate the amount of hydrolyzed ATP in µM.

4 Discussion

4.1 Basic studies on the chromatin remodeling capabilities of Lsh

The Snf2 family member Lsh is an essential epigenetic regulator protein. During embryonic development Lsh deficiency in mice results in perturbed heterochromatin organization accompanied by a genome-wide reduction of DNA methylation levels (Yan et al., 2003b) (Dennis, 2001). Loss of DNA methylation due to the absence of Lsh causes abnormalities in mitosis and meiosis, defects in gene imprinting and aberrant silencing of repetitive elements and stem cell genes (Fan et al., 2003) (La Fuente et al., 2006) (Fan et al., 2005) (Xi et al., 2009) (Dennis, 2001). Furthermore, Lsh was shown to interact with HDACs as well as *maintenance* and *de novo* DNA methyltransferases (Zhou et al., 2009) (Myant and Stancheva, 2007). Thus, Lsh plays an important role in the establishment of transcriptionally repressive chromatin during early developmental stages, mainly by affecting DNA methylation levels. However, the mechanistic properties of Lsh, which determine the crucial role of this enzyme for DNA methylation, have not been addressed. DNA methylation is repressed by nucleosomes, allowing DNA methylation only in the linker regions (Robertson et al., 2004) (Takeshima et al., 2006) (Felle et al., 2011a) (Schrader et al., 2015). Consequently, DNA in a nucleosomal complex requires active changes in nucleosome structure to render DNA accessible for DNA methyltransferases. Previous analyses of the methylation activity of the *de novo* DNA methyltransferases Dnmt3a and Dnmt3b and the *maintenance* DNA methyltransferase Dnmt1 in a nucleosomal context suggest that ATP-driven chromatin remodeling is required for efficient DNA methylation in chromatin (Felle et al., 2011a) (Schrader et al., 2015). Lsh belongs to the Snf2-like group of the Snf2 family that comprises enzymes such as *D. melanogaster* ISWI, mouse Chd1 and human Brg1, which are the catalytic core subunits of well-known ATP-dependent chromatin remodeling complexes (Flaus et al., 2006). Therefore, Lsh was supposed to mobilize nucleosomes in an ATP-dependent manner to regulate DNA accessibilty and facilitate DNA methylation. Since the proposed capability to move nucleosomes has not been proven yet, a detailed *in vitro* characterization of the chromatin remodeling functions of Lsh was perfromed. For this purpose, recombinant Lsh was expressed and purified, and subsequently used in binding assays, nucleosome mobilization assays and ATPase assays.

4.1.1 Lsh preferentially binds longer DNA, prefers nucleosomes with linkers to the nucleosomal core and binds cooperatively

As an initial step to nucleosome repositioning, remodelers require to recognize and bind specifically to the substrate. Lsh associates with chromatin *in vivo* as described by Yan and colleagues (Yan et al., 2003a). However, little is known about the binding mechanisms of Lsh. Here, a detailed biochemical analysis of the *in vitro* binding characteristics of Lsh towards naked DNA and nucleosomal DNA was done by applying two different techniques. A DNA binding assay using an ultra-low-range DNA marker already suggests cooperative binding behavior, as Lsh prefers to bind to longer free DNA fragments (chapter 3.3; Fig 3.3 A).

Using microscale thermophoresis, binding affinities were characterized based on the thermophoretic mobility of the binding partners in solution (chapter 3.3; Fig 3.3 B). In order to quantify binding affinities, the Hill equation was applied to the MST data. The Hill equation describes the fraction of a macromolecule saturated by a ligand as a function of the ligand concentration, and Hill values can then be used to determine cooperativity of ligand-enzyme binding (Hernan G Garcia, 2011). Hill values generated from MST data confirm that Lsh binds to DNA cooperatively, and binding to longer DNA molecules seems to enhance cooperativity. Cooperative binding dependent on the length of a substrate like DNA or RNA has been reported for some enzymes, such as the RNA-binding translocase RIG-I, the DNA repair protein Ku or the heterochromatin-associated protein MENT (Binder et al., 2011) (Ma and Lieber, 2001) (Springhetti et al., 2003). Furthermore, magnetic tweezer experiments and transmission electron microscopy demonstrate that the *S. cerevisiae* chromatin remodeling factor Isw1 binds DNA cooperatively (De Cian et al., 2012). Cooperativity depending on substrate length indicates multimerization of the protein, once it is bound to the substrate. However, Myant and Stancheva found that native Lsh is present as a monomer in nuclear extracts of human cells (Myant and Stancheva, 2007). The monomeric molecular mass of Lsh was determined by performing size-exclusion chromatography and sucrose-gradient sedimentation experiments (Myant and Stancheva, 2007). With striking analogy, the mass of the methyl-CpG-binding transcription factor MeCP2 was determined by applying the same methods, thereby deriving a mass of MeCP2 that is close to its predicted monomeric molecular weight (Klose and Bird, 2004). Interaction of Lsh with HDACs and Dnmts is suggested to happen transiently (Myant and Stancheva, 2007). Similarly, MeCP2 appears to interact rather transiently than stably with the Sin3-HDAC chromatin remodeling complex to mediate transcriptional repression (Klose and Bird, 2004) (Nan et al., 1998). By analogy with Lsh, MeCP2 binds DNA cooperatively and exhibits length-dependent binding affinity towards DNA. MeCP2 dimerizes upon binding to DNA as seen with atomic force microscopy (Ghosh

et al., 2010). In regard of these striking similarities to MeCP2, it is quite conceivable that Lsh forms multimers, once bound to DNA, which would explain its cooperative binding behavior. Another explanation for this behavior of Lsh may be the existence of more than one substrate binding site on the Lsh protein, and the binding of one substrate molecule facilitates the binding of a second and more substrate molecules.

Recent studies showed that the *maintenance* DNA methyltransferase Dnmt1 has length-dependent binding affinity towards DNA *in vitro*, propagating a DNA length-sensing activity of Dnmt1, and implying cooperative binding behavior. Furthermore, Dnmt1 preferentially binds to nucleosomes with long symmetric linker DNA (Schrader et al., 2015). Similar to Dnmt1, the results of the electrophoretic mobility shift assays with nucleosomes as substrates show preferred binding of Lsh to nucleosomes that have linkers, whereas the binding to the nucleosomal core is comparably weak (chapter 3.4; Figs 3.4 A– E). According to the MST data, even the nucleosomal core is bound cooperatively (chapter 3.4; Fig 3.4 F).

Yet, cooperative binding to nucleosomes increases in the presence of extranucleosomal DNA, suggesting extranucleosomal DNA as the main cause for cooperativity. Cooperative binding behavior of Lsh and its reported interaction with DNA methyltransferases (Myant and Stancheva, 2007) (Dunican et al., 2015) (Zhu et al., 2006) could present the basis for the effect of “methylation spreading” and the aberrant *de novo* methylation of CpG islands that is often observed in tumor cells (Graff et al., 1997).

Given DNA length-dependent cooperativity, a certain minimal linker length may be necessary for the stable association of Lsh with nucleosomes. In addition, based on the results of the gel retardation assays, symmetric linker DNA is beneficial to the binding of Lsh to nucleosomes, implying the binding of Lsh across the nucleosomal dyad to access both DNA linkers. In sum, Lsh could interact with nucleosomes as illustrated (Fig 4.1).

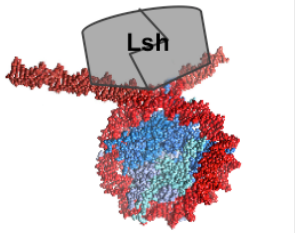

Fig 4.1: Cartoon illustrating the suggested binding mode of Lsh to nucleosomes.
Lsh binds cooperatively and could dimerize upon binding to nucleosomal DNA (grey line in the middle of the grey box illustrating Lsh). In doing so, Lsh probably crosses the nucleosomal dyad to contact the DNA at the entry/exit site of the nucleosome. DNA is shown in red, histones are shown in blue (modified and adapted from Schrader et al., PlosOne, 2015).

Narrowing DNA sizes in binding assays to determine the minimal length of DNA that is required for the stable interaction with nucleosomes, as well as DnaseI footprints to confirm crossing of the dyad axis, would provide further information about the binding mode of Lsh.

Additionally, binding studies with deletion mutants of Lsh could reveal the localization of DNA binding motifs (see chapter 4.6).
Enhanced affinity to nucleosomes in the presence of linker DNA is a characteristic that has been described for various remodeling enzymes. In contrast to the yeast SWI/SNF complex, that binds to the nucleosomal core with high affinity (Côté et al., 1998), a certain minimum of linker DNA is important for ISWI complexes in order to stably bind to mononucleosomes (Kagalwala et al., 2004) (Whitehouse et al., 2003) (Langst et al., 1999).
Longer extranucleosomal DNA has been reported to be essential for the ATPase motor protein Snf2H to form a stable protein-nucleosome interaction (He et al., 2006). Furthermore, Snf2H is known for cooperative nucleosome binding. Snf2H forms dimers implying direct protein-protein interactions as source for the cooperativity in binding affinities of Snf2H to nucleosomes (Racki et al., 2009).
Moreover, it was shown recently that the chromatin remodeling complex NoRC requires linker DNA for nucleosome binding and remodeling (Manelyte et al., 2014).
Taken together, these observations favor the hypothesis that the Snf2 family member Lsh regulates DNA methylation through the mobilization of nucleosomes.

4.1.2 Lsh does not remodel nucleosomes *in vitro*, and the *in vitro* ATPase activity of Lsh is not stimulated by DNA and nucleosomes

In contrast to most of the ATPase motor proteins of the Snf2-like group, Lsh does not seem to be part of a large protein complex (Myant and Stancheva, 2007). Nevertheless, ATPase subunits of chromatin remodeling complexes are capable to remodel nucleosomes *in vitro* by their own (Brehm et al., 2000) (Corona et al., 1999) (Phelan et al., 1999).
Further, it is known that DDM1, the *A. thaliana* homolog of Lsh, is able to reposition nucleosomes *in vitro* (Brzeski and Jerzmanowski, 2003). Murine Lsh and DDM1 share an overall amino acid sequence identity of about 45 %. However, murine Lsh seems to be incapable of moving nucleosomes (Burrage et al., 2013). During the presented work, the proposed chromatin remodeling capability of human Lsh was studied *in vitro*. End-positioned and centrally-positioned mononucleosomal templates, as well as a template with nucleosomes placed on different positions on the fragment, served as substrates in the nucleosome mobilization assays (chapter 3.5; Figs 3.5 A–D). Despite its ability to bind DNA and nucleosomes and its close relationship to ATPase subunits of well-described chromatin remodelers, Lsh did not exhibit chromatin remodeling activity *in vitro*. Since nucleosome mobilization is an ATP-driven process, ATPase assays were performed to investigate the protein's ATPase activity. For this purpose, different nucleosomes served as substrates, as substrate requirements can differ for each enzyme(chapter 3.6.2; Figs 3.7 A–D).

For instance, the ATPase of the yeast SWI/SNF complex is already maximally stimulated by free DNA (Boyer et al., 2000). In contrast, *D. melanogaster* Mi-2 is stimulated by nucleosomal DNA but not at all by free DNA (Brehm et al., 2000). Whereas Brg1 and BRM ATPase activities are stimulated to the same extent by nucleosomes and naked DNA, the ISWI ATPase is preferentially stimulated by nucleosomes (Corona et al., 1999) (Phelan et al., 1999).
The work presented here, shows that DNA and mononucleosomes, and even a nucleosomal array, did not stimulate the ATPase activity of Lsh by their own. Therefore, the performed basic *in vitro* studies suggest that Lsh does not mobilize nucleosomes in an ATP-dependent fashion. However, RNA was identified as a trigger of Lsh ATPase activity, and ATPase activity is further enhanced by nucleosomes in the presence of RNA (see chapter 4.3).
Yet it has to be proven, if the presence of a specific RNA (see chapter 4.3.5) induces the proposed chromatin remodeling activity of Lsh. Further, it cannot be ruled out that Lsh necessitates the interaction with one or more other proteins to show considerably strong ATPase and remodeling activity. Apart from this, Lsh could also possess a so far undefined domain inhibiting ATP binding or hydrolysis, and eventually chromatin remodeling, as has been reported for *D. melanogaster* ISWI (Clapier and Cairns, 2012). The needs for such requirements, and the generation of deletion mutants of Lsh to study the presence of domains inhibiting ATPase and chromatin remodeling activities, are discussed in chapter 4.6.

4.2 The role of Lsh in the recognition of the epigenetic landmark 5-hmC

5-hmC emerges when 5-mC is oxidized. Conversion of 5-mC to 5-hmC is catalyzed by Tet proteins that can successively oxidize 5-mC to 5-hmC, to 5-fC and to 5-caC (Tahiliani et al., 2009) (Ito et al., 2011). The oxidized 5-mC bases are thought to contribute to passive replication-dependent loss of 5-mC, as they may interfere with *maintenance* methylation during DNA replication. They do so by inhibiting UHRF1 binding or Dnmt1 activity, causing the progressive dilution of 5-hmC, and potentially 5-fC and 5-caC, through successive DNA replication cycles (Frauer et al., 2011) (Hashimoto et al., 2012). Besides, 5-hmC, 5-fC and 5-caC can be converted to cytosine via base excision repair mechanisms (BER). This suggests that these derivatives act as DNA demethylation intermediates but, in addition, also may have epigenetic signaling functions in their own right. 5-hmC shows unique distribution patterns in the genome (Xu et al., 2011) (Pastor et al., 2011) (Szulwach et al., 2011b), indicating that 5-hmC might play a role in altering chromatin structure and transcriptional regulation. Genome-wide analyses indicate association of 5-hmC with regulatory elements,

such as promoters and enhancers, and suggest that, depending on chromatin signatures, 5-hmC has regulatory functions in both activation and repression of transcription (Szulwach et al., 2011a) (Choi et al., 2014). To uncover functions of 5-hmC, 5-fC and 5-caC, several groups searched for readers for 5-mC and its oxidized derivates. For instance, the methyl-CpG-binding protein Mbd3, a key component of the chromatin remodeling complex NuRD (Zhang et al., 1999), can bind 5-hmC and unmodified cytosine, but not 5-mC, *in vitro,* and is proposed to associate with Tet1 (Hendrich and Bird, 1998) (Yildirim et al., 2011). Others showed selective binding of Mbd3 to 5-mC and 5-fC (Iurlaro et al., 2013) (Spruijt et al., 2013). Collectively, these studies open up the possibility that, amongst others, also chromatin remodelers such as the Mbd3/NuRD complex may be able to interpret signals of modified cytosines in the regulation of transcription or chromatin structure (Iurlaro et al., 2013) (Spruijt et al., 2013). During their screening approach for readers for oxidized derivates of 5-mC, Sprujit and colleagues identified Lsh as a reader for 5-hmC. They suggested that Lsh could participate in a DNA-repair-involved DNA demethylation pathway (Spruijt et al., 2013), as Lsh is known to promote phosphorylation of H2AX to γH2AX, and thereby contributes to efficient repair of DNA double-strand breaks (Burrage et al., 2013).
However, since Lsh is required for both *de novo* and *maintenance* DNA methylation cooperating with DNA methyltransferases and histone deacetylases (Dennis, 2001) (Myant and Stancheva, 2007) (Zhu et al., 2006) (Zhou et al., 2009), it is questionable wether Lsh has a role in DNA demethylation. Tet protein catalyzed hydroxy-methylation could rather serve to recruit Lsh to 5-hmC in order to mediate some of the regulatory functions of this novel epigenetic landmark.
To study the interplay between Lsh and 5-hmC, *in vitro* binding assays and ATPase assays were performed (chapter 3.8.1; Fig 3.9). MST data suggest a preferred binding of Lsh to hydroxy-methylated as well as methylated DNA over unmodified DNA, favoring the proposed role of Lsh as an epigenetic reader of 5-hmC. Yet, preferential binding to both 5-hmC and 5-mC, as detected by MST, is contradictory to the observations by Spruijt and colleagues, who detected Lsh as specifically binding to 5-hmC by applying a quantitative mass spectrometry-based proteomics approach (Spruijt et al., 2013). The use of divergent methods and DNA substrates might explain the differences in binding specificities. Identifying the DNA-binding domain of Lsh (see chapter 4.6) and structural analyses of this domain in a complex with 5-mC and 5-hmC, respectively, could further reveal, if there are preferences of Lsh towards 5-mC or 5-hmC. Furthermore, the E3 ubiqutin-protein ligase UHRF1 was discovered to bind 5-hmC and 5-mC-containing substrates with similar affinity via its SET and RING finger-associated (SRA) domain (Frauer et al., 2011). Recently, structural and biochemical analyses unveiled SRA domains as versatile readers of modified DNA, demonstrating that alterations in the binding pockets of SRA domains can tilt the binding preference from 5-mC

to 5-hmC (Zhou et al., 2014). Such alterations could also account for the almost identical binding affinities of Lsh to 5-mC and 5-hmC. However, an initial protein sequence alignment did not reveal a relationship between Lsh and SRA domain-containing proteins in terms of a shared SRA domain (data not shown).

The ATPase assays show stimulation of Lsh by hydroxy-methylated dinucleosomes.

In contrast, the ATPase activity of Lsh is essentially not stimulated by unmodified or methylated dinucleosomes (chapter 3.8.2; Figs 3.10–3.12).

Stimulation of Lsh ATPase activity by hydroxy-methylated dinucleosomes would provide indications pointing to an active involvement of Lsh in steps following the oxidation of 5-mC, i. e. functions of Lsh independent of its role in DNA methylation.

Recently, the role of the *S. cerevisiae* protein Cmr1 in DNA replication stress was assessed, pointing to the involvement of Cmr1 in maintaining genome integrity (Gallina et al., 2015). WDR76, the mammalian homolog of Cmr1, prefers binding to 5-hmC in comparison to 5-mC and interacts with Lsh (Spruijt et al., 2013) (Gallina et al., 2015). These findings would hint to a linked relevance of Lsh and 5-hmC to the regulation of chromatin structure in terms of a response to DNA damage. Indeed, emerging lines of evidence indicate that chromatin remodeling factors are recruited to DNA double-strand breaks (DSB), where they mobilize, evict, or disrupt nucleosomes, and thereby facilitate DNA damage repair (DDR) (Larsen et al., 2010) (Lan et al., 2010) (Hara and Sancar, 2002) (van Attikum et al., 2007) (Ura et al., 2001).

For instance, Brg1 stimulates nucleotide excision repair (Zhang et al., 2009), whereas the yeast chromatin remodeling enzymes SWI/SNF and Isw1 and Isw2 are suggested to be required for BER in chromatin (Menoni et al., 2007) (Nakanishi et al., 2007). These findings are substantiated by the severe inhibition of at least some DNA glycosylases by nucleosomal core particles (Beard et al., 2003) (Nilsen et al., 2002).

Consequently, stimulation of the ATPase and probably the remodeling activity of Lsh by hydroxy-methylated dinucleosomes would result in the opening of chromatin, facilitating DNA repair factors the access to DNA in order to maintain genome stability.

However, hydroxy-methylated dinucleosomes stimulated the ATPase activity of Lsh only under very well-defined experimental conditions (chapter 3.8.2; Fig 3.11). This complicates the interpretation of the biological relevance of the ATPase data. Nevertheless, Lsh might be active even at concentrations of ATP in the millimolar range. Yet, the background of non-hydrolyzed ATP may be too high to detect stimulatory effects in the *in vitro* ATPase assay setup, which is probably due to a low ATP hydrolysis rate.

4.3 The ATPase activity of Lsh is induced by RNA and enhanced by nucleosomes

4.3.1 Lsh binds to RNA with greater affinity than to DNA

Seeking for substrates with the potential to stimulate the ATPase activity of Lsh, the binding of Lsh to RNA was examined. EMSAs show the formation of a Lsh-RNA complex that is retarded in the native gel. MST data reveal binding of Lsh to a 30 nt long ssRNA molecule with higher affinity than to dsDNA of the same length and sequence (chapter 3.9.1; Fig 3.13). Similar Hill coefficients in the binding to ssRNA and dsDNA indicate similarities in the cooperative binding behavior of Lsh towards ssRNA and dsDNA. Length-dependent cooperative binding of Lsh (see 4.1.1) explains the almost identical n-values, as both substrates have a size of 30 nt. In this respect, Lsh does not seem to discriminate between RNA and DNA. The preferential binding of Lsh towards RNA is further illustrated by its inability to bind to ssDNA. In comparison to its ATPase activity in the presence of a 30 nt long ssRNA, Lsh shows higher ATPase activity in the presence of structured RNAs with sizes of 60 nt and 500 nt (as discussed in chapter 4.3.5). Consequently, Lsh might preferentially interact with structured RNAs or RNAs of sizes larger than 30 nt. Still, it would be of interest to directly show and quantify preferred binding towards RNAs of larger sizes than 30 nt and towards differently structured RNAs.
Direct binding of RNA has been reported for chromatin modifiying proteins like the histone-lysine methyltransferase Ezh2 or the chromodomain protein HP1 (Kaneko et al., 2010) (Muchardt et al., 2002), and interestingly, for the chromatin remodeling enzymes *D. melanogaster* ISWI and mammalian Brg1 and NoRC (Onorati et al., 2011) (Cajigas et al., 2015) (Mayer et al., 2008) (Manelyte et al., 2014). Furthermore, Dnmt1 as well as Dnmt3a were identified to bind to RNA *in vitro*. Strikingly, the association with specific RNA molecules is accompanied by enzymatic inhibition of the DNA methyltransferases (Zhang et al., 2015) (Holz-Schietinger and Reich, 2012) (Di Ruscio et al., 2014). This work shows binding of Lsh to RNA with greater affinity than to DNA, providing further indications for the importance of RNA to chromatin-associated proteins.

4.3.2 Nucleosomes contribute to RNA induced ATPase activity of Lsh

In view of the described affinity of Lsh towards RNA, the next step was to analyze the capability of RNA to stimulate the enzyme's ATPase activity. In doing so, total RNA was extracted from two different cell lines and two organisms. To exclude contaminating effects, different methods for RNA isolation had been applied. Overall, total RNA clearly stimulatd the ATPase activity of Lsh. In the presence of RNA, the ATPase activity of Lsh WT was in the range of 2–3-fold over the ATPase activity of KR as well as controls lacking RNA, independent of ATP concentrations (chapter 3.9.2; Fig 3.14). Realizing stimulation of the ATPase activity of Lsh by total RNA, nucleosomes were combined with total RNA in ATPase assays. Taking into consideration that complexity of the nucleosomal template might influence ATPase activity, mononucleosomes, differently DNA modified dinucleosomes and a nucleosomal array served as substrates. As expected, Lsh WT was about two times more active than KR when only total RNA was present. Throughout the experiments, Lsh WT and KR in combination solely with nucleosomes showed ATPase activity that was similar to the basal activity of WT and KR (chapter 3.9.3; Figs 3.16 A–C). While mononucleosomes in combination with RNA had essentially no additional effect on ATPase activity, ATPase assays with differently DNA modified dinucleosomes displayed a divergent picture. Unmodified and hydroxy-methylated dinucleosomes slightly enhanced ATPase activity in the presence of total RNA, whereas methylated dinucleosomes rather seemed to repress ATPase activity (chapter 3.9.3; Figs 3.16 A–B).

The data presented here are in contrast to studies on the chromatin remodeling enzyme ISWI. *S. cerevisiae* ISWI complexes did not reveal any differences in ATPase activity, when the complexes were incubated with either mono- or dinucleosomes (Krajewski and Reese, 2010), indicating a unique place for Lsh in the class of chromatin remodeling enzymes.

The modification status of the DNA template, unmodified or hydroxy-methylated, had no influence on the ATPase activity of Lsh. This argues against an active participation of Lsh in DNA demethylation. It is thus also unlikely that Lsh responds to the epigenetic signaling function of 5-hmC by mobilizing nucleosomes, as discussed in chapter 4.2.

The inhibition of the ATPase activity of Lsh by methylated nucleosomes is contradictory to the findings of Brzeski and colleagues, who showed that the DNA methylation status does not influence the ATPase activity of the *A. thaliana* homolog DDM1 (Brzeski and Jerzmanowski, 2003). Yet, regarding the suggested ability of Lsh to alter chromatin structure in order to facilitate the access to DNA for methyltransferases, methylated DNA would represent the final product. Therefore, it makes sense that a methylated nucleosomal substrate inhibits Lsh activity, which would be in accordance with a 'release' model, as proposed for ACF and Chd1. These machines were found to dissociate from the nucleosome

after remodeling, due to a reduced affinity to the end-products of the translocation reaction (Rippe et al., 2007).
The addition of a nucleosomal array to total RNA resulted in clearly pronounced catalytic activity of Lsh ATPase, indicating that nucleosome-enhanced ATPase activity depends on the complexity of the substrate (chapter 3.9.3; Fig 3.16 C). The binding experiments point to length-dependent cooperative binding and indicate preferred binding to nucleosomes with symmetric linkers, suggesting that Lsh contacts nucleosomes at the entry/exit site (chapters 3.3 and 3.4). Therefore, a flexible interaction with chromatin, as offered by a nucleosomal array, may be the cause for increased ATPase activity.
Activation of ATPase function by RNA is an unusual feature amongst ATPase subunits of chromatin remodeling complexes. Since remodelers move, eject or restructure nucleosomes in an ATP-dependent fashion, nucleosomal DNA represents the natural substrate that commonly stimulates ATPase activity (Clapier and Cairns, 2009). Indeed, RNA binding even inihibits ATPase and remodeling activity of at least some chromatin remodelers, such as NoRC and Brg1, most probably by competing with nucleosomes for the binding sites on the remodeling enzyme (Manelyte et al., 2014) (Cajigas et al., 2015). Corona and colleagues showed that the ATPase activity of *D. melanogaster* ISWI is clearly stimulated by nucleosomes but not by poly-A RNA (Corona et al., 1999). Interestingly, later studies revealed activating effects by the non-coding RNA hsrω on *D. melanogaster* ISWI ATPase. Yet, these studies indicate rather competing than synergistic effects of nucleosomes and hsrω RNA on the ATPase activity of ISWI (Onorati et al., 2011).
To sum up, the ATPase activity of Lsh is strengthened by nucleosomes in the presence of RNA, whereas nucleosomes by their own have no stimulatory effect.

4.3.3 Displacement of RNA by DNA and nucleosomes indicates a dynamic interaction between RNA and Lsh

Competitive EMSAs were done in order to understand the binding behavior of Lsh towards RNA in the context of chromatin. RNA appeared to be completely displaced from its binding site, when first a Lsh-RNA complex was formed and afterwards increasing amounts of DNA, either naked or in nucleosomal form, were added (chapter 3.9.4; Figs 3.17 A and 3.18 A). However, at lower concentrations of DNA or nucleosome up to at least equimolar amounts of DNA and RNA (Fig 3.17 A) or nucleosome and RNA (Fig 3.18 A), the RNA still associated with Lsh. In the vice-versa experiments, naked DNA or nucleosomal DNA in a complex with Lsh remained stably associated with the protein when titrating the RNA, even at excessive RNA concentrations (chapter 3.9.4; Figs 3.17 B and 3.18 B). Since there was no additional retarded band appearing in the gel shifts that would indicate simultaneous but individual

binding of Lsh to RNA and to DNA (naked or in nucleosomal form), and since signals overlapped at some points in the titration series, one can conclude that both RNA and DNA (naked or in nucleosomal form) interact with the same binding site of the protein.
As illustrated in Fig 3.13 B, Lsh binds to RNA with higher affinity than to DNA. Considering the displacement of RNA by DNA (naked or in nucleosomal form), and in view of the stability of a complex consisting of Lsh and DNA (naked or in nucleosomal form), Lsh probably binds to RNA with a high on/off-rate. In comparison, Lsh may interact with naked or nucleosomal DNA with a slow on/off-rate. Since RNA induces the ATPase activity of Lsh, such binding kinetics are maybe ATP-dependent (see chapter 4.3.4).
High affinity binding of Lsh to RNA with a relatively high on/off-rate would mean a dynamic interaction between Lsh and RNA. Interactions with high affinity binding caused by a high on/off-rate are rare, since high affinity interactions usually imply fast complex formation (high on-rate) combined with slow complex dissociation (slow off-rate) (de Mol et al., 2005). Yet, cases with high affinity binding caused by a high on/off-rate are reported (O'Connell et al., 2010) (de Mol et al., 2005). For instance, the uridine- or adenine/uridine-rich-stretches-RNA-binding protein (ARE-RBP) HuR, a protein contributing to the stability and translation of its target mRNAs, binds a U-rich ssRNA oligonucleotide with high on/off-rates in surface plasmon resonance (SPR) experiments (Kim et al., 2007). Applying the same technique, the *S. pombe* terminal-uridylyl-transferase (TUTase) Cid1, that stimulates mRNA decay, was reported to bind a 21-nucleotide RNA with high affinity at high on/off-rates (Yates et al., 2012). An interaction of Lsh with RNA at high on/off-rates would mean fast complex formation and fast complex dissociation. Short residence times of RNA probably imply short but frequently repeated periods of ATPase activity. In comparison, the Lsh-DNA or Lsh-nucleosome complex may take longer until it is formed but it probably has a relatively long half-life.
Figuratively, this would be beneficial for increased activity at the nucleosomal target site. A slow dissociation rate would explain why RNA cannot displace DNA and nucleosomes. Much higher concentrations of RNA would be needed to remove the DNA or nucleosome from its binding site on the protein. Additionaly, prolonging times when incubating the RNA with the Lsh-DNA or the Lsh-nucleosome complex could result in less stable complexes. The described binding behavior of Lsh to RNA in the presence of DNA or nucleosomes is schematically illustrated in Fig 4.2.

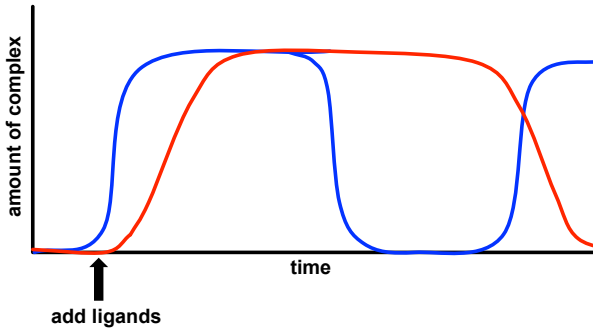

Fig 4.2: Competitive interactions with different rates of binding.
The time course of binding is shown for two interactions, one with relatively fast on-rate and off-rate (blue line), and one with relatively slow on-rate and off-rate (red line). Although the two reactions temporarily reach the same level of binding at equilibrium, the rates of binding and dissociation are quite different (according to Lim et al., Cell Signaling: Principles and mechanisms, Chapter 2: Principles and mechanisms of protein interactions, Garland Science, Taylor & Francis Group, LLC, 2015).

Accordingly, a model of the binding mode of Lsh could be described as follows: The interaction between Lsh and RNA is very dynamic and complex formation occurs rapidly. When Lsh recognizes nucleosomes, RNA is still bound, as the association of Lsh with chromatin is weak at first. Tighter binding to nucleosomes results in the displacement of RNA from Lsh. In turn, weakening the interaction between Lsh and nucleosomes should again enable RNA binding. At this point, it has to be stressed that the suggested slow on/off-rate in terms of binding of Lsh to nucleosomes is to be considered relative to the interaction between Lsh and RNA, and is based on *in vitro* binding experiments with only one or two substrates Lsh can choose. As steric effects in terms of surface chemistry as well as oligo-length influence binding, competitive binding studies with more complex nucleosomal substrates and differently structured RNAs could reveal further insights into the binding mechanism of Lsh. However, due to the complex environment in living cells, most reliable dissociation rates may be derived from fluorescence recovery after photobleaching (FRAP) analyses with GFP-tagged human Lsh to assay chromatin association dynamics *in vivo*.

4.3.4 ATP hydrolysis changes binding dynamics of Lsh

A wide variety of chromatin-associated proteins bind only transiently to chromatin in the nucleus of living cells. Tracking dynamic behavior in living cells by *in vivo* imaging methods such as FRAP revealed that many chromatin-associated proteins have a high turnover on chromatin with a residence time on the order of seconds (Phair et al., 2004). For example, the high-mobility group proteins HMGB1 and HMG-D have very high on/off-rates on chromatin (Thomas and Stott, 2012) (Ragab and Travers, 2003). Accordingly, these properties are crucial for generating high plasticity in genome expression, forming dynamic interaction networks *in vivo* (Phair et al., 2004) (Hager et al., 2009). Yet, chromatin-associated proteins exist in several, kinetically distinct populations, and are temporarily

immobilized upon their functional binding to distinct types of target sequences. Examples include RNA polymerases I and II, which become temporarily immobilized on target genes upon transcriptional engagement (Dundr et al., 2002) (Kimura et al., 2002), as well as DNA repair and replication factors upon association with repair and replication sites (Hoogstraten et al., 2002) (Sporbert et al., 2002) (Houtsmuller et al., 1999). The vast majority of human ISWI remodelers Snf2H and Snf2L was found to be highly mobile during G1/2 phase, binding only transiently to chromatin. However, ISWI remodelers were recruited to replication foci during S phase and to DNA repair sites. Thereby, the tightly bound fraction increased temporarily at those sites, which is suggested to promote translocation of target nucleosomes (Erdel et al., 2010). Cyclically occuring nucleosome translocation is a feature that was also reported for the remodeling complexes SWI/SNF and NuRD (George et al., 2009) (Métivier et al., 2003). Therefore, a continuous sampling mechanism was proposed for chromatin remodelers: Remodelers interact with nucleosomes dynamically and probe nucleosomes continuously. Upon the recognition of specific signals that induce their recruitment, remodeling enzymes reside at target sites and actively remodel nucleosomes (Erdel et al., 2011). Whereas mobility of human ISWI remodeling complexes appears to be independent of ATPase activity (Erdel et al., 2010), Lungu and colleagues suggest that the absence of a functional ATPase domain impairs the mobility of murine Lsh at pericentromeric heterochromatin. Applying FRAP, they compared dynamics of murine wild-type Lsh (Lsh WT) to the dynamics of its ATPase deficient version at heterochromatic sites. While Lsh WT exchanged rapidly between the bound state and the unbound state, ATPase deficient Lsh was comparably less mobile at pericentromeric heterochromatin (Lungu et al., 2015). Higher accumulation of the ATPase deficient version in comparison to WT hence suggests that an active ATPase is crucial for Lsh to retain its dynamic mobility.

Here, differences in the binding between human Lsh WT and KR were investigated in *in vitro* binding studies. In order to understand whether the capability of Lsh to hydrolyze ATP influences its binding behavior, EMSAs were carried out in the presence of ATP. Comparing the binding affinities of WT and KR to RNA, complex formation occured faster between Lsh WT and RNA than between KR and RNA (chapter 3.9.5; Fig 3.20). In competitive EMSAs with a pre-incubated Lsh-RNA complex and increasing amounts of nucleosomes, RNA was displaced from KR at lower amounts of nucleosomes when compared to the displacement of RNA from WT (chapter 3.9.5; Fig 3.21). Taking account of the stimulation of the ATPase activity by RNA, faster complex formation and slower dissociation of RNA from WT in comparison to KR demonstrate the importance of RNA to retain ATPase activity, especially when Lsh simultaneously interacts with nucleosomes. Therefore, RNA seems to be the limiting factor for the ATPase activity of Lsh. As a consequence, since nucleosomes still appear to displace RNA at some point, even in the presence of ATP, Lsh must be inactive

when it is tightly bound to nucleosomes. During the remodeling reaction, chromatin remodelers usually closely interact with their target nucleosome. This raises the question how Lsh could mobilize nucleosomes when only loose chromatin binding allows the simultaneous association with RNA that is essential for an active ATPase. Additional factors such as accessory proteins or certain chromatin modifications could be necessary to stimulate Lsh ATPase activity or at least stabilize the interaction between Lsh and RNA on chromatin. The RNA used in these experiments, a ssRNA oligonucleotide, is probably not the optimal substrate. Subsequent ATPase experiments with longer, structured RNAs showed increased ATPase activity of Lsh in comparison to its ATPase activity in the presence of ssRNA (see chapters 3.9.6 and 4.3.5). However, these ATPase assays were one-shot experiments, and mild stimulatory effects of the ssRNA on Lsh cannot be excluded from the data, particularly in the view of the findings discussed in this chapter. Yet, since differences in the binding behavior between WT and KR in the presence of ATP are quite small, the results need to be interpreted with caution. Nevertheless, our findings are in accordance with data from Lungu and colleagues, who suggest that Lsh is highly mobile and not tightly associated with chromatin when it is active. The inability to hydrolyze ATP though leads to its trapping on chromatin (Lungu et al., 2015).

4.3.5 The ATPase activity of Lsh is preferentially induced by structured RNAs

To elucidate the relevance of RNA structures for the enzyme's ATPase activity, differently structured RNAs were used in ATPase assays. Two different about 60 nt long RNAs that form stem-loops in solution and two about 500 nt long, highly structured RNAs originated from a long non-coding RNA, as well as a 30 nt long ssRNA oligonucleotide that is unable to fold into stem-loops, served as substrates (chapter 3.9.6; Figs 3.23 A–C). Generally, Lsh WT was at least two times more active than the KR mutant when structured, stem-loop forming RNAs were present, whereas the ATPase activity of Lsh was comparably weaker when Lsh was incubated with ssRNA. Overall, the data suggest that Lsh recognizes secondary structures of RNAs, such as stem-loops, which might be beneficial for the stimulation of its ATPase activity.

Still, the question remains what sort of RNA interacts specifically with Lsh. An increasing number of discoveries reveal the importance of non-coding RNAs to the control of the epigenetic landscape, as many non-coding RNAs physically associate with chromatin modifying and chromatin remodeling proteins, in order to regulate gene expression at specific loci (Khalil et al., 2009). In particular, long non-coding RNAs (lncRNAs) such as HOTAIR, Air, Evf2 and hsrω have been shown to target histone modifying proteins to

chromatin (Nagano et al., 2008) (Kaneko et al., 2010) and to functionally interact with chromatin remodeling enzymes, influencing their activity (Onorati et al., 2011) (Cajigas et al., 2015). Furthermore, long non-coding RNAs as well as microRNAs are increasingly being identified as potential regulators of DNA methylation (Yan et al., 2014) (Mohammad et al., 2010) (Merry et al., 2015). Considering this, a lncRNA or subset of lncRNAs might also associate with Lsh and regulate its function. Interestingly, very recently published RIP data show the interaction of Lsh with the lncRNA HOTAIR (Wang et al., 2015).
The presented data show only a very small fraction of RNAs that might interact with Lsh and stimulate its ATPase activity. Techniques such as RNA immunoprecipitation (RIP), or more advanced cross-linking immunoprecipitation (CLIP) techniques, followed by RNA-sequencing, would allow the genome-wide identification of RNAs that could specifically cooperate with Lsh.

4.3.6 Lsh – an RNA helicase?

This work shows that the ATPase activity of Lsh, a Snf2 family member, can be triggered by RNA. Like the Snf2 family, RNA helicases belong to the SF2 superfamily, as they are built around the SF2 characteristic catalytic core consisting of the DExx and the HELICc domains that contain the helicase motifs as well as the Q motif. Since RNA helicases are thus structurally related to the Snf2 family, one may draw functional similarities between Lsh and RNA helicases that require RNA binding to stimulate ATP hydrolysis.
There are two major classes of RNA helicase enzymes: the processive DExH class and the non-processive DEAD-box class. DExH members commonly use ATP to unwind short duplex RNA, based on directional translocation. In contrast, the DEAD-box helicases are ATP-dependent RNA-binding proteins that do not appear to translocate along nucleic acids. Instead, these proteins unwind duplexes by local strand separation, but can also catalyze RNA duplex annealing. RNA helicases generally function as part of large multicomponent assemblies, such as the spliceosome or the translation initiation machinery, and are involved in nearly all aspects of RNA metabolism. These include ribosome biogenesis, transcription and pre-mRNA splicing, microRNA (miRNA) processing, nonsense-mediated RNA decay (NMD), mRNA transport and protein translation. Furthermore, a number of RNA helicases have been shown to rearrange ribonucleoprotein (RNP) complexes in an active, ATP-dependent fashion (for reviews see (Pyle, 2008), (Linder and Jankowsky, 2011), and (Jankowsky, 2011)). Strikingly, several RNA helicases are also associated with diverse and seemingly unrelated functions, although those tasks are usually in addition to their RNA associated functions. For instance, the *D. melanogaster* DexH helicase maleless (MLE), an enzyme that shows clear RNA dependent ATPase activity (Izzo et al., 2008), was

documented to bind the MEP-1 and Mi-2 subunits of the chromatin remodeling complex NuRD, suggesting a role for MLE in nucleosome remodeling, apart from its functions in the male-specific lethal (MSL) complex that mediates dosage compensation (Cugusi et al., 2015). The DEAD-box helicase Ddx5 is involved in mRNA splicing, miRNA biogenesis, and also in transcriptional regulation. With regard to the latter, there is evidence that Ddx5 represses transcription, when it is targeted to constitutively active promoters and interacts with HDAC1 and Dnmt3a (Wilson et al., 2004) (Mpakali et al., 2012). Similar to Ddx5, Lsh was shown to associate with the *de novo* DNA methyltransferases Dnmt3a and Dnmt3b, as well as the histone deacetylases HDAC1 and HDAC2, in order to mediate gene silencing (Zhu et al., 2006) (Myant and Stancheva, 2007) (Zhou et al., 2009). Another example is the RNA helicase Rm62. Rm62 plays a role in processes such as alternative splicing, RNA export and RNA interference-mediated silencing. Studies in flies unveiled a direct interaction of Rm62 with the histone methyltransferase SU(VAR)3-9. Rm62-dependent recruitment of SU(VAR)3-9 to heat shock loci is responsible for H3K9 methylation and contributes to the establishment of transcriptionally inactive chromatin (Boeke et al., 2011). As for Rm62 and SU(VAR)3-9, a similar function was indicated for Lsh and the histone methyltransferase G9a. Myant and colleagues report cooperation between Lsh and G9a to silence pluripotency genes during lineage commitment and cell differentiation. Following efficient knock-down of *LSH*, ChIP data revealed impaired recruitment of G9a to promoters of pluripotency genes. However, their data do not show direct interactions between Lsh and G9a. Consequently, Lsh is suggested to promote chromatin remodeling, which facilitates the binding of G9a to a subset of genomic loci (Myant et al., 2011).

Taken together, a functional relationship between Lsh and RNA helicases cannot be ruled out. However, the helicase activity of Lsh has not been described to date. Furthermore, most RNA helicases display clear specificity for RNA, and published data showing RNA helicases making contacts to nucleosomes do not exist. ChIP analyses offer chromatin-association of some RNA helicases, such as Dbp2 or DDX21 (Cloutier et al., 2012) (Calo et al., 2015). Yet, nucleosome binding cannot be derived from ordinary ChIP experiments. The helicase could simply bind to nucleosome depleted regions, or linker regions without contacting the nucleosomes. Depending on crosslinking times, also proteins binding indirectly can immunoprecipitate; as many RNA helicases operate in large protein complexes, other components of the complex could mediate nucleosome binding. In addition, overexpression of a protein in cells followed by ChIP analyses may lead to false positive results.

This work demonstrates that Lsh can directly contact the nucleosomal core. It also shows that nucleosomes strengthen the ATPase activity of Lsh.

Moreover, Lsh contains Snf2-specific sequence motifs that are indicative of Snf2-specific structural features, distuingishing the Snf2 family from DexH and DEAD-box RNA helicases.

Therefore, Lsh is functionally more closely related to other members of the Snf2 family than to RNA helicases.

4.4 DNA methyltransferases do not activate Lsh ATPase *in vitro*

Lsh is known to regulate DNA methylation during development (Dennis, 2001). Knock-down of *LSH* gene expression in embryonic stem cells reduces DNA methylation at pluripotency genes, which is due to loss of *de novo* DNA methylation (Myant et al., 2011) (Zhu et al., 2006). Furthermore, embryos from Lsh knock-out mice have numerous organ and developmental defects (Sun, 2004), and deletion of Lsh in mice is accompanied by widespread decrease in CpG methylation, comprising about 30% of all cytosines in the CpG context (Yu et al., 2014). Recent studies suggest that a functional ATPase domain of Lsh is required for efficient CpG methylation and the association of Dnmt3b at target sites of repeat elements (Ren et al., 2015). Alltogether, these data prompted the investigation of the impact of Dnmts on the ATPase activity of Lsh *in vitro*. Therefore, recombinant Dnmt1, Dnmt3a and Dnmt3b2 were included in ATPase assays. Each Dnmt was titrated in the presence of either Lsh WT or Lsh KR in combination with a nucleosomal array. However, all tested Dnmts had no stimulatory effect on the ATPase activity of Lsh (chapter 3.10; Fig 3.25).
Accessory proteins or subunits of remodeling complexes are known to regulate ATPase activity and nucleosome mobilization of chromatin remodelers. In particular, C/EBPα is able to associate with Brg1 *in vitro* and to stimulate its ATPase activity (Inayoshi et al., 2006). The PHD- and chromodomains of Chd proteins like Chd4 and Chd1 are reported to regulate ATPase as well as remodeling activity (Watson et al., 2012) (Hauk et al., 2010), whereas actin-related proteins (ARPs) are critical components of the yeast chromatin remodeling complexes INO80 and RSC, as lack of ARPs reduces ATPase activity (Shen et al., 2003) (Szerlong et al., 2008). Several reports showed interactions of Lsh with Dnmts, suggesting complex formation in order to repress transcription (Zhu et al., 2006) (Myant and Stancheva, 2007) (Dunican et al., 2015). Yet such complexes would exist only transiently as Lsh exists as monomer in nuclear extracts of human cells (Myant and Stancheva, 2007). The results of the ATPase assays indicate that the cooperation of Lsh with Dnmts does not contribute to its ATPase activity and that other factors are required for ATPase stimulation.

4.5 Working model of the mechanism of action

The primary aim of this work was to study the mechanistic properties of Lsh that embody the basis for its well-documented importance for the establishment of transcriptionally inactive chromatin. In this respect, Lsh is supposed to remodel nucleosomes in an ATP-dependent fashion, regulating DNA accessibility. This is a crucial point during the setting of repressive DNA methylation marks, as DNA methyltransferases are unable to recognize and modify DNA in a nucleosomal context.

For a molecular characterization of Lsh, a detailed analysis of its binding behavior as well as ATPase and remodeling activity was performed *in vitro*. In sum, the data presented in this work can be illustrated and interpreted as shown in the following working model of the mechanism of action of Lsh (Fig 4.3):

According to FRAP analyses from Lungu and colleagues (Lungu et al., 2015) as well as results shown in the presented study, Lsh is probably not tightly associated with chromatin when it is active. Thus, upon RNA binding and stimulation of ATPase activity by RNA, Lsh could continuously sample nucleosomes by transiently binding and dissociating from nucleosomes, analogous to a continuous sampling model (Erdel et al., 2011) (see chapter 4.3.4). In this regard, RNA may not only trigger ATPase activity but also serve as a targeting factor. At target sites, an increased but still weak affinity to chromatin results in an increase in ATPase activity until Lsh stably associates with chromatin and the RNA is displaced from its binding site. Binding to chromatin may occur in the linker regions at the entry/exit sites of nucleosomes, and Lsh possibly multimerizes upon binding. In doing so, it possibly binds across the dyad axis of the nucleosome. Thereby, Lsh could spread in a nucleosomal array and in this way mark genomic regions *in vivo*. After dissociating from chromatin, Lsh may interact again with RNA.

Yet the question whether Lsh mobilizes nucleosomes remains unsolved. Alternatively, Lsh could function as an anchor protein with the ability to recognize specific epigenetic chromatin marks. Subsequently, Lsh might direct the organization of chromatin structure by recruiting Dnmts and HDACs and thereby facilitate gene silencing at specific genomic loci.

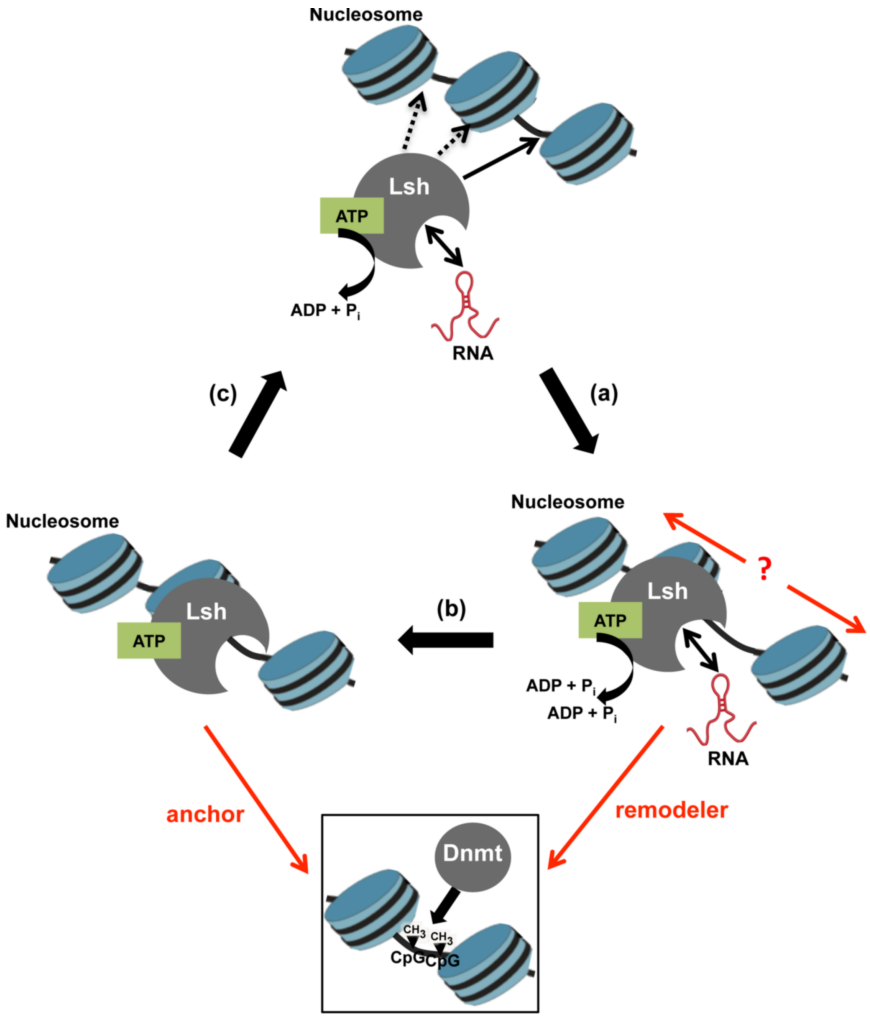

Fig 4.3: Working model of the mechanistic mode of action of Lsh.
Lsh interacts with chromatin transiently and probes nucleosomes when RNA is bound and stimulates its ATPase activity. At target sites like DNA repair sites or gene loci supposed to be silenced, concurrent binding to chromatin and RNA results in increased ATP hydrolysis **(a**). Increased and finally stable association of Lsh with chromatin accounts for the displacement of RNA. Eventually, this leads to an inactive ATPase **(b)**. Factors resulting in the weakening of the interaction with chromatin could enable repeated binding of RNA **(c)**. It remains an open question whether Lsh remodels nucleosomes. Being trapped on chromatin when inactive, Lsh could also act as a sort of anchor protein recruiting Dnmts in order to facilitate DNA methyation.

4.6 Perspectives

With a view to identify the interaction domain that is responsible for DNA and RNA binding, it was tried to generate deletion mutants of Lsh. In addition, it is possible that Lsh contains a so far undescribed inhibitory domain negatively influencing ATP binding or hydrolysis, as described for *D. melanogaster* ISWI (Clapier and Cairns, 2012). The deletion mutants could also serve to study the existence of such inhibitory domains in Lsh. However, either expression of the mutants failed or the elution fractions collected during purification attempts contained a number of contaminants (data not shown).

To date, it is not known whether Lsh contains domains with similarities to interaction domains of chromatin remodelers, such as plant homeodomain (PHD) fingers, chromodomains, bromodomains, HAND-SANT-SLIDE (HSS) domains and helicase-SANT-associated (HSA) domains. For this purpose, multiple sequence alignments were carried out with MSAProbs, a software tool that uses an accurate and well-documented multiple sequence alignment algorithm for protein sequences (Liu et al., 2010) (Gudyś and Deorowicz, 2014). The protein sequence of Lsh was compared to protein sequences of remodelers containing the interaction domain. The respective remodelers were selected from literature (remodelers with PHD domain: (Bienz, 2006); remodelers with bromodomain: (Jeanmougin et al., 1997); remodelers with HSS domain: (Grüne et al., 2003); remodelers with HSA domain: (Szerlong et al., 2008); remodelers with chromodomains: (Yap and Zhou, 2011)). According to the results of the sequence alignments, Lsh does not contain regions with motifs characteristic for PHD fingers, bromodomains and HSS domains (data not shown). In contrast, amino acids (aa) 30–115 and aa 142–206 of Lsh show overlaps with parts of HSA/post-HSA domains and chromodomains of chromatin remodelers (Fig 4.4).

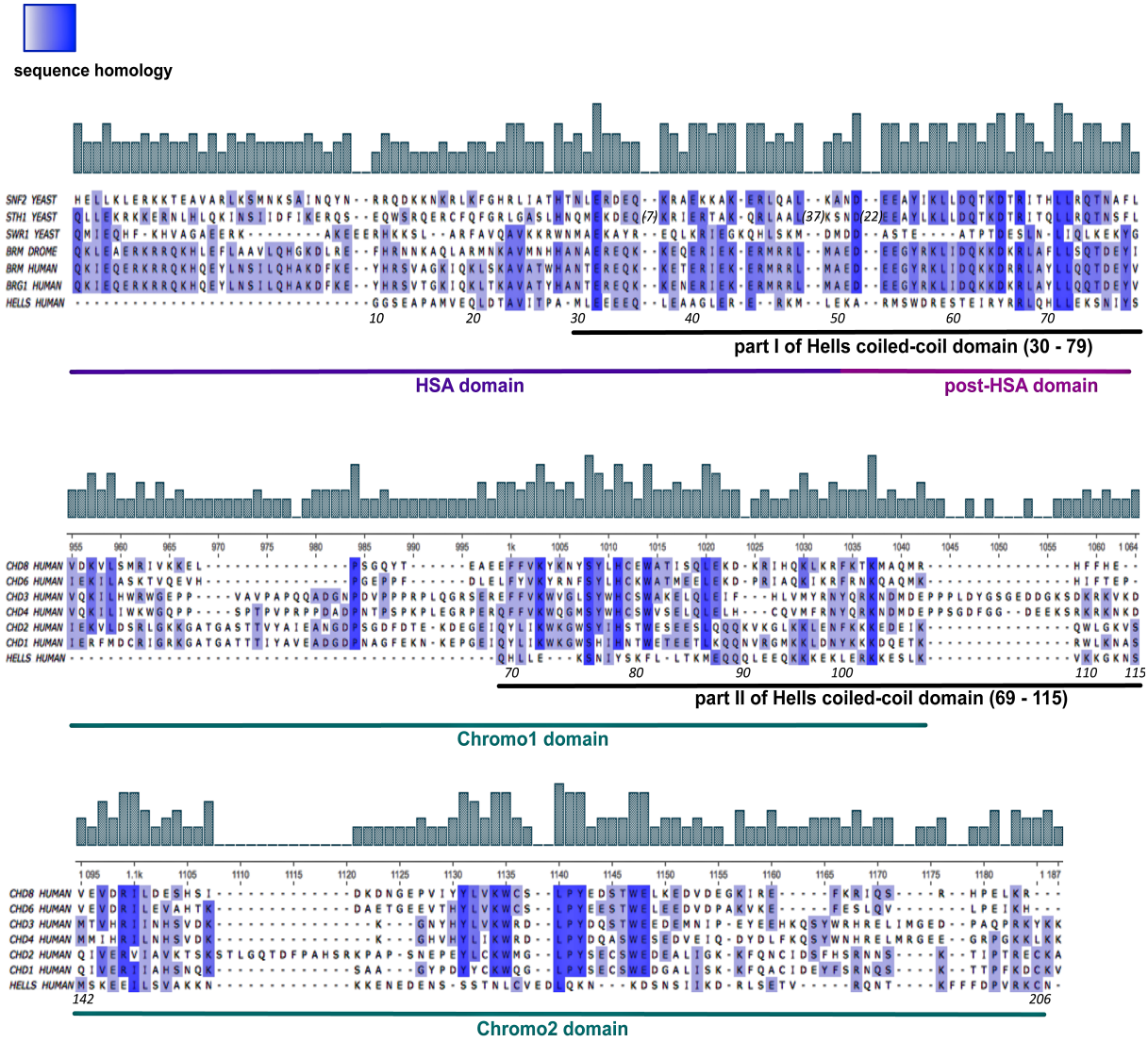

Fig 4.4: Multiple sequence alignments of Lsh (Hells) and HSA/post-HSA domains and chromodomains of chromatin remodelers.
Amino acids (aa) 10–79 of Lsh (referred to as Hells) are aligned to HSA/post-HSA domains of chromatin remodelers selected from Szerlong et al., Nature Struct. & Mol. Biol. 2008. Aa 69–115 and aa 142–206 of Lsh are aligned to chromodomains of chromatin remodelers selected from Yap and Zhou, Biochemistry 2008. Multiple sequence alignments were performed with MSAProbs and were visualized with the UGENE software tool. Numbers in brackets in one of the protein sequences (STH1 YEAST) show streches of amino acids that are not included in the rest of the protein sequences of the alignment. The degree of sequence similarity is color-coded and additionally indicated as bars on top of the alignments. A black line indicates the coiled-coil domain of Lsh. Violet lines indicate HSA/post-HSA domain, and turquoise lines indicate chromodomains.

Amino acids 30–115 represent the coiled-coil domain of Lsh. Coiled-coils are highly versatile protein motifs and can act as protein-protein interaction motifs, for example as dimerization domains in transcription factors and receptor kinases, or function as "zippers" in membrane fusion proteins. Besides being integral parts of molecular motors such as actins and kinesins, coiled-coil proteins with ATPase and GTPase domains often function in protein folding and DNA repair (Rose et al., 2005). Interestingly, the transcriptional repressor p66α and the methyl-binding domain protein MBD2, both components of the chromatin remodeling complex NURD, bind to each other via coiled-coils, and this coiled-coil interaction is

functionally important for MBD2-NURD mediated gene silencing (Gnanapragasam et al., 2011). Transferred to Lsh, the coiled-coil domain could be an interaction region responsible for the association with yet unknown but possibly important factors for the putative remodeling function of Lsh. In support of the suggested relevance for protein-protein interactions, the coiled-coil domain of Lsh and parts of HSA and post-HSA domains of remodelers share several amino acids (Fig 4.4). HSA domains of remodelers are binding platforms for actin and actin-related proteins (ARPs), and are supposed to contribute to the ATPase activity of ARP containing remodeling enzymes (Szerlong et al., 2008). For future experiments to identify functionally important interaction partners, one could try to isolate the coiled-coil domain and also generate a deletion version missing the coiled-coil domain and do pulldown assays, and afterwards look for differences in the fractions of bound proteins between WT the deletion mutants.

Furthermore, the multiple sequence alignments show that the coiled-coil domain (aa 69–115) and the region of Lsh comprising aa 142–aa 206 have protein sequence similarities with chromo1 and chromo2 domains of chromatin remodelers from the CHD family (Fig 4.4). Chromodomains usually serve as methylated histone-lysine binding motifs, facilitating recruitment to chromatin (Yap and Zhou, 2011). Thus it would be of interest to study whether Lsh prefers binding to nucleosomes containing methylated lysine residues to nucleosomes reconstituted with unmodified histones.

Clapier and Cairns defined two new regulatory regions on *D. melanogaster* ISWI, termed AutoN and NegC, which negatively regulate ATP hydrolysis (AutoN) or the coupling of ATP hydrolysis to DNA translocation (NegC). The AutoN domain contains a region similar to the so-called “basic patch“ of the histone H4 tail. Point mutations of the two arginine residues in this basic patch-like region have been found to increase ATPase activity and increase remodeling rates (Clapier and Cairns, 2012). According to multiple sequence alignments of Lsh and ISWI homologs, Lsh contains arginine residues at positions matching the two arginine residues in the basic patch-like region included in the AutoN domain of ISWI remodelers (Fig 4.5 A).

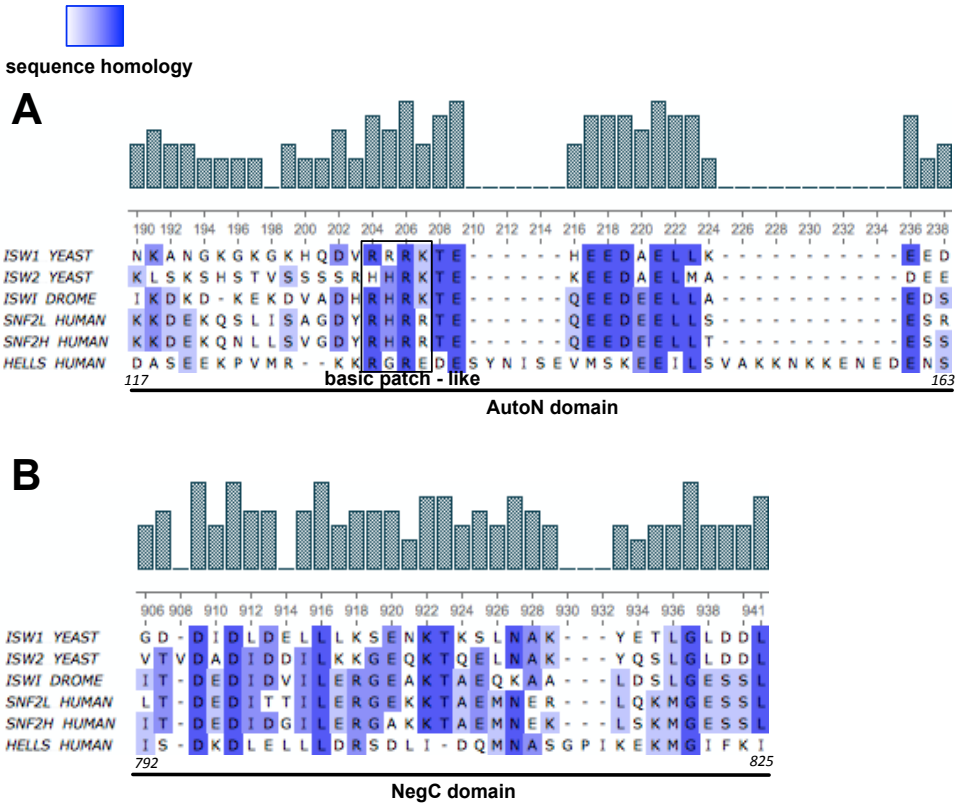

Fig 4.5: Multiple sequence alignments of Lsh (Hells) and AutoN and NegC domains of ISWI homologs. **(A)** The protein sequence (aa 117–163) of Lsh (referred to as Hells) is aligned to AutoN domains of ISWI remodelers. The basic patch-like region is highlighted in a rectangle. **(B)** The protein sequence (aa 792–825) of Lsh (referred to as Hells) is aligned to NegC domains of ISWI remodelers. AutoN and NegC domains were defined by Clapier and Cairns (Clapier and Cairns, 2012). Multiple sequence alignments were performed with MSAProbs and were visualized with the UGENE software tool. The degree of sequence similarity is color coded and additionally indicated as bars on top of the alignments. Black lines indicate the AutoN domain and the NegC domain.

Replacement of these two arginine residues with alanines, analogous to experiments done by Clapier and Cairns in terms of *D. melanogaster* ISWI, potentially increase the ATPase activity of Lsh. The alignments also show that Lsh shares a region (aa 792–aa 825) with similarity to NegC domains of ISWI remodelers (Fig 4.5 B). Assuming that Lsh remodels nucleosomes, deletion of this region possibly contributes to sliding activity.

5 Materials and Methods

5.1 Materials

Unless otherwise stated, all common chemicals and materials were purchased from GE Healthcare (Freiburg), Merck (Darmstadt), Invitrogen (Karlsruhe), Fermentas (St. Leon-Rot), New England Biolabs (Frankfurt am Main), Promega (Mannheim), Roche (Mannheim), Roth (Karlsruhe), Serva (Heidelberg), Bio-Rad (Munich), Stratagene/Agilent (Waldbronn), Sigma-Aldrich (Munich) and Qiagen (Hilden). Radioactive nucleotides were ordered at Hartmann Analytics (Brunswig).

5.1.1 Technical devices

Description	Supplier
Agarose gel UV imaging system	GelMax, Intas
Sonifier 250D	Branson
Fluorescence Image Readers	Fujifilm, GE Healthcare
FLA-3000, FLA-5000, Typhoon FLA 9500	
Chemiluminescence Image Reader	Fujifilm
LAS-3000	
Centrifuge Centrikon T-324	Kontron Instruments
PCR machines	Peqlab, Bio-Rad, Perkin Elmer
Peristaltic-pump LKB-P1	GE Healthcare
Tabletop centrifuge	Eppendorf
Trans-blot SD Semi-dry transfer cell	Bio-Rad
Thermomixer Compact	Eppendorf
Ultracentrifuge Centrikon T-1170	Kontron Instruments
OptimaTM L-80 XP	Beckman Coulter
Ultrospec 3100 pro	Amersham Biosciences
Uvikon Spectrophotometer 922	Kontron Instruments
Monolith NT.115 and NT.015T	NanoTemper Technologies
Purelab Ultra	ELGA
Axiovert 200M	Zeiss
Nanodrop ND-1000 Spectrophotometer	Peqlab

5.1.2 Software tools

Software	Application	Supplier
Multigauge V3.1	LAS reader viewer software	Fujifilm
Sigmaplot V12.5	graphical analysis software	Systat Software
RNAfold	RNA secondary structure prediction tool	(http://rna.tbi.univie.ac.at/cgi-bin/RNAfold.cgi)
Netprimer	primer design tool	Premierbiosoft (www.premierbiosoft.com)
BindN	RNA/DNA binding residue prediction tool	(http://bioinfo.ggc.org/bindn/)
VectorNTI V11	*in silico* cloning tool, organization tool	Invitrogen
NEB double digest finder	restriction digest tool	New England Biolabs (www.neb.com)
Reverse complement	nucleic acid reverse complement tool	(http://www.bioinformatics.org/sms/rev_comp.html)
MSAProbs	amino acid alignment tool	(http://msaprobs.sourceforge.net)
UGENE 1.20	nucleic acid and protein sequence editing and annotation tool	Unipro
Blast	comparative alignment and search tool	(http://blast.ncbi.nlm.nih.gov/Blast.cgi)
Protparam	protein parameter analysis tool	(http://web.expasy.org/protparam/)
ImageJ V1.48	image processing program	(open source)
4Peaks V1.7.1	DNA trace file viewer	Mekentosj
EMBOSS needle	pairwise protein sequence alignment tool	(http://www.ebi.ac.uk/Tools/psa/emboss_needle)
Phyre2	3-dimensional protein structure predicting tool	(www.sbg.bio.ic.ac.uk/phyre2/)

5.1.3 Chemicals and consumables

Description	Supplier
5-Methyl-dCTP	TriLink Biotechnologies
1.5 ml and 2 ml micro centrifuge tubes	Eppendorf/Sarstedt
15 ml and 50ml tubes	Sarstedt
Agarose (ME, LE GP and low melting)	Biozym
Ammonium acetate	Merck
Ammonium persulfate (APS)	Merck
ATP	Sigma
[γ-32P]-ATP (300Ci/mmol)	Hartmann Analytics
Bacto Agar	BD
Bacto Peptone	BD
Bacto Tryptone	BD
Barrier food wrap	Saran
Blue Gal	Invitrogen
Boric acid	Merck
Bradford reagent	Bio-Rad
Bromophenolblue	Serva
BSA (albumin fraction V)	Sigma
BSA purified	NEB
ß-Mercaptoethanol	Sigma
Cellculture flasks	Greiner
Columns, 1.5 ml, 35 µm filter pore	MoBiTec
Concentration tubes Microsep 10K, 30K	Omega
Coomassie G250	Serva
Cryovials	Roth
DEPC	Sigma
Dialysis membranes, 6–8 kD MWCO	Spectra Por
DMSO	Sigma
dATP, dGTP, dTTP	Genaxxon
dNTP mix	NEB/Qiagen
DTT	Roth
EDTA	Sigma
EGTA	Sigma
Ethidium bromide	Sigma
ETOH tech., p.a.	Merck

Description	Supplier
Filter paper Whatman 3MM	Whatman
Filter tips	Roth
Filter unit	Nalgene, 0.2 µm filter holes
Formaldehyde, 37%	Roth
Glass pipettes 5 ml and 10 ml	Hirschmann®
Glassware	Schott
Glycerin	Merck
Glycogen	Roche
HEPES	Roth
IPTG	Roche
Isopropanol p.a.	Merck
Laboratory film	Parafilm®
Lithium chloride	Sigma
Magnesium acetate	Merck
Magnesium chloride	Merck
Methanol p. a	Merck
Milk powder	Sucofin
Monolith NT115 standard treated capillaries	NanoTemper Technologies
MOPS	Roth
Nickel-NTA-agarose (Ni2+-beads)	Qiagen
Nitrocellulose membrane (GSWP, 0.22 µM)	Millipore
NP40	Sigma
Orange G	Sigma
Pasteur pipettes	Brand
PCR-reaction tubes 0.2 ml	Biozym
Petridishes and tissue culture dishes	Greiner, Sarstedt
Pipette tips	Gilson, Brand
PMSF	Sigma
Potassium chloride	Merck
Protein gel cassettes (disposable)	Invitrogen
Rotiphorese acrylamid-bisacrylamid	Roth
Siliconized 1.5 ml reaction tubes	Eppendorf, Bio-Rad

Description	Supplier
Sodium chloride	VWR
Sodium dodecyl sulfate (SDS)	Roth
Sodium phosphate mono-sodium salt	Merck
Sodium phosphate di-sodium salt	Merck
Sucrose	Roth
Sybr Safe	Invitrogen
Syringes and accessories	Roth
TCEP	Sigma
TEMED	Roth
TLC plates	Merckmillipore
Tris	Invitrogen
Triton X-100	Sigma
TRIzol	Ambion
Trypsin/EDTA (TC)	PAA
Tween 20	Sigma
Ultracentrifugation tubes for SW40 rotor	Beckman Coulter
Urea	Merck
X-tremeGENE	Roche
Yeast extract	BD
Chloroform	Roth
Fetal bovine serum	Sigma

5.1.4 Standard solutions

Stock solutions and buffers were prepared according to standard protocols (Sambrook and Russell, 2001) (Roche, 2011). Protease Inhibitor Cocktail (Roche) was freshly added. Common solutions are listed below.

Buffer	Composition
Annealing buffer	20 mM Tris-HCl pH 7.4 2 mM $MgCl_2$ 50 mM NaCl
EX-X buffers	20 mM Tris-HCl pH 7.6 1.5 mM $MgCl_2$ 0.5 mM EGTA 10% glycerol X mM KCl pH adjusted to 7.6 with HCl
Phosphate Buffered Saline (PBS)	140 mM NaCl 2.7 mM KCl 8.1 mM Na_2HPO_4 1.5 mM KH_2PO_4 pH adjusted to 7.4 with HCl
Tris Buffered Saline, 10x (10xTBS)	100 mM Tris 1.5 mM NaCl pH adjusted to 7.6 with HCl
TBST buffer	1xTBS with 0.1% Tween 20
TBST-milk	TBST buffer 5% (w/v) milk powder
TBST-BSA	TBST buffer 2.5% (w/v) BSA

Buffer	Composition
Transferbuffer (Towbin)	25 mM Tris 192 mM glycine 20% methanol 0.05% SDS
TBE buffer	90 mM Tris 90 mM boric acid 2 mM EDTA
TE buffer	10 mM Tris-HCl pH 7.6 1 mM EDTA
DNA sample buffer (10x)	50% glycerol 50 mM Tris-HCl pH 7.6 10 mM EDTA 0.05% (w/v) bromophenol blue and xylene cyanol
Orange G loading dye (10x)	50% glycerol 10 mM EDTA 0.05% (w/v) Orange G
SDS-protein sample buffer (5x)	300 mM Tris-HCl pH 6.8 10% (w/v) SDS 50% glycerol 5% ß-Mercaptoethanol 0.2 % (w/v) bromophenol blue
SDS-PAGE stacking buffer (4x)	0.5 M Tris 0.4 % SDS pH adjusted to 6.8 with HCl
SDS-PAGE separating buffer (4x)	1.5 mM Tris 0.4 % SDS pH adjusted to 8.8 with HCl

Buffer	Composition
SDS-PAGE running buffer	192 mM glycine 25 mM Tris 0.1% (w/v) SDS
Coomassie staining solution	45% water 45% methanol 10% acetic acid
MST sample buffer	50 mM HEPES pH 7.4 5 mM $MgCl_2$ 100 mM NaCl 0.05% (w/v) NP40
High salt buffer for chromatin assembly	10 mM Tris-HCl pH 7.6 2 M NaCl 1 mM EDTA 0.05% NP40 1 mM ß-Mercaptoethanol
Low salt buffer for chromatin assembly	10 mM Tris-HCl pH 7.6 50 mM NaCl 1 mM EDTA 0.05% NP40 1 mM ß-Mercaptoethanol
TLC developing buffer	0.5 M LiCl 1 M formic acid
MOPS buffer (10x)	20 mM NaAc 0.2 M MOPS 10 mM EDTA pH adjusted to 7.0 with 10 M NaOH

Buffer	Composition
RNA loading dye	1xMOPS 2.2 ml formaldehyde (37%) per 10 ml dye 50% formamide 0.05% (w/v) bromophenol blue
Lysis buffer I His-tag purification	50 mM Tris-HCl pH 7.6 100 mM KCl 0.1% NP40 Protease Inhibitor Cocktail (Roche)
Lysis buffer II His-tag purification	EX500 10 mM imidazole 0.1% NP40 0.01% ß-Mercaptoethanol Protease Inhibitor Cocktail (Roche)
Wash buffer His-tag purification	EX500 20 mM imidazole 0.1% NP40 0.01% ß-Mercaptoethanol Protease Inhibitor Cocktail (Roche)
Elution buffer His-tag purification	EX300 250 mM imidazole 0.1% NP40 0.01% ß-Mercaptoethanol Protease Inhibitor Cocktail (Roche)

5.1.5 Enzymes

Enzyme	Supplier
Antarctic Phosphatase	New England Biolabs
Micrococcus Nuclease (MNase)	Roche, Sigma
Proteinase K	Sigma
Restriction endonucleases	New England Biolabs
DNase I	Roche
RNase A	Roche
T4 polynucleotide kinase (PNK)	New England Biolabs
T4 DNA ligase	New England Biolabs
Taq DNA polymerase	Genaxxon
Herculase II Fusion Enzyme	Agilent
Phusion DNA polymerase	Finnzyme

5.1.6 Kits

Kit	Supplier
Herculase II Fusion Enzyme dNTP Combo PCR Kit	Agilent
QIAquick PCR purification Kit	Qiagen
QIAEX® Gel Extraction Kit	Qiagen
QIAprep Spin Miniprep Kit	Qiagen
Qiagen Plasmid Purification Midi Kit	Qiagen
PureLink™HiPure Plasmid Maxiprep Kit	Invitrogen
Super signal WEST Dura WB Kit	Pierce
Bac-to-Bac Baculovirus Expression System	Invitrogen
Gateway BP Clonase II Mix	Invitrogen
Gateway LR Clonase II Mix	Invitrogen
NucleoSpin RNA Kit	Macherey-Nagel
Dnmt Activity/Inhibition Assay Kit	Active Motif

5.1.7 Standard DNA and protein marker

Pre-stained protein marker PAGERuler	Fermentas
GeneRuler, ultra low range DNA marker	Fermentas
GeneRuler 1kb plus DNA marker	Fermentas

5.1.8 Protease inhibitors, RNase inhibitors and antibiotics

Substance	Supplier
Ampicillin	Sigma
Kanamycine	Sigma
Tetracycline	Sigma
Gentamycine	Sigma
Chloramphenicol	Roth
Penicillin/Streptomycine	Invitrogen/Gibco
Protease Inhibitor Cocktail	Roche
RNasin	Promega

5.1.9 Bacterial cell lines and media

Bacterial cell lines:

DH5alpha

description	general DNA plasmid propagation
resistance	none
genotype	F-φ80lacZΔM15 Δ(lacZYA-argF) U169 endA1 recA1 hsdR17 (rk-,mk+) supE44 thi-1 gyrA96 relA1 phoA

XL1 Blue

description	F´episome, general DNA plasmid propagation, blue/ white screening
resistance	tetracycline
genotype	recA1 endA1 gyrA96 thi-1 hsdR17 supE44 relA1 lac (F'proAB lacIqZDM15)

DH10EMBacYFP

description	*E. coli* strain that carries the baculoviral shuttle vector bMON14272 with a lowcopy number mini-F replicon with a kanamycine resitance marker and Tn7 transposon attachment sites within the LacZa peptide. The helper plasmid pMON7124 encodes for the transposase and confers resistance to tetracycline. YFP serves as virus performance marker.
resistance	kanamycine, tetracycline
genotype	F–ompT hsdSB (rB–mB–) gal dcm (DE3) pLysSRARE2

Media:

LuriaBertani (LB) medium

1.0% (w/v) Bacto-Tryptone

1.0% (w/v) NaCl

0.5% (w/v) Bacto-Yeast extract

Adjust pH to 7.0 with 10 M NaOH

Medium was autoclaved for 20 min at 120°C. Appropriate antibiotics were added in standard concentrations (Roche, 2011) prior to usage. For preparing plates, LB medium was mixed with 2 % agar and the appropriate antibiotics were added after cooling down to 50°C.

SOB medium

2 % (w/v) Bacto-Tryptone

10 mM NaCl

0.5% (w/v) Bacto-Yeast extract

2.5 mM KCl

10 mM $MgCl_2$*

Adjust pH to 7.0 with 10 M NaOH

* add before use

The medium was autoclaved for 20 min at 120°C.

5.1.10 Eukaryotic cell lines and media

HEK293

cell type	human embryonic kidney
growth conditions	37 °C, 5% CO_2, D-MEM-GlutaMAX, 10% FCS, 1% Pen/Strep
supplier	ATCC, cells were received second hand from I. Araya

HeLa

cell type	human cervix carcinoma
growth conditions	37 °C, 5% CO_2, D-MEM-GlutaMAX, 10% FCS, 1% Pen/Strep
supplier	ATCC, cells were received second hand from I. Araya

Sf21

cell type	insect cell line (*Spodoptera frugiperda*)
growth conditions	27°C, Sf-900^{TM} II SFM (Gibco), shaking (100 rpm)
supplier	cells were received second hand from L. Manelyte

5.1.11 Antibodies

Antibody	Supplier	Description	Dilution
HisProbe-HRP	ThermoFisher	none	1:1000
Penta His	Qiagen	mouse, monoclonal	1:3000
Anti-6x His-tag	Abcam	mouse, monoclonal	1:1000
Lsh (H-4; sc 46665)	Santa Cruz	mouse, monoclonal	1:1000

5.1.12 Oligonucleotides

All oligonucleotides used in this study were purchased from Eurofins MWG Operon and Integrated DNA Technologies. Oligonucleotides were diluted with MilliQ-water to a final concentration of 100 µM. Oligonucleotides for PCR amplification and sequencing reactions were designed to show a minimum of secondary structure, primer dimerization and with a melting temperature Tm of 60°C with the freely available Netprimer software provided by Premierbiosoft.

Unmodified DNA oligonucleotides:

Name; Orientation	Application; Amplicon and template	Sequence (5'–3')
TGP_30; for	cloning ; full-length Lsh WT and Lsh-Nterm template: pTriEXLsh10xC-His	CCTAGGGGGGACAAGTTTGTACAA AAAAGCAGGCTCCACCATGCCAGC GGAACGGCC
TGP_31; rev	cloning; full-length Lsh WT template: pTriEXLsh10xC-His	CCTAGGGGGGACCACTTTGTACAA GAAAGCTGGGTCAAACAAACATTC AGGACTGG
TGP_45; for	site-directed mutagenesis; full-length Lsh KR template: pDFB7LshWT6xC-His	GGATTGGGTAGAACAGTTCAGTG (in red: mismatched bases to create point mutation)
TGP_46; rev	site-directed mutagenesis; full-length Lsh KR template: pDFB7LshWT6xC-His	ACTGAACTGTTCTACCCAATCCC (in red: mismatched bases to create point mutation
TGP_54; for	cloning; Lsh-ATPase/Helicase domain and Lsh-ATPase domain template: pDFB7LshWT6xC-His	CCTAGGGGGGACAAGTTTGTACAA AAAAGCAGGCTCCACCATGCTTTG GGAAAATGGA
TGP_55; rev	cloning; Lsh-ATPase domain template: pDFB7LshWT6xC-His	CCTAGGGGGGACCACTTTGTACA AGAAAGCTGGGTCATCTGGCAACA AAAAGTTTAG
TGP_56; rev	cloning; Lsh-ATPase/Helicase domain template: pDFB7LshWT6xC-His	CCTAGGGGGGACCACTTTGTACAA GAAAGCTGGGTCATCTAAGAAATT CTTAGACA
TGP_58; rev	cloning; Lsh-Nterm template: pTriEXLsh10xC-His	CCTAGGGGGGACCACTTTGTACAA GAAAGCTGGGTCAAGCCATTCCA TGCCTTCTA
MF_77; for	MST; BN601 fragments generated by PCR on pGA4 BN601-m1	AGATCTTTTGAGGTCCGGTTCTT
MF_78 ; rev	MST; BN601 fragments generated by PCR on pGA4 BN601-m1	ATCTTAGTACGGAGAGGGAGCG
RM_08; for	ATPase assays; 601-10N-601 generated by PCR on pBS-601-10N-601	GCGAATTGGAGCTCCACCGC
RM_09; rev	ATPase assays; 601-10N-601 generated by PCR on pBS-601-10N-601	CGTCGTCATCCTTGTAATC

Name; Orientation	Application; Amplicon and template	Sequence (5'–3')
mDNA_-190; for	MST, EMSA and remodeling; rDNA promoter fragment -190/+90 template: pT7Blue-m-190+90	TATCAGTTCTCCGGGTTGTCAGGTC
AP_7; for	MST and EMSA; 0-NPS-0 template: pPCRScript_slo1-gla75	GATCCAGAATCCTGGTGCTGAG
AP_1; for	MST, EMSA, remodeling and ATPase assays; 77-NPS-77 template: pPCRScript_slo1-gla75	ATCTTTTGAGGTCCGGTTCTTT
AP_15; rev	ATPase assays; 77-NPS-77 template: pPCRScript_slo1-gla75	GTACAGAGAGGGAGAGTCACAAAAC
En3D_for	MST and EMSA	TCTTTTTTTTTTTTTTTCTTTTTTCCTCC
AIR down 20; rev	MST	GGAATCGTCCACGCGTTAGA
AIR down 35; rev	MST	CAAGGGGACGATTCCACGCGTTAGACGATTCCGCA
AIR down 60; rev	MST	GCACCGTGATTCGAGATCGCGACCTCAATCGGACGATTCCACGCGTTAGACGATTCCGCA

Modified DNA oligonucleotides:

Name; Orientation	Application; Amplicon and template	Modification	Sequence (5'–3')
fl TGP_2; for	MST; BN601 fragments template: pGA4 BN601-m1	5'-Cy5	AGATCTTTTGAGGTCCGGTTCTT
fl TGP_3; rev	MST; BN601 fragments template: pGA4 BN601-m1	5'-Cy3	ATCTTAGTACGGAGAGGGAGCG
mDNA_90; rev	MST, EMSA, remodeling; murine rDNA promoter fragment (190/+90) template: pT7Blue-m-190+90	5'-Cy5	GAATAGGCTGGACAAGCAAAACAGCC

Name; Orientation	Application; Amplicon	Modification	Sequence (5'–3')
fLP_26; rev	MST and EMSA; 0-NPS-0 template: pPCRScript_slo1-gla75	5'-Cy3	TAGCTGTATATATC TGACACATG
fLP_25; rev	MST, EMSA, remodeling 77-NPS-77; template: pPCRScript_slo1-gla75	5'-Cy3	GTACAGAGAGGGA GAGTCACAAAAC
En3D_rev	MST and EMSA	5'-Cy5	GGAGGAAAAAAGAA AAAAAAAAAAAAAA GA
AIR up 20; for	MST	5'-Cy5	TCTAACGCGTGGAC GATTCC
AIR up 35; for	MST	5'-Cy5	TGCGGAATCGTCTA ACGCGTGGAATCGT CCCCTTG
AIR up 60; for	MST	5'-Cy5	TGCGGAATCGTCTA ACGCGTGGAATCGT CCGATTGAGGTCG CGATCTCGAATCAC GGTGC

Modified RNA oligonucleotides:

Name; Orientation	Application; Amplicon	Modification	Sequence (5'–3')
En3D_RNA	MST and EMSA	5'-FAM	CCUCCUUUUUUCU UUUUUUUUUUUUU UCU

5.1.13 Plasmids

General plasmids:

Plasmid	Insert	Created by
pPCRScript_slo1-gla75	trimeric nucleosome positioning sequence NPS1 with rDNA and hsp70 DNA flankings	Sloning
pUC18 12x 601	12 repeats of 200 bp long 601 NPS in pUC18 plasmid	J. Widom
pGA4 BN601-m1	vector containing a modified 601 sequence	Mr. Gene

Plasmid	Insert	Created by
pBS-601-10N-601	2 repeats of 601 NPS sequence separated by 10 nucleotides of random sequence	J. Reese
pCMV14	CMV promoter containing vector	Stratagene
pT7Blue-m-190+90	murine rDNA promoter sequence (-190/+90)	L. Manelyte
pTriEx-Lsh-WT-10xC-His	human full-length Lsh WT with C-terminal 10xHis-tag	Mr. Gene

GATEWAY plasmids:

Plasmid	Insert	Created by
pDONR221	attP sites containing donor vector to create GOI containing entry clones by site specific recombination	Invitrogen
pDONR221-GOI	entry clones with the following GOIs: full-length (fl) Lsh, WT and KR, Lsh-ATPase domain, WT and KR, Lsh-ATPase/Helicase domain, WT and KR, Lsh-Nterm WT	T. Gross
pDM3-Lsh-N-Flag_C-His	destination vector with full-length Lsh WT gene and N-terminal Flag tag and C-terminal His-tag; the vector is suited for bacterial expression	T. Gross
pDM7-GOI-6xC-His	destination vectors with the following GOIs: Lsh-ATPase domain, WT and KR, Lsh-ATPase/Helicase domain, WT and KR, Lsh-Nterm WT; GOIs are fused to a C-terminal His-tag; the vector is suited for bacterial expression	T. Gross
pDFB7-GOI-6xC-His	destination vectors with the following GOIs: full-length (fl) Lsh, WT and KR, Lsh-ATPase/Helicase domain, WT and KR, Lsh-Nterm WT; GOIs are fused to a C-terminal His-tag; plasmids are used for recombination into baculovirus shuttle bacmid	T. Gross

5.1.14 Baculoviruses

Gene of interest (GOI)	Virus
human Lsh, WT and KR mutant	pDFB7-fl-LshWT-6xC-His and pDFB7-fl-LshKR-6xC-His were recombined into bacmid DNA, and recombinant viruses were generated
human Lsh AH, WT and KR mutant	ATPase domain in combination with Helicase domain of Lsh WT and KR (pDFB7-LshAH-WT-6xC-His and pDFB7-LshAH-KR-6xC-His) were recombined into bacmid DNA, and recombinant viruses were generated
human Lsh WT-Nterm, aa 1–234	N-terminus of Lsh WT (pDFB7-LshNterm-WT-6xC-His) was recombined into bacmid DNA, and recombinant virus was generated

5.1.15 Histones

Core histone octamers were purified from chicken erythrocytes and provided in the laboratory by E. Silberhorn.

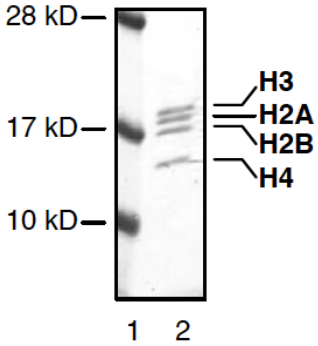

Fig 5.1: Histone octamers purified from chicken erythrocytes.
1 µg of octamers was loaded onto a 17% SDS gel and subsequently stained with coomassie blue. Bands of the four core histones H2A, H2B, H3 and H4 are depicted in lane 2 (adapted from J. Exler, PhD thesis, 2010).

5.2 Methods

All molecular work like preparation and transformation of chemically-competent bacteria with DNA, amplification of plasmid DNA in *E.coli*, purification, concentration determination, restriction enzyme digestion, ligation of DNA fragments, analysis of DNA on agarose and polyacrylamide gels, and amplification of DNA by polymerase chain reaction (PCR) was performed following standard protocols (Sambrook and Russell, 2001). Bacteria were cultured in LB medium, and appropriate antibiotics were added corresponding to the plasmid-encoded resistance. The plasmid DNA was isolated with DNA purification kits (Invitrogen/Qiagen). Isolation of DNA fragments from agarose gels was performed using the Qiagen Gel Extraction kit.

5.2.1 Working with DNA

5.2.1.1 Determination of DNA quality and quantity

The NanoDrop ND1000 spectrophotometer (Peqlab) was used to determine DNA concentration and purity by absorption measurements at 260 nm. Protein impurities can be determined by absorption measurement at 280 nm. The ratio $A^{260}/_{280}$ provides information about the purity of the DNA. DNA quality was additionally analyzed by agarose gel electrophoresis.

5.2.1.2 Polyacrylamide and agarose gel electrophoresis

Agarose gel electrophoresis was generally performed with gels containing 0.8–1.2 % (w/v) agarose in 1x TBE buffer, 1:10000 SYBR Safe (Invitrogen), in 1xTBE running buffer at a constant voltage of 100–120 V. DNA standard marker and samples were supplemented with 6x DNA loading dye. In contrast to agarose gel electrophoresis, DNA was separated by polyacrylamide gel electrophoresis (PAGE) in 0.4x TBE at 100 V. In order to remove unpolymerized acrylamide, gels were pre-runned for 30–45 min at 50–70 V. For visualization, the gels were stained in 0.4x TBE containing ethidiumbromide (0.5mg/ml) for 15 min and washed twice with distilled water for 10 min each.

5.2.1.3 Restriction enzyme digestion

Restriction enzymes were used at reaction conditions according to the manufacturer's recommendations concerning buffer, addition of BSA, incubation time and temperature (see www.neb.com). For analytical digestion 0.2–1 µg DNA was incubated with 5 units of the respective restriction endonuclease in a total volume of 25 µl. The preparative restriction enzyme digestion was usually done with 5–10 µg DNA using 4 units restriction endonuclease

per 1 µg DNA in a total volume of 50 µg. To check completion of enzyme digestion, DNA was electrophoretically separated using 0.8–1.2% TBE-agarose gels supplemented with SYBR Safe (Invitrogen).

5.2.1.4 DNA ligation

Ligation of sticky or blunt-ended DNA fragments was performed using the T4 DNA ligase (NEB). The molar ratio of insert to vector was kept in a range between 3/1–5/1. The ATP containing 10x ligase buffer was stored in aliquots at -20 °C. Ligation reaction was performed in a total volume of 20 µl at 16 °C overnight (O/N).

5.2.1.5 Polymerase chain reaction (PCR)

For PCR reactions used in cloning procedures, the Phusion polymerase (Finnzyme) was used according to the manufacturer's instructions. The PCR protocol was adjusted for each reaction concerning annealing temperature and time as well as elongation time. The general outline and a typical reaction mix are depicted in the tables below.

Cycle step	Temperature (°C)	Time	Number of cycles
Initial denaturation	98 °C	3 min	1
denaturation	98 °C	30 sec	20
annealing	50-60 °C (depends on primers)	30 sec	
extension	72 °C	30 sec + 30 sec/kb	
Final extension	72 °C	5 min	1

Reagents	Volumes
Primer for 10µM	2.5 µl
Primer rev 10µM	2.5 µl
dNTPs 10 mM	1 µl
Phusion-buffer 5x	10 µl
Phusion-pol.	0.5 µl
Template	200 ng
H_2O	33.5 µl minus µl template
Total volume	50 µl

5.2.1.6 Preparative DNA precipitation

DNA was precipitated (after PCR amplification, restriction digest, etc.) by addition of 0.5 volumes of 7.5 M ammonium acetate (pH 7.8) and 2.5 volumes of 100% icecold Ethanol (EtOH). Glycogen (0.5 µg/µl) was added to improve DNA precipitation. Samples were incubated on ice for 10 min, pelleted (4 °C, 13000 g, 15–30 min), washed with 70% EtOH and dissolved in either MilliQ-water or TE-buffer.

5.2.1.7 Colony PCR

Colony PCR was employed as a fast and quick method to screen for clones that contain the appropriate insert in correct orientation, before starting to grow colonies for plasmid isolation. Therefore, a pipette tip was dipped into a bacterial colony on an agar plate. One part of adhering cells was gridded on fresh LB plates containing the appropriate antibiotics, the rest was subsequently mixed with 20 µl water in a 0.2 ml PCR tube. Cells were opend for 10 min at 100 °C. Afterwards, 30 µl of colony PCR master mix were added to each PCR tube, and the reactions were subjected to the colony PCR programm. For colony PCR, a lab made Taq polymerase was used. The general outline and a typical reaction mix are depicted in the tables below.

Cycle step	Temperature (°C)	Time	Number of cycles
Initial denaturation	95 °C	5 min	1
denaturation	95 °C	30 sec	35
annealing	50-60 °C (depends on primers)	30 sec	
extension	72 °C	60 sec/kb	
Final extension	72 °C	5 min	1

Reagents	Volumes
Primer for 10µM	2.5 µl
Primer rev 10µM	2.5 µl
dNTPs 10 mM	1 µl
Taq-buffer 10x	5 µl
Taq-pol.	1 µl
(H_2O + colony)	(20 µl)
H_2O	18 µl
Total volume	50 µl

5.2.1.8 Annealing of oligonucleotides

Equimolar amounts of sense and complementary antisense oligonucleotides were diluted to the desired concentration in 1x annealing buffer. The samples were incubated at 95 °C for 10 min in a thermoblock. Afterwards, the thermoblock was switched off to slowly cool down reactions to room temperature for approximately 1–2 h. For annealings with fluorescently labeled oligonucleotides, the unlabeled strand was used in approximately 5% excess to guaranty complete annealing of all labeled oligonucleotides. This was done to avoid background signals from single-stranded (ss) fluorescently labeled oligonucleotides in the MST assays. Annealing reactions were analyzed by native PAGE.

5.2.1.9 Preparation of methylated, hydroxymethylated and unmodified BN601 DNA fragments

Methylated, hydroxymethylated and unmodified BN601 DNA fragments were generated by PCR, introducing methylated and hydroxymethylated cytosines by replacing dCTP in the dNTP mix either with methyl-dCTP (TriLink) or hydroxymethyl-dCTP (gift from Attila Nemeth). As template the plasmid pGA4 BN601-m1 (Mr. Gene) was used, which harbours an altered 601 nucleosome positioning sequence (BN601) such that the produced DNA fragments, each with a size of 310 bp, contained 25 evenly distributed CpG sites (Fig 5.2 A). To amplify methylated DNA fragments, the temperature in the denaturing steps was raised to 100 °C in order to destabilize the ^{m5}dC:dG base pairs and thus allow efficient amplification of the template (Wong and McClelland, 1991). For fluorescent labeling of the DNA fragments, one primer was attached either with Cy5 or Cy3 as cyanine fluorescent dye at its 5'-end. In the following, the PCR temperature settings and pipetting schemes to set up a 50 µl reaction are described.

Cycle step	Temperature (°C)	Time	Number of cycles
Initial denaturation	5-hmC: 95 °C 5-mC: 100 °C	2 min	1
denaturation	5-hmC: 95 °C 5-mC: 100 °C	15 sec	20
annealing	55 °C	20 sec	
extension	72 °C	25 sec	
Final extension	72 °C	5 min	1

Reagents	Volumes
Unlabeled primer 10 µM	2.5 µl
Labeled primer 10µM	0.5 µl
dNTPs 10 mM	1 µl
Phusion GC buffer 5x	10 µl
Phusion-pol.	0.5 µl
Template	10 ng
H_2O	35.5 µl - template
Total volume	50 µl

After PCR, the product was purified using the Qiaquick PCR Purification kit (Qiagen), and the concentration was determined on the Nanodrop photometer (PeqLab).
The DNA fragments contain two HpaII restriction sites, enabling analysis of incorporation of methyl- and hydroxymethyl-modifications by restriction endonuclease digestion with HpaII and its isoschizomer MspI (Fig 5.2). MspI and HpaII recognize the same sequence (CCGG) but are sensitive to different methylation status. HpaII cleaves only a completely unmodified

site, and any modification at either cytosine blocks cleavage. MspI cleaves unmodified CCGG sites and will recognize and cleave at 5-mC and 5-hmC but only if the internal C in the CCGG sequence is methylated or hydroxymethylated. If the external C is modifed, MspI cannot cleave. As we used dNTP mixes including methyl-dCTP or hydroxymethyl-dCTP, all cytosine residues are modified. Probably, MspI would recognize the internal modified C in CCGG but steric hindrances by the modified external C may expel recognition. This means that both HpaII and MspI are not able to cleave when all cytosine residues are modified. Subsequent to restriction endonuclease digestion, reactions were analyzed on a 15% native PAA gel. 5-hmC and 5-mC modified DNA fragments were not cleaved (Fig 5.2 B, lanes 6–7, and lanes 9–10). Cleavage of the unmodified DNA releases fragments with 8 bp (not seen on the gel), 75 bp and about 230 bp in size (Fig 5.2 B, lanes 3–4). There was a remaining part of unmodified DNA molecules that was not cleaved by MspI and HpaII due to incomplete digestion. Nevertheless, the restriction enzyme analyses enable the discrimination of modified and unmodified DNA fragments.

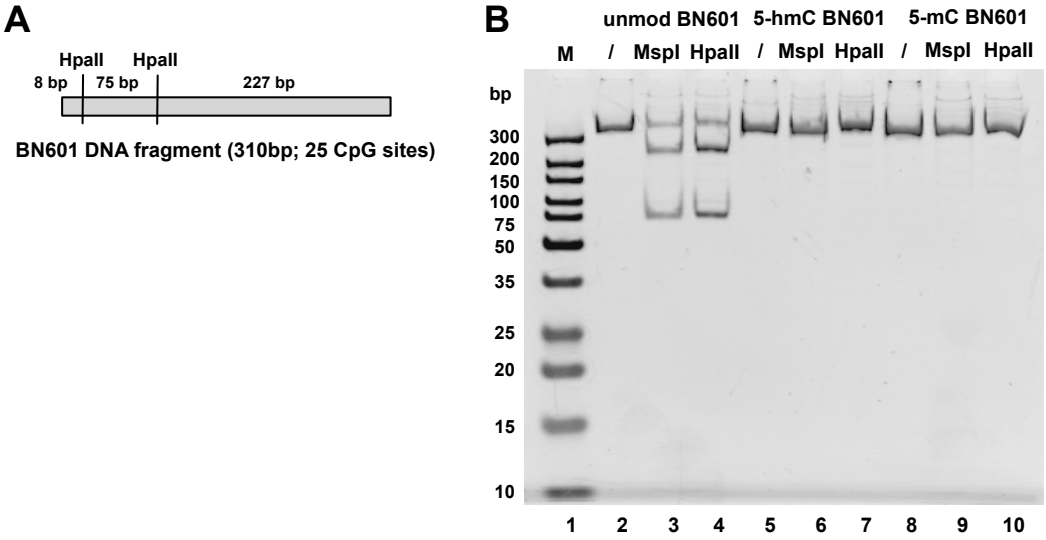

Fig 5.2: Analysis of incorporation of 5-hmC and 5-mC into the BN601 DNA fragment.
5-hmC and 5-mC modified and unmodified BN601 DNA fragments were generated by PCR and subsequently analyzed by restriction enzyme digestion. **(A)** Schematic illustration of the BN601 DNA fragment generated by PCR. The DNA fragment has a size of 310 bp and contains 25 CpG sites. HpaII restriction sites enable the discrimination between modified and unmodified DNA fragments. The relative positions of the HpaII restriction sites on the BN601 DNA fragment are indicated. **(B)** After PCR, incorporation of 5-hmC and 5-mC was analyzed by digestion of the DNA fragments with MspI and HpaII. Following restriction enzyme digestion, reactions were loaded on a 15% native PAA gel. For visualization, the gel was stained with ethidium bromide and destained with water. As controls (lanes 2, 5 and 8), DNA was incubated with buffer lacking the respective restriction endonuclease (indicated by /).

5.2.1.10 Site-directed mutagenesis

Site-directed mutagenesis was applied in order to create an ATPase inactive version of Lsh. Therefore, the lysine residue at position 254 was replaced by an arginine residue. This point mutation in the ATP-binding pocket of the protein abolishes ATP binding and hydrolysis. For this purpose, the plasmid containing the protein coding sequence of 6x His-tagged Lsh

(pDFB7-fl-LshWT-6xC-His) was purified from a dam+ *E. coli* strain (here DH5α) to ensure that all GATC sites are methylated for later digestion with DpnI. To introduce the point mutation, forward and reverse primers containing the appropriately changed nucleobases were designed with the PrimerX software tool (bioinformatics.org/primerx). Steps in primer design were performed according to the program's instructions and recommendations listed in the authors' program documentation and following recommendations listed in IDT's Mutagenesis Application Guide (IDT). The chosen primer pair was checked for predicted dimerization, hairpin formation and melting temperatures. Both primers contain 5' phosphorylated ends to allow the two ends to be ligated together following amplification. A standard PCR program was run with reduced cycle number using the proof-reading Phusion High-Fidelity DNA Polymerase (Finnzyme). Since the primers are positioned 'back to back', the entire template containing plasmid is copied. A high-fidelity polymerase does not displace the newly synthesized strands and stops after copying the plasmid when it returns to the 5' end of the primer resulting in nicked circular strands. After PCR, the DNA was precipitated, loaded on a 1.3% agarose gel, appropriate DNA bands were gel-eluted. Subsequently the DNA was subjected to DpnI digestion in order to remove the original plasmid. 600 ng of DNA were digested with 10 units DpnI in a total volume of 50 µl at 37 °C for 3 h. The reaction was cleaned-up using the Qiaquick PCR Purification kit. The final product was transformed into chemically competent bacteria to repair the nicks. Transformation and subsequent plasmid isolation were done according to standard protocols. Integrity of clones was checked by analytical restriction enzyme digestion followed by agarose gel electrophoresis. Presence of the point mutation and nucleobase sequence integrity of the plasmid were checked by sequencing the entire plasmid. Since the original plasmid vector is the pDFB7 vector, which is a pFastBac vector suited for protein expression in Sf21 insect cells, the generated plasmid containing the point mutation was ready to use for recombination into baculovirus bacmid DNA (see 5.2.5.5).

5.2.2 Working with RNA

In general, working with RNA needs to be performed under RNase-free conditions. RNAseZap was used to decontaminate surfaces, and RNA containing reactions were supplied with RNasin (Promega). For pipetting, filtertips were used and buffers were set up with sterilized MilliQ water.

5.2.2.1 Growing mammalian cells for isolation of total RNA

Work with mammalian cell lines was carried out according to standard protocols. All work was done under a sterile hood in laminar flow and all solutions and consumables were purchased sterile. The working space, gloves and devices were thoroughly wiped with 70%

ethanol before use. All cell lines used were cultivated in DMEM supplemented with 10% FCS and 1% penicillin/streptomycine. Cells were incubated at 37°C in a humified incubator with 5% CO_2. The medium was stored at 4 °C and pre-warmed to 37 °C in a water bath before usage. The medium of the cultures was changed every 2–3 days depending on the doubling time of the cells. At an estimated confluency of 80%, the cells were split. For this purpose, the medium was removed and a trypsin/EDTA solution was added to the cells. The cells were incubated at 37 °C for 5 min and the cells still not detached were removed from the surface by slightly tapping the culture dish. The trypsin reaction was stopped by adding culture medium three times the volume of trypsin/EDTA. The appropriate volume of cells was then transferred to a new flask or culture disk with fresh growth medium and again incubated at 37 °C, 5% CO_2.

5.2.2.2 Isolation of total RNA

Total RNA was isolated with the NucleoSpin RNA kit (Macherey-Nagel) or with TRIzol reagent (Ambion) according to the manufacturer's instructions. The resulting total RNA was stored at -80 °C.

5.2.2.3 Determination of RNA quality and quantity

The NanoDrop ND1000 spectrophotometer (Peqlab) was used to determine RNA concentration by absorption measurements at 260 nm as described previously. RNA quality was analyzed by agarose gel electrophoresis. The integrity of total RNA was analyzed by visual assessment of the 28S:18S rRNA ratio on formaldehyde agarose gels. A 1.3% agarose gel was prepared by dissolving 1.3 g agarose in 85 ml sterile DEPC treated water. The solution was cooled down to about 65 °C. Then, 10 ml pre-warmed 10x MOPS buffer and 5 ml of 37% formaldehyde were added, and the gel was poured into an electrophoresis tank. For sample preparation 1–3 µg of total RNA were mixed with 2 µl of 10x MOPS, 2 µl 37% formaldehyde and 9 µl formamide in a total volume of 20 µl. Samples were incubated at 65 °C for 10 min and cooled on ice. 2 µl of RNA loading buffer was added to each sample and samples were loaded. Gels were run in running buffer (1x MOPS, 12.3 M formaldehyde) and stained with ethidium bromide for visualization.

5.2.3 Protein biochemical methods

Proteins were purified and analyzed according to standard protocols (Sambrook and Russell, 2001). Generally, proteins were stored at -80 °C and kept on ice before starting an experiment.

5.2.3.1 Determination of protein concentrations

Protein concentrations were determined using the colorimetric assay described by Bradford (Bradford, 1976). In brief, a serial dilution of the protein of unknown concentration and one of BSA of known concentration were prepared in water. For measurements, constant amounts of protein assay dye (Bio-Rad) were added, and absorbance of samples and BSA was measured at 595 nm. Using absorbance and the known concentrations of BSA, a standard curve was set in order to determine the concentration of the diluted samples according to the calculated linear regression line and equation. Values were normalized to the diluted volumes of protein samples, and the mean of normalized values was calculated. Finally, molarities were calculated using the molecular weight of the protein.

5.2.3.2 Denaturating SDS-polyacrylamide gel electrophoresis (SDS-PAGE)

Quantitiy and quality of recombinant proteins was initially analyzed by SDS-polyacrylamide gel electrophoresis (SDS-PAGE). Separating and stacking gels were prepared according to standard protocols using ready-to-use polyacrylamide solutions from Roth (Rotigel 30%, 49:1). For electrophoresis, protein samples were mixed with Laemmli SDS-PAGE sample buffer, heat-denatured for 5 min at 95 °C and directly loaded onto the gel. Proteins were separated at 35 mA (4 mA/cm) until the dye front reached the bottom of the gel. The molecular weight of proteins was estimated by running pre-stained marker proteins (PAGE ruler, Fermentas) in parallel. Following electrophoresis, proteins were stained with Coomassie Brilliant Blue (0.1% Coomassie Blue in 10% acetic acid and 45% methanol) for 15 min on a slowly rocking platform and destained in water by repeated heating in a microwave.

5.2.3.3 Semi-dry western blot and immunodetection

Following separation by SDS-PAGE, proteins were transferred to PVDF membranes using the Bio-Rad ‘Trans-Blot SD Apparatus’ for 1 h and 20 min at 24 V and 2 mA/cm^2. For protein transfer, the PVDF membrane was soaked in 100% methanol and then incubated together with the gel in Towbin transfer buffer for 20 min. The PVDF membrane was placed between three gel-sized Whatman papers soaked in transfer buffer at the bottom and the gel plus two gel-sized Whatman papers soaked in transfer buffer on top. After transfer, the PVDF membrane was washed three times in TBST for 10–15 min each. Depending on the primary antibody, the membrane was incubated either in TBST containing 5% milk or TBST

containing 2.5% BSA for 1–2 h or O/N in order to reduce non-specific background. For immunodetection, the membrane was incubated with the appropriate antibody in TBST containing 5% milk or TBST containing 2.5% BSA at 4 °C O/N, slowly shaking. Afterwards, the membrane was washed three times in TBST for 10–15 min each and incubated for 1 h with a horseradish peroxidase-coupled (HRP) secondary antibody in TBST containing 5% milk. If HisProbe-HRP (ThermoFisher) was used, the membrane was only incubated with the His-probe in TBST containing 2.5% BSA at 4 °C for 2 h, since a second antibody is not needed. After three additional washes in TBST, antigen-antibody complexes were detected using the SuperSignal West Dura WB kit (ThermoFisher) and imaged with the image reader LAS-3000 (Fujifilm).

5.2.4 *E. coli* culture and methods

5.2.4.1 Liquid culture

For plasmid preparations a single colony was picked from an agar plate with a sterile tip, inoculated into LB or SOB medium supplemented with the respective antiobiotics and shaken O/N at 37 °C at 180 rpm. For standard preparations with the Qiaprep Spin Miniprep Kit (Qiagen), 5 ml cultures were used. For expression cultures, a small pre-culture was inoculated O/N at 30 °C to an OD_{600} of 3–5. This culture was then used to inoculate the expression culture to an OD_{600} of 0.1.

5.2.4.2 Glycerol stock

For long-term storage of bacterial cultures and convenient handling of frequently used bacterial strains, 850 µl of a liquid culture are mixed with 400 µl of 50% sterile glycerol and frozen at -80 °C.

5.2.4.2 Transformation of chemically competent bacteria

For transformation, 50 µl of chemically competent bacteria were thawed on ice and either 10 ng of purified plasmid DNA or 5 µl of ligation reaction were added. The suspension was mixed by gently tapping the tube and incubated on ice for 15–30 min. Cells were transformed by heat-shock for 45 seconds, then cooled down on ice for 5–10 min. 450 µl of LB or SOB medium without antibiotics were added, and the bacteria were incubated at 37 °C shaking at 600 rpm for 30 min in case of ampicillin resistance, or 1 h in case of kanamycin or chloramphenicol resistance. 50 µl and 200 µl of the mixture were plated on agar plates containing the appropriate antibiotics. Plates were incubated at 37 °C O/N.

5.2.5 GATEWAY cloning system

5.2.5.1 Introduction to the GATEWAY technology

To express human Lsh protein, a eukaryotic expression system was used. Insect cells derived from the Spodoptera frugiperda (Sf21) can be easily infected by a cell line specific virus, called baculovirus. The use of a recombinant virus carrying a gene-of-interest (GOI) allows high-level production of recombinant proteins in a eukaryotic cell system, including all kinds of post-translational modifications. Recombinant baculovirus were cloned with the GATEWAY cloning system from Invitrogen. The GATEWAY technology is a universal cloning method based on the site-specific recombination system of bacteriophage lambda, which facilitates the integration of lambda into the *E. coli* chromosome and allows the switch between the lytic and lysogenic pathway. The *in vitro* recombination reaction is mediated by a mixture of lambda and *E. coli* encoded recombination proteins (Clonase-enzyme mix). Lambda recombination occurs between site-specific attachment (att) sites: attB on the *E. coli* chromosome and attP on the lambda chromosome. The att sites serve as the binding site for recombination proteins. Upon lambda integration, recombination occurs between attB and attP sites to give rise to attL and attR sites. The actual crossover occurs between homologous 15 bp core regions on the two sites, but surrounding sequences are required as they contain the binding sites for the recombination The recombination proteins involved in the reaction differ depending upon whether lambda utilizes the lytic or lysogenic pathway. The lysogenic pathway is catalyzed by the bacteriophage λ Integrase (Int) and *E. coli* Integration Host Factor (IHF) proteins (BP Clonase™ enzyme mix) while the lytic pathway is catalyzed by the bacteriophage λ Int and Excisionase (Xis) proteins, and the *E. coli* Integration Host Factor (IHF) protein (LR Clonase™ enzyme mix).

Pathway	Reaction	Catalyzed by
Lysogenic	attB x attP → attL x attR	BP Clonase
Lytic	attL x attR → attB x attP	LR Clonase

BP Reaction: Facilitates recombination of an attB substrate (attB-PCR product or a linearized attB expression clone) with an attP substrate (donor vector) to create an attL containing entry clone (see diagram below). This reaction is catalyzed by the BP Clonase™ enzyme mix.

Fig 5.3: BP reaction–GATEWAY technology (adapted from the GATEWAY manual (Invitrogen)

LR Reaction: Facilitates recombination of an attL substrate (entry clone) with an attR substrate (destination vector) to create an attB-containing expression clone (see diagram below). This reaction is catalyzed by the LR Clonase™ enzyme mix.

Fig 5.4: LR reaction–GATEWAY technology (adapted from the GATEWAY manual (Invitrogen)

5.2.5.2 GATEWAY-vectors–overview

With this system, a GOI is first cloned into an entry vector. From this vector, the GOI can be transferred into destination vectors. Diverse protein-tags can be fused to the protein of interest by taking advantage of the availability of numerous destination vectors. Also for other expression systems like *E. coli*, yeast or mammalian cells, specific destination vectors are available and can be recombined with the same GOI-containing entry plasmid. Thus, the GATEWAY system allows not only efficient cloning of specific expression vectors, but also fast creation of large expression clone libraries. To enable recombinational cloning and efficient selection of entry or expression clones, most GATEWAY vectors contain two att sites flanking a cassette containing the following features: The *ccdB* gene for negative selection as well as the chloramphenicol resistance gene (CmR) for counterselection; both are present in all GATEWAY vectors. After a BP or LR recombination reaction, the cassette including the *ccdB* and CmR genes is replaced by the GOI to generate the entry clones and expression clones, respectively. The protein encoded by the *ccdB* gene interferes with *E. coli* DNA gyrase, thereby inhibiting growth of most *E. coli* strains (e. g. DH5α, TOP10, but not XL1 blue). Thus, presence of the *ccdB* gene allows a strong negative selection of non-recombined plasmids, reducing the number of false positive clones and fastening the process of clone selection. For propagation of *ccdB* gene containing vectors an *E. coli* strain carrying a mutation in the gyrase gene (*gyrA462*) that conferred resitance to the *ccdB* effects, like the DB3.1 strain, has to be used.

5.2.5.3 Creation of an entry clone

The protein coding sequence of human Lsh was PCR amplified using the proof-reading Phusion High Fidelity DNA polymerase (Finnzyme) and the plasmid pTriEx-h-Lsh-10xC-His. This plasmid was already available in the laboratory and had been used to try expression of 10x His-tagged human Lsh in bacteria. In addition to protein sequence specific nucleobases, primers contained corresponding sequences for attB sites for recombination, and AvrII restriction

enzyme recognition sites at the 5'-end of the primers to remove primer residues and primer dimers. Subsequent to PCR, the product was precipitated, digested with AvrII and gel-purified. Performing the BP reaction according to the manufacturer's instructions (BP Clonase II mix; Invitrogen) the purified attB-flanked PCR product was recombined with the GATEWAY donor vector pDONR221 to create entry clones.

5.2.5.4 Creation of a destination clone

In order to create an expression clone, an LR reaction was performed with the LR Clonase II mix (Invitrogen) as recommended by the manufacturer. In brief, a recombination between the Lsh gene containing entry vector with attL sites and kanamycine resistance gene and a destination vector suited for protein expression in Sf21 insect cells was performed. The pFastBac based destination vector, namely pDFB7, contains attR sites, ampicillin resitance gene, ccdB gene and chloramphenicol marker. An AcMNPV polyhedrin promoter allows high expression levels of the GOI in insect cells. Additionally, the vector encodes a C-terminal 6x His-tag and a SV40 late polyadenylation signal flanked by transposition elements (Tn7). The reaction mixture was then transformed into DH5α competent cells and plated onto LB_{Amp} plates. Only the bacteria containing a pDFB7-GOI plasmid were able to grow, since the ccdB gene was replaced with the GOI, and remaining entry vectors do not confer ampicillin resistance.

5.2.5.5 Recombination into baculovirus bacmid DNA

The Bac-to-Bac system based on improvements made by Imre Berger was applied to obtain recombinant baculoviruses. For this purpose, we used the *E.coli* strain DH10EMBacYFP (Berger et al., 2004) in which the bacmid DNA was modified in a way that the *v-cath* and *chiA* genes had been replaced by an ampicillin marker and LoxP sites. The *v-cath* gene encodes for a cathepsin L-like proteinase and the *chiA* gene for a chitinase that acts as a chaperone for proVCATH. The infected cells are thus less prone to cell lysis during infection and to proteolytic degradation, which results in a higher yield of full-length recombinant protein. The EYFP gene under the control of the polyhedrin promotor is inserted via Cre/Lox recombination and allows the monitoring of protein expression via fluorescence microscopy during the course of infection.

The pDFB7 vector including the GOI that is flanked by transposition elements (Tn7) was transformed into *E. coli* DH10EMBacYFP chemically competent cells that contain the bacmid DNA (tetracycline resistance marker) with the YFP marker and a helper-plasmid (encoding a kanamycin resistance marker and a transposase). The included transposase catalyzed the recombination of the Tn7 flanked region of the pDFB7 vector into the bacmid DNA, which also contains Tn7 transposition elements. Together with the GOI a gentamycin resistance marker

got integrated into the viral genome. Triple antibiotic and blue-white selection resulted in the selection of the recombinant bacmid DNA (transposition of the GOI + gentamycin into the bacmid DNA destroys the lacZ gene).

5.2.5.6 Transformation of DH10EMBacYFP cells

Chemically competent DH10EMBacYFP *E. coli* cells were transformed with pDEST-GOI plasmid (5 min incubation on ice, 45 sec at 42 °C, 5 min on ice). 250 µl of SOB medium were added to the cells and incubated additional 5-12 hours at 37 °C. All cells were plated on LB plates (50µg/ml kanamycine, 10µg/ml tetracycline, 7µg/ml gentamycine, 100µg/ml X-Gal, 40µg/ml IPTG) and incubated at 37°C for 24–36 hours. Ten out of approximately 50–60 colonies were white. Five colonies were picked and plated on fresh LB selective plates to verify the positive Tn7 transposition reaction.

5.2.5.7 Isolation of recombinant bacmid DNA and transformation in Sf21 insect cells

After transformation of the pFastBac construct into DH10EMBacYFP *E. coli* cells and successful transposition, recombinant bacmid DNA was purified from positive white transformants. To do so, a bacterial colony was picked in order to inoculate 2 ml LB medium supplied with 50µg/ml kanamycine, 7µg/ml gentamycine, and 10µg/ml tetracycline. Cells were grown O/N at 37 °C and 180 rpm. The liquid culture was then pelleted, and the supernatant was discarded. For alkaline cell lysis the pellet was resuspended in 300 µl buffer P1, followed by addition of 300 µl buffer P2 and 300 µl buffer N3 (see Qiagen's Miniprep kit for buffer composition). The sample was centrifuged for 10 min at 13.000 rpm, the pellet was discarded, and the supernatant was centrifuged for 3 min at 13.000 rpm. Having discarded the pellet again, the bacmid DNA in the supernatant was precipitated with isopropanol and washed twice with 70% EtOH. The pellet was air-dried and dissolved in 30 µl filter-sterilized water. Purified bacmid DNA was suitable for PCR analysis and transfection into Sf21 insect cells. The presence of the desired GOI in the high molecular weight bacmid DNA was verified by PCR (with a GOI and a bacmid specifc primer).

5.2.5.8 Transfection of Sf21 insect cells

The positive tested recombinant bacmid DNA was transfected into Sf21 cells (1x 10^6 cells in a well of a 6-well plate in 3 ml Sf-900 II medium (Invitrogen)) with X-tremeGENE (Roche) to produce a first viral stock. For every protein of interest, two bacmid clones were tested in duplicates, and controls (cells only and medium only) were included to determine the source of possible contaminations. 20 µl of bacmid DNA were mixed with 200 µl Sf-900 II medium. Per bacmid clone, 10 µl of X-tremeGENE (Roche) were first mixed with 90 µl Sf-900 II medium and then added to the bacmid DNA. The mixture was evenly distributed dropwise to the indicated wells. After 48–60 hours successful transfection could be monitored via

fluorescence microscopy as the bacmid contains the YFP marker. The supernatant, which is the initial virus, was taken and stored at 4 °C, leaving the cells on the 6-well plates This virus stock was amplified and used for protein expression (see 5.2.6.2 and following). 3 ml medium were added to the cells and incubated for about 48 hours. Afterwards, cells were harvested by first removing the medium and then collecting the cells in 500 µl PBS by scraping and transferring the cells to a 1.5 ml Eppendorf tube. Protease inhibitors were added, and the cells were sonified with a Branson Sonifier 250D (small tip, 30 seconds at 20% output control, constant). Generated cell extracts were supplemented with 6x protein loading dye, and recombinant protein expression was analyzed by SDS-PAGE and western blotting.

5.2.6 Sf21 insect cell culture and baculovirus protein expression

Baculoviruses are a group of large double-stranded (ds) DNA viruses infecting insects. They feature a narrow host range with each type of baculovirus being virulent only to a specific insect species, while not infecting other insects, plants or mammals. Autographa californica Nuclear Polyhedrosis Virus (AcNPV) is well-studied and together with *Spodoptera frugiperda* ovary cell culture (Sf21) a useful tool for recombinant protein expression. During the baculovirus life cycle, two different forms of virus are produced by the infected host cell: Extracellular virus particles bud during the early stage of infection (release 24 hours post infection) and spread infection to other organs of the insect. During the late stage of infection, occluded virus particles form in the nucleus of the host cell. The occluded virus consists of many nucleocapsids enveloped by a matrix mainly formed by polyhedrin, a structural protein expressed at very high levels. The polyhedrin matrix allows the virus to last in the environment after the death of the host. After ingestion of occluded virus, virions are released in the mid-gut of the next host and enter adjacent cells by endocytosis. *In vitro*, polyhedrin is not necessary for virus replication and can be deleted or replaced. As the polyhedrin promoter is the strongest promoter known at present, it allows high expression levels of heterologous proteins. In addition, the baculovirus genome and capsid structure tolerate insertions of sequence well, and therefore large coding sequences can be introduced (Berger et al., 2004) (Fitzgerald et al., 2006). In contrast to bacterial expression systems, baculovirus expression systems allow expression of large proteins providing also signal peptide cleavage, intron splicing, nuclear transport, phosphorylation, glycosylation and acetylation.

5.2.6.1 Culturing of Sf21 insect cells

Sf21 insect cells were cultivated in Sf-900 II medium (Invitrogen). Cells were grown as suspension cultures in Erlenmeyer flasks at approximately 100 rpm at 27 °C. For continuous and stable growth behavior, Sf21 cells were kept in logarithmic growth, i. e. at cell densities between 5x 10^5 and 2x 10^6 cells/ml. Since cells tend to adhere to the surface of the flasks, it is advisable to change the culture flask every 10 days. After use, culture vessels were washed with 10% acetic acid. Vessels were then sterilized twice by autoclaving and re-used.

5.2.6.2 Virus propagation by low MOI amplification

Amplification of baculovirus was undertaken to preserve the virus stock and to gain a higher titer of virus that was used for protein expression. MOI (multiplicity of infection) is defined as the number of baculoviruses/Sf21 cell. In order to avoid the accumulation of defective virus particles that reduces heterologous protein expression, baculovirus amplification with a MOI of 0.1 is optimal. Low MOI infection was performed in Erlenmeyer flasks with 25 ml culture volume and at a constant cell density of 10^6 cells/ml (always dilute back to this cell number). Once infected, Sf21 cells had to double once during the first 24 hours post infection (e. g. 10% of the cells were infected, whereas the other 90% doubled). Under these conditions, growth arrest was usually observed another 24 hours later. If the baculovirus titer was lower, it took some days (passages) until growth arrest was reached (after multiple rounds of virus amplification). Budded viruses were released starting from 24 hours after infection.
In general, viral supernatant was harvested 48 hours after the observed growth arrest.

5.2.6.3 Test-expression of recombinant proteins in Sf21 insect cells

Once the baculovirus was amplified, the viral titer for large-scale protein expression had to be determined. In Erlenmeyer flasks, 50 ml medium with 0.5x10^6 cells/ml were infected with varying amounts of virus (e.g. mock infection, 25, 50, 100, 150, 200 and 300 µl of baculovirus) and evenly distributed by shaking on a horizontal platform for about 48–96 hours hours at 27 °C. Daily growth behavior and infection process were documented, allowing a rough titer determination. Additionally, from each Erlenmeyer flask samples of 1x10^6 cells were harvested every 24 hours after infection, peletted and stored at -20°C. Having collected all samples during the course of the test-expression, each cell pellet was resuspended in 500 µl PBS, supplemented with protease inhibitors and sonicated using the Branson Sonifier 250D (small tip, 30 seconds at 20% output control, constant).
Generated cell extracts were supplemented with 6x protein loading dye, and recombinant protein expression was analyzed by SDS-PAGE and western blotting.

5.2.6.4 Protein expression in Sf21 insect cells

After determination of the optimal amount of baculovirus needed for sufficient protein expression a large scale expression was performed. Cells were grown in suspension in Erlenmeyer flasks (200 ml culture in 1l flasks) and infected at a cell density of $0.5x10^6$ cells/ml with the respective amount of baculovirus (as determined before with test infections). After 96 hours, cells were harvested by centrifugation for 5–10 min at 500 g, snap frozen in liquid nitrogen and stored at -80 °C until use. During the course of the protein expression, samples of $1x10^6$ cells were taken in order to monitor expression by SDS-PAGE and western blotting. Harvesting and sample preparation was performed as described (see 5.2.6.3).

5.2.7 Purification of recombinant proteins form Sf21 insect cells

5.2.7.1 Preparation of cell lysates

After optimizing protein expression, a typical large-scale purification was done with 1–3x 10^8 insect cells. Cell pellets containing recombinant His-tagged DNA methyltransferases expressed in Sf21 insect cells were already available in the laboratory and had not been produced during this work. Purification was performed in the cold room and samples were always kept on ice. Cell pellets were resuspended in 35 ml lysis buffer I (50 mM Tris pH 7.6, 100 mM KCl and 0.1% NP40). Protease inhibitors were added to buffers prior to use (one tablet complete EDTA-free protease inhibitor cocktail (Roche) per 50 ml buffer). The cell suspension was vortexed for 2 min and centrifuged for 10 min at 4500rpm. The pellet was resuspended in 10 ml lysis buffer II (EX500 with 10 mM imidazole, 0.1% NP40 and 0.01% ß-mercaptoethanol (ß-ME)). Subsequently, the suspension was further lysed by sonication with a Branson Sonifier 250D (big tip; 8x for 15 seconds at 50% amplitude and 50% duty cycle with a cooling period of 15 seconds in between). After incubation of the lysate at 4 °C for 15 min on an overhead wheel, the lysate was cleared by centrifugation for 40 min, 10.000 g and 4 °C. The supernatant was transferred to a 15 ml reaction tube and stored on ice.

5.2.7.2 Purification of His-tagged proteins

For affinity purification of His-tagged human Lsh wild-type, Lsh KR mutant as well as DNA methyltransferases Dnmt1, Dnmt3a, and Dnmt3b2, 500 µl of Ni-NTA agarose-slurry (Qiagen) were equilibrated in batch with lysis buffer II (EX500 with 10 mM imidazole, 0.1% NP40 and 0.01% ß-ME). Protease inhibitors were added to buffers prior to use (one tablet complete EDTA-free protease inhibitor cocktail (Roche) per 50 ml buffer). For equilibration, beads were washed four times in 2 ml of lysis buffer II and were spun down for 2 min at 100 g and 4 °C. Equilibrated beads were incubated with the supernatant from lysed cells for 90 min at 4 °C on an overhead shaker. Beads were spun down for 2 min at 100 g and 4 °C, and the flow-

through was discarded. The resin was washed four times with each 5 ml wash buffer (EX500 containing 20 mM imidazole, 0.1% NP40 and 0.01% ß-ME) and loaded onto a 1 ml mini-column after the last washing step. Bound proteins were eluted from the Ni-NTA-agarose by addition of 250 µl elution buffer (EX300 containing 0.1% NP40, 250 mM imidazole and 0.01% ß-ME) and incubation for 60 min at 4 °C on an overhead shaker. This elution step was repeated twice. Elution fractions were aliquoted, snap frozen in liquid nitrogen and stored at -80 °C. After the last elution step, beads were resuspended in 100 µl EX0. Samples collected during preparation of cell lysates and during protein purification were loaded on a 7.5% SDS gel to analyze purification efficiency by SDS-PAGE. Protein concentration was determined via Bradford assay using a BSA standard curve. After purification of Dnmts, Dnmt activity was tested with the Dnmt Activity/Inhibition Assay Kit (Active Motif) according to the manufacturer's instructions.

5.2.8 *In vitro* reconstitution of chromatin

5.2.8.1 Preparation of DNA fragments for nucleosome assembly by restriction digestion

The plasmid pUC18-12x-601 contains 12 repeats of the 601 nucleosome positioning sequence (NPS), flanked by restriction recognition sites to allow fast and specific production of DNA fragments for mononucleosome assembly by restriction endonuclease digestion. 180 µg of plasmid DNA (pUC18-12x-601) were digested with 300 units of restriction endonuclease (NotI and AvaI respectively) in a total volume of 150 µl supplemented with 0.1 mg/ml BSA, at 37 °C for 16 hours. Complete digestion was checked using 1% agarose gels supplemented with SYBR Safe (Invitrogen).

5.2.8.2 Preparation of DNA fragments for nucleosome assembly by PCR

5.2.8.2.1 Preparation of the DNA fragments 0-NPS-0 and 77-NPS-77:

To generate nucleosomal DNA fragments of specific sizes a PCR was performed. For production of the constructs '0-NPS-0' and '77-NPS-77' the pPCRScript_slo1-gla75 insert (referred to as Sloning DNA) was used, which consists of three repeats of the nucleosome positioning sequence 601 (Lowary and Widom, 1998) flanked by a partial rDNA promoter sequence (approximately 70bp) on the left and a partial HSP70 promoter sequence (approximately 70bp) on the right. Prior to use as a PCR template, the plasmid DNA was digested with BglII in preparative scale to hydrolyse the template down to monomers. To generate NPS constructs with flanking DNA of defined length, specific primer pairs were used. For the 601 sequence without linker DNA (referred to as 0-NPS-0) primer pairs AP7 and AP8 were used. The reverse primer AP8 hybridizes 5 bp upstream of the 3'-border of the

WID sequence, hence amplifying a 142 bp DNA fragment instead of 147 bp. The 77-NPS-77 construct with 77 bp DNA flanking the 601 sequence on both sides is 301 bp in size and was generated using primer pairs AP1 and AP15. Preparative PCR reaction was performed in 2 ml scale with 2 µg template DNA. The reaction mix was split into 20x 100 µl in 0.2 ml PCR tubes and reaction was started in a PCR cycler (PeqLab) under the following conditions.

Cycle step	Temperature (°C)	Time	Number of cycles
Initial denaturation	94 °C	2 min	1
denaturation	94 °C	40 sec	35
annealing	58 °C	40 sec	
extension	72 °C	40 sec	
Final extension	72 °C	10 min	1

Reagents	Volumes
Primer for 10µM	100 µl
Primer rev 10µM	100 µl
dNTPs 10 mM	40 µl
Taq buffer 10x	200 µl
Taq pol.	40 µl
Template	~2 µg (40 µl)
H_2O	1480 µl
Total volume	2000 µl

Reactions were cooled down to 4 °C, 10 ng/µl glycogen was added and PCR products were precipitated with 7.5 M ammonium acetate and ethanol. Purity was checked on a 1.5% agarose gel, and concentration was determined using the Nanodrop photometer (PeqLab).

5.2.8.2.2 Preparation of the DNA fragment -190/90:

The murine rRNA gene promoter fragment with 280 bp in size (ranging from 190 bp downstream and 90 bp upstream to the TSS) was amplified by PCR from the plasmid pT7Blue-m-190+90. PCR conditions for fragment production are as follows.

Cycle step	Temperature (°C)	Time	Number of cycles
Initial denaturation	95 °C	2 min	1
denaturation	95 °C	15 sec	20
annealing	60 °C	20 sec	
extension	72 °C	25 sec	
Final extension	72 °C	7 min	1

Reagents	Volumes
mDNA_-190 (for) 10µM	25 µl
mDNA_+90 Cy5 (rev) 10µM	25 µl
dNTPs 10 mM	10 µl
Phusion-buffer 5x	100 µl
Phusion-pol.	5 µl
Template	15 µl (500–750 ng)
H_2O	320 µl
Total volume	500 µl

The reaction mix was split into 5x 100 µl in 0.2 ml PCR tubes and reaction was started in a PCR cycler (PeqLab) The product was purified with the Qiaquick PCR Purification kit (Qiagen), analyzed on 5% native PAA gels, and DNA concentration was determined with the Nanodrop photometer (PeqLab).

5.2.8.2.3 Preparation of methylated, hydroxymethylated and unmodified 601-10N-601 DNA fragments:

Methylated, hydroxymethylated and unmodified 601-10N-601 DNA fragments were used to generate differently DNA modified dinucleosomes, allowing greater possibilities in terms of recognition of the nucleosomal substrate in contrast to mononucleosomes, and furthermore the examination whether epigenetic DNA modifications are preferably recognized and interpreted by the protein of interest. The 601-10N-601 DNA fragments were produced by PCR using the plasmid pBS 601-10N-601 as template. Methylated and hydroxymethylated cytosines were introduced by replacing dCTP in the dNTP mix either with methyl-dCTP (TriLink) or hydroxymethyl-dCTP (gift from Attila Nemeth). The DNA fragments have a size of about 390 bp, contain about 30 CpG sites and harbour two strong nucleosome positioning sequences (referred to as 601; (Lowary and Widom, 1998)) (Fig 5.5 A). Large scale PCR conditions for fragment production are described in the following.

Cycle step	Temperature (°C)	Time	Number of cycles
Initial denaturation	5-hmC and unmod.: 95 °C 5-mC: 100 °C	5 min	1
denaturation	5-hmC and unmod.: 95 °C 5-mC: 100 °C	20 sec	30
annealing	59 °C	30 sec	
extension	72 °C	30 sec	
Final extension	72 °C	10 min	1

5-hmC and unmod		5-mC	
Reagents	Volumes	Reagents	Volumes
RM 08 (for) 100 µM	4.8 µl	RM 08 (for) 100 µM	4.8 µl
RM 09 (rev) 100 µM	4.8 µl	RM 09 (rev) 100 µM	4.8 µl
dNTPs 25 mM	12.8 µl	dNTPs 25 mM	12.8 µl
Taq buffer 10x	160 µl	**Herculase** buffer 5x	320 µl
Taq pol.	32 µl	**Herculase**	32 µl
Template	16 ng	Template	16 ng
H_2O	1370 µl	H_2O	1225 µl
Total volume	1600 µl	Total volume	1600 µl

PCR products were precipitated with 7.5 M ammonium as described (see 5.2.1.6), purity was checked on 1.3% agarose gels, and concentration was determined using the Nanodrop photometer (PeqLab). Incorporation of methyl- and hydroxymethyl-modifications was analyzed by restriction endonuclease digestion with HpaII and its isoschizomer MspI. The amplified 601-10N-601 sequence contains four HpaII recognition sites, releasing fragments of 160 bp, 30 bp and 20 bp if cut (Fig 5.5 A). Subsequent to restriction endonuclease digestion, reactions were analyzed on a 3% agarose gel. As expected (see 5.2.1.9), cleavage of the unmodified DNA revealed DNA fragments with the size of 160 bp, 30 bp and 20 bp (Fig 5.5 B, lanes 3–4), whereas 5-hmC and 5-mC modified DNA fragments were not cleaved by MspI and HpaII (Fig 5.5 B, lanes 6–7, and lanes 9–10).

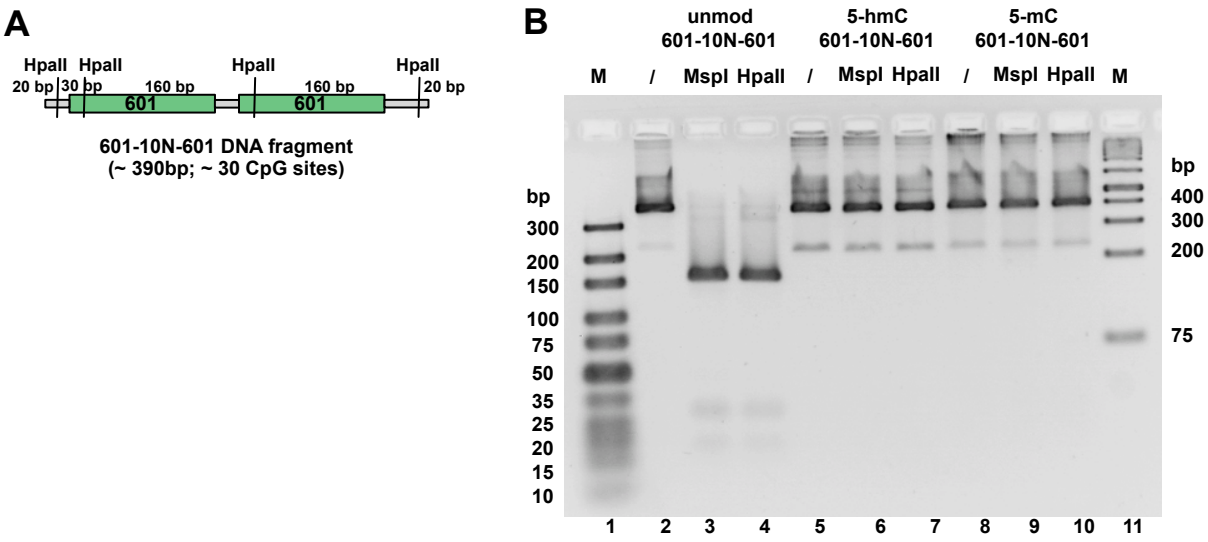

Fig 5.5: Analysis of incorporation of 5-hmC and 5-mC into the 601-10N-601 DNA fragment.
5-hmC and 5-mC modified and unmodified 601-10N-601 DNA fragments were generated by PCR and subsequently analyzed by restriction enzyme digestion. **(A)** Schematic illustration of the 601-10N-601 DNA fragment generated by PCR. The DNA fragment has a size of about 390 bp and contains about 30 CpG sites. HpaII restriction sites enable the discrimination between modified and unmodified DNA fragments. The relative positions of the HpaII restriction sites on the DNA fragment are indicated. The 601 nucleosome positioning sequences are highlighted in green. **(B)** After PCR, incorporation of 5-hmC and 5-mC was analyzed by digestion of the DNA fragments with MspI and HpaII. Following restriction enzyme digestion, reactions were loaded on a 3 % agarose gel. For visualization, the gel was stained with ethidium bromide and destained with water. As controls (lanes 2, 5 and 8), DNA was incubated with buffer lacking the respective restriction endonuclease (indicated by /).

5.2.8.3 Chromatin assembly by salt gradient dialysis

Nucleosomes were assembled from DNA and histones by the salt gradient dialysis technique according to Rhodes and Laskey (Rhodes and Laskey, 1989). Assembly reactions were performed in the lid of siliconized 1.5 ml tubes (Eppendorf). Dialysis membranes with a MWCO of 6–8 kD (Spectrapor) were pre-incubated for 5 min in high salt buffer (10 mM Tris/HCl pH 7.6, 2 M NaCl, 1 mM EDTA, 0.05% NP40, 1 mM ß-ME). The membrane was placed over the O-ring of a 1.5 ml tube and was fixed with the lid containing a hole in the middle of the lid. Tubes were placed in a styrofoam floater and transferred to a 3 liter beaker filled with 300 ml high salt buffer, containing a magnetic stirrer. Air bubbles below each membrane were removed with a bent pasteur pipette. Beakers were protected from light, if the DNA in the assembly reaction was fluorescently labeled. Finally, the assembly reaction was pipetted onto the lid. 3 liter of low salt buffer (10 mM Tris/HCl pH 7.6, 50 mM NaCl, 1 mM EDTA, 0.05% NP40, 1 mM ß-ME) were pumped into the beaker with a flow rate of about 150 ml–300 ml per hour at room temperature. Hence, salt concentration decreased slowly from 2 M to 227 mM allowing a specific assembly of the histone octamers onto the given DNA fragment.

When the optimal histone:DNA ratio had been determined, nucleosomes were assembled in large scale. In general, 25 µg of DNA were mixed with an optimal amount of histones in high salt buffer, supplemented with 200 ng/µl BSA, in a final volume of 250 µl. The assembly mix was split into 5x 50 µl before loading into the dialysis chambers. Quality of mononucleosomes and dinucleosomes was directly checked on 5% native PAA gels in 0.4x TBE run for 1 h at 100 V. To control the assembly of poly-nucleosomes on plasmid DNA (pUC18 12x 601), a partial MNase digestion was done (see below). Nucleosomes were stored at 4°C, protected from light if the DNA was fluorescently labeled.

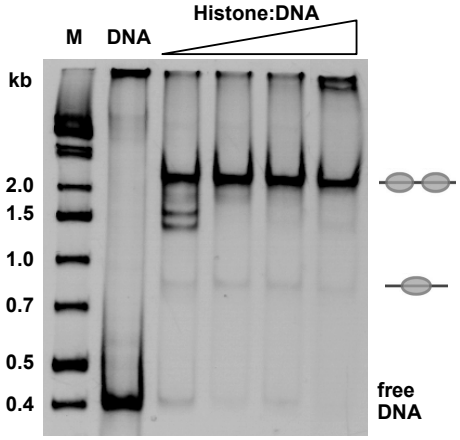

Fig 5.6: Analysis of a typical *in vitro* chromatin assembly.
Chromatin was reconstituted on 601-10N-601 DNA with chicken histones, resulting in the assembly of dinucleosomes. The ratio of histones to DNA was increased stepwise to determine the optimal histone:DNA ratio for large scale assembly. Assemblies were analyzed on 5% native PAA gels. The naked 601-10N-601 DA fragment serves as control. Sketches indicate mono- and dinucleosomes.

5.2.8.4 Chromatin analysis by micrococcal nuclease (MNase) digestion

Micrococcal nuclease (MNase) cleaves DNA preferentially in the linker region between individual nucleosomes. Partial MNase digestion generates a so-called nucleosomal ladder, thereby allowing qualitative analysis of the obtained grade of chromatin. Typically, 2 µg of chromatin was partially digested with 0.625 units/µl of MNase for 30, 60 and 270 seconds in the presence of 3 mM $CaCl_2$ and 200 ng/µl BSA at room temperature. The reaction was stopped by the addition of 0.2 volumes of stop solution (4% SDS, 100 mM EDTA), supplemented with proteinase K (10 µg / reaction) and glycogen (10 µg) and deproteinized for 1 hour at 45 °C. The DNA was purified by ethanol precipitation (0.5 vol 7.5 M NH_4Ac and 2.5 volumes 100% ethanol were added, incubated for 10 min on ice, centrifuged for 15 min at 13,000 rpm and washed once with 70% ethanol), air dried, dissolved in 10 µl loading buffer and analyzed on 1.3% agarose gels. Gels were stained with ethidium bromide and destained in water.

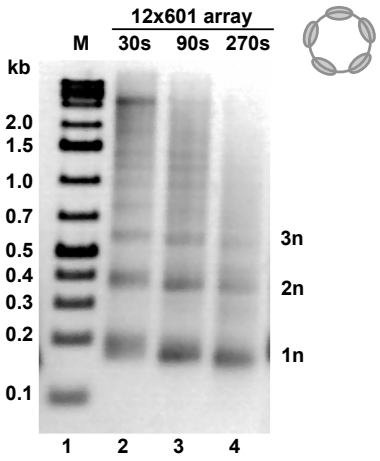

Fig 5.7: Partial MNase digestion of *in vitro* assembled circular chromatin.
Circular chromatin was assembled on pUC18 12x601 plasmid DNA with chicken histones by salt gradient analysis. 2 µg of chromatin were digested with MNase. Reaction was stopped after 30, 60 and 270 sec incubation time (lanes 2–4). After digestion with proteinase K DNA was precipitated and analyzed on a 1.3% agarose gel stained with ethidium bromide. The nucleosomal ladder generated by the MNase digestion is shown, and mono- di- and trinucleosomes are indicated (1n–3n).

5.2.9 Functional assays

5.2.9.1 DNA binding assay

To analyze the binding characteristics of Lsh to small DNA fragments, binding assays using an ultra-low-range DNA marker (Thermo Scientific) were carried out.
Increasing concentrations of Lsh (125 nM–1 µM) were titrated to the DNA (125 ng ultra low range DNA marker) in binding buffer (20mM Tris pH 7.6, 30mM KCl, 5mM EDTA, 1mM DTT, 10% glycerol) in a final volume of 20 µl. The concentration of monovalent anions (Cl^-) and cations (K^+) was adjusted to 100 mM. Reactions were incubated for 30 min at 26°C, and DNA-protein complexes were separated from unbound DNA on 12% native PAA gels in 0.4x TBE. After a pre-run of the native PAA gels at 50 V for 45 min, samples were loaded on the gels, and gels were run for 90 min at 100 V. To follow migration, DNA loading dye was loaded as marker. The gels were stained with ethidium bromide, destained with water and analyzed on the gel documentation system (Bio-Rad).

5.2.9.2 Electrophoretic mobility shift assay (EMSA)

Interactions of Lsh with nucleosomes, DNA and RNA were analyzed by electrophoretic mobility shift assays (EMSA). The ability of proteins such as transcription factors or DNA binding proteins to bind to DNA, RNA or nucleosomes can be assessed according to the running behavior in a polyacrylamide gel system. If binding occurs, the mobility of the complex is impaired resulting in either a slower migration velocity (shift) or a complete loss of migration, i.e the complex cannot enter the gel and is retained in the pocket.

5.2.9.2.1 Analysis of protein-nucleosome interactions by EMSA:

Positioned mononucleosomes were used to study protein-nucleosome interactions. Typically, reactions were prepared in a 20 µl total volume in EX buffer containing 20 mM Tris/HCl pH 7.6, 1.5 mM $MgCl_2$, 0.5 mM EGTA, 10% glycerol, 1mM DTT and 200 ng/µl BSA. The concentration of monovalent anions (Cl^-) and cations (K^+/Na^+) was adjusted to 100 mM. 125 nM–1 µM of protein was titrated to constant amounts of unlabeled or fluorescently labeled nucleosomal DNA (usually 10–20 nM). Samples were incubated for 30 min at 30 °C. Afterwards, complexes were separated from free nucleosomal DNA by native PAGE. Reactions were loaded on pre-electrophorezed 5% native PAA gels in 0.4x TBE buffer and run for 60–75 min at 100V. Orange G DNA loading dye was used to monitor the running time. After separation, the nucleosomal DNA was visualized on a fluorescence image reader (FLA-5000; Fuji), or by staining with ethidium bromide and documentation with the gel documentation system (Bio-Rad).
To test the influence of ATP on the binding characteristics of Lsh to mononucleosomes, 25 nM of fluorescently labeled nucleosomes were incubated with increasing concentrations (35

nM–2.5 µM) of either Lsh wild-type or Lsh KR mutant. ATP concentrations were kept constant (1 mM). Apart from this, the analysis of the binding of Lsh to mononucleosomes was performed as described before.

5.2.9.2.2 Analysis of protein-RNA interactions by EMSA:

In general, analysis was done as described for protein-nucleosome interactions, but reactions were prepared in EX buffer containing 150 mM KCl, 20 mM Tris/HCl pH 7.6, 1.5 mM $MgCl_2$, 0.5 mM EGTA and 10% glycerol. 12.5 nM–1.6 µM Lsh were titrated to 25 nM FAM labeled single stranded RNA. Samples were incubated for 30 min at 30 °C. Afterwards, Lsh/RNA complexes were separated from free RNA by native PAGE. Reactions were loaded on pre-electrophorezed 5% native PAA gels in 0.4x TBE buffer and run for 20 min at 100V. Subsequently, RNA was visualized on a fluorescence image reader (FLA-5000; Fuji).

To test the influence of ATP on the binding characteristics of Lsh to RNA, 25 nM of fluorescently labeled single-stranded RNA were incubated with increasing concentrations (75 nM–2.5 µM) of either Lsh wild-type or Lsh KR mutant. ATP concentrations were kept constant (1 mM). Apart from this, the analysis of the binding of Lsh to RNA was performed as described before.

5.2.9.3 Competitive EMSA

In order to analyze the stability of complexes consisting of Lsh and either RNA, DNA or nucleosomes, competitive EMSAs were carried out. Complexes were formed by incubating 1.6 µM of Lsh with 50 nM of fluorescently labeled RNA, DNA or mononucleosomes at 30°C for 5 min in EX buffer containing 300 mM KCl, 20 mM Tris/HCl pH 7.6, 1.5 mM $MgCl_2$, 0.5 mM EGTA and 10% glycerol. Subsequently, the complex was mixed with a dilution series of the competing substrate. The dilution series ranged from 6 nM–1.6 µM, and was prepared in EX buffer containing 20 mM Tris/HCl pH 7.6, 1.5 mM $MgCl_2$, 0.5 mM EGTA and 10% glycerol in a total volume of 10 µl. 10 µl of complex were added to each 10 µl of dilution series. Thus, final concentrations of the competing substrate varied from 3 nM–800 nM, and final concentration of Lsh was 400 nM in a complex with 25 nM RNA, DNA or nucleosome in a final buffer composition of 150 mM KCl, 20 mM Tris/HCl pH 7.6, 1.5 mM $MgCl_2$, 0.5 mM EGTA and 10% glycerol. The mixture was incubated for 15 min at 30 °C. Reactions were analyzed on 5% native PAA gels. Gels were pre-run for 30 min at 50 V, reactions were loaded, and gels were run for 20–45 min at 100 V. Documentation was done on a Typhoon FLA 9500 laser scanner (GE Healthcare). Since the competing binding partners were differently labeled, filters of the device were set to scan both fluorophores at the same time. For visual inspection, images of the individual fluorescent substrates were overlaid.

To test the influence of ATP on the stability of the Lsh/RNA complex at increasing concentrations of mononucleosomes, competitive EMSAs were performed in the presence of constant amounts of ATP (1mM). For complex formation, Lsh wild-type and Lsh KR mutant were incubated with fluorescently labeled single-stranded RNA as described before. Lsh/RNA complexes were mixed with increasing concentrations of fluorescently labeled mononucleosomes, varying from 12.5 nM to 800 nM final concentrations. Apart from this, experiments were performed as described before.

5.2.9.4 Microscale thermophoresis (MST)

5.2.9.4.1 The concept of microscale thermophoresis:

The microscale thermophoresis (MST) technology enables the quantitative measurement of molecular interactions in solution. The theoretical background of the method and its usage for a wide array of different assays is published (Baaske et al., 2010) (Wienken et al., 2011). In general, the method is based on the thermophoretic movement of molecules along an induced temperature gradient. This movement is determined by parameters such as size, charge and hydration shell of a molecule. Since binding to another molecule is thought to influence all these parameters, the interaction leads to changes in thermophoretic behavior. Basically, these changes are recorded by the Monolith MST device (NanoTemper) in the form of thermophoresis profiles that can be used to generate binding curves and calculate K_d or EC_{50} values.

The principal setup of an MST experiment is illustrated in Fig 5.8 A. A prerequisite for MST measurements on the used MST devices was the fluorescent labeling of one of the two binding partners for detection by the optics of the device. The molecule bearing the fluorescent label is usually kept at constant concentrations, and a serial dilution of the putative binding partner is titrated to the labeled molecules. Sample mixtures are then sucked into glass capillaries that are placed onto a tray, which is put into the MST device. The typical progress of an MST experiment is depicted in Fig 5.8 B. Turning on the laser, a temperature gradient is induced, and the molecules begin to move. The molecule movement is measured over a certain time frame. Afterwards, the laser is switched off, and back diffusion of the molecules starts. For analysis during this work, the most important part of the created curves are the thermophoresis signals, i. e. the time points representing the overall thermophoretic behavior of the whole complex formed by the two binding partners. These signals are determined by changes in size, charge and hydration shell. Fig 5.8 C shows differences in the thermophoretic curves that are induced by the binding events. One can clearly distinguish the thermophoretic curves of the different states of unbound, partially-bound and fully-bound molecules in the reactions. These differences are translated into binding curves by plotting the normalized thermophoresis data against the concentrations of

the non-labeled binding partner. From these binding curves, K_d constants and EC_{50} values can be calculated by using the law of mass action or the Hill equation (Fig 5.8 D).

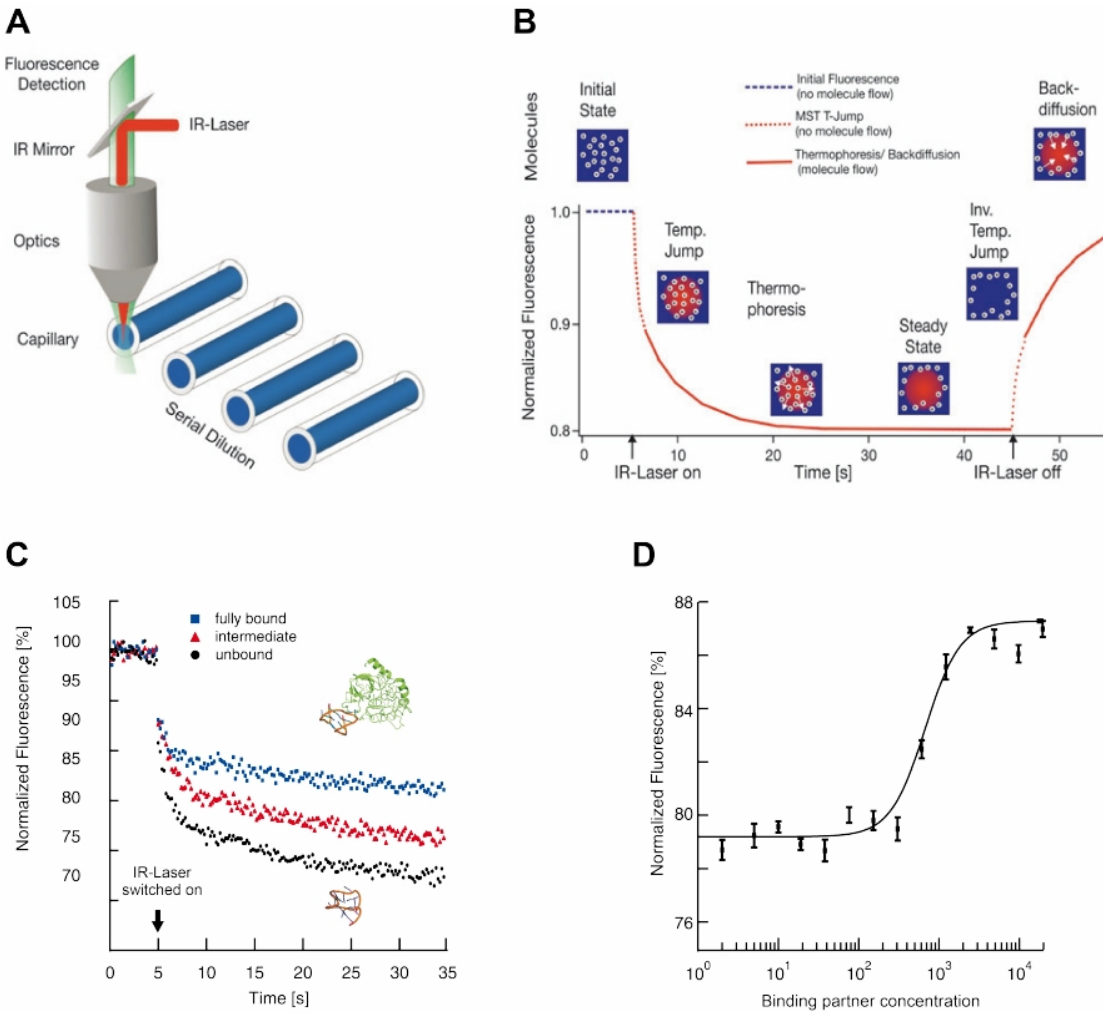

Fig 5.8: The concept of microscale thermophoresis.
(A) Setup of the Monolith MST device including a fluorescence detector, an IR-laser for temperature gradient induction and glas capillaries containing the reaction partners. **(B)** General outline of a thermophoresis experiment. Upon induction of the laser the molecules start to align themselves to the temperature gradient. These early time points describe the temperature jump behavior. At later time points, the molecules move along the temperature gradient according to their size, charge and hydration shell. This defines the thermophoresis data. Afterwards, a steady-state is reached, then the laser is switched off, and the molecules diffuse back. **(C)** Upon binding, the thermophoretic movement of the molecules changes, which can be seen in the curves, from unbound state (black) to partially-bound (red) and finally fully-bound state (blue). **(D)** Data from thermophoresis or temperature jump signals can be plotted against the concentrations of the unlabeled binding partner to generate binding curves, from which K_D and EC_{50} values can be calculated. (Pictures are adapted from Jerabek-Willemsen et al., 2011, and Baaske et al., 2010).

5.2.9.4.2 Analysis of protein-DNA and protein-RNA interactions with MST:

Prior to setting up up reactions, aggregates were removed by centrifuging protein solutions and nucleic acid stock solutions for 5 min at 13.000 g at 4 °C. For the protein, a 2:1 dilution series was prepared in EX buffer with 200 mM KCl and no glycerol or NP40 (200 mM KCl, 20 mM Tris/HCl pH 7.6, 1.5 mM $MgCl_2$, 0.5 mM EGTA) in final volumes of 10 µl. The DNA or

RNA mastermix was prepared in EX buffer without KCl, glycerol and NP40 (20 mM Tris/HCl pH 7.6, 1.5 mM $MgCl_2$, 0.5 mM EGTA). 10 µl of the mastermix were added to each protein dilution to get a final molar DNA or RNA concentration of 20–40 nM in a total volume of 20 µl. Reactions were mixed by pipetting and sucked into standard treated glass capillaries. Reactions were incubated in the MST device at 30 °C for 10–15 min before starting the measurements at 30 °C with an LED power of 50% and MST powers of 20%, 40% and 80% and a laser-on time of 40 sec. For data evaluation, the thermophoresis signals were normalized to fraction bound (X) by X = (Y(c)-Min)/(Max-Min). EC_{50} values were obtained according to the Hill equation corrected for the minimum (Min) and maximum (Max) values of the binding curve: Y(c) = Min+(Max-Min)/(1+(EC_{50}/c)^n) with 'Y(c)' being the thermophoresis signal, and 'c' the variable concentration of the respsective protein. Final data analysis of collected technical and biological replicates was done with SigmaPlot (Systat Software).

5.2.9.4.3 Analysis of protein-nucleosome interactions with MST:

In general, analysis was done as described for protein-DNA and protein-RNA interactions, but nucleosomes were not centrifuged, and samples were prepared in siliconized reaction tubes (Biozym) and supplemented with 200 ng/µl BSA. The 2:1 dilution series of the protein and the nucleosome mastermix were prepared in EX buffer with 100 mM KCl and no glycerol or NP40 (200 mM KCl, 20 mM Tris/HCl pH 7.6, 1.5 mM $MgCl_2$, 0.5 mM EGTA). 10 µl of the nucleosome mastermix were added to each 10 µl of each protein dilution to get a final molar concentration of nucleosomes of 50 nM in a total volume of 20 µl.

5.2.9.5 Nucleosome mobilization assay

By using the nucleosome mobilization assay, one can visualize nucleosome movement catalyzed by ATP-dependent nucleosome remodeling factors on the single molecule level (Langst et al., 1999). The nucleosome sliding assay relies on the fact that the location of a histone octamer on a DNA fragment affects its electrophoretic mobility in native PAA gels. Centrally-positioned nucleosomes migrate slower than nucleosomes positioned at an end of a DNA fragment. All reactions were performed in siliconized tubes (Biozym). A typical reaction contained 30 nM (if the DNA was fluorescently labeled) or 100 nM nucleosomes (if the DNA was not labeled) with defined translational positions and 1 mM ATP in a total volume of 20 µl in EX buffer (20 mM Tris/HCl pH 7.6, 1.5 mM $MgCl_2$, 0.5 mM EGTA and 10% glycerol) supplemented with 1 mM DTT and 200 ng/µl BSA. The concentration of monovalent anions (Cl^-) and cations (K^+/Na^+) was adjusted to 90 mM. Nucleosomes were incubated with 50 nM–800 nM of enzyme, as indicated in the respective figure legend (see 3.5), for 60 min at 30 °C. The reaction was stopped by the addition of 1.5 µg competitor DNA (plasmid DNA) and further incubated for 10 min. Nucleosome positions were analyzed on 5% native PAA

gels in 0.4 % TBE buffer. Gels were pre-run for 30 min and run for 60–90 min at 100 V. Optimal migration was controlled by using Orange G DNA loading dye as a marker. After separation the nucleosomal DNA was visualized on a fluorescence image reader (FLA-5000; Fuji), or by staining with ethidium bromide and documentation with the gel documentation system (Bio-Rad).

5.2.9.6 ATPase assay

ATPase assays were performed in the presence of [γ-32P]-ATP (0.2 µCi/µl) with various substrates to analyze specific substrate-dependent ATPase activity. Protein, non-radioactive ATP and putative ATPase stimulating substrates such as DNA, RNA and nucleosomes were mixed together with radioactive ATP in final 10 µl reaction volumes at concentrations as indicated in the respective figure legends. Usually, reactions contained 120 mM KCl, 20 mM Tris/HCl pH 7.6, 1.5 mM $MgCl_2$, 0.5 mM EGTA, 10% glycerol and 1mM DTT. Reactions were kept on ice and incubated for 40–60 min at 30 °C. Afterwards, the samples were put back on ice. 1 µl aliquots of each sample were spotted onto a thin layer chromatography (TLC) plate (Merck). TLC plates were transferred to a chamber containing 1 M LiCl and 0.5 M formic acid to separate the hydrolyzed phosphate from unreacted ATP. Plates were dried, wrapped in Saran foil, and radioactive energy on the plates was exposed to a phosphor imaging screen for 11–12 hours. Screens were read using the FLA-3000 phosphor imaging system (Fuji). ATP and hydrolyzed phosphate spots were quantified using the multigauge software (Fuji). The percentage of hydrolyzed ATP was calculated according to the following equation: $\%_{(\text{hydrolyzed ATP})} = P_i*100/(P_i + ATP_{\text{non-hydr}})$, where P_i was the signal intensity of hydrolyzed ATP and $ATP_{\text{non-hydr}}$ the signal intensity of non-hydrolyzed ATP. The percentage of hydrolyzed ATP was corrected for background activity arising from non-radioactive ATP and substrates such as RNA, or preparations of purified DNA methyltransferases. Corrected values were then used to calculate the amount of hydrolyzed ATP in µM.

6 Appendix

Repetitions of ATPase assays using unmodified dinucleosomes

A) 100 µM ATP; varying concentrations of Lsh WT and KR and varying concentrations of nucleosomes

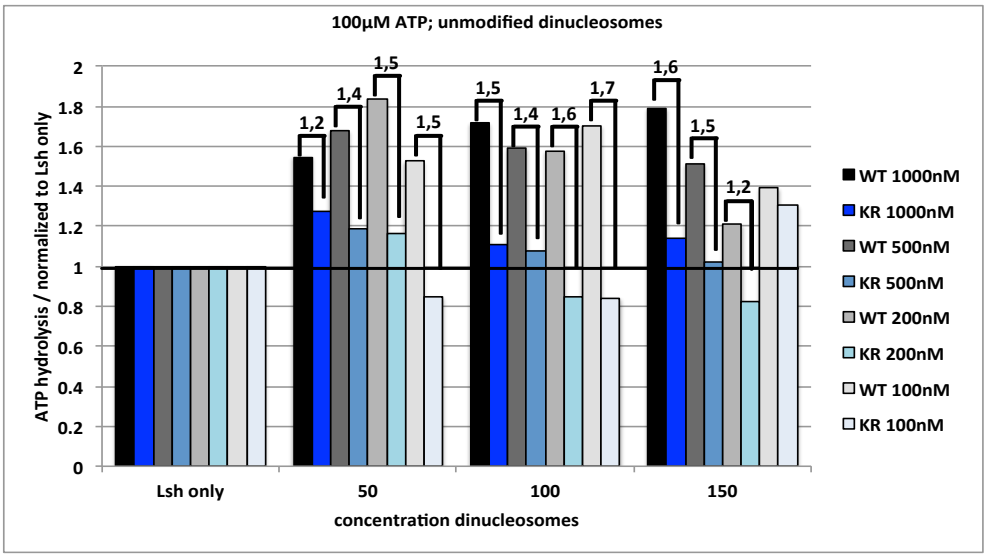

B) 10 µM ATP; varying concentrations of Lsh WT and KR and varying concentrations of nucleosomes

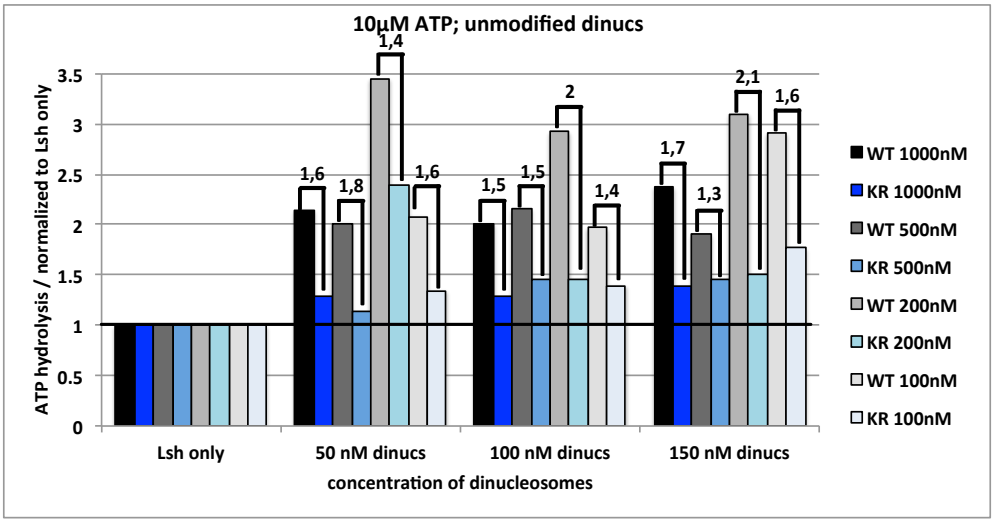

Analysis of the influence of unmodified dinucleosomes on the ATPase activity of Lsh.
The effect of unmodified dinucleosomes on the ATPase activity of Lsh was studied at **(A)** 100 µM ATP and **(B)** 10 µM ATP. Nucleosome concentrations varied from 50 to 150 nM, and concentrations of Lsh WT and KR varied from 100 nM to 1000 nM, as indicated. WT is illustrated in black and grey scale bars, KR in blue scale and white bars. Reactions were carried out in 10 µl volumes in the presence of the indicated amount of ATP (non-radioactive) and minor amounts of radioactive ATP (0.2 µCi/µl). Reactions were incubated for 45 min at 30 °C, then pipetted onto a TLC plate to separate the hydrolyzed phosphate from unreacted ATP. The percentage of hydrolyzed ATP was calculated according to the equation: $\%_{(\text{hydrolyzed ATP})} = P_i*100/(P_i + ATP_{\text{non-hydr}})$, and was corrected for background activity arising from non-radioactive ATP. Corrected values were then used to calculate the amount of hydrolyzed ATP in µM. Afterwards, values were normalized to Lsh only (WT and KR lacking nucleosomes). WT and corresponding KR were compared to each other, and calculated ratios are displayed, if values for WT are > 1 and exceed values for the corresponding KR. Values > 1 for WT were compared to Lsh only (corresponds to a value = 1, indicated by a black line), if values for the corresponding KR are < 1. Values < 1 can be ignored as signal intensities are weaker than for Lsh only.

Repetitions of ATPase assays using hydroxy-methylated dinucleosomes

A) 100 µM ATP; varying concentrations of Lsh WT and KR and varying concentrations of nucleosomes

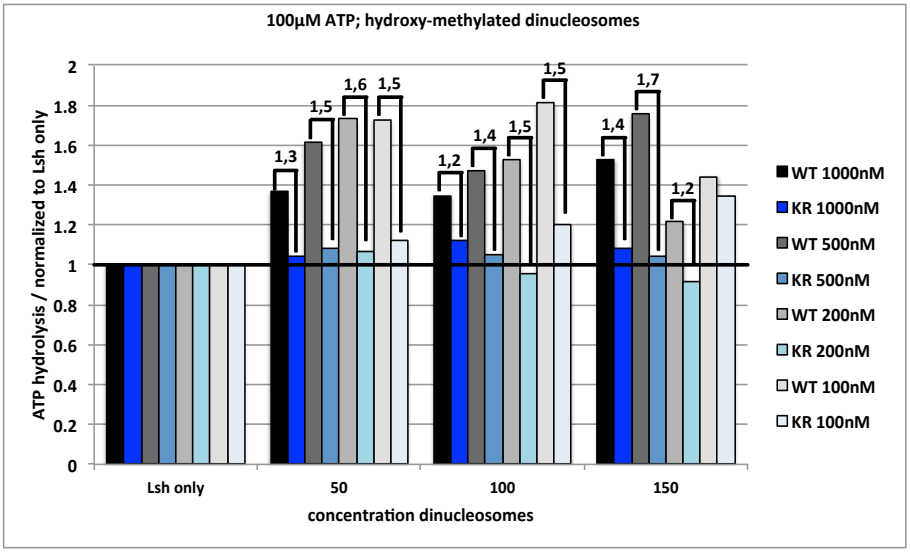

B) 10 µM ATP; varying concentrations of Lsh WT and KR and varying concentrations of nucleosomes

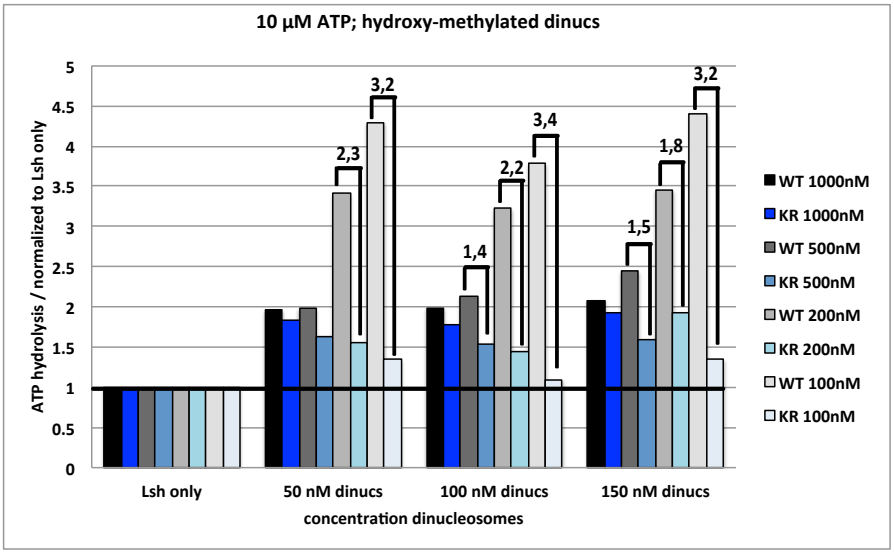

Analysis of the influence of hydroxy-methylated dinucleosomes on the ATPase activity of Lsh.
The effect of hydroxy-methylated dinucleosomes on the ATPase activity of Lsh was studied at **(A)** 100 µM ATP and **(B)** 10 µM ATP. Nucleosome concentrations varied from 50 to 150 nM, and concentrations of Lsh WT and KR varied from 100 nM to 1000 nM, as indicated. WT is illustrated in black and grey scale bars, KR in blue scale and white bars. Reactions were carried out in 10 µl volumes in the presence of the indicated amount of ATP (non-radioactive) and minor amounts of radioactive ATP (0.2 µCi/µl). Reactions were incubated for 45 min at 30 °C, then pipetted onto a TLC plate to separate the hydrolyzed phosphate from unreacted ATP. The percentage of hydrolyzed ATP was calculated according to the equation: $\%_{(\text{hydrolyzed ATP})} = P_i*100/(P_i + ATP_{\text{non-hydr}})$, and was corrected for background activity arising from non-radioactive ATP. Corrected values were then used to calculate the amount of hydrolyzed ATP in µM. Afterwards, values were normalized to Lsh only (WT and KR lacking nucleosomes). WT and corresponding KR were compared to each other, and calculated ratios are displayed, if values for WT are > 1 and exceed values for the corresponding KR. Values > 1 for WT were compared to Lsh only (corresponds to a value = 1, indicated by a black line), if values for the corresponding KR are < 1. Values < 1 can be ignored as signal intensities are weaker than for Lsh only.

ATPase assay with total RNA as substrate

In order to confirm the stimulating effect of RNA on the ATPase activity of Lsh, RNA was isolated from HEK293 cells using the NucleoSpin® RNA isolation kit (Macherey-Nagel) instead of TRIzol.

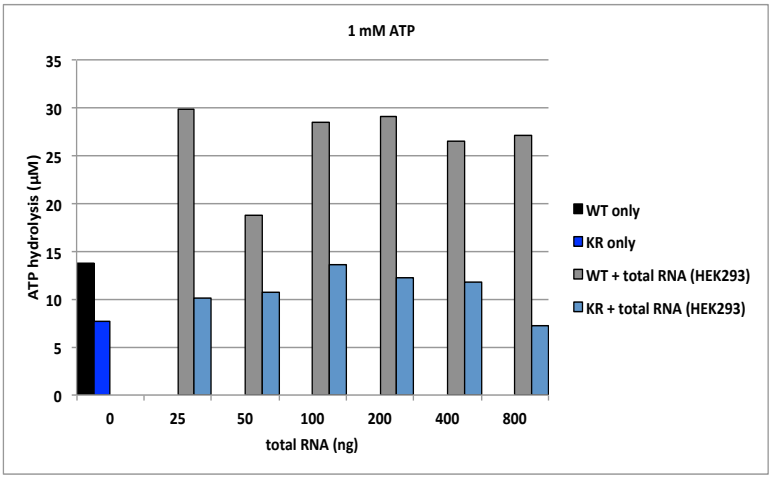

Effect of total RNA on the ATPase activity of Lsh.
The ATPase activity of Lsh was studied using total RNA as substrate. Increasing amounts of total RNA (25 ng–800 ng) isolated from HEK293 cells were incubated with 200 nM of Lsh WT (grey bars) and Lsh KR (light blue bars) in the presence of 1 mM non-radioactive ATP. Lsh WT (black bars) and Lsh KR (dark blue bars) lacking total RNA in the mixture served as controls. Reactions were incubated with minor amounts of radioactive ATP (0.2 µCi/µl) for 45 min at 30 °C in a volume of 10 µl, and were pipetted onto a TLC plate to separate hydrolyzed phosphate from unreacted ATP. Percentage of hydrolyzed ATP was calculated according to the equation: $\%_{(hydrolyzed\ ATP)} = P_i*100/(P_i + ATP_{non\text{-}hydr})$, and was corrected for background activity arising from non-radioactive ATP and total RNA preparations. Corrected values were used to calculate hydrolyzed ATP in µM.

Sequences of RNAs used in binding- and ATPase assays

EN3D_ssRNA (synthetic oligo)
CCUCCUUUUUUCUUUUUUUUUUUUUUUCU

L10 (precursor miRNA_fly)
GUUGGGGGACAUUGAUCUCGGAGACGGCGGUUUAACUGAUCCAUUCUCUCACAUCACUUCCC
UCACAG

L17 (precursor miRNA_fly)
CCUGGAGGGGGGCACUGCGCAAGCAAAGCCAGGGACCCUGAGAGGCUUUGCUUCCUGCUCC
CCUAG

T546 (part from lncRNA TINCR_human)
GGGCGGGCGGAGCGCGGGCGCGGCGGGGGCGGGCGGCCAGGCUAGUCGGGCGGGUGCGCG
GGGCGCUCGGGGCCCGGGGCCAGAGCUGGAGCCGGAGCCGGGCGGGCGCCAUGGAGGGGC
UGCGGCGGGGGCUGUCGCGCUGGAAGCGCUACCACAUCAAGGUGCACCUGGCGGACGAGGC
GCUGCUGCUACCGCUGACCGUGCGGCCGCGGGACACGCUCAGCGACCUGCGCGCCCAGCUG
GUGGGCCAGGGCGUGAGCUCCUGGAAGCGCGCCUUCUACUACAACGCGCGGCGGCUGGACG
ACCACCAGACGGUGCGCGACGCGCGCCUGCAGGACGGCUCGGUGCUGCUGCUCGUCAGCGA
CCCCAGGUAGUCUGGGUUGGAGGAGGCAGAGCCAUGACCAAGGGGACCUGGGUACUGGCUG
AAGGAAUAGGCUGGGGUAGAGGGCACUUUUGGAAGGCACUUCUCCUGCCUCCCGGGAGCCUA
GAUCUCACUCCAGGGUCUGGGCUCCCAGGUGGACCAU

T3460(part from lncRNA TINCR_human)
GGGGGUGCCGAGGCUACGCAUGUCCUCGAGGGCCGUGUACACUCUCCAGGCACCAUGGGCG
GAGGCGCCAGAGGCUGGGAAGAAAUAAUGUUUUAGUUAAGAGUCCUGUUGGCUGCAGGACUC
AGAGCAUGGACAGGUGGAUAGUAAAUCACCACCACGGGGACAGCCGUGCCCAGACUGUGCGU
UUGCUUAGCUCGGGGACAGCACUUGGCCCGGGGUCUCCUGCUCGCCUCCCUUCAGAGCAUC
UGCCAAACUUCGGGCAUCUACCCUGCAAUUCCCGCUUGGCUGAGAGGAGGGGGAGAAGGAGG
GGAAGAGAGAGGAGCCCCACUUCACUCCGGCAGGCAGACCUGCUGGAGCUGCUUUGCAGAAU
GACUUGGGUCUUGCUGGCCCCUGGGUGUGCCUGGAGGGGGGUCUUCCUAUCCCCCUCCACC
UCUCCCCUUGGUGCCUAACCCAGGACUUUGUCCCCAGAGACCCACUGUGUGCCCCCUGGAGC
UCCUCCUAGAGCAGAGUCUGCUGCUGUCUGU

7 Acknowledgements

Abschließend möchte ich allen Leuten danken, die diese Arbeit ermöglicht haben.

Zunächst möchte ich Prof. Dr. Gernot Längst für die Vergabe der Doktorarbeit und deren Begutachtung danken. Ich möchte mich auch dafür bedanken, dass ich die Arbeit in seiner Arbeitsgruppe durchführen durfte, und mir seine fachliche Betreuung und Ratschläge immer wieder neue Einblicke in die Thematik ermöglichten.
Außerdem gilt mein Dank Prof. Dr. Michael Rehli für die Übernahme des Zweitgutachtens und, zusammen mit PD Dr. Attila Nemeth, das Mentoring im Rahmen meiner Doktorarbeit, von welchem ich profitieren konnte.
Neben Prof. Dr. Gernot Längst und Prof. Dr. Michael Rehli danke ich den weiteren Mitgliedern des Prüfungsausschusses, Prof. Dr. Wolfgang Seufert, Prof. Dr. Klaus Grasser und PD Dr. Joachim Griesenbeck, für die Bewertung und Prüfung meiner Dissertation.
Bei der gesamten Arbeitsgruppe Längst sowie allen anderen Mitgliedern des “House of the Ribosome” bedanke ich mich für die Unterstützung und die insgesamt sehr gute und angenehme Arbeitsatmosphäre. Es hat einem so manch anstrengenden Arbeitstag erleichtert.
An dieser Stelle möchte ich auch all meinen Freunden für die bisherige gemeinsame Zeit danken. Ich danke dabei auch meiner Freundin für ihre Geduld, ihren Rückhalt und Zuspruch.
Ein ganz besonderer Dank gilt meiner Familie, die stets an mich glaubt, mich unterstützt und für mich da ist.

8 Bibliography

Abdalla, H., Yoshizawa, Y., and Hochi, S. (2009). Active demethylation of paternal genome in mammalian zygotes. J. Reprod. Dev. *55*, 356–360.

Achour, M., Jacq, X., Rondé, P., Alhosin, M., Charlot, C., Chataigneau, T., Jeanblanc, M., Macaluso, M., Giordano, A., Hughes, A.D., et al. (2008). The interaction of the SRA domain of ICBP90 with a novel domain of DNMT1 is involved in the regulation of VEGF gene expression. Oncogene *27*, 2187–2197.

Aoyagi, S., Wade, P.A., and Hayes, J.J. (2003). Nucleosome sliding induced by the xMi-2 complex does not occur exclusively via a simple twist-diffusion mechanism. Journal of Biological Chemistry *278*, 30562–30568.

Arand, J., Spieler, D., Karius, T., Branco, M.R., Meilinger, D., Meissner, A., Jenuwein, T., Xu, G., Leonhardt, H., Wolf, V., et al. (2012). In vivo control of CpG and non-CpG DNA methylation by DNA methyltransferases. PLoS Genet *8*, e1002750.

Arita, K., Ariyoshi, M., Tochio, H., Nakamura, Y., and Shirakawa, M. (2008). Recognition of hemi-methylated DNA by the SRA protein UHRF1 by a base-flipping mechanism. Nature *455*, 818–821.

Baaske, P., Wienken, C.J., Reineck, P., Duhr, S., and Braun, D. (2010). Optical Thermophoresis for Quantifying the Buffer Dependence of Aptamer Binding. Angew. Chem. Int. Ed. *49*, 2238–2241.

Bachman, K.E., Rountree, M.R., and Baylin, S.B. (2001). Dnmt3a and Dnmt3b are transcriptional repressors that exhibit unique localization properties to heterochromatin. Journal of Biological Chemistry *276*, 32282–32287.

Bacolla, A., Pradhan, S., Roberts, R.J., and Wells, R.D. (1999). Recombinant human DNA (cytosine-5) methyltransferase. II. Steady-state kinetics reveal allosteric activation by methylated dna. Journal of Biological Chemistry *274*, 33011–33019.

Bannister, A.J., and Kouzarides, T. (2005). Reversing histone methylation. Nature *436*, 1103–1106.

Bao, Y., and Shen, X. (2007). INO80 subfamily of chromatin remodeling complexes. Mutat Res *618*, 18–29.

Barbaux, S., Gascoin-Lachambre, G., Buffat, C., Monnier, P., Mondon, F., Tonanny, M.-B., Pinard, A., Auer, J., Bessières, B., Barlier, A., et al. (2012). A genome-wide approach reveals novel imprinted genes expressed in the human placenta. Epigenetics *7*, 1079–1090.

Barlow, D.P., and Bartolomei, M.S. (2014). Genomic Imprinting in Mammals. Cold Spring Harbor Perspectives in Biology *6*, a018382–a018382.

Bartolomei, M.S., Zemel, S., and Tilghman, S.M. (1991). Parental imprinting of the mouse H19 gene. Nature *351*, 153–155.

Bashtrykov, P., Jankevicius, G., Jurkowska, R.Z., Ragozin, S., and Jeltsch, A. (2014). The UHRF1 Protein Stimulates the Activity and Specificity of the Maintenance DNA Methyltransferase DNMT1 by an Allosteric Mechanism. Journal of Biological Chemistry *289*, 4106–4115.

Beard, B.C., Wilson, S.H., and Smerdon, M.J. (2003). Suppressed catalytic activity of base excision repair enzymes on rotationally positioned uracil in nucleosomes. Proc Natl Acad Sci USA *100*, 7465–7470.

Becker, P.B., and Hörz, W. (2002). ATP-DEPENDENT NUCLEOSOME REMODELING. Annu. Rev. Biochem. *71*, 247–273.

Berger, I., Fitzgerald, D.J., and Richmond, T.J. (2004). Baculovirus expression system for heterologous multiprotein complexes. Nat Biotechnol *22*, 1583–1587.

Berkyurek, A.C., Suetake, I., Arita, K., Takeshita, K., Nakagawa, A., Shirakawa, M., and Tajima, S. (2014). The DNA Methyltransferase Dnmt1 Directly Interacts with the SET and RING Finger-associated (SRA) Domain of the Multifunctional Protein Uhrf1 to Facilitate Accession of the Catalytic Center to Hemi-methylated DNA. Journal of Biological Chemistry *289*, 379–386.

Bernstein, B.E., Mikkelsen, T.S., Xie, X., Kamal, M., Huebert, D.J., Cuff, J., Fry, B., Meissner, A., Wernig, M., Plath, K., et al. (2006). A bivalent chromatin structure marks key developmental genes in embryonic stem cells. Cell *125*, 315–326.

Bestor, T.H. (2000). The DNA methyltransferases of mammals. Human Molecular Genetics *9*, 2395–2402.

Bestor, T., Laudano, A., Mattaliano, R., and Ingram, V. (1988). Cloning and sequencing of a cDNA encoding DNA methyltransferase of mouse cells. The carboxyl-terminal domain of the mammalian enzymes is related to bacterial restriction methyltransferases. Journal of Molecular Biology *203*, 971–983.

Bienz, M. (2006). The PHD finger, a nuclear protein-interaction domain. Trends Biochem Sci *31*, 35–40.

Binder, M., Eberle, F., Seitz, S., Mücke, N., Hüber, C.M., Kiani, N., Kaderali, L., Lohmann, V., Dalpke, A., and Bartenschlager, R. (2011). Molecular mechanism of signal perception and integration by the innate immune sensor retinoic acid-inducible gene-I (RIG-I). Journal of Biological Chemistry *286*, 27278–27287.

Bird, A. (2002). DNA methylation patterns and epigenetic memory. Genes Dev *16*, 6–21.

Boeke, J., Bag, I., Ramaiah, M.J., Vetter, I., Kremmer, E., Pal-Bhadra, M., Bhadra, U., and Imhof, A. (2011). The RNA helicase Rm62 cooperates with SU(VAR)3-9 to re-silence active transcription in Drosophila melanogaster. PLoS ONE *6*, e20761.

Bostick, M., Kim, J.K., Estève, P.-O., Clark, A., Pradhan, S., and Jacobsen, S.E. (2007). UHRF1 plays a role in maintaining DNA methylation in mammalian cells. Science *317*, 1760–1764.

Bouazoune, K., and Kingston, R.E. (2012). Chromatin remodeling by the CHD7 protein is impaired by mutations that cause human developmental disorders. Proceedings of the National Academy of Sciences *109*, 19238–19243.

Bouazoune, K., Mitterweger, A., Längst, G., Imhof, A., Akhtar, A., Becker, P.B., and Brehm, A. (2002). The dMi-2 chromodomains are DNA binding modules important for ATP-dependent nucleosome mobilization. Embo J *21*, 2430–2440.

Boyer, L.A., Logie, C., Bonte, E., Becker, P.B., Wade, P.A., Wolffe, A.P., Wu, C., Imbalzano, A.N., and Peterson, C.L. (2000). Functional delineation of three groups of the ATP-

dependent family of chromatin remodeling enzymes. Journal of Biological Chemistry *275*, 18864–18870.

Boyer, L.A., Latek, R.R., and Peterson, C.L. (2004). The SANT domain: a unique histone-tail-binding module? Nat. Rev. Mol. Cell Biol. *5*, 158–163.

Bönisch, C., Nieratschker, S.M., Orfanos, N.K., and Hake, S.B. (2008). Chromatin proteomics and epigenetic regulatory circuits. Expert Rev Proteomics *5*, 105–119.

Bradford, M.M. (1976). Rapid and Sensitive Method for Quantitation of Microgram Quantities of Protein Utilizing Principle of Protein-Dye Binding. Anal. Biochem. *72*, 248–254.

Brehm, A., Langst, G., Kehle, J., Clapier, C.R., Imhof, A., Eberharter, A., Müller, J., and Becker, P.B. (2000). dMi-2 and ISWI chromatin remodelling factors have distinct nucleosome binding and mobilization properties. Embo J *19*, 4332–4341.

Brehm, A., Tufteland, K.R., Aasland, R., and Becker, P.B. (2004). The many colours of chromodomains. Bioessays *26*, 133–140.

Brosh, R.M., and Matson, S.W. (1995). Mutations in motif II of Escherichia coli DNA helicase II render the enzyme nonfunctional in both mismatch repair and excision repair with differential effects on the unwinding reaction. J. Bacteriol. *177*, 5612–5621.

Brzeski, J., and Jerzmanowski, A. (2003). Deficient in DNA Methylation 1 (DDM1) Defines a Novel Family of Chromatin-remodeling Factors. Journal of Biological Chemistry *278*, 823–828.

Burrage, J., Termanis, A., Geissner, A., Myant, K., Gordon, K., and Stancheva, I. (2013). The SNF2 family ATPase LSH promotes phosphorylation of H2AX and efficient repair of DNA double-strand breaks in mammalian cells. Journal of Cell Science *125*, 5524–5534.

Cajigas, I., Leib, D.E., Cochrane, J., Luo, H., Swyter, K.R., Chen, S., Clark, B.S., Thompson, J., Yates, J.R., Kingston, R.E., et al. (2015). Evf2 lncRNA/BRG1/DLX1 interactions reveal RNA-dependent inhibition of chromatin remodeling. Development *142*, 2641–2652.

Calo, E., Flynn, R.A., Martin, L., Spitale, R.C., Chang, H.Y., and Wysocka, J. (2015). RNA helicase DDX21 coordinates transcription and ribosomal RNA processing. Nature *518*, 249–253.

Campos, E.I., and Reinberg, D. (2009). Histones: annotating chromatin. Annu. Rev. Genet. *43*, 559–599.

Cao, J., and Yan, Q. (2012). Histone ubiquitination and deubiquitination in transcription, DNA damage response, and cancer. Front Oncol *2*, 26.

Celeste, A., Fernandez-Capetillo, O., Kruhlak, M.J., Pilch, D.R., Staudt, D.W., Lee, A., Bonner, R.F., Bonner, W.M., and Nussenzweig, A. (2003). Histone H2AX phosphorylation is dispensable for the initial recognition of DNA breaks. Nat Cell Biol *5*, 675–679.

Chedin, F., Lieber, M.R., and Hsieh, C.-L. (2002). The DNA methyltransferase-like protein DNMT3L stimulates de novo methylation by Dnmt3a. Proc Natl Acad Sci USA *99*, 16916–16921.

Chen, T., and Li, E. (2006). Establishment and maintenance of DNA methylation patterns in mammals. Curr. Top. Microbiol. Immunol. *301*, 179–201.

Chen, T., Tsujimoto, N., and Li, E. (2004). The PWWP domain of Dnmt3a and Dnmt3b is required for directing DNA methylation to the major satellite repeats at pericentric heterochromatin. Molecular and Cellular Biology *24*, 9048–9058.

Chen, T., Ueda, Y., Dodge, J.E., Wang, Z., and Li, E. (2003). Establishment and maintenance of genomic methylation patterns in mouse embryonic stem cells by Dnmt3a and Dnmt3b. Molecular and Cellular Biology *23*, 5594–5605.

Choi, I., Kim, R., Lim, H.-W., Kaestner, K.H., and Won, K.-J. (2014). 5-hydroxymethylcytosine represses the activity of enhancers in embryonic stem cells: a new epigenetic signature for gene regulation. BMC Genomics *15*, 670.

Clapier, C.R., Langst, G., Corona, D.F., Becker, P.B., and Nightingale, K.P. (2001). Critical role for the histone H4 N terminus in nucleosome remodeling by ISWI. Molecular and Cellular Biology *21*, 875–883.

Clapier, C.R., and Cairns, B.R. (2009). The Biology of Chromatin Remodeling Complexes. Annu. Rev. Biochem. *78*, 273–304.

Clapier, C.R., and Cairns, B.R. (2012). Regulation of ISWI involves inhibitory modules antagonized by nucleosomal epitopes. Nature 1–6.

Cloutier, S.C., Ma, W.K., Nguyen, L.T., and Tran, E.J. (2012). The DEAD-box RNA helicase Dbp2 connects RNA quality control with repression of aberrant transcription. J. Biol. Chem. *287*, 26155–26166.

Corona, D.F., Langst, G., Clapier, C.R., Bonte, E.J., Ferrari, S., Tamkun, J.W., and Becker, P.B. (1999). ISWI is an ATP-dependent nucleosome remodeling factor. Molecular Cell *3*, 239–245.

Cosgrove, M.S., Boeke, J.D., and Wolberger, C. (2004). Regulated nucleosome mobility and the histone code. Nature Structural & Molecular Biology *11*, 1037–1043.

Côté, J., Peterson, C.L., and Workman, J.L. (1998). Perturbation of nucleosome core structure by the SWI/SNF complex persists after its detachment, enhancing subsequent transcription factor binding. Proc Natl Acad Sci USA *95*, 4947–4952.

Côté, J., Quinn, J., Workman, J.L., and Peterson, C.L. (1994). Stimulation of GAL4 derivative binding to nucleosomal DNA by the yeast SWI/SNF complex. Science.

Craig, J.M. (2005). Heterochromatin--many flavours, common themes. Bioessays *27*, 17–28.

Cugusi, S., Kallappagoudar, S., Ling, H., and Lucchesi, J.C. (2015). The Drosophila Helicase Maleless (MLE) is Implicated in Functions Distinct From its Role in Dosage Compensation. Mol. Cell Proteomics *14*, 1478–1488.

Datta, J., Majumder, S., Bai, S., Ghoshal, K., Kutay, H., Smith, D.S., Crabb, J.W., and Jacob, S.T. (2005). Physical and functional interaction of DNA methyltransferase 3A with Mbd3 and Brg1 in mouse lymphosarcoma cells. Cancer Res. *65*, 10891–10900.

Davey, C.A., Sargent, D.F., Luger, K., Maeder, A.W., and Richmond, T.J. (2002). Solvent mediated interactions in the structure of the nucleosome core particle at 1.9 a resolution. Journal of Molecular Biology *319*, 1097–1113.

De Cian, A., Praly, E., Ding, F., Singh, V., Lavelle, C., Le Cam, E., Croquette, V., Piétrement, O., and Bensimon, D. (2012). ATP-independent cooperative binding of yeast Isw1a to bare

and nucleosomal DNA. PLoS ONE *7*, e31845.

de Koning, A.P.J., Gu, W., Castoe, T.A., Batzer, M.A., and Pollock, D.D. (2011). Repetitive elements may comprise over two-thirds of the human genome. PLoS Genet *7*, e1002384.

de Mol, N.J., Catalina, M.I., Dekker, F.J., Fischer, M.J.E., Heck, A.J.R., and Liskamp, R.M.J. (2005). Protein flexibility and ligand rigidity: a thermodynamic and kinetic study of ITAM-based ligand binding to Syk tandem SH2. ChemBioChem *6*, 2261–2270.

DeChiara, T.M., Robertson, E.J., and Efstratiadis, A. (1991). Parental imprinting of the mouse insulin-like growth factor II gene. Cell *64*, 849–859.

Denis, H., Ndlovu, '.N., and Fuks, F. (2011). Regulation of mammalian DNA methyltransferases: a route to new mechanisms. EMBO Rep. *12*, 647–656.

Dennis, K. (2001). Lsh, a member of the SNF2 family, is required for genome-wide methylation. Genes Dev *15*, 2940–2944.

Di Ruscio, A., Ebralidze, A.K., Benoukraf, T., Amabile, G., Goff, L.A., Terragni, J., Figueroa, M.E., De Figueiredo Pontes, L.L., Alberich-Jorda, M., Zhang, P., et al. (2014). DNMT1-interacting RNAs block gene-specific DNA methylation. 1–10.

Dorigo, B., Schalch, T., Kulangara, A., Duda, S., Schroeder, R.R., and Richmond, T.J. (2004). Nucleosome arrays reveal the two-start organization of the chromatin fiber. Science *306*, 1571–1573.

Dovey, O.M., Foster, C.T., and Cowley, S.M. (2010). Histone deacetylase 1 (HDAC1), but not HDAC2, controls embryonic stem cell differentiation. Proceedings of the National Academy of Sciences *107*, 8242–8247.

Du, J., Nasir, I., Benton, B.K., Kladde, M.P., and Laurent, B.C. (1998). Sth1p, a Saccharomyces cerevisiae Snf2p/Swi2p homolog, is an essential ATPase in RSC and differs from Snf/Swi in its interactions with histones and chromatin-associated proteins. Genetics *150*, 987–1005.

Duerr, H., Flaus, A., Owen-Hughes, T., and Hopfner, K.-P. (2006). Snf2 family ATPases and DExx box helicases: differences and unifying concepts from high-resolution crystal structures. Nucleic Acids Research *34*, 4160–4167.

Dundr, M., Hoffmann-Rohrer, U., Hu, Q., Grummt, I., Rothblum, L.I., Phair, R.D., and Misteli, T. (2002). A kinetic framework for a mammalian RNA polymerase in vivo. Science *298*, 1623–1626.

Dunican, D.S., Pennings, S., and Meehan, R.R. (2015). Lsh Is Essential for Maintaining Global DNA Methylation Levels in Amphibia and Fish and Interacts Directly with Dnmt1. BioMed Research International *2015*, 1–12.

Dürr, H., Körner, C., Müller, M., Hickmann, V., and Hopfner, K.-P. (2005). X-ray structures of the Sulfolobus solfataricus SWI2/SNF2 ATPase core and its complex with DNA. Cell *121*, 363–373.

Ebbert, R., Birkmann, A., and Schüller, H.J. (1999). The product of the SNF2/SWI2 paralogue INO80 of Saccharomyces cerevisiae required for efficient expression of various yeast structural genes is part of a high-molecular-weight protein complex. Mol. Microbiol. *32*, 741–751.

Erdel, F., Krug, J., Längst, G., and Rippe, K. (2011). Targeting chromatin remodelers: Signals and search mechanisms. BBA - Gene Regulatory Mechanisms *1809*, 497–508.

Erdel, F., Schubert, T., Marth, C., Laengst, G., and Rippe, K. (2010). Human ISWI chromatin-remodeling complexes sample nucleosomes via transient binding reactions and become immobilized at active sites. Proc Natl Acad Sci USA *107*, 19873–19878.

Eyss, von, B., Maaskola, J., Memczak, S., Ilmann, K.M.O., Schuetz, A., Loddenkemper, C., Tanh, M.-D., Otto, A., Muegge, K., Heinemann, U., et al. (2011). The SNF2-like helicase HELLS mediates E2F3-dependent transcription and cellular transformation. Embo J 1–14.

Fan, T., Hagan, J.P., Kozlov, S.V., Stewart, C.L., and Muegge, K. (2005). Lsh controls silencing of the imprinted Cdkn1c gene. Development *132*, 635–644.

Fan, T., Schmidtmann, A., Xi, S., Briones, V., Zhu, H., Suh, H.C., Gooya, J., Keller, J.R., Xu, H., Roayaei, J., et al. (2008). DNA hypomethylation caused by Lsh deletion promotes erythroleukemia development. Epigenetics *3*, 134–142.

Fan, T., Yan, Q., Huang, J., Austin, S., Cho, E., Ferris, D., and Muegge, K. (2003). Lsh-deficient murine embryonal fibroblasts show reduced proliferation with signs of abnormal mitosis. Cancer Res. *63*, 4677–4683.

Fatemi, M., Hermann, A., Gowher, H., and Jeltsch, A. (2002). Dnmt3a and Dnmt1 functionally cooperate during de novo methylation of DNA. Eur. J. Biochem. *269*, 4981–4984.

Fatemi, M., Hermann, A., Pradhan, S., and Jeltsch, A. (2001). The activity of the murine DNA methyltransferase Dnmt1 is controlled by interaction of the catalytic domain with the N-terminal part of the enzyme leading to an allosteric activation of the enzyme after binding to methylated DNA. Journal of Molecular Biology *309*, 1189–1199.

Feinberg, A.P. (2004). The epigenetics of cancer etiology. Semin. Cancer Biol. *14*, 427–432.

Felle, M., Hoffmeister, H., Rothammer, J., Fuchs, A., Exler, J.H., and Langst, G. (2011a). Nucleosomes protect DNA from DNA methylation in vivo and in vitro. Nucleic Acids Research *39*, 6956–6969.

Felle, M., Joppien, S., Nemeth, A., Diermeier, S., Thalhammer, V., Dobner, T., Kremmer, E., Kappler, R., and Langst, G. (2011b). The USP7/Dnmt1 complex stimulates the DNA methylation activity of Dnmt1 and regulates the stability of UHRF1. Nucleic Acids Research *39*, 8355–8365.

Fellinger, K., Rothbauer, U., Felle, M., Längst, G., and Leonhardt, H. (2009). Dimerization of DNA methyltransferase 1 is mediated by its regulatory domain. J. Cell. Biochem. *106*, 521–528.

Felsenfeld, G., Burgess-Beusse, B., Farrell, C., Gaszner, M., Ghirlando, R., Huang, S., Jin, C., Litt, M., Magdinier, F., Mutskov, V., et al. (2004). Chromatin boundaries and chromatin domains. Cold Spring Harb. Symp. Quant. Biol. *69*, 245–250.

Fischle, W. (2008). Talk is cheap--cross-talk in establishment, maintenance, and readout of chromatin modifications. Genes Dev *22*, 3375–3382.

Fischle, W., Wang, Y., and Allis, C.D. (2003a). Histone and chromatin cross-talk. Current Opinion in Cell Biology *15*, 172–183.

Fischle, W., Wang, Y., Jacobs, S.A., Kim, Y., Allis, C.D., and Khorasanizadeh, S. (2003b).

Molecular basis for the discrimination of repressive methyl-lysine marks in histone H3 by Polycomb and HP1 chromodomains. Genes Dev *17*, 1870–1881.

Fitzgerald, D.J., Berger, P., Schaffitzel, C., Yamada, K., Richmond, T.J., and Berger, I. (2006). Protein complex expression by using multigene baculoviral vectors. Nat Meth *3*, 1021–1032.

Flaus, A., Martin, D.M.A., Barton, G.J., and Owen-Hughes, T. (2006). Identification of multiple distinct Snf2 subfamilies with conserved structural motifs. Nucleic Acids Research *34*, 2887–2905.

Frauer, C., Hoffmann, T., Bultmann, S., Casa, V., Cardoso, M.C., Antes, I., and Leonhardt, H. (2011). Recognition of 5-hydroxymethylcytosine by the Uhrf1 SRA domain. PLoS ONE *6*, e21306.

Fuks, F., Hurd, P.J., Deplus, R., and Kouzarides, T. (2003a). The DNA methyltransferases associate with HP1 and the SUV39H1 histone methyltransferase. Nucleic Acids Research *31*, 2305–2312.

Fuks, F., Hurd, P.J., Wolf, D., Nan, X., Bird, A.P., and Kouzarides, T. (2003b). The methyl-CpG-binding protein MeCP2 links DNA methylation to histone methylation. Journal of Biological Chemistry *278*, 4035–4040.

Gallina, I., Colding, C., Henriksen, P., Beli, P., Nakamura, K., Offman, J., Mathiasen, D.P., Silva, S., Hoffmann, E., Groth, A., et al. (2015). Cmr1/WDR76 defines a nuclear genotoxic stress body linking genome integrity and protein quality control. Nat Commun *6*, 6533.

Gangaraju, V.K., and Bartholomew, B. (2007). Mechanisms of ATP dependent chromatin remodeling. Mutat Res *618*, 3–17.

Gaspar-Maia, A., Alajem, A., Polesso, F., Sridharan, R., Mason, M.J., Heidersbach, A., Ramalho-Santos, J., McManus, M.T., Plath, K., Meshorer, E., et al. (2009). Chd1 regulates open chromatin and pluripotency of embryonic stem cells. Nature *460*, 863–868.

Geiman, T.M., Tessarollo, L., Anver, M.R., Kopp, J.B., Ward, J.M., and Muegge, K. (2001). Lsh, a SNF2 family member, is required for normal murine development. Biochim Biophys Acta *1526*, 211–220.

Geiman, T.M., Sankpal, U.T., Robertson, A.K., Zhao, Y., Zhao, Y., and Robertson, K.D. (2004). DNMT3B interacts with hSNF2H chromatin remodeling enzyme, HDACs 1 and 2, and components of the histone methylation system. Biochem. Biophys. Res. Commun. *318*, 544–555.

George, A.A., Schiltz, R.L., and Hager, G.L. (2009). Dynamic access of the glucocorticoid receptor to response elements in chromatin. Int. J. Biochem. Cell Biol. *41*, 214–224.

Georgel, P.T., Tsukiyama, T., and Wu, C. (1997). Role of histone tails in nucleosome remodeling by Drosophila NURF. Embo J *16*, 4717–4726.

Ghosh, R.P., Horowitz-Scherer, R.A., Nikitina, T., Shlyakhtenko, L.S., and Woodcock, C.L. (2010). MeCP2 binds cooperatively to its substrate and competes with histone H1 for chromatin binding sites. Molecular and Cellular Biology *30*, 4656–4670.

Gibbons, R.J., McDowell, T.L., Raman, S., O'Rourke, D.M., Garrick, D., Ayyub, H., and Higgs, D.R. (2000). Mutations in ATRX, encoding a SWI/SNF-like protein, cause diverse changes in the pattern of DNA methylation. Nat. Genet. *24*, 368–371.

Gnanapragasam, M.N., Scarsdale, J.N., Amaya, M.L., Webb, H.D., Desai, M.A., Walavalkar, N.M., Wang, S.Z., Zu Zhu, S., Ginder, G.D., and Williams, D.C. (2011). p66Alpha-MBD2 coiled-coil interaction and recruitment of Mi-2 are critical for globin gene silencing by the MBD2-NuRD complex. Proceedings of the National Academy of Sciences *108*, 7487–7492.

Goll, M.G., and Bestor, T.H. (2005). Eukaryotic cytosine methyltransferases. Annu. Rev. Biochem. *74*, 481–514.

Gowher, H., and Jeltsch, A. (2001). Enzymatic properties of recombinant Dnmt3a DNA methyltransferase from mouse: the enzyme modifies DNA in a non-processive manner and also methylates non-CpG [correction of non-CpA] sites. Journal of Molecular Biology *309*, 1201–1208.

Gowher, H., Stockdale, C.J., Goyal, R., Ferreira, H., Owen-Hughes, T., and Jeltsch, A. (2005). De novo methylation of nucleosomal DNA by the mammalian Dnmt1 and Dnmt3A DNA methyltransferases. Biochemistry *44*, 9899–9904.

Graff, J.R., Herman, J.G., Myöhänen, S., Baylin, S.B., and Vertino, P.M. (1997). Mapping patterns of CpG island methylation in normal and neoplastic cells implicates both upstream and downstream regions in de novo methylation. Journal of Biological Chemistry *272*, 22322–22329.

Grewal, S.I.S., and Jia, S. (2007). Heterochromatin revisited. Nat. Rev. Genet. *8*, 35–46.

Grüne, T., Brzeski, J., Eberharter, A., Clapier, C.R., Corona, D.F.V., Becker, P.B., and Müller, C.W. (2003). Crystal structure and functional analysis of a nucleosome recognition module of the remodeling factor ISWI. Molecular Cell *12*, 449–460.

Gudyś, A., and Deorowicz, S. (2014). QuickProbs—A Fast Multiple Sequence Alignment Algorithm Designed for Graphics Processors. PLoS ONE *9*, e88901.

Guo, J.U., Su, Y., Zhong, C., Ming, G.-L., and Song, H. (2011). Hydroxylation of 5-methylcytosine by TET1 promotes active DNA demethylation in the adult brain. Cell *145*, 423–434.

Guschin, D., Geiman, T.M., Kikyo, N., Tremethick, D.J., Wolffe, A.P., and Wade, P.A. (2000). Multiple ISWI ATPase complexes from xenopus laevis. Functional conservation of an ACF/CHRAC homolog. Journal of Biological Chemistry *275*, 35248–35255.

Hager, G.L., McNally, J.G., and Misteli, T. (2009). Transcription Dynamics. Molecular Cell *35*, 741–753.

Han, P., Li, W., Lin, C.-H., Yang, J., Shang, C., Nurnberg, S.T., Jin, K.K., Xu, W., Lin, C.-Y., Lin, C.-J., et al. (2014). A long noncoding RNA protects the heart from pathological hypertrophy. Nature *514*, 102–106.

Hancock, R. (2012). Structure of metaphase chromosomes: a role for effects of macromolecular crowding. PLoS ONE *7*, e36045.

Hara, R., and Sancar, A. (2002). The SWI/SNF chromatin-remodeling factor stimulates repair by human excision nuclease in the mononucleosome core particle. Molecular and Cellular Biology *22*, 6779–6787.

Hashimoto, H., Horton, J.R., Zhang, X., Bostick, M., Jacobsen, S.E., and Cheng, X. (2008). The SRA domain of UHRF1 flips 5-methylcytosine out of the DNA helix. Nature *455*, 826–829.

Hashimoto, H., Liu, Y., Upadhyay, A.K., Chang, Y., Howerton, S.B., Vertino, P.M., Zhang, X., and Cheng, X. (2012). Recognition and potential mechanisms for replication and erasure of cytosine hydroxymethylation. Nucleic Acids Research *40*, 4841–4849.

Hata, K., Okano, M., Lei, H., and Li, E. (2002). Dnmt3L cooperates with the Dnmt3 family of de novo DNA methyltransferases to establish maternal imprints in mice. Development *129*, 1983–1993.

Hauk, G., McKnight, J.N., Nodelman, I.M., and Bowman, G.D. (2010). The Chromodomains of the Chd1 Chromatin Remodeler Regulate DNA Access to the ATPase Motor. Molecular Cell *39*, 711–723.

He, X., Fan, H.-Y., Narlikar, G.J., and Kingston, R.E. (2006). Human ACF1 alters the remodeling strategy of SNF2h. Journal of Biological Chemistry *281*, 28636–28647.

He, Y.-F., Li, B.-Z., Li, Z., Liu, P., Wang, Y., Tang, Q., Ding, J., Jia, Y., Chen, Z., Li, L., et al. (2011). Tet-mediated formation of 5-carboxylcytosine and its excision by TDG in mammalian DNA. Science *333*, 1303–1307.

Hendrich, B., and Bird, A. (1998). Identification and characterization of a family of mammalian methyl-CpG binding proteins. Molecular and Cellular Biology *18*, 6538–6547.

Hermann, A., Gowher, H., and Jeltsch, A. (2004a). Biochemistry and biology of mammalian DNA methyltransferases. Cell. Mol. Life Sci. *61*, 2571–2587.

Hermann, A., Goyal, R., and Jeltsch, A. (2004b). The Dnmt1 DNA-(cytosine-C5)-methyltransferase methylates DNA processively with high preference for hemimethylated target sites. Journal of Biological Chemistry *279*, 48350–48359.

Hernan G Garcia, J.K.N.O.J.A.T.R.P. (2011). Thermodynamics of Biological Processes. Meth. Enzymol. *492*, 27.

Ho, L., and Crabtree, G.R. (2010). Chromatin remodelling during development. Nature *463*, 474–484.

Ho, L., Jothi, R., Ronan, J.L., Cui, K., Zhao, K., and Crabtree, G.R. (2009). An embryonic stem cell chromatin remodeling complex, esBAF, is an essential component of the core pluripotency transcriptional network. Proceedings of the National Academy of Sciences *106*, 5187–5191.

Hoffmann, I., Roatsch, M., Schmitt, M.L., Carlino, L., Pippel, M., Sippl, W., and Jung, M. (2012). The role of histone demethylases in cancer therapy. Mol Oncol *6*, 683–703.

Holz-Schietinger, C., and Reich, N.O. (2012). RNA modulation of the human DNA methyltransferase 3A. Nucleic Acids Research *40*, 8550–8557.

Hoogstraten, D., Nigg, A.L., Heath, H., Mullenders, L.H.F., van Driel, R., Hoeijmakers, J.H.J., Vermeulen, W., and Houtsmuller, A.B. (2002). Rapid switching of TFIIH between RNA polymerase I and II transcription and DNA repair in vivo. Molecular Cell *10*, 1163–1174.

Horn, P.J., and Peterson, C.L. (2002). Molecular biology. Chromatin higher order folding--wrapping up transcription. Science *297*, 1824–1827.

Houtsmuller, A.B., Rademakers, S., Nigg, A.L., Hoogstraten, D., Hoeijmakers, J.H., and Vermeulen, W. (1999). Action of DNA repair endonuclease ERCC1/XPF in living cells. Science *284*, 958–961.

Hu, J.C. (2000). A guided tour in protein interaction space: coiled coils from the yeast proteome. Proc Natl Acad Sci USA *97*, 12935–12936.

Hu, L., Li, Z., Cheng, J., Rao, Q., Gong, W., Liu, M., Shi, Y.G., Zhu, J., Wang, P., and Xu, Y. (2013). Crystal structure of TET2-DNA complex: insight into TET-mediated 5mC oxidation. Cell *155*, 1545–1555.

Huang, J. (2004). Lsh, an epigenetic guardian of repetitive elements. Nucleic Acids Research *32*, 5019–5028.

Huang, N., Banavali, N.K., and MacKerell, A.D. (2003). Protein-facilitated base flipping in DNA by cytosine-5-methyltransferase. Proc Natl Acad Sci USA *100*, 68–73.

Huisinga, K.L., Brower-Toland, B., and Elgin, S.C.R. (2006). The contradictory definitions of heterochromatin: transcription and silencing. Chromosoma *115*, 110–122.

Inayoshi, Y., Miyake, K., Machida, Y., Kaneoka, H., Terajima, M., Dohda, T., Takahashi, M., and Iijima, S. (2006). Mammalian chromatin remodeling complex SWI/SNF is essential for enhanced expression of the albumin gene during liver development. Journal of Biochemistry *139*, 177–188.

Inoue, A., and Zhang, Y. (2011). Replication-dependent loss of 5-hydroxymethylcytosine in mouse preimplantation embryos. Science *334*, 194.

Inoue, A., Shen, L., Dai, Q., He, C., and Zhang, Y. (2011). Generation and replication-dependent dilution of 5fC and 5caC during mouse preimplantation development. Cell Res. *21*, 1670–1676.

Iqbal, K., Jin, S.-G., Pfeifer, G.P., and Szabó, P.E. (2011). Reprogramming of the paternal genome upon fertilization involves genome-wide oxidation of 5-methylcytosine. Proceedings of the National Academy of Sciences *108*, 3642–3647.

Ito, S., D'Alessio, A.C., Taranova, O.V., Hong, K., Sowers, L.C., and Zhang, Y. (2010). Role of Tet proteins in 5mC to 5hmC conversion, ES-cell self-renewal and inner cell mass specification. Nature *466*, 1129–1133.

Ito, S., Shen, L., Dai, Q., Wu, S.C., Collins, L.B., Swenberg, J.A., He, C., and Zhang, Y. (2011). Tet proteins can convert 5-methylcytosine to 5-formylcytosine and 5-carboxylcytosine. Science *333*, 1300–1303.

Iurlaro, M., Ficz, G., Oxley, D., Raiber, E.-A., Bachman, M., Booth, M.J., Andrews, S., Balasubramanian, S., and Reik, W. (2013). A screen for hydroxymethylcytosine and formylcytosine binding proteins suggests functions in transcription and chromatin regulation. *14*, 1–1.

Iyer, L.M., Tahiliani, M., Rao, A., and Aravind, L. (2009). Prediction of novel families of enzymes involved in oxidative and other complex modifications of bases in nucleic acids. Cell Cycle *8*, 1698–1710.

Izzo, A., Regnard, C., Morales, V., Kremmer, E., and Becker, P.B. (2008). Structure-function analysis of the RNA helicase maleless. Nucleic Acids Research *36*, 950–962.

Jacobson, R.H., Ladurner, A.G., King, D.S., and Tjian, R. (2000). Structure and function of a human TAFII250 double bromodomain module. Science *288*, 1422–1425.

Jankowsky, E. (2011). RNA helicases at work: binding and rearranging. Trends Biochem Sci

36, 19–29.

Jarvis, C.D., Geiman, T., Vila-Storm, M.P., Osipovich, O., Akella, U., Candeias, S., Nathan, I., Durum, S.K., and Muegge, K. (1996). A novel putative helicase produced in early murine lymphocytes. Gene *169*, 203–207.

Jeanmougin, F., Wurtz, J.M., Le Douarin, B., Chambon, P., and Losson, R. (1997). The bromodomain revisited. Trends Biochem Sci *22*, 151–153.

Jeddeloh, J.A., Stokes, T.L., and Richards, E.J. (1999). Maintenance of genomic methylation requires a SWI2/SNF2-like protein. Nat. Genet. *22*, 94–97.

Jeltsch, A. (2002). Beyond Watson and Crick: DNA methylation and molecular enzymology of DNA methyltransferases. ChemBioChem *3*, 274–293.

Jia, D., Jurkowska, R.Z., Zhang, X., Jeltsch, A., and Cheng, X. (2007). Structure of Dnmt3a bound to Dnmt3L suggests a model for de novo DNA methylation. Nature *449*, 248–251.

Kagalwala, M.N., Glaus, B.J., Dang, W., Zofall, M., and Bartholomew, B. (2004). Topography of the ISW2-nucleosome complex: insights into nucleosome spacing and chromatin remodeling. Embo J *23*, 2092–2104.

Kaneko, S., Li, G., Son, J., Xu, C.-F., Margueron, R., Neubert, T.A., and Reinberg, D. (2010). Phosphorylation of the PRC2 component Ezh2 is cell cycle-regulated and up-regulates its binding to ncRNA. Genes Dev *24*, 2615–2620.

Kato, Y., Kaneda, M., Hata, K., Kumaki, K., Hisano, M., Kohara, Y., Okano, M., Li, E., Nozaki, M., and Sasaki, H. (2007). Role of the Dnmt3 family in de novo methylation of imprinted and repetitive sequences during male germ cell development in the mouse. Human Molecular Genetics *16*, 2272–2280.

Keyes, W.M., Pecoraro, M., Aranda, V., Vernersson-Lindahl, E., Li, W., Vogel, H., Guo, X., Garcia, E.L., Michurina, T.V., Enikolopov, G., et al. (2011). ΔNp63α Is an Oncogene that Targets Chromatin Remodeler Lsh to Drive Skin Stem Cell Proliferation and Tumorigenesis. Stem Cell *8*, 164–176.

Khalil, A.M., Guttman, M., Huarte, M., Garber, M., Raj, A., Rivea Morales, D., Thomas, K., Presser, A., Bernstein, B.E., van Oudenaarden, A., et al. (2009). Many human large intergenic noncoding RNAs associate with chromatin-modifying complexes and affect gene expression. Proceedings of the National Academy of Sciences *106*, 11667–11672.

Khavari, P.A., Peterson, C.L., Tamkun, J.W., Mendel, D.B., and Crabtree, G.R. (1993). BRG1 contains a conserved domain of the SWI2/SNF2 family necessary for normal mitotic growth and transcription. Nature *366*, 170–174.

Khorasanizadeh, S. (2004). The nucleosome: from genomic organization to genomic regulation. Cell *116*, 259–272.

Kim, H.S., Kuwano, Y., Zhan, M., Pullmann, R., Mazan-Mamczarz, K., Li, H., Kedersha, N., Anderson, P., Wilce, M.C.J., Gorospe, M., et al. (2007). Elucidation of a C-rich signature motif in target mRNAs of RNA-binding protein TIAR. Molecular and Cellular Biology *27*, 6806–6817.

Kimura, H., Sugaya, K., and Cook, P.R. (2002). The transcription cycle of RNA polymerase II in living cells. The Journal of Cell Biology *159*, 777–782.

Klose, R.J., and Bird, A.P. (2004). MeCP2 behaves as an elongated monomer that does not stably associate with the Sin3a chromatin remodeling complex. Journal of Biological Chemistry *279*, 46490–46496.

Kornberg, R.D. (1974). Chromatin structure: a repeating unit of histones and DNA. Science *184*, 868–871.

Kouzarides, T. (2007). Chromatin Modifications and Their Function. Cell *128*, 693–705.

Krajewski, W.A., and Reese, J.C. (2010). SET domains of histone methyltransferases recognize ISWI-remodeled nucleosomal species. Molecular and Cellular Biology *30*, 552–564.

Kretz, M., Siprashvili, Z., Chu, C., Webster, D.E., Zehnder, A., Qu, K., Lee, C.S., Flockhart, R.J., Groff, A.F., Chow, J., et al. (2013). Control of somatic tissue differentiation by the long non-coding RNA TINCR. Nature *493*, 231–235.

Kriaucionis, S., and Bird, A. (2003). DNA methylation and Rett syndrome. Human Molecular Genetics *12 Spec No 2*, R221–R227.

La Fuente, De, R., Baumann, C., Fan, T., Schmidtmann, A., Dobrinski, I., and Muegge, K. (2006). Lsh is required for meiotic chromosome synapsis and retrotransposon silencing in female germ cells. Nat Cell Biol *8*, 1448–1454.

Lan, L., Ui, A., Nakajima, S., Hatakeyama, K., Hoshi, M., Watanabe, R., Janicki, S.M., Ogiwara, H., Kohno, T., Kanno, S.-I., et al. (2010). The ACF1 complex is required for DNA double-strand break repair in human cells. Molecular Cell *40*, 976–987.

Langst, G., Bonte, E.J., Corona, D.F., and Becker, P.B. (1999). Nucleosome movement by CHRAC and ISWI without disruption or trans-displacement of the histone octamer. Cell *97*, 843–852.

Larsen, D.H., Poinsignon, C., Gudjonsson, T., Dinant, C., Payne, M.R., Hari, F.J., Rendtlew Danielsen, J.M., Menard, P., Sand, J.C., Stucki, M., et al. (2010). The chromatin-remodeling factor CHD4 coordinates signaling and repair after DNA damage. The Journal of Cell Biology *190*, 731–740.

Längst, G., and Becker, P.B. (2004). Nucleosome remodeling: one mechanism, many phenomena? Biochim Biophys Acta *1677*, 58–63.

Lee, D.W., Zhang, K., Ning, Z.Q., Raabe, E.H., Tintner, S., Wieland, R., Wilkins, B.J., Kim, J.M., Blough, R.I., and Arceci, R.J. (2000). Proliferation-associated SNF2-like gene (PASG): a SNF2 family member altered in leukemia. Cancer Res. *60*, 3612–3622.

Lehnertz, B., Ueda, Y., Derijck, A.A.H.A., Braunschweig, U., Perez-Burgos, L., Kubicek, S., Chen, T., Li, E., Jenuwein, T., and Peters, A.H.F.M. (2003). Suv39h-mediated histone H3 lysine 9 methylation directs DNA methylation to major satellite repeats at pericentric heterochromatin. Curr. Biol. *13*, 1192–1200.

Leonhardt, H., Page, A.W., Weier, H.U., and Bestor, T.H. (1992). A targeting sequence directs DNA methyltransferase to sites of DNA replication in mammalian nuclei. Cell *71*, 865–873.

LeRoy, G., Loyola, A., Lane, W.S., and Reinberg, D. (2000). Purification and characterization of a human factor that assembles and remodels chromatin. Journal of Biological Chemistry *275*, 14787–14790.

Li, E., Bestor, T.H., and Jaenisch, R. (1992). Targeted mutation of the DNA methyltransferase gene results in embryonic lethality. Cell *69*, 915–926.

Li, E. (2002). Chromatin modification and epigenetic reprogramming in mammalian development. Nat. Rev. Genet. *3*, 662–673.

Li, G., and Reinberg, D. (2011). Chromatin higher-order structures and gene regulation. Current Opinion in Genetics & Development *21*, 175–186.

Li, H., Rauch, T., Chen, Z.-X., Szabó, P.E., Riggs, A.D., and Pfeifer, G.P. (2006). The histone methyltransferase SETDB1 and the DNA methyltransferase DNMT3A interact directly and localize to promoters silenced in cancer cells. Journal of Biological Chemistry *281*, 19489–19500.

Linder, P., and Jankowsky, E. (2011). From unwinding to clamping — the DEAD box RNA helicase family. Nature Publishing Group *12*, 505–516.

Linxweiler, W., and Hörz, W. (1984). Reconstitution of mononucleosomes: characterization of distinct particles that differ in the position of the histone core. Nucleic Acids Research *12*, 9395–9413.

Liu, N., Peterson, C.L., and Hayes, J.J. (2011). SWI/SNF- and RSC-Catalyzed Nucleosome Mobilization Requires Internal DNA Loop Translocation within Nucleosomes. Molecular and Cellular Biology *31*, 4165–4175.

Liu, N., Wang, M., Deng, W., Schmidt, C.S., Qin, W., Leonhardt, H., and Spada, F. (2013). Intrinsic and extrinsic connections of Tet3 dioxygenase with CXXC zinc finger modules. PLoS ONE *8*, e62755.

Liu, Y., Schmidt, B., and Maskell, D.L. (2010). MSAProbs: multiple sequence alignment based on pair hidden Markov models and partition function posterior probabilities. Bioinformatics *26*, 1958–1964.

Long, H.K., Blackledge, N.P., and Klose, R.J. (2013). ZF-CxxC domain-containing proteins, CpG islands and the chromatin connection. Biochem Soc Trans *41*, 727–740.

Lorenz, R., and Bernhart, S. (2011). ViennaRNA Package 2.0. … For Molecular Biology.

Lowary, P.T., and Widom, J. (1998). New DNA sequence rules for high affinity binding to histone octamer and sequence-directed nucleosome positioning. Journal of Molecular Biology *276*, 19–42.

Luger, K., and Richmond, T.J. (1998). DNA binding within the nucleosome core. Curr. Opin. Struct. Biol. *8*, 33–40.

Luger, K., Mäder, A.W., Richmond, R.K., Sargent, D.F., and Richmond, T.J. (1997). Crystal structure of the nucleosome core particle at 2.8 A resolution. Nature *389*, 251–260.

Luger, K. (2006). Dynamic nucleosomes. Chromosome Res *14*, 5–16.

Lungu, C., Muegge, K., Jeltsch, A., and Jurkowska, R.Z. (2015). An ATPase-Deficient Variant of the SNF2 Family Member HELLS Shows Altered Dynamics at Pericentromeric Heterochromatin. Journal of Molecular Biology 1–13.

Lusser, A., and Kadonaga, J.T. (2003). Chromatin remodeling by ATP-dependent molecular machines. Bioessays *25*, 1192–1200.

Lusser, A., Urwin, D.L., and Kadonaga, J.T. (2005). Distinct activities of CHD1 and ACF in ATP-dependent chromatin assembly. Nature Structural & Molecular Biology *12*, 160–166.

Ma, Y., and Lieber, M.R. (2001). DNA length-dependent cooperative interactions in the binding of Ku to DNA. Biochemistry *40*, 9638–9646.

Maga, G., and Hubscher, U. (2003). Proliferating cell nuclear antigen (PCNA): a dancer with many partners. Journal of Cell Science *116*, 3051–3060.

Maiti, A., and Drohat, A.C. (2011). Thymine DNA glycosylase can rapidly excise 5-formylcytosine and 5-carboxylcytosine: potential implications for active demethylation of CpG sites. J. Biol. Chem. *286*, 35334–35338.

Manelyte, L., and Längst, G. (2013). Chromatin Remodelers and Their Way of Action. (InTech).

Manelyte, L., Strohner, R., Gross, T., and Längst, G. (2014). Chromatin targeting signals, nucleosome positioning mechanism and non-coding RNA-mediated regulation of the chromatin remodeling complex NoRC. PLoS Genet *10*, e1004157.

Margueron, R., and Reinberg, D. (2010). Chromatin structure and the inheritance of epigenetic information. Nat. Rev. Genet. *11*, 285–296.

Martens, J.H.A., O'Sullivan, R.J., Braunschweig, U., Opravil, S., Radolf, M., Steinlein, P., and Jenuwein, T. (2005). The profile of repeat-associated histone lysine methylation states in the mouse epigenome. Embo J *24*, 800–812.

Martienssen, R., and Henikoff, S. (1999). The House & Garden guide to chromatin remodelling. Nat. Genet. *22*, 6–7.

Mayer, C., Neubert, M., and Grummt, I. (2008). The structure of NoRC-associated RNA is crucial for targeting the chromatin remodelling complex NoRC to the nucleolus. EMBO Rep. *9*, 774–780.

Mellor, J., and Morillon, A. (2004). ISWI complexes in Saccharomyces cerevisiae. Biochim Biophys Acta *1677*, 100–112.

Menoni, H., Gasparutto, D., Hamiche, A., Cadet, J., Dimitrov, S., Bouvet, P., and Angelov, D. (2007). ATP-dependent chromatin remodeling is required for base excision repair in conventional but not in variant H2A.Bbd nucleosomes. Molecular and Cellular Biology *27*, 5949–5956.

Merry, C.R., Forrest, M.E., Sabers, J.N., Beard, L., Gao, X.-H., Hatzoglou, M., Jackson, M.W., Wang, Z., Markowitz, S.D., and Khalil, A.M. (2015). DNMT1-associated long non-coding RNAs regulate global gene expression and DNA methylation in colon cancer. Human Molecular Genetics *24*, 6240–6253.

Métivier, R., Penot, G., Hübner, M.R., Reid, G., Brand, H., Kos, M., and Gannon, F. (2003). Estrogen receptor-alpha directs ordered, cyclical, and combinatorial recruitment of cofactors on a natural target promoter. Cell *115*, 751–763.

Mjelle, R., Hegre, S.A., Aas, P.A., Slupphaug, G., Drabløs, F., Sætrom, P., and Krokan, H.E. (2015). Cell cycle regulation of human DNA repair and chromatin remodeling genes. DNA Repair *30*, 53–67.

Moarefi, A.H., and Chedin, F. (2011). ICF syndrome mutations cause a broad spectrum of

biochemical defects in DNMT3B-mediated de novo DNA methylation. Journal of Molecular Biology *409*, 758–772.

Mohammad, F., Mondal, T., Guseva, N., Pandey, G.K., and Kanduri, C. (2010). Kcnq1ot1 noncoding RNA mediates transcriptional gene silencing by interacting with Dnmt1. Development *137*, 2493–2499.

Morgan, H.D., Santos, F., Green, K., Dean, W., and Reik, W. (2005). Epigenetic reprogramming in mammals. Human Molecular Genetics *14 Spec No 1*, R47–R58.

Mortusewicz, O., Schermelleh, L., Walter, J., Cardoso, M.C., and Leonhardt, H. (2005). Recruitment of DNA methyltransferase I to DNA repair sites. Proc Natl Acad Sci USA *102*, 8905–8909.

Mpakali, A., G Kotini, A., and Spella, M. (2012). P68/Ddx5 RNA Helicase Interacts and Co-Localizes In vivo with the De Novo DNA Methyltransferases Dnmt3a1 and Dnmt3a2. Journal of Proteomics & Bioinformatics *05*.

Muchardt, C., Guilleme, M., Seeler, J.-S., Trouche, D., Dejean, A., and Yaniv, M. (2002). Coordinated methyl and RNA binding is required for heterochromatin localization of mammalian HP1alpha. EMBO Rep. *3*, 975–981.

Mueller-Planitz, F., Klinker, H., Ludwigsen, J., and Becker, P.B. (2012). The ATPase domain of ISWI is an autonomous nucleosome remodeling machine. Nature Structural & Molecular Biology *20*, 82–89.

Murawska, M., Kunert, N., van Vugt, J., Längst, G., Kremmer, E., Logie, C., and Brehm, A. (2008). dCHD3, a novel ATP-dependent chromatin remodeler associated with sites of active transcription. Molecular and Cellular Biology *28*, 2745–2757.

Myant, K., and Stancheva, I. (2007). LSH Cooperates with DNA Methyltransferases To Repress Transcription. Molecular and Cellular Biology *28*, 215–226.

Myant, K., Termanis, A., Sundaram, A.Y.M., Boe, T., Li, C., Merusi, C., Burrage, J., Heras, J.I.D.L., and Stancheva, I. (2011). LSH and G9a/GLP complex are required for developmentally programmed DNA methylation. Genome Research *21*, 83–94.

Nabel, C.S., Jia, H., Ye, Y., Shen, L., Goldschmidt, H.L., Stivers, J.T., Zhang, Y., and Kohli, R.M. (2012). AID/APOBEC deaminases disfavor modified cytosines implicated in DNA demethylation. Nat. Chem. Biol. *8*, 751–758.

Nagano, T., Mitchell, J.A., Sanz, L.A., Pauler, F.M., Ferguson-Smith, A.C., Feil, R., and Fraser, P. (2008). The Air noncoding RNA epigenetically silences transcription by targeting G9a to chromatin. Science *322*, 1717–1720.

Nakanishi, S., Prasad, R., Wilson, S.H., and Smerdon, M. (2007). Different structural states in oligonucleosomes are required for early versus late steps of base excision repair. Nucleic Acids Research *35*, 4313–4321.

Nan, X.S., Ng, H.H., Johnson, C.A., Laherty, C.D., Turner, B.M., Eisenman, R.N., and Bird, A. (1998). Transcriptional repression by the methyl-CpG-binding protein MeCP2 involves a histone deacetylase complex. Nature *393*, 386–389.

Nilsen, H., Lindahl, T., and Verreault, A. (2002). DNA base excision repair of uracil residues in reconstituted nucleosome core particles. Embo J *21*, 5943–5952.

Nongkhlaw, M., Gupta, M., Komath, S.S., and Muthuswami, R. (2012). Motifs Q and I Are Required for ATP Hydrolysis but Not for ATP Binding in SWI2/SNF2 Proteins. Biochemistry *51*, 3711–3722.

O'Connell, D.J., Bauer, M.C., O'Brien, J., Johnson, W.M., Divizio, C.A., O'Kane, S.L., Berggård, T., Merino, A., Akerfeldt, K.S., Linse, S., et al. (2010). Integrated protein array screening and high throughput validation of 70 novel neural calmodulin-binding proteins. Mol. Cell Proteomics *9*, 1118–1132.

Ogawa, O., Eccles, M.R., Szeto, J., McNoe, L.A., Yun, K., Maw, M.A., Smith, P.J., and Reeve, A.E. (1993). Relaxation of insulin-like growth factor II gene imprinting implicated in Wilms' tumour. Nature *362*, 749–751.

Okano, M., Bell, D.W., Haber, D.A., and Li, E. (1999). DNA methyltransferases Dnmt3a and Dnmt3b are essential for de novo methylation and mammalian development. Cell *99*, 247–257.

Okano, M., Xie, S., and Li, E. (1998). Cloning and characterization of a family of novel mammalian DNA (cytosine-5) methyltransferases. Nat. Genet. *19*, 219–220.

Okuwaki, M., and Verreault, A. (2004). Maintenance DNA methylation of nucleosome core particles. Journal of Biological Chemistry *279*, 2904–2912.

Olins, D., and Olins, A. (2003). Chromatin history: our view from the bridge. Nat. Rev. Mol. Cell Biol. *4*, 809–814.

Oliver, A.W., Jones, S.A., Roe, S.M., Matthews, S., Goodwin, G.H., and Pearl, L.H. (2005). Crystal structure of the proximal BAH domain of the polybromo protein. Biochem. J. *389*, 657–664.

Onorati, M.C., Lazzaro, S., Mallik, M., Ingrassia, A.M.R., Carreca, A.P., Singh, A.K., Chaturvedi, D.P., Lakhotia, S.C., and Corona, D.F.V. (2011). The ISWI chromatin remodeler organizes the hsrω ncRNA-containing omega speckle nuclear compartments. PLoS Genet *7*, e1002096.

Pang, K.C., Frith, M.C., and Mattick, J.S. (2006). Rapid evolution of noncoding RNAs: lack of conservation does not mean lack of function. Trends in Genetics *22*, 1–5.

Pastor, W.A., Pape, U.J., Huang, Y., Henderson, H.R., Lister, R., Ko, M., McLoughlin, E.M., Brudno, Y., Mahapatra, S., Kapranov, P., et al. (2011). Genome-wide mapping of 5-hydroxymethylcytosine in embryonic stem cells. Nature *473*, 394–397.

Pennings, S., Meersseman, G., and Bradbury, E.M. (1991). Mobility of positioned nucleosomes on 5 S rDNA. Journal of Molecular Biology *220*, 101–110.

Peters, A.H.F.M., Kubicek, S., Mechtler, K., O'Sullivan, R.J., Derijck, A.A.H.A., Perez-Burgos, L., Kohlmaier, A., Opravil, S., Tachibana, M., Shinkai, Y., et al. (2003). Partitioning and plasticity of repressive histone methylation states in mammalian chromatin. Molecular Cell *12*, 1577–1589.

Pfaffeneder, T., Spada, F., Wagner, M., Brandmayr, C., Laube, S.K., Eisen, D., Truss, M., Steinbacher, J., Hackner, B., Kotljarova, O., et al. (2014). Tet oxidizes thymine to 5-hydroxymethyluracil in mouse embryonic stem cell DNA. Nat. Chem. Biol. *10*, 574–581.

Phair, R.D., Scaffidi, P., Elbi, C., Vecerova, J., Dey, A., Ozato, K., Brown, D.T., Hager, G., Bustin, M., and Misteli, T. (2004). Global Nature of Dynamic Protein-Chromatin Interactions

In Vivo: Three-Dimensional Genome Scanning and Dynamic Interaction Networks of Chromatin Proteins. Molecular and Cellular Biology *24*, 6393–6402.

Phelan, M.L., Sif, S., Narlikar, G.J., and Kingston, R.E. (1999). Reconstitution of a core chromatin remodeling complex from SWI/SNF subunits. Molecular Cell *3*, 247–253.

Poot, R.A., Dellaire, G., Hülsmann, B.B., Grimaldi, M.A., Corona, D.F., Becker, P.B., Bickmore, W.A., and Varga-Weisz, P.D. (2000). HuCHRAC, a human ISWI chromatin remodelling complex contains hACF1 and two novel histone-fold proteins. Embo J *19*, 3377–3387.

Pradhan, S., Bacolla, A., Wells, R.D., and Roberts, R.J. (1999). Recombinant human DNA (cytosine-5) methyltransferase. I. Expression, purification, and comparison of de novo and maintenance methylation. Journal of Biological Chemistry *274*, 33002–33010.

Pradhan, S., and Estève, P.-O. (2003). Mammalian DNA (cytosine-5) methyltransferases and their expression. Clin. Immunol. *109*, 6–16.

Pyle, A.M. (2008). Translocation and Unwinding Mechanisms of RNA and DNA Helicases. Annu. Rev. Biophys. *37*, 317–336.

Qin, W., Leonhardt, H., and Pichler, G. (2014). Regulation of DNA methyltransferase 1 by interactions and modifications. Nucleus (Austin, Tex) *2*, 392–402.

Qiu, C., Sawada, K., Zhang, X., and Cheng, X. (2002). The PWWP domain of mammalian DNA methyltransferase Dnmt3b defines a new family of DNA-binding folds. Nat. Struct. Biol. *9*, 217–224.

Racki, L.R., Yang, J.G., Naber, N., Partensky, P.D., Acevedo, A., Purcell, T.J., Cooke, R., Cheng, Y., and Narlikar, G.J. (2009). The chromatin remodeller ACF acts as a dimeric motor to space nucleosomes. Nature *462*, 1016–1021.

Ragab, A., and Travers, A. (2003). HMG-D and histone H1 alter the local accessibility of nucleosomal DNA. Nucleic Acids Research *31*, 7083–7089.

Rainier, S., Dobry, C.J., and Feinberg, A.P. (1995). Loss of imprinting in hepatoblastoma. Cancer Res. *55*, 1836–1838.

Regha, K., Latos, P.A., and Spahn, L. (2006). The imprinted mouse Igf2r/Air cluster--a model maternal imprinting system. Cytogenet. Genome Res. *113*, 165–177.

Ren, J., Briones, V., Barbour, S., Yu, W., Han, Y., Terashima, M., and Muegge, K. (2015). The ATP binding site of the chromatin remodeling homolog Lsh is required for nucleosome density and de novo DNA methylation at repeat sequences. Nucleic Acids Research *43*, 1444–1455.

Rhee, I., Bachman, K.E., Park, B.H., Jair, K.-W., Yen, R.-W.C., Schuebel, K.E., Cui, H., Feinberg, A.P., Lengauer, C., Kinzler, K.W., et al. (2002). DNMT1 and DNMT3b cooperate to silence genes in human cancer cells. Nature *416*, 552–556.

Rhodes, D., and Laskey, R.A. (1989). Assembly of nucleosomes and chromatin in vitro. Meth. Enzymol. *170*, 575–585.

Rice, P., Longden, I., and Bleasby, A. (2000). EMBOSS: the European Molecular Biology Open Software Suite. Trends in Genetics *16*, 276–277.

Richmond, E., and Peterson, C.L. (1996). Functional analysis of the DNA-stimulated ATPase domain of yeast SWI2/SNF2. Nucleic Acids Research *24*, 3685–3692.

Richmond, T.J., and Davey, C.A. (2003). The structure of DNA in the nucleosome core. Nature *423*, 145–150.

Rippe, K., Schrader, A., Riede, P., Strohner, R., Lehmann, E., and Laengst, G. (2007). DNA sequence- and conformation-directed positioning of nucleosomes by chromatin-remodeling complexes. Proc Natl Acad Sci USA *104*, 15635–15640.

Robertson, A.K., Geiman, T.M., Sankpal, U.T., Hager, G.L., and Robertson, K.D. (2004). Effects of chromatin structure on the enzymatic and DNA binding functions of DNA methyltransferases DNMT1 and Dnmt3a in vitro. Biochem. Biophys. Res. Commun. *322*, 110–118.

Robertson, K.D. (2002). DNA methylation and chromatin - unraveling the tangled web. Oncogene *21*, 5361–5379.

Robinson, P.J.J., and Rhodes, D. (2006). Structure of the “30 nm” chromatin fibre: a key role for the linker histone. Curr. Opin. Struct. Biol. *16*, 336–343.

Roche (2011). Lab FAQS. 1–397.

Rodríguez-Campos, A., and Azorín, F. (2007). RNA is an integral component of chromatin that contributes to its structural organization. PLoS ONE *2*, e1182.

Rose, A., Schraegle, S.J., Stahlberg, E.A., and Meier, I. (2005). Coiled-coil protein composition of 22 proteomes--differences and common themes in subcellular infrastructure and traffic control. BMC Evol. Biol. *5*, 66.

Rossetto, D., Avvakumov, N., and Côté, J. (2012). Histone phosphorylation: a chromatin modification involved in diverse nuclear events. Epigenetics *7*, 1098–1108.

Rottach, A., Leonhardt, H., and Spada, F. (2009). DNA methylation-mediated epigenetic control. J. Cell. Biochem. *108*, 43–51.

Rountree, M.R., Bachman, K.E., Herman, J.G., and Baylin, S.B. (2001). DNA methylation, chromatin inheritance, and cancer. Oncogene *20*, 3156–3165.

Routh, A., Sandin, S., and Rhodes, D. (2008). Nucleosome repeat length and linker histone stoichiometry determine chromatin fiber structure. Proceedings of the National Academy of Sciences *105*, 8872–8877.

Ryan, D.P., Sundaramoorthy, R., Martin, D., Singh, V., and Owen-Hughes, T. (2011). The DNA-binding domain of the Chd1 chromatin-remodelling enzyme contains SANT and SLIDE domains. Embo J *30*, 2596–2609.

Saksouk, N., Simboeck, E., and Déjardin, J. (2015). Constitutive heterochromatin formation and transcription in mammals. Epigenetics & Chromatin *8*, 3.

Sambrook, J., and Russell, D.W. (2001). Molecular Cloning (CSHL Press).

Santoro, R., Li, J., and Grummt, I. (2002). The nucleolar remodeling complex NoRC mediates heterochromatin formation and silencing of ribosomal gene transcription. Nat. Genet. *32*, 393–396.

Santos-Rosa, H., Schneider, R., Bernstein, B.E., Karabetsou, N., Morillon, A., Weise, C., Schreiber, S.L., Mellor, J., and Kouzarides, T. (2003). Methylation of histone H3 K4 mediates association of the Isw1p ATPase with chromatin. Molecular Cell *12*, 1325–1332.

Sarma, K., Cifuentes-Rojas, C., Ergun, A., Del Rosario, A., Jeon, Y., White, F., Sadreyev, R., and Lee, J.T. (2014). ATRX directs binding of PRC2 to Xist RNA and Polycomb targets. Cell *159*, 869–883.

Schalch, T., Duda, S., Sargent, D.F., and Richmond, T.J. (2005). X-ray structure of a tetranucleosome and its implications for the chromatin fibre. Nature *436*, 138–141.

Schiesser, S., Hackner, B., Pfaffeneder, T., Müller, M., Hagemeier, C., Truss, M., and Carell, T. (2012). Mechanism and Stem-Cell Activity of 5-Carboxycytosine Decarboxylation Determined by Isotope Tracing. Angew. Chem. Int. Ed. *51*, 6516–6520.

Schrader, A., Gross, T., Thalhammer, V., and Längst, G. (2015). Characterization of Dnmt1 Binding and DNA Methylation on Nucleosomes and Nucleosomal Arrays. PLoS ONE *10*, e0140076.

Shen, L., and Zhang, Y. (2013). 5-Hydroxymethylcytosine: generation, fate, and genomic distribution. Current Opinion in Cell Biology *25*, 289–296.

Shen, X., Mizuguchi, G., Hamiche, A., and Wu, C. (2000). A chromatin remodelling complex involved in transcription and DNA processing. Nature *406*, 541–544.

Shen, X., Ranallo, R., Choi, E., and Wu, C. (2003). Involvement of actin-related proteins in ATP-dependent chromatin remodeling. Molecular Cell *12*, 147–155.

Shikauchi, Y., Saiura, A., Kubo, T., Niwa, Y., Yamamoto, J., Murase, Y., and Yoshikawa, H. (2009). SALL3 interacts with DNMT3A and shows the ability to inhibit CpG island methylation in hepatocellular carcinoma. Molecular and Cellular Biology *29*, 1944–1958.

Slotkin, R.K., and Martienssen, R. (2007). Transposable elements and the epigenetic regulation of the genome. Nat. Rev. Genet. *8*, 272–285.

Smallwood, S.A., Tomizawa, S.-I., Krueger, F., Ruf, N., Carli, N., Segonds-Pichon, A., Sato, S., Hata, K., Andrews, S.R., and Kelsey, G. (2011). Dynamic CpG island methylation landscape in oocytes and preimplantation embryos. Nat. Genet. *43*, 811–814.

Smith, C.L., and Peterson, C.L. (2005). A Conserved Swi2/Snf2 ATPase Motif Couples ATP Hydrolysis to Chromatin Remodeling. Molecular and Cellular Biology *25*, 5880–5892.

Smith, Z.D., and Meissner, A. (2013). DNA methylation: roles in mammalian development. Nat. Rev. Genet. *14*, 204–220.

Smith, Z.D., Chan, M.M., Mikkelsen, T.S., Gu, H., Gnirke, A., Regev, A., and Meissner, A. (2012). A unique regulatory phase of DNA methylation in the early mammalian embryo. Nature *484*, 339–344.

Song, J., Teplova, M., Ishibe-Murakami, S., and Patel, D.J. (2012). Structure-based mechanistic insights into DNMT1-mediated maintenance DNA methylation. Science *335*, 709–712.

Sporbert, A., Domaing, P., Leonhardt, H., and Cardoso, M.C. (2005). PCNA acts as a stationary loading platform for transiently interacting Okazaki fragment maturation proteins. Nucleic Acids Research *33*, 3521–3528.

Sporbert, A., Gahl, A., Ankerhold, R., Leonhardt, H., and Cardoso, M.C. (2002). DNA polymerase clamp shows little turnover at established replication sites but sequential de novo assembly at adjacent origin clusters. Molecular Cell *10*, 1355–1365.

Springhetti, E.M., Istomina, N.E., Whisstock, J.C., Nikitina, T., Woodcock, C.L., and Grigoryev, S.A. (2003). Role of the M-loop and reactive center loop domains in the folding and bridging of nucleosome arrays by MENT. Journal of Biological Chemistry *278*, 43384–43393.

Spruijt, C.G., Gnerlich, F., Smits, A.H., Pfaffeneder, T., Jansen, P.W.T.C., Bauer, C., Münzel, M., Wagner, M., Müller, M., Khan, F., et al. (2013). Dynamic Readers for 5-(Hydroxy)Methylcytosine and Its Oxidized Derivatives. Cell *152*, 1146–1159.

Strahl, B.D., and Allis, C.D. (2000). The language of covalent histone modifications. Nature *403*, 41–45.

Strohner, R., Nemeth, A., Jansa, P., Hofmann-Rohrer, U., Santoro, R., Langst, G., and Grummt, I. (2001). NoRC--a novel member of mammalian ISWI-containing chromatin remodeling machines. Embo J *20*, 4892–4900.

Strohner, R., Wachsmuth, M., Dachauer, K., Mazurkiewicz, J., Hochstatter, J., Rippe, K., and Längst, G. (2005). A “loop recapture” mechanism for ACF-dependent nucleosome remodeling. Nature Structural & Molecular Biology *12*, 683–690.

Suetake, I., Miyazaki, J., Murakami, C., Takeshima, H., and Tajima, S. (2003). Distinct enzymatic properties of recombinant mouse DNA methyltransferases Dnmt3a and Dnmt3b. Journal of Biochemistry *133*, 737–744.

Suetake, I., Shinozaki, F., Miyagawa, J., Takeshima, H., and Tajima, S. (2004). DNMT3L stimulates the DNA methylation activity of Dnmt3a and Dnmt3b through a direct interaction. Journal of Biological Chemistry *279*, 27816–27823.

Sun, L.Q. (2004). Growth retardation and premature aging phenotypes in mice with disruption of the SNF2-like gene, PASG. Genes Dev *18*, 1035–1046.

Szerlong, H., Hinata, K., Viswanathan, R., Erdjument-Bromage, H., Tempst, P., and Cairns, B.R. (2008). The HSA domain binds nuclear actin-related proteins to regulate chromatin-remodeling ATPases. Nature Structural & Molecular Biology *15*, 469–476.

Szulwach, K.E., Li, X., Li, Y., Song, C.-X., Han, J.W., Kim, S., Namburi, S., Hermetz, K., Kim, J.J., Rudd, M.K., et al. (2011a). Integrating 5-hydroxymethylcytosine into the epigenomic landscape of human embryonic stem cells. PLoS Genet *7*, e1002154.

Szulwach, K.E., Li, X., Li, Y., Song, C.-X., Wu, H., Dai, Q., Irier, H., Upadhyay, A.K., Gearing, M., Levey, A.I., et al. (2011b). 5-hmC-mediated epigenetic dynamics during postnatal neurodevelopment and aging. Nat. Neurosci. *14*, 1607–1616.

Tahiliani, M., Koh, K.P., Shen, Y., Pastor, W.A., Bandukwala, H., Brudno, Y., Agarwal, S., Iyer, L.M., Liu, D.R., Aravind, L., et al. (2009). Conversion of 5-methylcytosine to 5-hydroxymethylcytosine in mammalian DNA by MLL partner TET1. Science *324*, 930–935.

Takeshima, H., Suetake, I., and Tajima, S. (2008). Mouse Dnmt3a preferentially methylates linker DNA and is inhibited by histone H1. Journal of Molecular Biology *383*, 810–821.

Takeshima, H., Suetake, I., Shimahara, H., Ura, K., Tate, S.-I., and Tajima, S. (2006). Distinct DNA methylation activity of Dnmt3a and Dnmt3b towards naked and nucleosomal

DNA. Journal of Biochemistry *139*, 503–515.

Tao, Y., Xi, S., Briones, V., and Muegge, K. (2010). Lsh Mediated RNA Polymerase II Stalling at HoxC6 and HoxC8 Involves DNA Methylation. PLoS ONE *5*, e9163.

Tao, Y., Xi, S., Shan, J., Maunakea, A., Che, A., Briones, V., Lee, E.Y., Geiman, T., Huang, J., Stephens, R., et al. (2011). Lsh, chromatin remodeling family member, modulates genome-wide cytosine methylation patterns at nonrepeat sequences. Proc Natl Acad Sci USA *108*, 5626–5631.

Thomas, J.O., and Stott, K. (2012). H1 and HMGB1: modulators of chromatin structure. Biochem Soc Trans *40*, 341–346.

Thomä, N.H., Czyzewski, B.K., Alexeev, A.A., Mazin, A.V., Kowalczykowski, S.C., and Pavletich, N.P. (2005). Structure of the SWI2/SNF2 chromatin-remodeling domain of eukaryotic Rad54. Nature Structural & Molecular Biology *12*, 350–356.

Ura, K., Araki, M., Saeki, H., Masutani, C., Ito, T., Iwai, S., Mizukoshi, T., Kaneda, Y., and Hanaoka, F. (2001). ATP-dependent chromatin remodeling facilitates nucleotide excision repair of UV-induced DNA lesions in synthetic dinucleosomes. Embo J *20*, 2004–2014.

van Attikum, H., Fritsch, O., and Gasser, S.M. (2007). Distinct roles for SWR1 and INO80 chromatin remodeling complexes at chromosomal double-strand breaks. Embo J *26*, 4113–4125.

Vaquero, A., Loyola, A., and Reinberg, D. (2003). The constantly changing face of chromatin. Sci Aging Knowledge Environ *2003*, RE4.

Varga-Weisz, P.D., and Becker, P.B. (2006). Regulation of higher-order chromatin structures by nucleosome-remodelling factors. Current Opinion in Genetics & Development *16*, 151–156.

Wang, R., Shi, Y., Chen, L., Jiang, Y., Mao, C., Yan, B., Liu, S., Shan, B., Tao, Y., and Wang, X. (2015). The ratio of FoxA1 to FoxA2 in lung adenocarcinoma is regulated by LncRNA HOTAIR and chromatin remodeling factor LSH. Sci Rep *5*, 17826.

Waseem, A., Ali, M., Odell, E.W., Fortune, F., and Teh, M.-T. (2010). Downstream targets of FOXM1: CEP55 and HELLS are cancer progression markers of head and neck squamous cell carcinoma. Oral Oncol. *46*, 536–542.

Watson, A.A., Mahajan, P., Mertens, H.D.T., Deery, M.J., Zhang, W., Pham, P., Du, X., Bartke, T., Zhang, W., Edlich, C., et al. (2012). The PHD and Chromo Domains Regulate the ATPase Activity of the Human Chromatin Remodeler CHD4. Journal of Molecular Biology *422*, 3–17.

Weber, C.M., and Henikoff, S. (2014). Histone variants: dynamic punctuation in transcription. Genes Dev *28*, 672–682.

West, S.C. (1997). Processing of recombination intermediates by the RuvABC proteins. Annu. Rev. Genet. *31*, 213–244.

Whitehouse, I., Stockdale, C., Flaus, A., Szczelkun, M.D., and Owen-Hughes, T. (2003). Evidence for DNA translocation by the ISWI chromatin-remodeling enzyme. Molecular and Cellular Biology *23*, 1935–1945.

Wienken, C.J., Baaske, P., Duhr, S., and Braun, D. (2011). Thermophoretic melting curves

quantify the conformation and stability of RNA and DNA. Nucleic Acids Research *39*, e52–e52.

Wilson, B.G., and Roberts, C.W.M. (2011). SWI/SNF nucleosome remodellers and cancer. Nature Publishing Group *11*, 481–492.

Wilson, B.J., Bates, G.J., Nicol, S.M., Gregory, D.J., Perkins, N.D., and Fuller-Pace, F.V. (2004). The p68 and p72 DEAD box RNA helicases interact with HDAC1 and repress transcription in a promoter-specific manner. BMC Mol. Biol. *5*, 11.

Wong, K.K., and McClelland, M. (1991). PCR with 5-methyl-dCTP replacing dCTP. Nucleic Acids Research *19*, 1081–1085.

Woodcock, C.L., and Dimitrov, S. (2001). Higher-order structure of chromatin and chromosomes. Current Opinion in Genetics & Development *11*, 130–135.

Woodcock, C.L., and Horowitz, R.A. (1995). Chromatin organization re-viewed. Trends Cell Biol. *5*, 272–277.

Woodcock, C.L. (2006). Chromatin architecture. Curr. Opin. Struct. Biol. *16*, 213–220.

Wutz, A. (2011). Gene silencing in X-chromosome inactivation: advances in understanding facultative heterochromatin formation. Nat. Rev. Genet. *12*, 542–553.

Xi, S., Geiman, T.M., Briones, V., Guang Tao, Y., Xu, H., and Muegge, K. (2009). Lsh participates in DNA methylation and silencing of stem cell genes. Stem Cells *27*, 2691–2702.

Xi, S., Zhu, H., Xu, H., Schmidtmann, A., Geiman, T.M., and Muegge, K. (2007). Lsh controls Hox gene silencing during development. Proc Natl Acad Sci USA *104*, 14366–14371.

Xie, S., Wang, Z., Okano, M., Nogami, M., Li, Y., He, W.W., Okumura, K., and Li, E. (1999). Cloning, expression and chromosome locations of the human DNMT3 gene family. Gene *236*, 87–95.

Xu, Y., Wu, F., Tan, L., Kong, L., Xiong, L., Deng, J., Barbera, A.J., Zheng, L., Zhang, H., Huang, S., et al. (2011). Genome-wide regulation of 5hmC, 5mC, and gene expression by Tet1 hydroxylase in mouse embryonic stem cells. Molecular Cell *42*, 451–464.

Xu, Y., Xu, C., Kato, A., Tempel, W., Abreu, J.G., Bian, C., Hu, Y., Hu, D., Zhao, B., Cerovina, T., et al. (2012). Tet3 CXXC domain and dioxygenase activity cooperatively regulate key genes for Xenopus eye and neural development. Cell *151*, 1200–1213.

Yan, J., Guo, X., Xia, J., Shan, T., Gu, C., Liang, Z., Zhao, W., and Jin, S. (2014). MiR-148a regulates MEG3 in gastric cancer by targeting DNA methyltransferase 1. Med. Oncol. *31*, 879.

Yan, Q., Cho, E., Lockett, S., and Muegge, K. (2003a). Association of Lsh, a regulator of DNA methylation, with pericentromeric heterochromatin is dependent on intact heterochromatin. Molecular and Cellular Biology *23*, 8416–8428.

Yan, Q., Huang, J., Fan, T., Zhu, H., and Muegge, K. (2003b). Lsh, a modulator of CpG methylation, is crucial for normal histone methylation. Embo J *22*, 5154–5162.

Yan, Z., Wang, Z., Sharova, L., Sharov, A.A., Ling, C., Piao, Y., Aiba, K., Matoba, R., Wang, W., and Ko, M.S.H. (2008). BAF250B-associated SWI/SNF chromatin-remodeling complex is required to maintain undifferentiated mouse embryonic stem cells. Stem Cells *26*, 1155–

1165.

Yang, L., Rau, R., and Goodell, M.A. (2015). DNMT3A in haematological malignancies. Nature Publishing Group *15*, 152–165.

Yap, K.L., and Zhou, M.-M. (2011). Structure and Mechanisms of Lysine Methylation Recognition by the Chromodomain in Gene Transcription. Biochemistry *50*, 1966–1980.

Yates, L.A., Fleurdépine, S., Rissland, O.S., De Colibus, L., Harlos, K., Norbury, C.J., and Gilbert, R.J.C. (2012). Structural basis for the activity of a cytoplasmic RNA terminal uridylyl transferase. Nature Structural & Molecular Biology *19*, 782–787.

Yildirim, O., Li, R., Hung, J.-H., Chen, P.B., Dong, X., Ee, L.-S., Weng, Z., Rando, O.J., and Fazzio, T.G. (2011). Mbd3/NURD complex regulates expression of 5-hydroxymethylcytosine marked genes in embryonic stem cells. Cell *147*, 1498–1510.

Yu, W., McIntosh, C., Lister, R., Zhu, I., Han, Y., Ren, J., Landsman, D., Lee, E., Briones, V., Terashima, M., et al. (2014). Genome-wide DNA methylation patterns in LSH mutant reveals de-repression of repeat elements and redundant epigenetic silencing pathways. Genome Research *24*, 1613–1623.

Zeng, W., Baumann, C., Schmidtmann, A., Honaramooz, A., Tang, L., Bondareva, A., Dores, C., Fan, T., Xi, S., Geiman, T., et al. (2011). Lymphoid-Specific Helicase (HELLS) Is Essential for Meiotic Progression in Mouse Spermatocytes. Biology of Reproduction *84*, 1235–1241.

Zhan, S., Shapiro, D.N., and Helman, L.J. (1994). Activation of an imprinted allele of the insulin-like growth factor II gene implicated in rhabdomyosarcoma. J. Clin. Invest. *94*, 445–448.

Zhang, G., Estève, P.-O., Chin, H.G., Terragni, J., Dai, N., Corrêa, I.R., and Pradhan, S. (2015). Small RNA-mediated DNA (cytosine-5) methyltransferase 1 inhibition leads to aberrant DNA methylation. Nucleic Acids Research *43*, 6112–6124.

Zhang, H., Zhang, X., Clark, E., Mulcahey, M., Huang, S., and Shi, Y.G. (2010). TET1 is a DNA-binding protein that modulates DNA methylation and gene transcription via hydroxylation of 5-methylcytosine. Cell Res. *20*, 1390–1393.

Zhang, L., Zhang, Q., Jones, K., Patel, M., and Gong, F. (2009). The chromatin remodeling factor BRG1 stimulates nucleotide excision repair by facilitating recruitment of XPC to sites of DNA damage. Cell Cycle *8*, 3953–3959.

Zhang, Y., and Reinberg, D. (2001). Transcription regulation by histone methylation: interplay between different covalent modifications of the core histone tails. Genes Dev *15*, 2343–2360.

Zhang, Y., Ng, H.H., Erdjument-Bromage, H., Tempst, P., Bird, A., and Reinberg, D. (1999). Analysis of the NuRD subunits reveals a histone deacetylase core complex and a connection with DNA methylation. Genes Dev *13*, 1924–1935.

Zhang, Y., Smith, C.L., Saha, A., Grill, S.W., Mihardja, S., Smith, S.B., Cairns, B.R., Peterson, C.L., and Bustamante, C. (2006). DNA translocation and loop formation mechanism of chromatin remodeling by SWI/SNF and RSC. Molecular Cell *24*, 559–568.

Zhao, H., and Chen, T. (2013). Tet family of 5-methylcytosine dioxygenases in mammalian development. J. Hum. Genet. *58*, 421–427.

Zhao, J., Sun, B.K., Erwin, J.A., Song, J.-J., and Lee, J.T. (2008). Polycomb proteins targeted by a short repeat RNA to the mouse X chromosome. Science *322*, 750–756.

Zhao, Q., Rank, G., Tan, Y.T., Li, H., Moritz, R.L., Simpson, R.J., Cerruti, L., Curtis, D.J., Patel, D.J., Allis, C.D., et al. (2009). PRMT5-mediated methylation of histone H4R3 recruits DNMT3A, coupling histone and DNA methylation in gene silencing. Nature Structural & Molecular Biology *16*, 304–311.

Zhou, R., Han, L., Li, G., and Tong, T. (2009). Senescence delay and repression of p16INK4a by Lsh via recruitment of histone deacetylases in human diploid fibroblasts. Nucleic Acids Research *37*, 5183–5196.

Zhou, T., Xiong, J., Wang, M., Yang, N., Wong, J., Zhu, B., and Xu, R.-M. (2014). Short Article. Molecular Cell *54*, 879–886.

Zhou, Y., and Grummt, I. (2005). The PHD finger/bromodomain of NoRC interacts with acetylated histone H4K16 and is sufficient for rDNA silencing. Curr. Biol. *15*, 1434–1438.

Zhu, H., Geiman, T.M., Xi, S., Jiang, Q., Schmidtmann, A., Chen, T., Li, E., and Muegge, K. (2006). Lsh is involved in de novo methylation of DNA. Embo J *25*, 335–345.

Zillner, K., Jerabek-Willemsen, M., Duhr, S., Braun, D., Längst, G., and Baaske, P. (2011). Microscale Thermophoresis as a Sensitive Method to Quantify Protein: Nucleic Acid Interactions in Solution. In Methods in Molecular Biology, (New York, NY: Springer New York), pp. 241–252.